

The Role of the Integrin $\beta 3$ Adhesome in Angiogenesis

Samuel J. Atkinson

A thesis submitted for the degree of Doctor of
Philosophy (Ph.D.) in Biomolecular Science

University of East Anglia
School of Biological Sciences

August 2018

© This copy of the thesis has been supplied on condition that anyone who consults it is understood to recognise that its copyright rests with the author and that use of any information derived there from must be in accordance with current UK Copyright Law. In addition, any quotation or extract must include full attribution.

Contents

Abstract.....	6
List of Figures	7
List of Tables	9
Acknowledgements.....	10
Chapter one – Introduction	11
Angiogenesis	11
Hypoxia	12
VEGF Pathway	13
Other Pathways in Angiogenesis.....	17
Angiogenesis in Cancer	19
Figure 1-1 Hif1a Pathway Under Hypoxia and Normoxia	22
Figure 1-2 VEGF-A Splice Variants.....	23
Integrins	24
Inside-out Signalling.....	24
Outside-in Signalling	25
Focal Adhesions	27
Integrin Trafficking.....	28
Cross Talk	28
Integrin β 3.....	29
Figure 1-3 Model of the Inactive and Active Confirmations of Integrins.....	32
The Adhesome	33
Methodology.....	33
Contents of the Adhesome	34
Figure 1-4 Protein Domains Found in the Adhesome.....	36
Microtubules.....	37
Function	38
Regulation	38
Interactions with Focal Adhesions	39
Microtubules in Angiogenesis.....	40
Figure 1-5 Overview of Microtube Assembly and Behaviour in Cell Migration.....	41
Aims	43
Chapter two – Materials and Methods.....	44
Reagents.....	44
Mice and Genotyping.....	44

Endothelial Cell Isolation and Immortalisation.....	44
Focal Adhesion Enrichment	45
Western Blotting.....	46
Silver Staining.....	46
Mass Spectrometry	46
Adhesion Assay	46
Immunocytochemistry	47
Nucleofection.....	47
Live Cell Imaging	48
Cell Viability.....	48
Random Migration	48
In Vivo Tumour Assay.....	49
Immunohistochemistry.....	49
Microtubule Cold Stability Assay	49
Active Rac1 Assay.....	50
Statistical Analysis.....	50
Antibodies	51
Chapter three – Isolation and Mass Spectrometry of the Endothelial Cell Adhesome	53
Development of Adhesome Enrichment Method.....	53
Figure 3-1 Adhesome Proteins Can be Crosslinked in Endothelial cells and Poly-l-Lysine Functions as a Negative Control	59
Figure 3-2 Higher Pressure Washing Reduced Sample Complexity	60
Figure 3-3 Endothelial Cells Adhere to Fibronectin and Poly-l-Lysine	62
Quality Control and Experimental Design Development of Adhesome Enrichment.....	63
Figure 3-4 Silver Staining as an Indication for Successful Adhesome Enrichment	65
Figure 3-5 Experimental Design for Defining the Endothelial Adhesome Incorporating Silver Staining Quality Control	67
Optimisation of MaxQuant Label Free Quantification	68
Table 3-1 MaxQuant Test Runs – Parameter Optimisation	73
Figure 3-6 Reactions of DSP, DPBBP, DTT and IAA in Protein Mass Spectrometry.....	74
Table 3-2 MaxQuant Test Runs – Protein Modification.....	75
Chapter four – Analysis of the Endothelial Cell and Integrin β 3 Dependent Adhesomes	76
Statistical Analysis of the Endothelial Cell Adhesome	76
Figure 4-1 Correlations between Adhesome Samples.....	82
Figure 4-2 Hierarchical Clustering of the Endothelial Adhesome	83
Table 4-1 Enrichment Analysis of the Endothelial Adhesome	85

Figure 4-3 Interaction Map of Fibronectin Clustered Proteins in the Endothelial Adhesome	88
Statistical Analysis of the Integrin $\beta 3$ Dependent Adhesome	90
Table 4-2 Enrichment Analysis of the $\beta 3^{+/-}$ Endothelial Adhesome	98
Table 4-3 Enrichment Analysis of the $\beta 3^{-/-}$ Endothelial Adhesome	100
Figure 4-4 Interaction Map of the $\beta 3$ Dependent Adhesome	102
Figure 4-5 Tubulins in the $\beta 3^{+/-}$ Adhesome	104
Figure 4-6 Microtubule Regulators in the $\beta 3$ Dependent Adhesome	106
Statistical Analysis of Endothelial Adhesome with c(RGDfV) Treatment	107
Figure 4-7 Analysis of the c(RGDfV) Treated Adhesome	109
Chapter five – Microtubule Behaviour in Integrin $\beta 3$ Depleted Angiogenesis	110
Microtubules in Endothelial Cells	110
Figure 5-1 Microtubule and Actin Cytoskeletons in Endothelial Cells	116
Figure 5-2 Microtubule Targeting to Focal Adhesions in Endothelial Cells	118
Figure 5-3 Microtubule Live Imaging in Endothelial Cells	120
Microtubule Inhibitors in Endothelial Cells	122
Figure 5-4 Use of Microtubule Inhibitors in Endothelial Cells	125
Figure 5-5 Random Migration in $\beta 3$ Depleted Endothelial Cells with Microtubule Inhibitors	126
Figure 5-6 Random Migration in Microtubule Inhibitor Treated Endothelial Cells with Alternative Modes of $\beta 3$ Inhibition	128
Microtubule Inhibitors in vivo	130
Figure 5-7 Constitutive Integrin $\beta 3$ Depletion in Tumour Vasculature	133
Figure 5-8 Inducible Integrin $\beta 3$ Depletion in Tumour Vasculature	135
Chapter six – Mechanisms of Integrin $\beta 3$ Regulation of Microtubule Stability	136
Microtubule Stability in Integrin $\beta 3$ Depleted Cells	136
Figure 6-1 Cold Stable Microtubule Staining in $\beta 3$ Depleted Endothelial Cells	139
Figure 6-2 Cold Soluble Microtubules in $\beta 3$ Depleted Endothelial Cells	140
$\beta 3$ Dependent Microtubule Stability Regulators in Endothelial Cells	141
Figure 6-3 Rcc2 Regulates Microtubule Stability in Endothelial Cells	144
Figure 6-4 Anxa2 Regulates Microtubule Stability in Endothelial Cells	145
Rac1 Drives Microtubule Stability in $\beta 3$ Depleted Endothelial Cells	147
Figure 6-5 Rac1 Inhibition Decreases Microtubule Stability in $\beta 3$ Depleted Endothelial Cells	150
Figure 6-6 Rcc2 and Anxa2 Dependent Microtubule Stability is driven by Rac1 in Endothelial Cells	152

Figure 6-7 Active Rac1 Associates with Different Microtubule Regulators in Itb3 Depleted Endothelial Cells	154
Chapter seven – Discussion	156
Modes of Integrin β 3 Inhibition	156
Figure 7-1 Effects of Different Modes of β 3 Inhibition During Angiogenesis	160
Microtubule Regulation by Integrin β 3.....	161
Figure 7-2 Possible Mechanisms Behind β 3 Regulation of Microtubules.....	165
Microtubules as Targets for Integrin β 3 Treatment Escape	166
Further Work – Other Adhesome Targets	169
Appendix	171
Supplementary Figures	171
Figure 1 Comparison of Microscopy Techniques	171
Figure 2 Resistance to Mebendazole treatment by β 3 Depleted Endothelial Cells	173
Figure 3 Random Migration of β 3 Depleted Endothelial Cells.....	174
Figure 4 Dual Knockdown of Rcc2 and Anxa2 Cumulatively Increases Microtubule Stability	175
Figure 5 Hsp90 Inhibition in β 3 Depleted Endothelial Cell Migration	176
Figure 6 Non-normalised Random Migration of Endothelial Cells with Microtubule Inhibitors	177
Supplementary Tables	178
Table 1 Raw MaxQuant Output of the Endothelial Adhesome	178
Table 2 LFQ of the Endothelial Adhesome.....	179
Table 3 β 3+/- Endothelial Cell Adhesome.....	180
Table 4 β 3-/- Endothelial Cell Adhesome	181
Table 5 c(RGDfV) Treated Endothelial Cell Adhesome	182
Table 6 Mass Spectrometry of Rcc2 Pulldown.....	183
Abbreviations	184
References	191

Abstract

Angiogenesis, the formation of new blood vessels from those that already exist, plays an essential role in development, homeostasis and tumour growth. As such, targeting angiogenesis is seen as crucial in treatment of cardiovascular diseases or cancer. Therapies directed against vascular endothelial growth factor and its major receptor, VEGFR2 (vascular endothelial growth factor receptor 2), whilst effective in a number of cancers, are not without side-effects due to the role this signalling pathway plays in vascular homeostasis. Because of their restricted expression, fibronectin binding endothelial integrins, especially $\alpha\beta3$ - and $\alpha5\beta1$ -integrins, have emerged as alternative anti-angiogenic targets to neovasculature, particularly in the case of $\beta3$. However, neither global nor conditional knockouts of these integrins block tumour angiogenesis beyond acute deletions, and clinical trials of blocking antibodies and peptides directed against these extracellular matrix receptors have been disappointing. To gain novel insight into how $\alpha\beta3$ -integrin regulates outside-in signal transmission, in this thesis we have optimised an enrichment and mass spectrometry workflow to undertake an unbiased analysis of the molecular composition of the mature endothelial adhesome, and profiled changes that occur when $\beta3$ -integrin function or expression are manipulated. In so doing, we have uncovered $\beta3$ -integrin dependent changes in microtubule behaviour that affect cell migration and offered some potential explanations as to why current inhibitors have failed clinical trials. $\beta3$ negatively regulates microtubule stability/targeting to focal adhesions and these changes are driven by Rcc2 (Regulator of Chromatin Condensation 2) and Anxa2 (Annexin A2) regulation of Rac1 (Ras-related C3 botulinum toxin substrate 1). As a result, cell migration, angiogenesis and tumour growth in the absence of $\beta3$ are susceptible to low doses of clinically relevant microtubule inhibitors.

List of Figures

Figure 1-1 Hif1a Pathway Under Hypoxia and Normoxia	22
Figure 1-2 VEGF-A Splice Variants.....	23
Figure 1-3 Model of the Inactive and Active Conformations of Integrins	32
Figure 1-4 Protein Domains Found in the Adhesome.....	36
Figure 1-5 Overview of Microtubule Assembly and Behaviour in Cell Migration.....	41
Figure 3-1 Adhesome Proteins Can be Crosslinked in Endothelial cells and Poly-L-Lysine Functions as a Negative Control	59
Figure 3-2 Higher Pressure Washing Reduced Sample Complexity.....	60
Figure 3-3 Endothelial Cells Adhere to Fibronectin and Poly-L-Lysine	62
Figure 3-4 Silver Staining as an Indication for Successful Adhesome Enrichment	65
Figure 3-5 Experimental Design for Defining the Endothelial Adhesome Incorporating Silver Staining Quality Control	67
Figure 3-6 Reactions of DSP, DPBBP, DTT and IAA in Protein Mass Spectrometry	74
Figure 4-1 Correlations between Adhesome Samples.....	82
Figure 4-2 Hierarchical Clustering of the Endothelial Adhesome	83
Figure 4-3 Interaction Map of Fibronectin Clustered Proteins in the Endothelial Adhesome	88
Figure 4-4 Interaction Map of the $\beta 3$ Dependent Adhesome	102
Figure 4-5 Tubulins in the $\beta 3$ +/- Adhesome	104
Figure 4-6 Microtubule Regulators in the $\beta 3$ Dependent Adhesome.....	106
Figure 4-7 Analysis of the c(RGDfV) Treated Adhesome	109
Figure 5-1 Microtubule and Actin Cytoskeletons in Endothelial Cells	116
Figure 5-2 Microtubule Targeting to Focal Adhesions in Endothelial Cells	118
Figure 5-3 Microtubule Live Imaging in Endothelial Cells.....	120
Figure 5-4 Use of Microtubule Inhibitors in Endothelial Cells	125
Figure 5-5 Random Migration in $\beta 3$ Depleted Endothelial Cells with Microtubule Inhibitors	126
Figure 5-6 Random Migration in Microtubule Inhibitor Treated Endothelial Cells with Alternative Modes of $\beta 3$ Inhibition.....	128
Figure 5-7 Constitutive Integrin $\beta 3$ Depletion in Tumour Vasculature.....	133
Figure 5-8 Inducible Integrin $\beta 3$ Depletion in Tumour Vasculature	135
Figure 6-1 Cold Stable Microtubule Staining in $\beta 3$ Depleted Endothelial Cells	139

Figure 6-2 Cold Soluble Microtubules in β 3 Depleted Endothelial Cells	140
Figure 6-3 Rcc2 Regulates Microtubule Stability in Endothelial Cells.....	144
Figure 6-4 Anxa2 Regulates Microtubule Stability in Endothelial Cells	145
Figure 6-5 Rac1 Inhibition Decreases Microtubule Stability in β 3 Depleted Endothelial Cells	150
Figure 6-6 Rcc2 and Anxa2 Dependent Microtubule Stability is driven by Rac1 in Endothelial Cells.....	152
Figure 6-7 Active Rac1 Associates with Different Microtubule Regulators in Itb3 Depleted Endothelial Cells.....	154
Figure 7-1 Effects of Different Modes of β 3 Inhibition During Angiogenesis	160
Figure 7-2 Possible Mechanisms Behind β 3 Regulation of Microtubules.....	165
Supplementary Figure 1 Comparison of Microscopy Techniques	171
Supplementary Figure 2 Resistance to Mebendazole treatment by β 3 Depleted Endothelial Cells.....	173
Supplementary Figure 3 Random Migration of β 3 Depleted Endothelial Cells.....	174
Supplementary Figure 4 Dual Knockdown of Rcc2 and Anxa2 Cumulatively Increases Microtubule Stability	175
Supplementary Figure 5 Hsp90 Inhibition in β 3 Depleted Endothelial Cell Migration.....	176
Supplementary Figure 6 Non-normalised Random Migration of Endothelial Cells with Microtubule Inhibitors	177

List of Tables

Table 3-1 MaxQuant Test Runs – Parameter Optimisation	73
Table 3-2 MaxQuant Test Runs – Protein Modification.....	75
Table 4-1 Enrichment Analysis of the Endothelial Adhesome	85
Table 4-2 Enrichment Analysis of the $\beta 3+/-$ Endothelial Adhesome	98
Table 4-3 Enrichment Analysis of the $\beta 3-/-$ Endothelial Adhesome	100

Supplementary Tables

Table 1 Raw MaxQuant Output of the Endothelial Adhesome	178
Table 2 LFQ of the Endothelial Adhesome.....	179
Table 3 $\beta 3+/-$ Endothelial Cell Adhesome.....	180
Table 4 $\beta 3-/-$ Endothelial Cell Adhesome	181
Table 5 α (RGDfV) Treated Endothelial Cell Adhesome	182
Table 6 Mass Spectrometry of Rcc2 Pulldown.....	183

Acknowledgements

Two very important people were essential in supporting me during these four years, in the development of this thesis and in helping me realise my ambition to become a research scientist.

Firstly, I cannot find the words to properly express my gratitude for eternal support I've had from my supervisor Dr Stephen Robinson during and before my PhD. He consistently went above and beyond his duty as a supervisor to take on additional roles including: mentor, lab partner, father figure and best friend. All whilst showing incredible generosity and patience towards me but still finding the time to run a world-class research programme – it has been an absolute honour to be a part of the Robinson lab. I hope one day I can repay his kindness but also pay it forward by learning from his excellent example in running a busy lab group.

Secondly, the amazing (soon to be) Dr Alex Liu has shown me unlimited kindness, caring, support and encouragement through the good and bad times. All of this and more whilst undertaking her own demanding PhD has shown me her capability for great things and I look forward to the rest of our lives together. I cannot thank my wonderful fiancé Alex enough for everything she has done.

None of this would have been possible without the support of both Alex and Stephen. Therefore I would like to dedicate this thesis to the both of you for making it happen!

I would also like to thank my supervisory team Professor Dylan Edwards and Professor Uli Mayer for their feedback and advice as well as other members of UEA for their input into the project including Dr Mette Mogensen and Dr Paul Thomas. Additionally, a special thanks for all the present and past members of the Robinson and Edwards groups for putting up with me, giving constructive feedback and helping in the lab – including: Veronica, Liz, Sophie, Aleks, Ben, Abdullah, Rob, Wesley, Jordi and Kate. Finally I have to thank Dr Tim Ellison and Dr Christian Roghi for preparing me for this PhD during their fantastic supervision of my summer and masters projects.

Chapter one – Introduction

Angiogenesis

The definition of angiogenesis is the formation of new vasculature from existing vessels. Animals with a blood supply need to develop a functioning vascular system during embryogenesis and maintain this throughout their lives. Animals continue to grow, develop and respond to their environment long after birth and as a result, angiogenesis must also be able to continue beyond embryogenesis to facilitate this.

Oxygen does not diffuse through tissue quick enough to satisfy the respiratory needs of most cell types, hence cells typically cannot survive beyond 50 to 100 μm from an oxygen source¹. Complex organisms therefore will need a vascular system to move oxygenated blood around the body and re-oxygenate blood in specialised organs such as lungs for air breathing animals or gills for water breathing animals. The vascular system is then also used to deliver nutrients necessary for tissues to function and remove waste products. In mammals the vascular system consists of arteries, veins and capillaries all with the same basic structure of a lumen which allows for blood flow, a layer of endothelial cells connected by tight, adherens and gap junctions², a shared basement membrane around the endothelial cells³ and then a number of supporting cells called pericytes or smooth muscle cells with additional layers such as an adventitia in larger vessels to provide elastic support⁴. Endothelial cells are the key cell type in vasculature, forming the endothelium which faces the blood on one side and the rest of the body on the other where they control the movement of substrates and cells between them⁵.

Before angiogenesis can occur, vasculogenesis must first occur to develop the initial vasculature of an animal de novo. Vasculogenesis and angiogenesis share many aspects, such as regulation by similar growth factors that target endothelial cells and that vasculogenesis will create the vessels from which angiogenesis occurs later to develop smaller vessels such as capillaries⁶. In embryonic vasculogenesis, hemangioblasts develop in the extra-embryonic mesoderm in the yolk sac at 7.5 days post gestation in mice⁷. Hemangioblasts are multipotent stem cells that form and reside in “blood islands”, resembling the bone marrow stem cell niche in adults, where they give rise to both the hematopoietic and endothelial lineages⁸. Hemangioblasts begin to form VEGFR2 positive angioblasts which form vessels directly in the adjacent mesoderm by further differentiating into VEGFR2 and VE-cadherin (Vascular endothelial cadherin) positive endothelial cells, both key markers of endothelial identity; angioblasts also circulate through the primitive

vasculature to form embryonic blood vessels throughout the rest of the embryo and in the initial vascularisation of organs which develop later such as kidneys or lungs^{9,10}. Continued vasculogenesis in the embryo lays down the foundation for the development of the heart and the primitive vascular plexus which is further developed and remodelled by angiogenesis to give rise to the complete vascular system¹¹.

Angiogenesis itself can occur by two main mechanisms – intussusceptive and sprouting. Intussusceptive angiogenesis involves an existing vessel becoming bifurcated by the protrusion of opposing vessel walls and contact of the endothelial cells, a formation of a transluminal pillar and invasion of fibroblasts and pericytes which results in the separation of the lumen into two spaces¹². Sprouting angiogenesis will be the main focus of this thesis and referred to from now on as just “angiogenesis”.

Hypoxia

Hypoxia is one of the most potent drivers of angiogenesis and it is a clear signal that the metabolic demands for oxygen are not being met within tissues. Hypoxia could be triggered by a sudden increase in cellular activity, such as during embryonic development, or after disruption of existing blood vessels during traumatic injuries¹³. A family of “hypoxia inducible factors” such as Hif1a (Hypoxia inducible factor 1 alpha subunit) are the primary mechanism behind hypoxia triggered signalling. Activity of prolyl-hydroxylase enzymes such as PHD2 (Prolyl hydroxylase domain containing protein 2) are dependent on molecular oxygen, which provides the means behind oxygen sensing intracellularly¹⁴. PHD2 and related enzymes use molecular oxygen to hydroxylate prolyl or asparaginyl residues with one oxygen atom and use the other atom to convert 2-oxoglutarate to carbon dioxide. 2-oxoglutarate is a key intermediate in the citric acid cycles, the generation of which is dependent on sufficient glucose for acetyl-CoA generation and sufficient oxygen in the electron transport chain, proving another pathway for Egn1 to react to oxygen levels as well as glucose availability¹⁵. In normoxia, Egn1 is able to hydroxylate a proline residue in two very highly conserved oxygen dependent degradation domains of Hif1a¹⁶ which initiates binding to an E3 ubiquitin ligase complex via Vhl (Von Hippel-Lindau tumour suppressor)¹⁷. Once bound to Vhl, Hif1a is ubiquitinated and targeted for degradation by the proteasome¹⁸. Therefore under normoxia cellular levels of Hif1a are low and angiogenesis is not triggered. During hypoxia however, Egn1 is not able to function without sufficient oxygen and Hif1a is not sent for degradation. Hif1a is continually expressed in order to allow response to changing oxygen levels, so without degradation

levels begin to rise at which point Hif1a is translocated to the nucleus where it binds Hif1b¹⁹. Once in the nucleus other cofactors such as Ep300 (E1a binding protein p300) and Crebbp (Creb binding protein) bind to form a functioning transcription complex that target hypoxia response elements²⁰. Many genes contain these hypoxia response elements in their promoters such as VEGF (Vascular endothelial growth factor) and Epo (Erythropoietin), with a significant proportion being involved in angiogenesis; for a full list see review by Wenger et al²¹ and an overview of the process can be seen in figure 1-1. Hif1a's ability to activate genes such as Nos2 (Nitric oxide synthase 2) and Slc2a1 (Solute carrier family 2, facilitated glucose transporter member 1) which produces nitric oxide to increase blood flow and increase glucose availability for glycolysis/anaerobic oxidation respectively^{22,23}. These outcomes serve to both increase oxygen supply and decrease oxygen demand in an attempt to temporarily achieve normoxia; Hif1a's primary target, VEGF, is the means by which a longer term solution to hypoxia is achieved.

VEGF Pathway

The VEGF family of proteins includes VEGF-A, VEGF-B, VEGF-C, VEGF-D and Pgf (Placental growth factor)²⁴ and the family can be expanded further by considering the splice variants of VEGF-A, VEGF-B and Pgf as well as the further post translational processing of VEGF-A, VEGF-C and VEGF-D²⁵. VEGF-A, as the most studied VEGF protein, has many splice variants including VEGF-A₁₂₁, VEGF-A₁₄₅, VEGF-A₁₄₈, VEGF-A₁₆₅, VEGF-A₁₈₃, VEGF-A₁₈₉ and VEGF-A₂₀₆ with VEGF-A₁₆₅ been considered the prototype, and potentially most relevant to our studies, isoform²⁶. Examples of how the different splice variants are formed from the VEGF-A transcript are shown in figure 1-2. Even the splice variants of a single VEGF can have widely different roles in angiogenesis such as the VEGF-A isoforms which can be divided into pro-angiogenic VEGF-A_{xxx} and anti-angiogenic VEGF-A_{xxx}b groups²⁷. As well as the exact form being expressed, the gradient of VEGF in a tissue is also important for regulating the direction and strength of an angiogenic response through guidance of the chemotactic response of endothelial cells²⁸. This gives another mechanism for which angiogenic responses can be regulated, using the ability of some isoforms of VEGF, such as VEGF-A₁₆₅ to bind glycosaminoglycans within heparin side chains found in perlecan in tissues or syndecan on cell surfaces²⁹. This sequestration of VEGF limits the diffusion distance, keeping the angiogenic response local, and also creates a kind of VEGF store that can be released by MMPs (Matrix metalloproteases)³⁰ such as when MMP9 is secreted by neutrophils during inflammation or in cancer angiogenesis³¹.

Given the complexity of the roles of VEGF isoforms and considering our studies are primarily focused on the endothelial cells which receive these signals it is more useful to focus on the VEGF receptors. Three main VEGF receptors are known – VEGFR1, VEGFR2 and VEGFR3, all of which are receptor tyrosine kinases, meaning they undergo dimerization upon ligand binding, activation of intrinsic tyrosine kinase activity and autophosphorylation of tyrosine in the intracellular domains which creates binding sites for downstream signalling molecules³². VEGFR1 is able to bind VEGF-A, VEGF-B and PlGF, and has a particularly high affinity for VEGF-A than the other receptors, but has very low intrinsic tyrosine kinase activity³³. Additionally a soluble form of VEGFR1 is also produced, meaning that both the membrane and soluble forms compete with the other VEGF receptors for VEGF and as a result is considered anti-angiogenic due to its ability to prevent VEGF from reaching pro-angiogenic receptors³⁴. VEGFR3 is important in lymphatic endothelium and is primarily a receptor for VEGF-C in order to activate Akt1 (AKT serine/threonine kinase 1) although has been known to form a heterodimer with VEGFR2 to activate Erk1 (Extracellular regulated kinase 1) in response to certain isoforms of VEGF-A and C^{35,36}.

VEGFR2 is the main pro-angiogenic receptor in angiogenesis. Canonical activation of VEGFR2 starts with the binding of appropriate ligands including VEGF-A splice variants and some processed VEGF-C and D forms which induces formation of a VEGFR2 heterodimer³⁷, whereas non-canonical activation involves mechanical stimuli to activate tyrosine phosphorylation often through VE-cadherin involvement³⁸. It is worth noting that VEGFR2 heterodimers such as VEGFR1-2, which is thought to suppress VEGFR-2 tyrosine phosphorylation by the VEGFR1's higher affinity for VEGF³⁹ and direct inhibition by a PI3K- α (Phosphatidylinositol 4,5-bisphosphate 3-kinase catalytic subunit α isoform) pathway⁴⁰. The formation of signalling of the VEGFR2 homodimer can be augmented by co-receptors. The main VEGF co-receptor, Nrp1 (Neuropilin-1), can also bind VEGF-A allowing it to form a complex with the VEGFR2 homodimer enhancing its downstream signalling effects⁴¹, this role of Nrp1 can be somewhat antagonised by binding with Sem3a (Semaphorin 3a) preventing VEGFR2 association⁴². Classifying Nrp1's role in VEGF-A driven angiogenesis as simply a co-receptor underrates its importance in generating sufficient downstream VEGFR2 signalling, as highlighted by the fact that global and endothelial specific knockouts of Nrp1 result in early embryonic lethality^{43,44}. Efnb2, another key co-receptor, can also form complexes with VEGFR2 to spatially control VEGFR2 patterning on cell surfaces which helps to control directionality of angiogenic responses by binding with ephrin receptors and also assist in VEGFR2 internalisation which is essential for

downstream signalling in response to VEGF-A binding^{45,46}. VEGFR2 can also form complexes with integrins. Complexes with $\beta 1$ occur when VEGF-A is bound to ECM (Extracellular matrix) that the integrin also binds to, localising the whole complex to focal adhesions and results in prolonged activation of VEGF signalling. This combined $\beta 1$ /VEGFR2 binding and localisation to the area of VEGF-A loaded ECM is not able to happen with soluble VEGF⁴⁷. $\beta 3$ is known to interact with VEGFR2 in the presence of vitronectin, the primary ligand for $\alpha v\beta 3$ but not its alternative ligands such as fibronectin⁴⁸. The $\beta 3$ /VEGFR2 complex involves several other partners such as Src and Sdc1 (Syndecan-1) (both components of focal adhesions) and when activated, it promotes substantial cross activation of both the integrin and the VEGF receptor pathways, enhancing angiogenesis^{49,50}. VEGFR2 can also form complexes with VE-cadherin where it participates in the flow sensing signalling of VE-cadherin through VEGFR2's PI3K-alpha and Erk1 signalling pathways⁵¹. Different complexes of VEGFR2 form a network of interactions where different co-receptors and VEGF ligands control the rate and specificity of downstream signalling from VEGFR2. For example $\beta 3$ can negatively regulate angiogenesis by sequestering Nrp1, preventing its pro-angiogenic association with VEGFR2⁵².

Once activated, VEGFR2 induces several well-known pathways involved in endothelial cell activation, proliferation and migration, which are all key for angiogenesis, such as the Phospholipase c gamma 1-Erk1/2, PI3K-alpha-Akt1-Mtor (Mechanistic Target Of Rapamycin) and Src pathways⁵³. Activated VEGFR2 binds Phospholipase c gamma 1 which catalysis the breakdown of PIP₂ (Phosphatidylinositol 4,5-bisphosphate) to IP₃ (Inositol triphosphate) and DAG (Diacylglycerol)²⁵. IP₃ in turn triggers the release of intracellular calcium stores from the endoplasmic reticulum via the calcium channel/IP₃ receptor Itpr3⁵⁴. Calcium and DAG together activate Pkcb (Protein kinase C beta) which in turn drives the Raf1 (Raf-1 proto-oncogene, serine/threonine kinase)/Mapk pathway⁵⁵. Targets of Erk1/2 include cyclins, cyclin-dependent kinases and Myc which increases endothelial cell proliferation as well as post-translational regulation of Fak1 (Focal adhesion kinase 1) and Pxn, promoting endothelial cell migration^{55,56}. Calcium released from the Phospholipase c gamma 1-Erk1/2 pathway also binds Calm1, allowing it to bind and activate Ppp3cc⁵⁷ which dephosphorylates the transcription factor Nfatc1 (Nuclear factor of activated T-cells 1), allowing it to enter the nucleus and increase the expression of many angiogenesis related genes⁵⁸ as well as decrease the expression of VEGFR1 which prevents VEGF from being sequestered and increasing its availability for VEGFR2 signaling⁵⁹.

The PI3K-alpha-Akt1-Mtor pathway starts with activation of PI3K-alpha by Src or VE-cadherin recruited to VEGFR2⁶⁰. PI3K-alpha then converts PIP₂ to PIP₃ (Phosphatidylinositol 3,4,5-trisphosphate) which binds to and activates Akt1. Akt1 and PI3K-alpha have many downstream targets that are involved in endothelial cell survival, proliferation and apoptosis⁶¹ as well as vascular permeability and maturation in established vessels⁶². An important downstream target of this PI3K-alpha pathway is Mtor, which has its main inhibitor Tsc2 (Tuberous sclerosis 2) deactivated by Akt1 phosphorylation and is also phosphorylated directly by Akt1⁶³. Mtor, once activated, drives angiogenesis by promoting endothelial cell Fak1 and actin cytoskeleton remodeling which assists in adhesion to ECM⁶⁴. Src recruitment via the Tsad adaptor also gives VEGFR2 another pathway it can signal by to regulate endothelial cell junctions and vascular permeability⁶⁵. Major Src substrates also include key focal adhesion proteins Fak1 and Pxn, and cytoskeletal components aiding with endothelial cell migration by promoting focal adhesion turnover and cell shape changes^{66,67}. Whilst hypoxia driven VEGF expression is the main driver behind most angiogenesis is it not the only one that should be considered. Other growth factors and cytokines play important roles such as transforming growth factors, fibroblast growth factors, epidermal growth factors, angiopoietins and more⁶⁸. Many of these play tissue and situation specific roles in angiogenesis, helping local vasculature deciding in judging the balance of pro and anti-angiogenic signals, especially given the fact that hypoxia is subjective in tissues and is relative to the local physiological norm i.e. normoxia for the prostate would be severely hypoxic for the heart^{69,70}.

Many of the VEGF effects described so far prepare and start angiogenic processes in endothelial cells. For example, VEGF signalling will begin to activate the quiescent endothelial cells in existing vasculature, by causing them to loosen their cell-cell junctions and start to degrade the shared basement membrane using proteases⁷¹. The majority of the pathways utilised by VEGFR2 also increase endothelial cell proliferation, generating enough endothelial cells to form the new vessels at the site of hypoxia⁷². VEGFR2 signalling also guides directional migration in endothelial cells towards the source of the VEGF, through the influences on focal adhesion proteins Fak1 and Pxn as well as driving Cdc42 (Cell division cycle 42) directed migration through Phospholipase c beta 3⁷³. This process needs to be carefully controlled to ensure that endothelial cells migrate towards the hypoxic area but still maintain a connection to the existing vasculature to connect to the circulatory system. Endothelial cells organise themselves into a leading tip cell that moves towards the source of VEGF and a trailing line of connected stalk cells⁷⁴. Endothelial cells

express several Notch receptors which are transmembrane receptors for a number of cell surface Notch ligands including Dll4 (Delta like canonical notch ligand 4) also expressed on endothelial cells⁷⁵. VEGFR2 signalling induces filopodia extension, centralising VEGF sensing and guiding endothelial cells towards the source of VEGF; the leading endothelial cell with filopodia is known as the tip cell^{74,76}. Only one tip cell is needed to guide the connected stalk of other endothelial cells towards the source of VEGF, hence the tip cell phenotype is suppressed in other endothelial cells leading them to become stalk cells. VEGFR2 signalling does this by increasing expression of Dll4, which then binds to Notch receptors on adjacent cells⁷⁷. The notch receptor is then cleaved by membrane bound ADAM10 (A disintegrin and metalloproteinase domain) and , ADAM17 or other proteases, releasing the Notch intracellular cytoplasmic domain⁷⁸. This domain acts as a transcription factor to target many Notch responsive genes, as well as suppressing the expression of VEGFR2⁷⁹. As a result, the endothelial cell closest to the source of VEGF will express the most Dll4 becoming the tip cell and signalling the others to become stalk cells, ensuring the orderly extension of the stalk to the source of VEGF⁸⁰. Stalk cells are not totally unresponsive to VEGF however, those closest to the source will proliferate the most compared to those at the base of the sprout but this is not thought to be nearly as important for the progression of the sprout as the pulling force generated by the migration of the tip cell^{76,81}.

Other Pathways in Angiogenesis

Before, throughout and after the directional migration of the endothelial cells towards a VEGF source, constant ECM turnover is required⁸² which requires adaptation in the repertoire of ECM receptors in endothelial cells. Quiescent endothelial cells normally express integrins such as $\alpha 1\beta 1$, $\alpha 2\beta 1$, $\alpha 3\beta 1$, $\alpha 5\beta 1$, $\alpha 6\beta 1$, $\alpha 6\beta 4$ and $\alpha v\beta 5$, the majority of which bind laminins or collagens found within the basement membrane of the vessel. During angiogenesis, fibronectin and vitronectin are laid down by the endothelial cells themselves or fibroblasts. As these ECM components are not found commonly in basement membranes⁸²⁻⁸⁴, there is the sudden switch in endothelial cells to express appropriate ECM receptors such as $\alpha v\beta 3$ and more $\alpha 5\beta 1$. ECM degradation is also a key step in angiogenesis, for example, tip cells are known to produce and cluster MMP14 at the leading edge in order to degrade ECM and create a path through the 3D matrix for which the developing sprout will migrate, which leaves behind a space for the eventual mature tube of the capillary^{85,86}. Endothelial cells produce a variety of ECM components including collagens, fibronectin and laminins, with the exact mixture of ECMs deposited depending on the

maturity or progress of angiogenesis. This allows endothelial cells to produce a provisional ECM whilst migrating and forming new vessels but a more basal-like ECM once vessels begin to mature^{87,88}.

Lumen formation is an important step in angiogenesis, forming the hollow space for blood flow within vessels, and this begins early in angiogenesis once stalk cells have formed⁸⁹. Two distinct mechanisms are thought to be responsible for lumen formation in stalk cells: one involving a process called intracellular or cell hollowing and another called extracellular or cord hollowing. Cdc42, Rac1 and MMP14 are all important to both of these mechanisms^{89,90}. MMP14 is particularly important in lumen formation and the creation of the vascular guidance tunnel by proteolysis of the interstitial ECM started by the migrating tip cell⁹¹. Adhesion to the surrounding ECM is also important in lumen formation, with integrins relevant to the local ECM composition being important such as $\alpha 2\beta 1$ for collagen matrices⁹² or $\alpha 5\beta 1$ and $\alpha v\beta 3$ for three dimensional fibrin matrices⁹³. Integrins and Cdc42 are critical in establishing apical-basal polarity in endothelial cells, which is required to ensure all cells in the new sprout are orientated correctly to the luminal and abluminal surfaces⁹⁴. Once polarised, endothelial cells respond to continuing VEGF signalling by activating several Rho-dependent kinases such as Rock1 (Rho associated coiled-coil containing protein kinase 1) through VEGFR2. Rock1 then inhibits actin depolymerisation and phosphorylates Mlc, driving the assembly of an actomyosin complex that opens up the space between opposing endothelial cells to produce the lumen⁹⁵. Finally, in order for the lumen to become useful and a blood flow achievable, a loop including the nearest currently perfused vessel must form in a process known as vessel anastomosis⁹⁶. Multiple sprouts will be recruited to a hypoxic area, eventually leading to two tip cells from different sprouts coming into contact where a concentration of tissue macrophages facilitates cell-cell contacts between them using VE-cadherin and leads to eventual fusing to produce a closed loop^{97,98}. Once a loop has formed there is now a complete path for blood to flow from the existing vessel towards the hypoxic area and then back towards the original vessel. The initiation of blood flow acts as a potent trigger for vessel maturation and stabilisation, as a lack of flow is an indicator of unsuccessful angiogenesis and leads to regression of the sprouts – a process that happens naturally during the formation of mature vascular beds⁹⁹. Blood flow can be sensed by endothelial cells using a variety of mechanosensory complexes and triggers the strengthening of cell-cell contacts primarily via VE-cadherin, deposition of basement membranes and recruitment of pericytes to strengthen the vessel, additionally giving it the smooth muscle tools to control blood flow in the future^{100,101}.

Angiogenesis in Cancer

Angiogenesis is a tightly controlled event important during many physiological processes such as embryonic development, growth, wound healing and more but due to its complexity, can go wrong or be co-opted in many pathologies⁹⁶. In cancer for example, tumours grow to just a few mm across without a vascular supply and subsequently, the induction of angiogenesis is considered a key milestone in progression of the disease termed the “angiogenic switch”¹⁰². For example the RIP-Tag mouse model of spontaneous pancreatic cancer shows a dramatic induction of angiogenesis in a subset of hyperplastic islets at 7 to 12 weeks, transforming the subset from benign carcinomas in situ to malignant tumours – a process dependent on VEGF as the main driver of angiogenesis^{103,104}. In these situations non transformed endothelial cells have been hijacked by transformed tumour cells to connect them to the circulatory system. This model is driven by the expression of the SV40T oncogene with a rat insulin promoter¹⁰⁵. Whilst the RIP-Tag model has provided many insights into the biology of angiogenesis in tumours, it has failed to produce meaningful clinical progress for most patients with pancreatic cancer. This is likely due to the type of pancreatic cancer observed in the model, a neuroendocrine origin tumour, which is much rarer than the types that occur in patients such as pancreatic ductular adenocarcinomas which are very poorly vascularised, demonstrating that angiogenesis may not always be essential for tumour growth^{106,107}. Poor vascularisation is common in cancers, and even within vascularised tumours there will be significant pockets of hypoxia owing to tumour heterogeneity – these areas often contain the most malignantly transformed cells due to the changes make to their metabolism to cope with the lack of oxygen^{13,108,109}. Even if angiogenesis is dispensable for tumour growth, tumours that recruit a blood supply can use it to seed distant metastatic sites through the bloodstream¹¹⁰.

Cancers often have lower oxygen requirements than surrounding tissues due to the Warburg effect where they favour glycolysis to produce intermediate metabolites for DNA synthesis and cell growth¹¹¹. This still creates a huge demand for glucose, amino acids and other nutrients hence the need for angiogenesis is still present. Hypoxia is a mixed blessing for cancer cells as it can mean a lack of oxygen, however the stabilisation of Hif1a will upregulate metabolism, migration and survival genes benefiting cancer progression as well as the production of VEGF¹⁰⁹. Tumours produce high levels of VEGF, due to hypoxia, benefits of other Hif1a targets and the common mutation of targets such as Ras genes that

increase VEGF production¹¹². Even with rampant angiogenesis, there is never enough blood supply to satisfy the continual growth of the tumour or penetrate the hypoxic core resulting in chronic VEGF release¹¹³. Experiments carried out comparing spikes of VEGF production using adenovirus vectors to chronic VEGF production showed that acute VEGF results in mature and regularly spaced vessels, just like physiological angiogenesis, however chronic VEGF results in chaotic, large and leaky vessels with poor blood flow like in tumours¹¹⁴. Leaky and inefficient vasculature is common in tumours due to the constant stimulation with VEGF; normal angiogenesis requires VEGF levels to fall eventually as VEGF stimulation increases vascular permeability by loosening endothelial cell-cell contacts¹¹⁵.

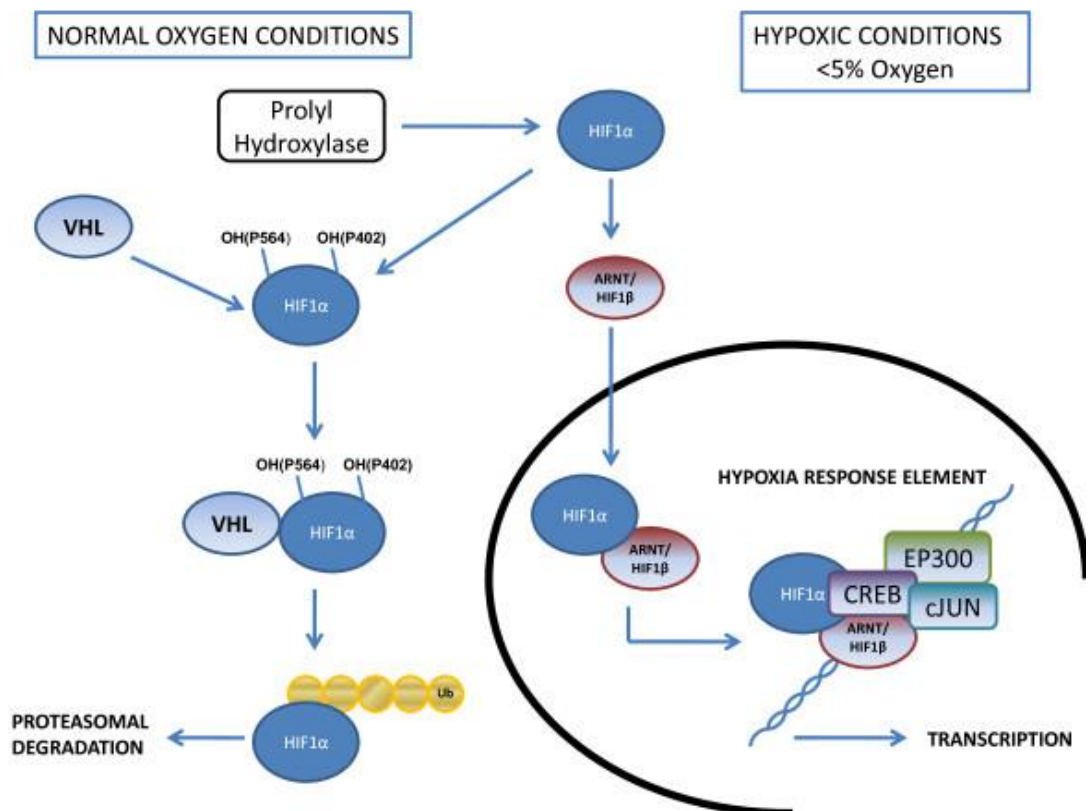
Tumours also promote angiogenesis by a number of other means. For example they recruit and convert resident fibroblasts to cancer activated fibroblasts (CAFs) which are known to promote angiogenesis by production of VEGF, Il6 (Interleukin 6) and other cytokines which results in the kind of aberrant vessels seen in tumours^{116,117}. Conversion of fibroblasts is thought to be an irreversible process leading to a continual increase in these pro-angiogenic signals over time, again creating leaky vasculature¹¹⁸. This means the factors produced by CAFs are important to consider in designing anti-angiogenic or anti-cancer therapies, as well as the factors produced by the tumour. Just like myofibroblasts in wound healing, CAFs produce large amounts of ECM including fibronectin, which promotes endothelial cell activation and migration via fibronectin binding integrins^{115,119}. Deposition of large amounts of ECM, combined with the large number of cancer cells, results in a busy cancer stroma that is stiffer and highly crosslinked and both of these features promote angiogenesis by increased integrin signalling^{120,121}. These ECMs hold large amounts of VEGF and other growth factors/cytokines that are liberated upon breakdown by the MMPs also produced by CAFs¹²². Tumours also recruit and transform immune cells giving rise to a large resident population of tumour associated macrophages¹²³. Several potential explanations exist for the pro-angiogenesis phenotypes of high levels of immune cells in tumours, including the production of MMP9 by immune cells to degrade ECM to release VEGF and other factors, which further antagonises the leakiness of vessels, drawing in more immune cells¹²⁴. Constant recruitment of fibroblasts and immune cells in tumours, driving sustained and aberrant angiogenesis gave rise to the idea that cancers are “wounds that never heal”¹²⁵.

Preventing angiogenesis from occurring is therefore an attractive anti-cancer therapy. Firstly, cancer cells themselves originate due to mutations in their genomes and retain the ability to mutate further genes during their development. As a result cancers can quickly

develop resistance to chemotherapy by mutating targeted genes, degrading drugs, suppressing apoptosis pathways or increasing drug efflux¹²⁶. Endothelial cells, even those co-opted into providing tumour vasculature, have a stable genome meaning that their options for developing resistance are fewer and hence the goal of preventing or regressing tumour vasculature is a good strategy¹²⁷. Secondly, as tumour vasculature is chaotic and poorly organised, the overall perfusion of tumours is often quite low compared to normal tissue. This means that even with a highly effective chemotherapeutic agent, it will be difficult to deliver a sufficient dose to the tumour. Some anti-angiogenic therapies have been designed to prune the weaker vessels of the tumour to leave a more mature and stable network, a process known as vessel normalisation, with the goal of increasing perfusion and delivery of a second chemotherapeutic drug to the tumour¹²⁸.

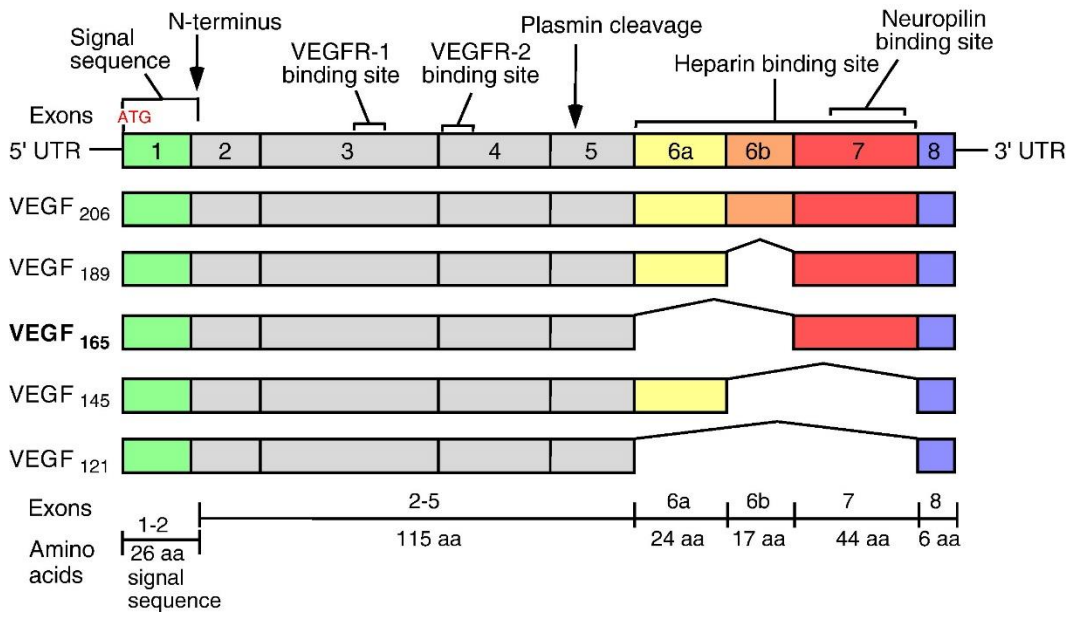
VEGF was the one of the landmark discoveries in angiogenesis research and ultimately led to the development of bevacizumab, a monoclonal antibody against VEGF, for use initially in colorectal cancer where it has increased progression free survival in combination with chemotherapeutic drugs such as 5-fluorouracil¹²⁹. Bevacizumab treatment was found to normalise tumour vasculature within 12 hours, with a reduction in blood flow but crucially no change in uptake of radionucleotide labelled glucose; within a combination therapy setting this means it would reduce vascularisation of the tumour but improve the delivery of the chemotherapeutic¹³⁰. Reducing VEGF levels would halt the chronic VEGF phenotype of tumours mentioned above, allowing unnecessary vessels to regress and others to mature/stabilise¹³¹. Bevacizumab is also being applied to other conditions with pathological angiogenesis such as wet macular degeneration where it causes leaky vessels to regress¹³². Anti-angiogenic therapies based on interfering with VEGF signalling are prone to treatment escape as alternative growth factors can also be powerful angiogenic stimuli. Tumours can switch to producing other growth factors or produce ever increasing amounts of VEGF, taking advantage of the poor delivery of the anti-VEGF agent in tumours, by selection of subclones with these properties within the tumour¹³³. Other mechanisms of treatment escape include vessel mimicry by tumour cells, induction of intussusceptive angiogenesis or pro-angiogenic signalling from CAFs or immune cells¹³⁴. The next stage in many areas of angiogenesis research is to understand precisely why previous anti-angiogenesis drugs have failed in certain cases: by looking closer at the mechanism of the drug and understanding better how endothelial cells respond to them.

Figure 1-1 Hif1a Pathway Under Hypoxia and Normoxia



Hypoxia response pathway diagram showing the differential pathways of Hif1a under normoxic and hypoxic conditions. This includes the proteasomal degradation of Hif1a after ubiquitination and the induction of hypoxia response element containing genes. Taken from Thirlwell et al¹³⁵

Figure 1-2 VEGF-A Splice Variants



Differential splicing of the mRNA transcript with 8 possible exons and binding/cleavage sites shown (top). Resulting VEGF-A isoforms 206, 189, 165, 145 and 121 are formed from different combinations of these exons. Figure taken from Holmes et al¹³⁶

Integrins

Cell adhesion and migration is dependent on interactions with the ECMs surrounding cells. Many types of ECM receptors exist in cells but the most important type for considering endothelial cell adhesion and migration are integrins¹³⁷. Integrins are a family of 24 heterodimeric cell surface receptors composed of 18 possible alpha and 8 possible beta subunits, where different combinations of alpha and beta subunits form receptors with unique ligand specificity such as towards collagens, laminins or RGD (Arginine, glycine, asparagine tri-peptide) containing proteins¹³⁸. The fibronectin receptors $\alpha5\beta1$ and $\alpha v\beta3$ are of particular interest in endothelial cell adhesion and migration due to their prominent associations with angiogenesis¹³⁹. As well as simply mediating adhesion to the ECM, integrins are also key signalling molecules. Successful ligation to an ECM is useful information to a cell that needs to be passed inwards in a process known as outside-in signalling whereas the activation of the integrin in the first place, to be able to bind ECM, is known as inside-out signalling¹⁴⁰.

Integrins consist of a large extracellular domain, a transmembrane domain and a short cytoplasmic tail. The shape of the extracellular domain is regulated to control the ability of the integrin to bind ligands i.e. its activation, such as in leukocytes where their ICAM1 (Intracellular adhesion molecule 1) and VCAM1 (Vascular cell adhesion protein 1) binding integrins are only activated at sites of infection, to ensure they arrest in blood vessels at the correct location¹⁴¹. Interactions between the transmembrane domains of integrin heterodimers confer a bent structure to the extracellular domain keeping it inactive¹⁴², which can be seen in figure 1-3 where the proximity of the transmembrane domains causes the subunits to fold down together. Mutations that affect interactions of the transmembrane domains such as G708N of $\beta3$ leave the integrin heterodimer constitutively active with much higher affinity for ligand binding¹⁴³. Two important and conserved interaction sites in the transmembrane domain are both thought to need disruption in order to result in complete integrin activation termed the inner and outer membrane clasps; the angle of the transmembrane domains relative to the membrane and each other is crucial in ensuring both these clasps can interact with each other and is controlled by binding of factors to the cytoplasmic tails¹⁴⁴.

Inside-out Signalling

Tln1 (Talin 1) is a critical regulator of integrin activation, as can be seen in figure 1-3 where separation of the transmembrane domains permits the integrin to assume its active

confirmation. Its head domain binds to integrin beta cytoplasmic tails to contribute to activation and its rod domain binds directly to actin and to Vinculin, which also links to the actin, helping establish a strong connection between integrins and the actin cytoskeleton^{145,146}. The Tln1 rod domain contains another integrin beta cytoplasmic tail binding site allowing the linking of multiple integrins¹⁴⁷. Tln1 is often the final step in integrin activation so can be used as a marker of focal adhesions, where integrins cluster together at sites of adhesion¹⁴⁸. Members of the kindlin family, such as Kindlin-1, Kindlin-2 and Kindlin-3, are important co-activators of integrins along with Tln1 and share a similar FERM domain that allows localisation and binding to integrin beta tails¹⁴⁹. Some studies have suggested that Kindlin-2 in endothelial cells activates $\alpha\beta3$ whilst Kindlin-3 activates $\alpha5\beta1$ with some overlapping functions (endothelial cells do not express Kindlin-1), but this does not seem consistent across different sources of endothelial cells^{144,150}. For example other studies show that Kindlin-3 deletion in mice phenocopies Glanzmann thrombasthenia, a condition which is caused low levels of $\beta3$ in platelets resulting in chronic bleeding from a lack of platelet aggregation and binding to fibrinogen^{151,152}.

Unlike Tln1, kindlins are not thought to activate integrins directly but instead do so through the many proteins they recruit to the cytoplasmic tail the integrins¹⁵³. One of these proteins, Ilk (Integrin linked kinase), binds directly to Kindlin-2 and acts as a scaffold to recruit further activation proteins such as Pxn and Parvin alpha¹⁵⁴. Another important interactor known as Migfilin also binds directly to Kindlin-2 and is recruited during integrin activation, knockouts of which have been shown to impair integrin activation, cell spreading and focal adhesion formation¹⁵⁵. The binding of Migfilin is thought to act as a switch in integrin activation because of its proposed mechanism of action where it displaces Filamin-a from the integrin cytoplasmic tail¹⁵⁶. Filamin-a is an actin crosslinking protein involved in regulating the actin cytoskeleton but it is also thought to have roles in recruiting integrins to membrane regions where actin protrusions are forming^{157,158}. Filamin-a however is an integrin inhibitor, possibly preventing premature activation of integrins once recruited to the actin cytoskeleton until Migfilin displaces it¹⁵⁹.

Outside-in Signalling

Once integrins have been sufficiently activated, with their extracellular domains in an open confirmation, they can bind their respective ligands. Successful ligation of ECM is an important signal controlling many cellular processes for example survival, with a lack of ECM ligation often triggering a form of cell death called anoikis¹⁶⁰. Integrin cytoplasmic tails

are themselves though have no inherent enzymatic activity, therefore they need to recruit signalling proteins directly or via adaptors¹⁶¹. Ligand binding to integrins induces a conformational change throughout the protein, resulting in the recruitment of the outside-in signalling machinery to the cytoplasmic tail¹⁶². Fak1, like Tln1 and kindlins, contains a FERM domain, which normally is bound to the kinase domain of Fak1. Integrin ligand engagement recruits Fak1 to the integrin beta cytoplasmic tail via the FERM domain, freeing up the kinase domain to autophosphorylate Y397 and partially activate Fak1¹⁶³. This initial phosphorylation recruits Src, which itself is activated by conformational changes induced by interaction with Fak1, resulting in further phosphorylation and activation of Fak1¹⁶⁴. The Fak1/Src signalling complex is one of the most important outside-in signalling complexes created by integrin ligation¹⁶³. Fak1/Src phosphorylates Bcar1 (Breast Cancer Anti-Estrogen Resistance Protein 1) creating SH2 (Src homology domain 2) domain binding sites for proteins such as Crk (CRK proto-oncogene, adaptor protein)¹⁶⁵ then Bcar1 and Crk in turn regulate the actin cytoskeleton and promotes migration through Dock1 (Dedicator of cytokinesis 1) and Rac1¹⁶⁶. Further complexes recruited to activated Fak1/Src include Grb7 (Growth factor receptor bound protein 7) and PI3K-alpha^{167,168} which work together to regulate cell migration via Rac1 in their respective signalling pathways^{169,170}. Other important downstream targets of Fak1/Src are several RhoA (Ras homologue family member A) family kinases which regulate actomyosin to control cell migration¹⁷¹.

Pxn is a well-known scaffold protein recruited to integrins to regulate outside-in signalling and is often used as a focal adhesion marker¹⁷². Pxn is phosphorylated and recruited by Fak/Src, which also creates SH2 sites for proteins like Crk to bind as mentioned above¹⁷³. Pxn also contains domains that bind Vinculin which functions as a link to the actin cytoskeleton¹⁷⁴.

Some of the proteins that played a role in the activation of integrin are still bound to the integrin beta cytoplasmic tails and play a role in outside-in signalling. Recently, Tln1 has been found to be a mediator of the mechanosensory abilities of integrins¹⁷⁵. Due to its position between the integrins and the actin cytoskeleton¹⁴⁵, tln1 is in a unique position to measure the force being applied on the actin cytoskeleton by the integrin by using its rod domains R1 to R13 where bundles of these rod domains are pulled apart by the tension generated upon cell adhesion either by unzipping domains or shearing between them¹⁷⁶. RIAM (Rap1-Interacting GTP Adapter Molecule) is a protein that binds to R3 of Tln1 to recruit it to the plasma membrane in order to support activation of integrins but upon unzipping of this domain its binding site is lost and is replaced by Vinculin, a process which

supports the maturation of a focal adhesion as tension forces increase¹⁷⁷. Increasing tension across Tln1 rod domains gradually unwinds the whole molecule, revealing binding sites for more molecules such as Kank1 (KN Motif and Ankyrin Repeat Domains 1) which recruits microtubules to mature focal adhesions¹⁷⁸.

Focal Adhesions

Often a concentration of integrins will be found on the same area of the plasma membrane, such as where a large collagen fibre or fibronectin fibril contacts the cell. These matrices can have binding sites for more than one integrin heterodimer at a time; additionally ECMs such as collagen and fibronectin can interact and crosslink each other, resulting in a clustering of integrin binding sites^{179–181}. Therefore the integrins on the cell surface will also cluster forming large protein complexes known as focal adhesions¹⁸². Integrins, direct and indirect interaction partners make up focal adhesions which in total can contain several hundred different proteins¹⁸³. When focal adhesions first begin to form, with clusters of activated integrins binding their ligands, they are known as nascent adhesions. These nascent adhesions can be triggered to mature depending on the migratory needs of the cell such as by the Tln1 domain tension mechanism mentioned earlier^{184,185}. When considering fibronectin adhesion, focal adhesions can be considered nascent if they rely on $\beta 1$ for adhesion but mature if they rely on $\beta 3$ ¹⁸⁶. Whereas other classification systems divide them into fibrillar adhesions containing $\beta 1$ only, which give the cell high mobility, and focal adhesions containing both $\beta 1$ and $\beta 3$, which generate strong tension forces¹⁸⁷. Focal adhesions are able to support cell mobility by being the main structures upon which cells migrate. In order to do this they must be dynamic structures that can assemble where needed at the leading edge of the cell but disassemble at the retracting edge, whilst still providing enough anchorage for actomyosin driven cell migration in-between assembly and disassembly¹⁸⁸. Fibrillar adhesions are particularly good at aiding cell migration because they extend in the direction of migration from the edge of a mature focal adhesion, then disassemble from the rear edge at the same time which creates a tread milling adhesion that provides anchorage precisely where needed for the migrating cell to pull against¹⁸⁹. Tln1, as an activator of integrins and key tension sensor, is an excellent promoter of focal adhesion maturation under the appropriate conditions as well as other proteins such as RhoA and Rock1 which assist in linking focal adhesions to actin stress fibres formed during cell migration^{188,190} Focal adhesion disassembly, which is as important for cell migration as focal adhesion assembly, and is regulated by several

factors including microtubules, Kif5b (Kinesin family member 5B), Dnm2 (Dynamin-2), Fak1 dephosphorylation, and Capn2 (Calpain 2)¹⁹¹⁻¹⁹³.

Integrin Trafficking

As outlined above, focal adhesions must be able to assemble and disassemble in order to allow successful migration of the cell. The key components of the adhesions, such as integrins, will need to be trafficked to and from the adhesive fronts of the cell. Many different pathways control internalisation, recycling and degradation of integrins from the cell surface, for a full review see Bridgewater et al¹⁹⁴. The way integrins are trafficked depends on the situation and cell type. For example proteins important in angiogenesis such as Nrp1 have been shown to promote the internalisation of active $\alpha 5\beta 1$ during adhesion to fibronectin in Rab6 containing endosomes¹⁹⁵. Recycling of integrins back to the surface in endothelial cells is also important for migration and tube formation in vitro which is controlled by Arf6 (ADAP-ribosylation factor 6) particularly in HGF mediated angiogenesis¹⁹⁶. Many of the components of integrin trafficking pathways, like Arf6, are shared by other trafficking pathways such as the VEGF pathway where it acts downstream of VEGFR2 to control Rac1 activation¹⁹⁷. Therefore when assessing the roles of integrins in angiogenesis it will be important to also consider the knock on effects any manipulation will have on other pathways.

Microtubules have an important role on the trafficking of many cargos (see later). They can participate in the trafficking of integrins by providing a polarised pathway from the centre of the cell to the adhesive front at the edge when they target focal adhesions¹⁹⁶.

Microtubules that target focal adhesions can induce rapid disassembly such as when Mapk4k (Mitogen-Activated Protein Kinase Kinase Kinase Kinase 4) is targeted to microtubule tips via EB2 and then recruits GEFs (Guanine exchange factors) to activate Arf6 triggering integrin internalisation¹⁹⁸

Cross Talk

Integrins are known for their ability to cross talk to other pathways, particularly growth factor receptor pathways such as VEGFR2 or Egfr (Epidermal growth factor receptor), therefore the impact of integrins on cell behaviour can be dramatic¹⁹⁹. Sometimes this cross talk is vital for the action of the integrin itself such as where Egfr signalling via Pkcb is

required for $\alpha\beta 5$ directed migration on vitronectin²⁰⁰. Other examples include $\alpha 6$ integrins which can associate with ErbB2 (Erb-B2 receptor tyrosine kinase 2 or HER2) to promote cell invasion and proliferation much in the same way that the activated growth factor heterodimer of Errb2/Egfr would²⁰¹. Many of the molecules mentioned earlier in integrin signalling themselves are involved in receptor tyrosine kinase responses, particularly Src downstream of growth factor receptors such as Egfr, Met and various Gpcrs (G protein coupled receptors)²⁰². Src, acting downstream from these receptors, can influence many of the same pathways activated by integrins including PI3K-alpha and create phosphorylated binding sites for SH2 domain containing adaptors such as Grb7^{203,204}

Integrin $\beta 3$

Fibronectin binding integrins play a particularly important role in angiogenesis. $\alpha\beta 3$ is a vitronectin/fibronectin/von Willebrand factor receptor that is upregulated in angiogenic vasculature²⁰⁵. Often $\beta 3$ is the target of manipulation in studies on endothelial cells as the only compatible alpha subunit is αv , whereas αv can form heterodimers with $\beta 3$ or $\beta 5$; manipulations of αv could therefore result in unwanted disruption of $\beta 5$ ²⁰⁶. Early studies indicated that $\beta 3$ could be a pro-angiogenic molecule due to the timing of its upregulation and because blockade of the integrin induced apoptosis in endothelial cells²⁰⁷, which was thought to be because of the loss of anti-apoptotic signalling from Fak1/Src²⁰⁸. $\beta 3$ is known to exhibit extensive cross talk with VEGFR2, particularly when bound together after engagement with vitronectin, resulting in Src dependent cross-phosphorylation and activation of both molecules^{48,209}. Cross-activation between $\beta 3$ and VEGFR2 has also been observed via PI3K-alpha²¹⁰. These findings led to the development of $\alpha\beta 3$ inhibitors designed to halt tumour angiogenesis such as Cilengitide[®], a cyclic RGD mimetic resembling the $\alpha\beta 3$ binding site of fibronectin, which entered clinical trials. Despite promising *in vitro* and *in vivo* studies, where Cilengitide[®] caused apoptosis of endothelial cells, slowed migration and reduced the growth of tumours^{210,211}, it ultimately failed in phase III²¹². Cilengitide[®] was well tolerated in patients due to the restriction of $\alpha\beta 3$ to only actively proliferating vasculature, and it exhibited good pharmacokinetics such as by being able to cross the blood brain barrier leading to the suggestion that failure was due to the choice of target²¹³. Detailed investigations into the effects of Cilengitide[®] on endothelial cells and angiogenesis revealed that whilst high doses of the RGD-mimetic did inhibit angiogenesis, low doses actually promoted it, providing clues that $\beta 3$ may not have been the purely pro-angiogenic molecule it was thought to be²¹⁴.

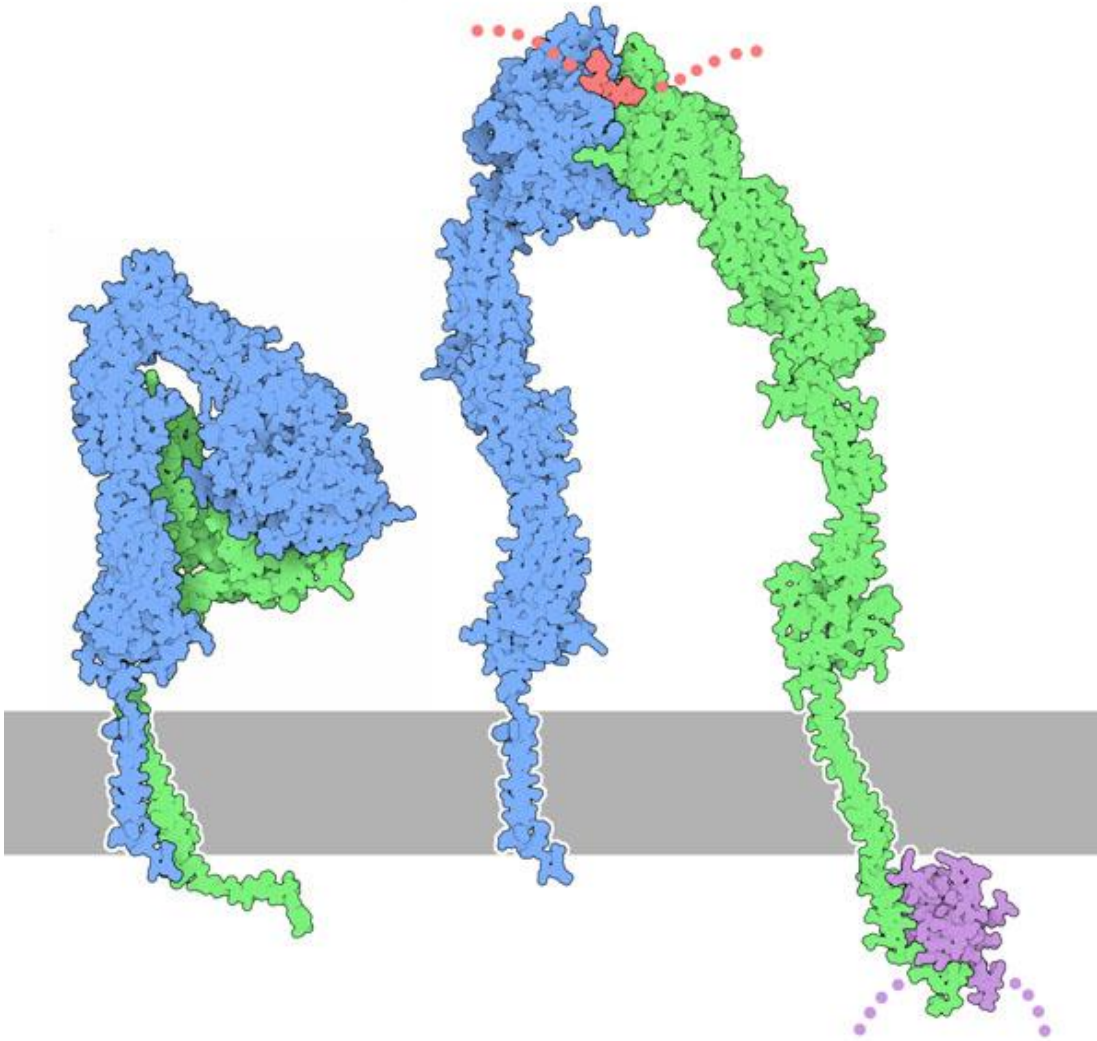
Further investigations have confirmed $\beta 3$ can have anti-angiogenic roles. $\beta 3$ -null mice exhibit enhanced pathological angiogenesis²¹⁵. VEGFR2 has been shown to be a key protein responsible for $\beta 3$ -null phenotypes as it is upregulated to increase pro-angiogenic signalling as well as cause an increase in VEGF dependent permeability without $\beta 3$ ^{216,217}. Previously it was thought that $\beta 3$ and VEGFR2 were cross-activating by promoting increased signalling in each other's downstream pathways, so it was initially strange that $\beta 3$ appeared to be suppressing VEGFR2 effects. An explanation for this came when it was discovered that $\beta 3$ bound to the VEGF co-receptor Nrp1, and prevented its association with VEGFR2⁵². Co-depletion of Nrp1 and $\beta 3$ leads to a significant reduction in tumour angiogenesis, backing up the suggestion that $\beta 3$ limits Nrp1/VEGFR2 associations and pro-angiogenic signalling²¹⁸. Pharmacological inhibition of Nrp1 however is not likely to be as straight forward as with $\beta 3$, or tolerated as well in patients, due to the fact that constitutive deletions of Nrp1 are lethal in mice embryonically⁴³. However a small deletion of the cytoplasmic tail of Nrp1 does still synergise with $\beta 3$ inhibition in preventing angiogenesis without the embryonic lethality^{218,219}. $\beta 3$ also has other known anti-angiogenic roles such as being the receptor for tumstatin, a fragment of basement membrane collagen IV released during MMP9 degradation common in angiogenesis and tumour growth, acting as a kind of negative feedback²²⁰.

Defining an integrin like $\beta 3$ as simply pro or anti-angiogenic is likely an over simplification that has complicated the field of angiogenesis research. Evidence has arisen that the precise contribution of $\beta 3$ to angiogenesis is context dependent for example pro-tumorigenic in the brain but anti-tumorigenic in ovarian cancer^{221,222}. An interesting interpretation of $\beta 3$ is that it is indeed pro-angiogenic, but depletion of this integrin leads to compensation in endothelial cells to account for its loss and that this compensation results in a net gain of angiogenic potential. This was highlighted by recent studies that showed a short term depletion of $\beta 3$ reduced angiogenesis and tumour growth but long term depletion increased both²²³. Regardless of $\beta 3$'s actual role in angiogenesis, it is still of use as a targeting aid in delivering payloads to angiogenic vasculature²²⁴.

Whilst this compensation method is not currently known, it is worth considering the other major fibronectin binding integrin in endothelial cells $\alpha 5\beta 1$. Much of the integrin signalling cascade of $\beta 3$ is common to $\beta 1$ and it is also expressed at higher levels on angiogenic vasculature²²⁵. Like $\beta 3$, $\beta 1$ is also known to have pro and anti-angiogenic functions such as the binding of endostatin in a similar way to $\beta 3$ binding tumstatin²²⁶. $\beta 1$ also has its own relationship with Nrp1¹⁹⁵. The precise nature of $\beta 3$ compensation in endothelial cells, and

whether this involves β_1 or another mechanism, is something that was investigated in this thesis.

Figure 1-3 Model of the Inactive and Active Conformations of Integrins



A realistic model of the inactive conformation of integrin $\alpha\text{IIb}\beta_3$ (left) and a hypothetical model of the active integrin (right). Alpha chains (blue), beta chains (green), Talin-1 (purple) and a fragment of fibronectin (red). Image created by the RCSB Protein Data Bank based on crystal structures ^{142,227-229}.

The Adhesome

The adhesome is a vast network of proteins involved in regulating cell-matrix adhesions including adhesion, signalling and structural proteins²³⁰. The adhesome of any given cell is matrix dependent, but on integrin ligating ECMs it will include at its core the focal adhesion but also an expanded network of other types of adhesion sites and supporting cytoskeletons etc²³¹. An overview of families of proteins known to be present in focal adhesions can be seen in figure 1-4.

Methodology

Adhesion research papers using traditional biochemistry approaches had identified about 160 adhesome members²³⁰. A step change in methodology to a non-candidate adhesome member identification process came in the form of protein mass spectrometry, made possible by advances such as commercial iron trap mass spectrometers²³², which soon increased the number of known adhesome proteins to over 2000¹⁸⁶. Quantitative mass spectrometry is critical to understanding how the stoichiometry of adhesome members would change upon a gene deletion or drug challenge²³³, this would be a useful feature to understand how compensation for the loss of $\beta 3$ for example is achieved as some adhesome proteins are essential for endothelial cell migration and need to be recruited by other means. Several strategies can be employed to achieve quantitative mass spectrometry, most of which make use of heavy isotopes of carbon, nitrogen or hydrogen to change the mass of peptides in a predictable way to assist in identification/quantification. These include: metabolic labelling, where organisms or cultures are fed labelled nutrients which are incorporated into their proteins naturally; chemical labelling, where a reaction is carried out to couple isotope containing moieties to proteins; spike-in controls, where pre-labelled peptide libraries are added in with samples of interest during mass spectrometry to generate quantifications by comparison; and label-free, where no labelling or spiking is carried out²³⁴. Label-free quantitative mass spectrometry has been made possible by advances in quantification algorithms and improved accuracy of mass spectrometers, which simplifies experimental designs by omitting labelling steps also reducing the costs from the expensive isotopes²³⁵. Whole cell proteomics, i.e. mass spectrometry of whole cell lysates, whilst useful in some studies is not appropriate for identifying adhesome members. Peptide coverage of higher organism proteomes is still very low despite steady gains, meaning that abundant proteins in whole cell lysates would likely be identified instead of more interesting transiently interacting

members of the adhesome²³⁶. Instead some kind of purification is needed to enrich for adhesome proteins before mass spectrometry to decrease background but also increase the likelihood of protein identification/quantification. Crosslinking compounds have been used to covalently link adhesome proteins to substrates of interest such as fibronectin to assist in enrichment^{186,237}. Chemically reversible crosslinkers are often used which have predictable target sites in peptides, which allow them to be used successfully in mass spectrometry where their modifications that affect peptide masses can be accounted for to still give accurate quantification^{238,239}.

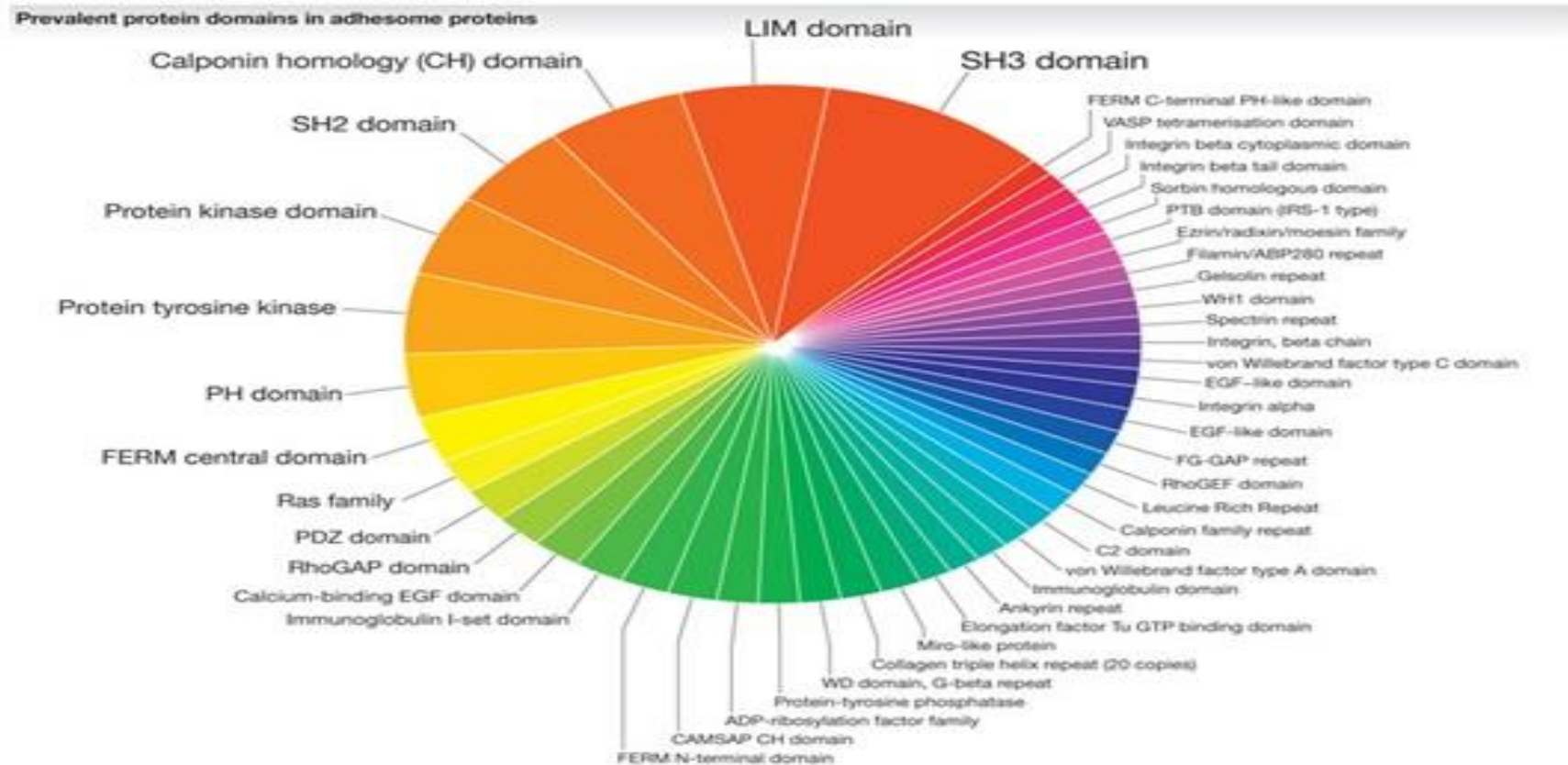
Contents of the Adhesome

Previous adhesome studies have shown that an entire class of adhesome components, LIM domain proteins, are recruited to nascent focal adhesions during their development to mature focal adhesions and that this recruitment is dependent on the ability of the cell to sense matrix stiffness through integrin engagement and Myh2 (Myosin heavy chain 2) activity²³³. Pxn is an example of an important LIM domain protein recruited during focal adhesion maturation¹⁵⁴. Others include Zyx (Zyxin), recruited during stress sensing to reinforce the link between focal adhesions and the actin cytoskeleton or Migfilin, carrying out the same role as Zyx but also linking to Filamin-a^{155,240}. Further adhesome studies found this Myh2 sensing was dependent on $\alpha 5$ containing integrins which lead to the maturation of focal adhesions and use of αv integrins, which were not further dependent on Myh2 but instead regulated the response to the matrix stiffness indicated by $\alpha 5$, therefore cooperation between both $\alpha 5\beta 1$ and $\alpha v\beta 3$ was needed to achieve the correct sensing and response to matrix stiffness¹⁸⁶. Work by Schiller et al^{186,233} highlighted the usefulness of Gene Ontology services, where datasets are provided that can be used to annotate quantitative mass spectrometry results to allow the identification of an entire class of proteins with similar domains, structures or functions that are co-regulated rather than only being able to identify single proteins^{241,242} and an example of this analysis can be seen in figure 1-4. Other studies of the adhesome have used mass spectrometry to identify proteins that were not previously known to have adhesion roles. For example Rcc2 was originally identified as a microtubule regulator, often found in the nucleus particularly during cell division, but was identified as having a negative role in cell spreading by interacting with other adhesome members Rac1 and Arf6^{243,244}. Finally the fields of adhesome research are being advanced further with the use of more advanced tools such

as activation state dependent antibodies which have been used to discover that active $\alpha 5\beta 1$ recruits microtubules to focal adhesions but the inactive integrin does not²³⁷.

Whilst there have been several thousand proteins identified in published adhesome studies, comparison between them has identified a core consensus adhesome of only 60 proteins²⁴⁵. These 60 represent the proteins absolutely essential for forming adhesions, and the thousands of other proteins are the matrix and cell-dependent proteins that can participate in cell adhesion. The majority of adhesome studies mentioned so far have been carried out in fibroblasts and none have been published studying endothelial cells. Additionally no study has been carried out to identify the role of $\beta 3$ in regulating the adhesome in cells. It is very likely that the inclusion of certain proteins in the non-consensus adhesome depends greatly on the integrins available, matrix and cell type. Endothelial specific proteins such as Nrp1 interact with integrins, focal adhesion proteins and regulate focal adhesion turnover, potentially making the endothelial adhesome unique compared to other cell types^{52,246,247}. Other endothelial specific proteins such as VE-cadherin also influence focal adhesions through crosstalk with integrins via RhoA and other connections^{248,249}. Crosstalk between integrins and growth factor receptors discussed earlier is common in many cell types, and endothelial cells have a unique complement of receptors including the VEGF receptors which are known to influence cell adhesion by phosphorylation of Fak1 through Src and Hsp90 (Heat shock protein 90)²⁵⁰.

Figure 1-4 Protein Domains Found in the Adhesome



An overview of the types of protein domain families often found in the adhesome by mass spectrometry experiments and their relative abundances by shown by area. Adapted from Schiller and Fässler²⁵¹.

Microtubules

Microtubules are a major type of cytoskeleton in mammalian cells, with the others being the actin cytoskeleton and the intermediate filament network. They are made up of primarily alpha and beta tubulin monomers, with 4 other tubulin families that play supporting roles in the microtubule filament²⁵². Alpha and beta tubulin monomers come together to form dimers, these dimers then polymerise, alpha contacting beta, with other dimers to form a protofilament and 13 protofilaments are complexed together to form the hollow tube of the microtubule structure (shown in figure 1-5A); the alpha then beta structure gives microtubules a polarity with the first beta monomer exposed as the minus end and the last alpha monomer exposed as the plus end²⁵³. Dimers can only be added or removed from the microtubule at the plus end meaning that the balance of polymerised and free tubulin controls the fate of the microtubule²⁵⁴. Tubulins are GTPases meaning they bind GTP (Guanine tri-phosphate) and hydrolyse it to GDP (Guanine di-phosphate), when bound to GTP, tubulin dimers are able to polymerise into microtubules, but shortly afterwards hydrolysis occurs and GDP tubulin is prone to disassembly²⁵⁵. However often more GTP bound tubulin is incorporated onto the plus end of the microtubule, blocking the earlier bound GDP tubulin from disassembly. The delay between tubulin addition at the plus end and the hydrolysis of GTP creates a "GTP cap" that protects the microtubule from disassembly²⁵⁴, also shown in figure 1-5A. Microtubules can exhibit dynamic instability, meaning they can switch rapidly from growing and shrinking behaviours. If addition of GTP bound tubulin monomers slows, then the hydrolysis of GDP will catch up and reach the end of the microtubule, where exposed GDP bound tubulin will fall off followed by a chain reaction of depolymerisation along the microtubule known as catastrophe. At any point, bound GTP tubulin can bind to the shrinking plus end to "rescue" the microtubule and re-establish the GTP cap allowing stable growth²⁵⁶. Control of the dynamic instability of microtubules is carried out by a vast array of proteins that bind to the plus end and regulate polymerisation, depolymerisation, GTP hydrolysis and direction of the growth known as +TIPS (Microtubule plus end tracking proteins)²⁵⁷. Other proteins that regulate microtubule behaviour that bind to tubulin dimers are known as MAPs (Microtubule associated proteins) such as Map6 which stabilises microtubules to halt cold induced disassembly²⁵⁸. Low temperatures cause spontaneous microtubule disassembly of unprotected microtubules and so cold stability can be a useful assay in determining if microtubules are being actively protected by MAPs or +TIPs^{259,260}.

Function

Microtubules have both structural and transportation roles in cells, meaning that targeting of their growth direction is key for ensuring the correct function. Microtubules for example interact with two major types of motor proteins: dyneins which move cargo to the minus end of the microtubule and kinesins which move cargo to the plus end²⁶¹. Entire vesicles can be coupled to these motor proteins, for example vesicles containing proteins from the golgi apparatus for exocytosis are carried along microtubules leading to the cell membrane²⁶². Microtubule networks are needed to give structural support to the retracting edge of migrating cells, but must also be able to shrink so they do not hinder the full retraction, hence the need for dynamic and controlled growth/shrinkage²⁶³. Microtubules can also affect cell migration by direct association with focal adhesions, delivering Dyn2 to disassemble focal adhesions via Fak1 interactions¹⁹¹.

Regulation

As described above, microtubules have a complicated existence with multiple opportunities for regulatory proteins to influence their behaviour by binding tubulin monomers, dimers and the microtubule polymer. Many of these interaction sites are binding sites for microtubule targeting drugs. Most drugs fall into two categories: those that destabilise the microtubule and those that stabilise them. Both categories commonly interfere with cell division and migration, due to those processes relying on the dynamic instability of microtubules and hence too stable or unstable networks will hinder them, making microtubule targeting drugs attractive anti-cancer agents²⁶⁴. Three sites have been characterised in microtubules where drugs are known to bind. The taxane site is found in the GDP bound active site of beta tubulins, and drugs which bind here force a conformational change in the tubulin to resemble that of the GTP bound tubulins, inhibiting disassembly like the GTP cap²⁶⁵. Taxanes such as paclitaxel and epothilones such as epothilone B are examples of clinically used drugs which stabilise microtubules this way^{266,267}. The “vinca site”, named for where vinca alkaloid drugs bind, is again found near the active site of beta tubulins but of the GTP confirmation, preventing GTP hydrolysis but importantly binds to the alpha and beta tubulin dimer inducing premature assembly in solution and preventing existing microtubules from being extended²⁶⁸. Vinca site binding drugs, such as vinblastine, also bind to plus ends of microtubules and produce a slight curve in the protofilaments, preventing them from assembling properly. This process is also

known as an end-poisoning mechanism^{269,270}. The other site, known as the colchicine site, is found on the interface of the alpha and beta tubulin dimerisation site. Drugs such as colchicine are microtubule destabilisers that prevent microtubule assembly and induce their disassembly when colchicine bound dimers are incorporated into the microtubule²⁷¹. The vast array of drugs available make manipulating microtubules in vitro and in vivo possible.

Interactions with Focal Adhesions

Microtubules have been observed targeting nascent focal adhesions as well as inducing the disassembly of mature focal adhesion, suggesting they have multiple roles to play in focal adhesion dynamics^{191,272}. Microtubules can influence the formation of focal adhesions via Rac1 by activating Rac1 GEFs at membrane protrusions to promote adhesion after protrusion during cell migration²⁷³. Rac1 activity is important in regulating microtubule behaviour in addition to the actin cytoskeleton and focal adhesions, therefore these processes will compete for the attention of activated Rac1 and as a result will be linked^{274,275}. As well as inducing focal adhesion assembly after membrane protrusion, microtubules also deliver the integrins to this area via transport proteins²⁷⁶. After focal adhesions formation, microtubules continue to deliver components to focal adhesions, transforming them into mature focal adhesions²⁷⁷. This attraction to focal adhesions is often termed microtubule capture, as various +TIPS such as Clip1 (CAP-Gly domain containing linker protein 1) can become linked to focal adhesions²⁷⁸. Microtubules themselves participate in the protrusion of the cell membrane at the leading edge, but also, their stimulation of focal adhesion formation subsequently leads to their capture at adhesions favouring the maturation of focal adhesions only where integrin ligation occurs will lead to further delivery of cargo by microtubules in a kind of feedback loop²⁷⁹.

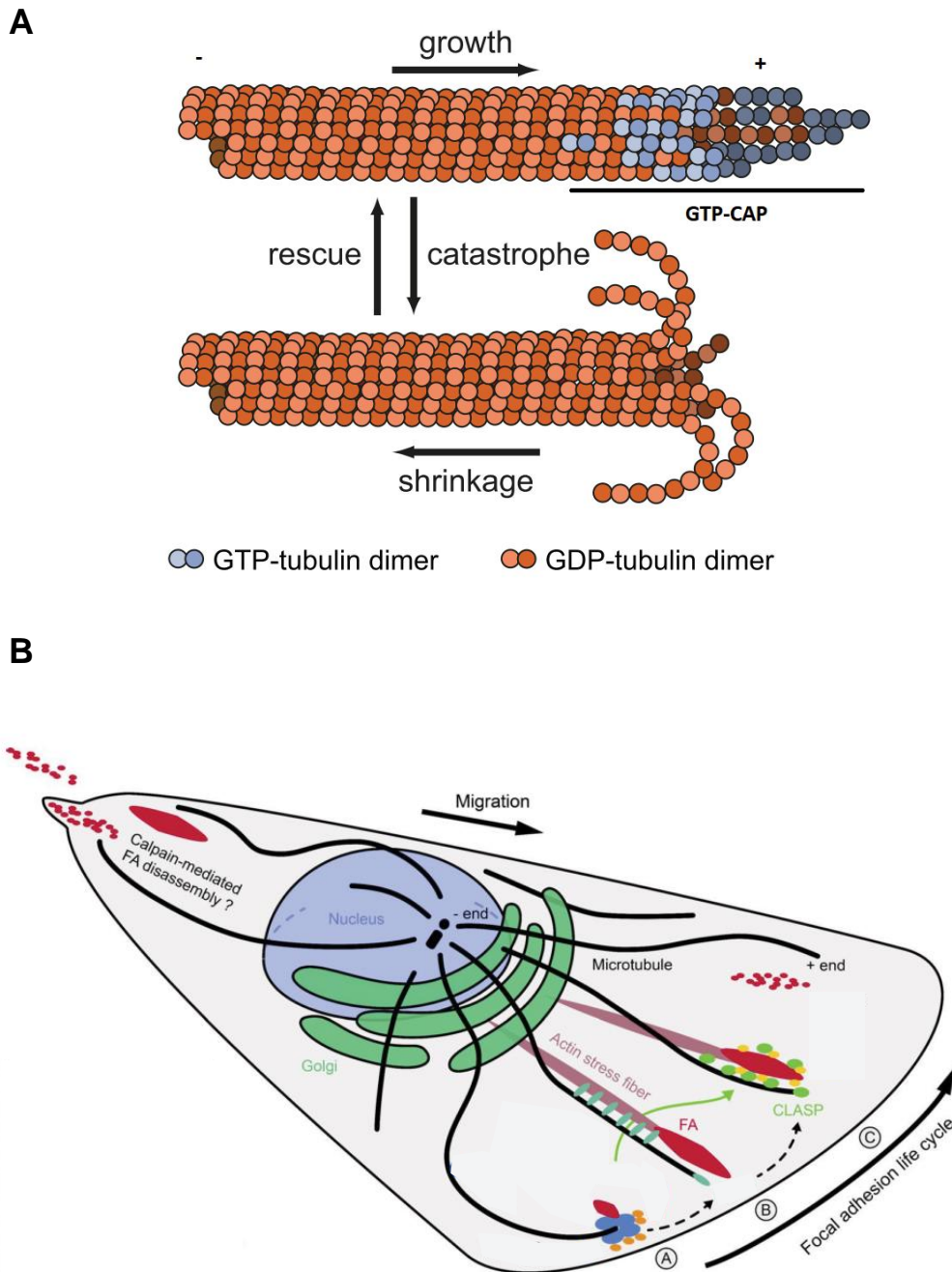
Microtubules have been observed targeting mature focal adhesion at the rear of a migrating cell to stimulate their disassembly and cause detachment, allowing the cell to contract the rear edge to move forward²⁸⁰. Microtubules target these mature focal adhesions by growing parallel to actin fibres towards the terminus where the adhesion is found, in a process dependent on crosslinkers of microtubules and actin such as spectraplakins like Macf1 (Microtubule actin crosslinking factor 1)²⁸¹; in contrast the targeting of nascent adhesions at the front of the cell seems dependent on microtubule capture by the focal adhesion as mentioned above, possibly because the actin cytoskeletal links to these adhesions haven't yet matured. Without Macf1, microtubules at the rear

edge of migrating cells are disorganised and focal adhesion turnover is reduced confirming this alternative mechanism of microtubule targeting to focal adhesions²⁸². Microtubule induced disassembly of focal adhesions is not one way, as upon focal adhesion disassembly the microtubule also undergoes catastrophe in a Pxn dependent process²⁸³. Figure 1-5B shows a brief overview of different ways microtubules can target focal adhesions.

Microtubules in Angiogenesis

Cell adhesion and migration are critical processes in angiogenesis, therefore microtubule dynamics have strong influences on endothelial cell behaviour, with microtubules known to regulate endothelial cell migration^{284,285}. Aside from regulating focal adhesions, microtubules are also known to influence angiogenesis by controlling VEGFR2 internalisation, as shown when microtubule disruption lead to an accumulation of VEGFR2 on the surface of endothelial cells²⁸⁶. As a result, microtubule inhibitors are increasingly used in tumours due to both their anti-cancer and anti-angiogenic effects, as both outcomes will serve to shrink tumours and often the endothelial cells respond to better to lower, sub-toxic, doses of the inhibitors than cancer cells which often develop resistance^{126,264,287}. Several microtubule inhibiting drugs are being evaluated for anti-angiogenic treatment such as paclitaxel²⁸⁸ and some are being used in combination with other types of chemotherapeutics such as fosbretabulin, which has very strong anti-angiogenic effects such as vessel loss and endothelial cell death^{289,290}.

Figure 1-5 Overview of Microtubule Assembly and Behaviour in Cell Migration



A The 13 protofilament cylinder structure and key processes highlighting the dynamic instability of microtubules. GTP-tubulin dimers adding to the plus end (top) allow growth of the microtubule whereas subsequent hydrolysis to GDP-tubulin allows the filament to shrink. The area between the plus end and the point of hydrolysis is known as the GTP-cap. Figure adapted from Bowne-Anderson et al²⁵⁶. **B** A schematic showing how microtubules can interact with focal adhesions across their lifecycle during cell migration. Microtubules can sometimes be targeted to nascent adhesions (A) or track along actin fibres to existing focal adhesions (B). Recruitment to mature focal adhesions can occur via adaptors via

proteins such as Clasps or Clips (C). Focal adhesions have been observed increase disassembly at the rear of the cell when they are targeted by microtubules. Adapted from Stehbens et al²⁹¹

Aims

Given that $\beta 3$ presents such an interesting target for anti-angiogenic therapy, this project was designed to add to existing knowledge of the role of $\beta 3$ in the endothelial adhesome in an attempt to explain why compensation for the loss of the integrin occurs. This compensation for the loss of the integrin²¹⁵ has resulted in disappointing outcomes when targeting it in vivo. Candidate based approaches have identified proteins such as Nrp1 which can enhance angiogenesis upon loss of $\beta 3$ ²¹⁸ leading us to believe there could be other undiscovered mechanisms. A non-candidate approach would be needed to help uncover the full role of $\beta 3$ in the adhesome, which could be used to manipulate angiogenesis in combination with $\beta 3$ targeting.

To fulfil the above objectives, more detailed aims include:

1. Develop a non-candidate approach that can be used to uncover the role of $\beta 3$ in the adhesome
2. Define the endothelial adhesome for the first time to provide a robust dataset to refer back to upon $\beta 3$ depletion and to confirm our non-candidate approach was valid by confirming the presence of expected angiogenic proteins based on literature
3. Use our validated method to define the adhesome of $\beta 3^{+/+}$, $\beta 3^{+/-}$ and $\beta 3^{-/-}$ endothelial cells as well as those under treatment with c(RGDfV) (Cyclo(-Arg-Gly-Asp-D-Phe-Val) trifluoroacetate). This data can then be used to identify the roles of Integrin $\beta 3$ in the adhesome and compensation pathways for its loss
4. Target the identified compensation pathways as a potential anti-angiogenic treatment in vitro and in vivo
5. Once pathways are validated and confirmed useful, then elucidate the molecular mechanism behind them by further mining adhesome data and other available datasets

Chapter two – Materials and Methods

Reagents

All reagents were purchased from Sigma-Aldrich (Poole, UK) unless stated otherwise and all antibodies used are listed in table 2.1. VEGF-A₁₆₄, hereafter referred to as VEGF was made according to Krilleke et al²⁹². EMD66203, referred to as c(RGDfv), was purchased from

Mice and Genotyping

All mice used were from a mixed C57BL6/129 background. $\beta 3^{-/-}$ mice were obtained from $\beta 3^{+/-}$ x $\beta 3^{+/-}$ crosses, where each mouse had a single $\beta 3$ knockout allele, also generating $\beta 3^{+/+}$ littermates. Original $\beta 3$ knockout mice were obtained from Hodivala-Dilke et al¹⁵¹. Pdgfb (Platelet derived growth factor subunit b) tamoxifen inducible cre (referred to as Pdgfb cre) mice were obtained from Marcus Fruttiger²⁹³ (UCL, London, UK) and Tie1 (Tyrosine-protein kinase receptor 1) constitutively driven cre (referred to as Tie1 cre) mice were obtained from Reinhard Fässler²⁹⁴ (Max Planck, Martinsried, Germany). Both cre lines were crossed to $\beta 3$ floxed mice²⁹⁵ obtained from Jochen Schneider (University of Luxembourg, Luxembourg) to generate double $\beta 3$ floxed cre positive or negative littermates. All animal experiments were performed in accordance with UK Home Office regulations and the European Legal Framework for the Protection of Animals used for Scientific Purposes (European Directive 86/609/EEC).

Endothelial Cell Isolation and Immortalisation

Mouse ECs were isolated from the lungs of mixed C57BL6/129 background mice. The lungs were finely chopped with scalpels and then digested with collagenase type I solution. 0.2% (w/v) collagenase type I solution was prepared in PBS (Phosphate buffered saline) with 1mM MgCl₂ and CaCl₂, allowed to auto-digest for 1 hour at 37°C, diluted in half with more PBS with 1mM MgCl₂ and CaCl₂ and supplemented with DNase at 1 to 1000 dilution. After 1 hour of digestion at 37°C, lungs were passed 3 times through a 19 gauge needle and then once through a 21 gauge needle. Lung digests were then centrifuged at 400 g for 5 minutes and resuspended in mouse lung endothelial cell medium prepared as per Reynolds and Hodivala-Dilke²⁹⁶, consisting of DMEM/F12 20% FBS with penicillin/streptomycin, glutamine and 50 mg L⁻¹ endothelial mitogen (Biogenesis). The cells were then plated on 0.1% gelatin, 10 μ l ml⁻¹ collagen and 10 μ l ml⁻¹ fibronectin coated T75 flasks. After 24 hours flasks were washed once with PBS to remove non adhered cells. Once flasks were confluent, they were positively sorted for ICAM2 (BD Biosciences Clone 3C4). 3 ml of PBS with 1 to 1000 dilution of ICAM2 was incubated directly on the lung culture flask at 4°C for 30 minutes on a rocker.

Antibody solution was removed and the flask washed with ice cold PBS before adding a sheep anti-rat IgG dynabeads (ThermoFisher) solution at 1 to 1000 in 3 ml media then incubated for 30 minutes at 4°C on a rocker. Beads solution was removed and cells washed twice with ice cold PBS before trypsinisation. The cell solution was then placed in a magnetised tube rack and non-bead coated cells removed with a media wash. Finally, the cells were removed from the rack, resuspended in media then plated on a coated T25 flask as above. A second round of sorting was carried out a week later.

Immortalisation was carried out as per Robinson et al⁵². Briefly, primary endothelial cells were treated with polyoma-middle-T-antigen containing retrovirus media (supernatant of GgP+E cell line from ATCC) supplemented with 8 µg ml⁻¹ polybrene for 6 hours at 37°C. Afterwards retrovirus media was removed and replaced with mouse lung endothelial cell medium. Retrovirus exposure was repeated the next day. Immortalisation was confirmed by culture for 4 weeks and were subsequently used in experiments up till passage 20. Endothelial identity was routinely checked by flow cytometry as per Ellison et al²¹⁸.

Focal Adhesion Enrichment

Focal adhesion enrichment for mass spectrometry was developed by Schiller et al²³³ and adapted for endothelial cells. IMMLECs (Immortalised mouse lung endothelial cells) were starved in serum-free OptiMEM® (ThermoFisher) for 3 hours and seeded at 6 x 10⁶ cells per plate in 10 cm plates that were previously coated with 10 µg ml⁻¹ fibronectin or 0.01% poly-L-lysine (Mw 150,000 to 300,000) in PBS overnight at 4°C and blocked in 1% BSA (Bovine serum albumin) in PBS for 1 hours at room temperature. Cells were adhered for 90 minutes to allow for mature focal adhesions to form and either stimulated with 30 ng ml⁻¹ VEGF at 37°C in the last 10 minutes or not at all. Cells were washed in PBS with 1 mM CaCl₂ and 1 mM MgCl₂ before being incubated with 0.05 mM DPDPB (1,4-Bis[3-(2-pyridylidithio)propionamido]butane) and 0.5 mM DSP (Dithiobis(succinimidyl propionate) for 5 minutes to crosslink focal adhesions to the plate. This reaction was quenched with 1 M Tris-HCl pH 7.5 before cells were lysed in RIPA (Radioimmunoprecipitation assay buffer) for 30 minutes on ice with occasional agitation. RIPA was collected without scraping, and the plates were blasted with a high-shear flow jet of RO (Reverse osmosis) water to remove cell debris. The flow of RO water was approximately 7 litres per minute through a 20mm diameter tube compressed to 1 mm to form a nozzle. Crosslinked proteins were eluted with 2 ml DTT (Dithiothreitol) buffer (25 mM Tris-HCl pH 7.5, 10 mM NaCl, 0.1% SDS, 100 mM DTT) for 1 hour at 60°C in a sealed and humidified chamber. 8 ml of acetone was added to this solution and left overnight at -20°C to allow the proteins to precipitate with

10 μ l GlycoBlue™ Coprecipitant (ThermoFisher). Samples were centrifuged at 13,000 g for 30 minutes and the acetone layer removed. The pellet was then resuspended in 30 μ l EB buffer (3% SDS, 60 mM sucrose, 65 mM Tris-HCl pH 6.8) before being used in western blotting, silver staining or mass spectrometry (see below) as the “crosslinked material”

Western Blotting

Protein samples were homogenised using acid-washed glass beads in a Tissue Lyser (Qiagen) at 50 Hz for 2 minutes before being centrifuged at 12,000 g for 10 minutes at room temperature and then quantified using DC™ Protein Assays (Bio-Rad) where appropriate. Samples were loaded onto 10% SDS-PAGE (Sodium dodecyl sulphate polyacrylamide gel electrophoresis) gels then transferred to a nitrocellulose membrane and incubated for 1 hour in 5% milk powder in PBS with 0.1% Tween 20 followed by overnight incubation in primary antibody diluted 1:1000 in BSA in PBS with 0.1% Tween 20 at 4°C. The membranes were then washed 3 times using PBS with 0.1% Tween 20 before being incubated with the appropriate horseradish peroxidase conjugated secondary antibody (Dako) diluted 1:2000 in 5% BSA in PBS with 0.1% Tween 20 for 1 hour at room temperature. The blot was visualised using Pierce® ECL Western Blotting Substrate kit (ThermoFisher) and chemiluminescence detected in a LAS-3000 darkroom (Fujifilm UK Ltd).

Silver Staining

Silver staining was carried out on 2 μ l of the crosslinked material samples from focal adhesion enrichments carried out as above along with 2 μ l of total cell lysates as controls. These samples were run on 10% SDS-PAGE gels before being silver stained using the Pierce™ Silver Stain Kit (ThermoFisher).

Mass Spectrometry

Three good quality crosslinked material samples, as determined by silver staining, were pooled together and analysed three times by label-free mass spectrometry at the Fingerprints Proteomics Facility, Dundee University, Dundee, UK as per Schiller et al²³³. Peptides were identified and quantified using MaxQuant software with the Andromeda peptide database.

Adhesion Assay

96 well plates were coated in 10 μ g ml⁻¹ fibronectin in PBS overnight at 4°C then blocked with 1% BSA in PBS for 1 hour at room temperature. 20,000 cells were seeded into each well and allowed to adhere for 90 minutes. Cells were then washed with PBS with 1 mM

MgCl₂ and 1 mM CaCl₂ 3 times to remove non adhered cells and fixed with 4% PFA (Paraformaldehyde) for 10 minutes at room temperature. After a further PBS wash, cells were stained with 1% methylene blue in 10 mM borate buffer pH 8.5/50% methanol for 30 minutes at room temperature. Excess stain was removed with RO water before a 50% 0.1 M HCl/50% ethanol destain solution was used for 10 minutes at room temperature. The destain solution was then moved to a new plate and read absorbance was measured at 630 nm. Adhesion assay was adapted from Ellison et al²¹⁸.

Immunocytochemistry

20,000 IMMLECs were seeded onto FN (Fibronectin) coated/BSA blocked coverslips (acid washed and baked before coating) and adhered for 90 minutes before being washed with PBS and immersed in -20°C methanol for 20 minutes. Coverslips were then washed with PBS, blocked for 10 minutes at room temperature with 0.5% BSA, 1% goat serum (or 1% donkey serum where anti-Nrp1 antibody was used) in PBS with Triton X-100 and incubated with primary antibody diluted 1:250 for 1 hour at room temperature. After subsequent PBS washes, the coverslips were incubated with the appropriate goat (or donkey for anti-Nrp1 staining) raised Alexa-Fluor® (ThermoFisher) conjugate secondary antibodies diluted 1:500. Coverslips were washed again in PBS before being mounted onto slides using Prolong® Gold with DAPI (ThermoFisher).

Simultaneous tubulin and actin staining was carried out using PHEMO fixation²⁹⁷. 20,000 cells were seeded onto FN coated/BSA blocked coverslips (acid washed and baked before coating) and adhered for 90 minutes. Coverslips were then washed with PBS at 37°C and fixed with PHEMO buffer (68 mM PIPES, 25 mM HEPES, 15 mM EGTA and 3 mM MgCl₂) with 3.7% PFA and 0.05% glutaraldehyde for 10 minutes at 37°C. 2 further washes in PHEMO buffer were carried out for 10 minutes each at 37°C before a final wash in PBS at room temperature. Blocking and staining was then carried out as above but with phalloidin diluted 1:100 in PBS to stain actin filaments (ThermoFisher A12380).

Nucleofection

All plasmid constructs and siRNAs were transfected into IMMLECs using nucleofection, a highly effective method of transfecting endothelial cells without using viruses²⁹⁸. After trypsinisation and counting, 1 x 10⁶ cells were resuspended into 100 µl of transfection buffer (200 mM HEPES, 137 mM NaCl, 5 mM KCl, 6 mM D-glucose, 7 mM Na₂HPO₄) and mixed with 3 µg of ON-TARGET plus SMARTpool siRNA (Dharmacon), ON-TARGET plus Non-targeting Control Pool siRNA or GFP-Pxn plasmid (Maddy Parsons, King's College London,

London, UK). Nucleofection was carried out using an Amaxa™ Nucleofector II (Lonza) on the T-005 setting.

Live Cell Imaging

IMMLECs were transfected with a GFP-tagged Pxn cDNA expression (provided by Maddy Parsons²⁹⁹) construct by nucleofection and allowed to recover overnight before a fraction were seeded on FN coated/BSA blocked coverslips (acid washed and baked before coating) and adhered for 3 hours. Cells were then treated with 100 nM SiR-Tubulin and 1 μ M verapamil (Cytoskeleton Inc CY-SC002) overnight. Coverslips were then imaged individually on an Axiovert (Zeiss) inverted microscope where one image of a GFP-positive cell was taken every minute for 30 minutes at 37°C and 5% CO₂ in green and far-red channels. During imaging media was replaced with phenol-free OptiMEM® with 2% FBS containing 100 nM SiR-Tubulin and 1 μ M verapamil. The total area of adhesive fronts was assessed by measuring the growth of GFP-Pxn positive areas between the 1st and 30th image and then the number of microtubules that entered the adhesive front over 30 minutes were counted.

Cell Viability

96 well plates were coated in 10 μ g ml⁻¹ fibronectin in PBS overnight at 4°C then blocked with 1% BSA in PBS for 1 hour at room temperature. 10,000 IMMLECs were seeded into each well and were allowed to adhere for 3 hours. Cells were then treated with a wide range of microtubule inhibiting agents overnight before being washed with PBS and fixed with 4% PFA for 10 minutes at room temperature. Methylene blue staining and analysis was carried as above for adhesion assays. Experiments were repeated using a narrower range of microtubule inhibiting drugs to find the exact dose at which 90% of cells survived compared to untreated control.

Random Migration

24 well plates were coated with 10 μ g ml⁻¹ fibronectin in PBS overnight at 4°C and then blocked with 1% BSA for 1 hour at room temperature. 10,000 ECs were seeded per well and allowed to recover overnight. Media was then replaced with media containing one of the following microtubule targeting agents: 5 nM Paclitaxel (Abcam 120143), 1 nM Etoposide (Abcam 141271), 10 μ M Colchicine (Abcam 120663), 0.4 μ M Mebendazole (Abcam 141246), 0.5 μ M Fostretablin (Sigma-Aldrich SML1131) or 1 μ M Eribulin provided by Katherine Weilbaecher (Washington University, St Louis, USA) (DMSO (Dimethyl sulfoxide) was used as a control). Alternatively, 0.08 μ M Tanespimycin (Abcam 171433) as an Hsp90

inhibitor was used. A phase contrast image was taken of each well every 20 minutes using an inverted Axiovert (Zeiss) microscope for 15 hours at 37°C and 5% CO₂. The ImageJ plugin MTrackJ³⁰⁰ was then used to manually track individual cells and the speed of random migration was calculated.

In Vivo Tumour Assay

The syngenic mouse lung carcinoma cell line (derived from C57BL6 mice) CMT19T was used in all tumour experiments, as per Steri et al²²³. Under anaesthetic, mice were injected subcutaneously in the flank with 1×10^6 cells. Tumours then grew for 7 days, at which point they were palpable through the skin, before the mice were treated with 0.15 mg kg^{-1} Eribulin intravenously once a week for 2 weeks or $8 \text{ mg Doxorubicin kg}^{-1}$ at day 11 and 14 via intraperitoneal injection. After 21 days mice were culled and tumours were excised, photographed and measured for volume using a digital caliper. Tumours were bisected along the midline, fixed overnight in 4% paraformaldehyde, preserved for several days in cryoprotectant (20% sucrose, 2% poly(vinylpyrrolidone) in PBS), embedded in gelatin (8% gelatin, 20% sucrose, 2% poly(vinylpyrrolidone) in PBS) before being snap frozen and stored at -80°C.

Immunohistochemistry

5 µm cryosections were prepared from frozen tumours and stained as described previously²²³. Images were acquired on an AxioPlan (Zeiss) epifluorescent microscope. Additionally, scans of complete sections were achieved using the AxioVision MosaiX plugin. Tissue area and vessel counts were obtained using ImageJ, as described in Ellison et al²¹⁸.

Microtubule Cold Stability Assay

Microtubule cold stability assays were carried out as described in Ochoa et al²⁵⁹. Briefly: 750,000 ECs were seeded per well of a 6 well plate (FN coated/BSA blocked as described earlier) and allowed to adhere for 75 minutes at 37°C before being moved to ice for 15 minutes. Cells were then washed with PBS and then 100 µl of PEM buffer (80 µM PIPES pH 6.8, 1 mM EGTA, 1 mM MgCl₂, 0.5% Triton X-100 and 25% (w/v) glycerol for 3 minutes. A second brief wash was performed with 50 µl PEM buffer. All PEM buffer was collected and pooled together with 150 µl EB buffer (3% SDS, 60mM Sucrose, 65mM Tris-HCL pH 6.8) at 2X concentration. Remaining material on the plate was then extracted using 300µl of EB buffer. Samples were then used in Western blotting analysis.

Additionally, the same procedure was used on ECs adhered to FN coated/BSA blocked coverslips (acid washed and bake-sterilised before coating). They were seeded as per the immunocytochemistry method then underwent the cold stability assay as above except that, immediately after PEM washing, the slides were immersed in -20°C 100% methanol for 20 minutes. Coverslips were stained as in the rest of the immunocytochemistry method.

In some cases the Rac1 inhibitor NSC23766 (Abcam 142161) was used during the cold stability assay. Cells were adhered for 60 minutes at 37°C before being treated with 50 µM NSC23766 or DMSO control for 15 minutes at 37°C. Cells were then moved to ice for a final 15 minutes before finishing the procedure as above.

Active Rac1 Assay

6 x 10⁶ ECs were seeded onto FN coated/BSA blocked 10 cm plates and allowed to adhere for 90 minutes. Rac1 Activation Magnetic Beads Pulldown Assay kit (Millipore 17-10393) was then used per manufacturer's instructions by lysine cells in MLB (Magnesium lysis buffer) before using Pak1-PBD (P21 (Rac1) activated kinase 1 – P21 binding domain) beads to pull-down active Rac1. Pull-down material was then loaded directly onto a gel for western blotting.

Statistical Analysis

All graphs presented show the mean as the bar height ± standard error of the mean. Statistical significances between means were calculated using Student's t-test where ns, *, **, *** and **** represent $p > 0.05$, $p \leq 0.05$, $p \leq 0.01$, $p \leq 0.001$ and $p \leq 0.0001$ respectively.

Significance analysis of microarrays³⁰¹ was carried out within the Perseus statistics package³⁰² using 250 randomisations in a permutation based false discovery rate of 0.01 for truncation with an S0 cut-off of 1 to identify statistically significant proteins between two samples.

Antibodies

Target	Supplier	Catalogue	Conjugate	Application
Acta2	Abcam	124964		Immunohistochemistry
Anxa2	Abcam	41803		Western Blotting
Emcn (Endomucin)	Santa Cruz Biotechnology	65495		Immunohistochemistry
Filamin-a	Abcam	76289		Western Blotting
Gapdh (Glyceraldehyde-3-phosphate dehydrogenase)	Abcam	9484		Western Blotting
Goat	ThermoFisher	A-11055	Alexa® 488	Immunocytochemistry
Hspa1a (Heat shock protein family A (Hsc70) member 1A)	Santa Cruz Biotechnology	7298		Western Blotting
β3	Cell Signalling	4702		Western Blotting
Erk1/Erk2	Cell Signalling	4695		Western Blotting
Mouse	Dako	P0447	Horse radish peroxidase	Western Blotting
Mouse	ThermoFisher	A-11004	Alexa® 568	Immunocytochemistry
Nrp1	Cell Signalling	3725		Western Blotting
Nrp1	R and D Systems	AF566		Immunocytochemistry
Ptk1	Cell Signalling	3285		Western Blotting

Pxn	Abcam	32084		Western Blotting / Immunocytochemistry
Rabbit	Dako	P0448	Horse radish peroxidase	Western Blotting
Rabbit	ThermoFisher	A-11008	Alexa® 488	Immunocytochemistry / Immunohistochemistry
Rac1	Merck	05-389		Western Blotting
Rat	ThermoFisher	A-11077	Alexa® 568	Immunohistochemistry
Rcc2	Abcam	70788		Western Blotting
Tln1	Sigma	T3287		Western Blotting / Immunocytochemistry
Tuba (pan)	Abcam	7291		Western Blotting
Tuba (pan)	Abcam	52866		Immunocytochemistry
Vim (Vimentin)	Cell Signalling	5741		Western Blotting

List of all primary and secondary antibodies used.

Chapter three – Isolation and Mass Spectrometry of the Endothelial Cell Adhesome

The aim of this chapter is to optimise and adapt the adhesome enrichment technique developed by Schiller et al²³³ to work with endothelial cells. Quality control methods are also needed to ensure efficient use of mass spectrometry time. Additionally, the configuration of MaxQuant required testing in order to successfully identify proteins modified during the adhesome enrichment.

Development of Adhesome Enrichment Method

Focal adhesions and the wider adhesome are known to consist of over 2400 proteins, although across multiple experiments and cell types the absolute core consensus is only about 60 proteins²⁴⁵. Cell matrix, integrin availability, cell type and culture conditions can all make a big difference to the adhesome, therefore it was important that we devised a method to specifically identify the endothelial cell adhesome before we could study the role $\beta 3$ plays in its composition.

All adhesome proteins could, in theory, be identified from a whole cell lysate by western blotting or mass spectrometry techniques. However many components of the adhesome are transient in nature: associating with one another upon events such as matrix engagement, engaging downstream effectors or de-associating with each other upon focal adhesion maturation. Even the core of the adhesome, the integrins, can exchange freely with the cytoplasmic pool by internalisation or recycling as well as move diffusely across the cell membrane in the right conditions³⁰³. Trafficking of integrins, for example, can include endocytosis from the membrane and degradation or recycling via, for example, Rab4 (Ras-related protein 4) or Rab11/Arf6 pathways¹⁹⁴. Whole cell analysis could capture integrins at any of these points, complicating analysis, so we decided it was necessary to enrich for proteins present in adhesion complexes under defined conditions. An effective enrichment would give us a snapshot of the adhesome which could then be compared to previous studies in other cells and provide us with a means to study how $\beta 3$ affects the composition of the adhesome.

Historically, identification of focal adhesion components was carried out by co-immunoprecipitations for the desired integrin, such as when Nrp1 was identified as a component with $\beta 3$ containing focal adhesions⁵². In order to reduce non-specific interactions with the antibody, stringent lysis buffers are used which can prevent transient

or weak interactions. Unless an activation-state specific antibody is used to immunoprecipitate, which exist for $\beta 1$ ³⁰⁴ but not mouse $\beta 3$, then integrins in other cell compartments (as mentioned earlier) would also be precipitated. Additionally this would not have allowed us to study the adhesome in $\beta 3$ deficient cells.

At least two suitable techniques have been developed to enrich for adhesome complexes and have so far been applied to fibroblasts. One method developed by Humphries et al²⁴⁴ employs (ECM) ligand coated beads to pull down adhesion complexes from cell lysates and chemical crosslinking to preserve transient interactors before purification. Another method by Schiller et al²³³ allows cells to adhere on matrix coated dishes, followed by chemical crosslinking of dish/matrix/adhesion complexes and high shear flow washing to remove non adhesome material. The Humphries et al method has greater flexibility of ligand choice (any whole or part of an ECM molecule could be used) as the cells can be grown on any substrate before lysis and pulldown using beads coated with ligand of interest. Whereas the Schiller et al method requires the ECM to be something that the cells will adhere to natively without other required matrices because it is these attachments to the ECM that will become the adhesome sample. In this case, assisting cells that may not adhere to a single component ECM with additional matrices could complicate analysis. Using beads to pull down complexes in cell lysates could also run the risk of isolating $\beta 3$ from any cell compartment that has the potential to be activated and bind matrix as it is possible during cell lysis and homogenisation that aberrant activation could occur. We therefore decided to adapt the Schiller et al method for use in endothelial cells as we thought this would provide a better snapshot of proteins actively involved in cell adhesion in a more physiologically relevant setting. The downside was that cells can also stick to substrates using non-integrin adhesions (which would also be crosslinked) but this was overcome by using a PLL (Poly-L-lysine) negative control to identify these adhesion components as cells will still adhere to PLL treated surfaces³⁰⁵.

As adhesome enrichment had not been carried out on endothelial cells before we therefore used conditions outlined by Schiller et al for fibroblasts as a starting point where cells are allowed to adhere onto fibronectin for 90 minutes before being crosslinked for 5 minutes, lysed with RIPA for 30 minutes and then shear washed. Crosslinking with the cell permeant reversible crosslinkers DSP and DPDPB for only 5 minutes was designed to allow the highest ratio of adhesome to non adhesome protein crosslinking. DSP (also known as Lomant's reagent) can crosslink primary amines such as the N-terminus of peptides and the side chain of lysine that are approximately 1.2 nm across proteins in a complex³⁰⁶. DPDPB

crosslinks thiol groups (such as those found on the amino acid cysteine) approximately 1.99 nm apart²³⁸. Both DSP and DPDBP can be reversed by thiol-based reducing agents such as DTT allowing any crosslinked proteins to be eluted and analysed. A five minute incubation with both crosslinkers before carrying out the remainder of the adhesome enrichment protocol and then western blotting showed that the DSP/DPDBP combination could diffuse into cells, crosslink proteins and prevent adhesome components from being washed away (figure 3-1A). Nrp1 and β 3, previously reported members of the adhesome³⁰⁷, were detected in the crosslinked material and not the untreated indicating the crosslinkers were functional under the conditions used. Additionally Hspa1a and Fak1, as intracellular members of the adhesome¹⁸⁶, were also detected with crosslinker treatment meaning DSP and DPDBP were able to successfully diffuse through the cell membrane. The absence of Nrp1, β 3, Hspa1a and Fak1 in the non-crosslinked (DMSO control) elution shows these proteins do not bind sufficiently to the matrix to avoid being blasted away during washing. Control lysates taken from the RIPA used to break apart the cells showed that crosslinking did not disrupt important epitopes required for immunoblotting.

The next step in optimising the protocol was to check that the cells adhered to the PLL negative control (also see figure 3-3) and that it was functioning correctly as such. As seen in figure 3-1B there was less β 3, Hspa1a and Gapdh detected in the crosslinked material from cells adhered to PLL than fibronectin. Proteins expected to be involved in adhering to fibronectin such as β 3 were only enriched when cells adhered to fibronectin and not PLL suggest the crosslinking was specific to adhesion complexes. In the RIPA derived samples there were equal amounts of all immunoblotted proteins in the PLL and fibronectin conditions indicating that IMMLECs are able to adhere to PLL in 90 minutes. It was also important to test that cells deficient in β 3 (genetically heterozygous cells) are still able to adhere to both fibronectin and PLL to allow subsequent investigations into the role of β 3 in the adhesome. In the crosslinked material, fibronectin adhered samples, roughly equal amounts of Hspa1a and Gapdh were detected in β 3+/+ and β 3+/- cells meaning the β 3+/- cells had no trouble adhering. There was less β 3 however but this was expected due to the genetic differences in the cells – also reflected in the RIPA samples.

Whilst the crosslinking, general enrichment, acetone precipitation and PLL as a negative control were working successfully in endothelial cells; a problem, identified in figure 3-1B, was that Gapdh was also been detected in the crosslinked material samples. Gapdh, a key housekeeping gene involved in glycolysis, is commonly used as a loading control³⁰⁸ hence its use on figure 3-1B. However unlike Hspa1a, another commonly used loading control³⁰⁹,

Gapdh is not found in reported adhesomes^{186,233,237,310}. The combination of two loading controls, Gapdh and Hspa1a, has shown that the enrichment process was still not specific enough and allowed too many non-adhesome proteins to be detected in the final western blots. Alternatively the crosslinkers may be penetrating too deep into the cell and crosslinking cytoplasmic material, which could have been explored further if other optimisation steps failed. A range of optimisation attempts were carried out and the solution was to change from a benchtop RO water system (Milli-Q® EMD Millipore) to an industrial scale RO plant which provided much higher water pressure for the high shear flow washing stage.

Figure 3-2A shows the result of the water pressure optimisation. Of the crosslinked material samples, a single lane is marked with an * to show that this sample was shear washed with the Milli-Q® system whereas the remaining were washed with the higher pressure RO plant. The low pressure * sample showed a higher intensity signal for all antibodies tested. Importantly, the Gapdh signal had now been removed in the higher pressure washed samples hence the adhesome enrichment had been successful and did not include non-adhesome proteins. To ascertain the depth of crosslinking achieved (i.e. how far the crosslinkers diffused past the cell membrane) we also looked at the signalling molecules Erk1 and Erk2. These proteins, also known as Erk1/2, have many roles in signalling cascades within cells but are also known to translocate to focal adhesions to facilitate outside-in signalling upon cell adhesion³¹¹. Our ability to detect small and potentially transient members of the adhesome using crosslinkers would give a greater meaning to the studies performed later. Additionally, as an alternative focal adhesion marker to Fak1 (seen in figure 3-1A), Tln1 has been detected in the crosslinked material samples even with the higher pressure washing. Tln1 recruitment to integrins requires that Fak1 binds first and begins signalling for the generation of a focal adhesion³¹². Therefore we were confident that IMMLECs were forming mature and functional focal adhesions during the 90 minute adhesion to fibronectin in the conditions used for adhesome enrichment. High pressure washing had also not affected our ability to enrich for Nrp1, β 3 and Hspa1a. A reversible Ponceau-S stain on the nitrocellulose membrane used for immunoblotting in figure 3-2A is shown in figure 3-2B. The * lane again showed many more bands than the higher pressure washed lanes and resembled the adjacent RIPA lysates. Higher pressure shear washing was therefore useful to further remove non-adhesome cell contents and leave behind only crosslinked proteins.

In the same experiment we also tested if VEGF, the main growth factor implicated in angiogenesis³¹³, could affect the ability of cells to adhere to fibronectin and prevent a successful adhesome enrichment although it was also likely that because VEGF can promote migration of endothelial cells directly or through interaction with Nrp1, it could actually enhance adhesion³¹⁴. This could result in an increased detection of proteins in PLL negative controls with VEGF stimulation but, as seen in figure 3-2A, this was not the case. Being able to use VEGF without affecting the adhesome enrichment procedure would prove useful later to help us define the endothelial cell adhesome.

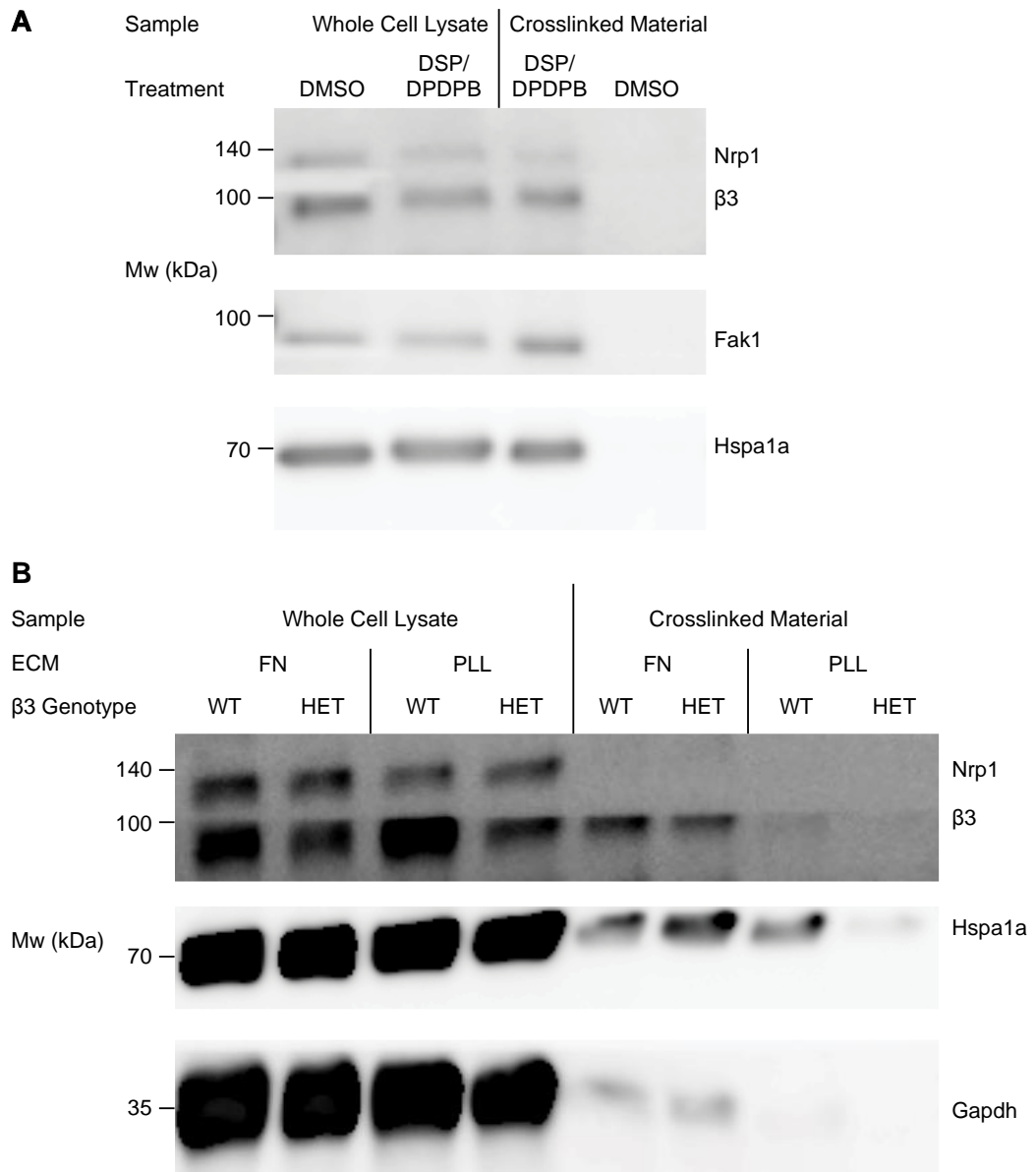
Despite increasing the water pressure during optimisation, another problem became evident. Figures 3-2A, B and C have biological repeats from different preparations included on the same western blots; there was a noticeable inconsistency with the intensity of the detected signals. This is particularly evident in figure 3-2C where the Filamin-a signal varied widely between the duplicate +VEGF crosslinked material samples. As a focal adhesion protein that links the actin cytoskeleton to integrins and regulates their activation/downstream signalling³¹⁵, it should have shown a consistent signal, especially since all the samples generated in figure 3-2C came from $\beta 3^{+/+}$ cells. The same sample with a high FlnA also showed an abnormally high Vim signal whereas one of the - VEGF samples was completely missing a Vim signal. As an intermediate filament, Vim is found to associate with $\beta 3$ positive adhesions in endothelial cells³¹⁶ and so it should have been present in adhesome enriched samples and at consistent levels in $\beta 3^{+/+}$ cells. Pxn, another focal adhesion marker like Tln1 and FAK³¹⁷ also showed the inconsistency between biological repeats. Taken together these observations suggest that the water pressure used may still not be high enough to achieve consistent adhesome enrichments. This was problematic considering we did not have access to an even higher pressure RO water source. We speculated however that we were on the cusp of having sufficient water pressure and that western blotting consisting of Gapdh and multiple focal adhesion markers would be sufficient to identify the successful adhesome enrichments from the unsuccessful ones. However it was not practical to use this method in further identification of the endothelial cell adhesome because it required western blotting of the whole sample, leaving none remaining for non-candidate analysis.

Another reason why we could not have used western blotting in further analysis of the endothelial adhesome was highlighted by Nrp1 immunoblots (figures 3-1B and 3-2A). The intensity of Nrp1 signals were sometimes below the limit of detectability in western blotting. Using protein arrays to immunoblot for several hundred proteins at once to profile

the endothelial adhesome would also not have been practical for the same reason. It was likely that many of the adhesome proteins were represented in the adhesome at even lower amounts than Nrp1. Scaling up our adhesome enrichment protocol beyond 6 million IMMLECs per sample would have been impossible practically and economically, leaving the only other solution to defining the adhesome being mass spectrometry.

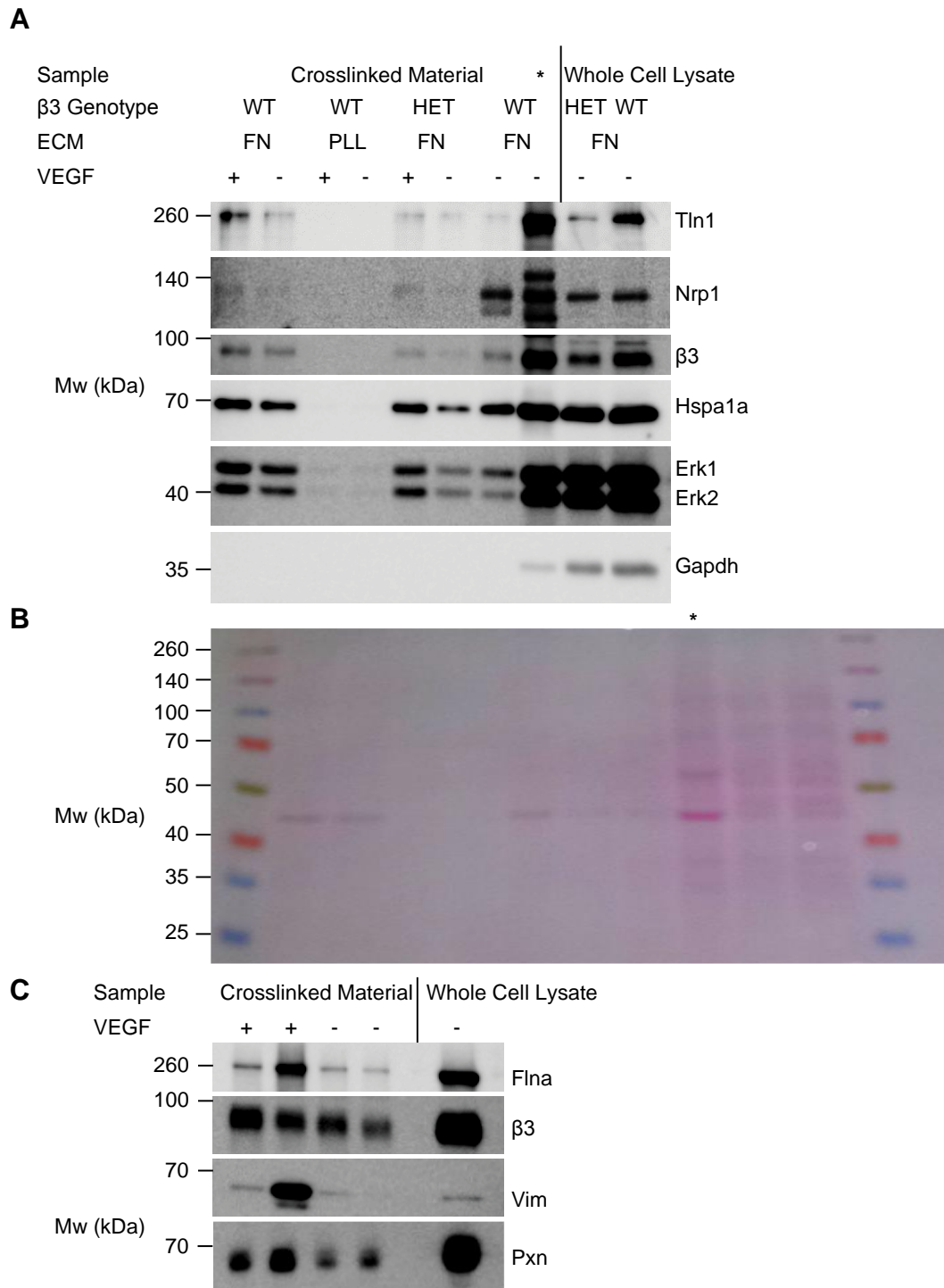
Finally, as seen in figure 3-3, we confirmed the conditions chosen for adhering cells for use in adhesome enrichments produce focal adhesions matching the observations made in figures 3-1 and 3-2. Tln1 was not found in adhesome samples when adhered to PLL and no focal adhesions structures are observed in cell staining of $\beta 3^{+}/+$ IMMELCs unlike when fibronectin coating is used. Nrp1 staining followed the same pattern but also overlapped with Tln1 staining when cells adhered to fibronectin, again confirming that Nrp1 was a member of the adhesome as observed in figures 3-1 and 3-2. The fact that cells were still present to be stained after two washes when adhered to PLL (indicated by the DAPI signals showing a cell nucleus present) double confirmed that IMMLEC cells are able to adhere to PLL successfully. In the development of the adhesome enrichment technique. Schiller et al²³³ carried out staining experiments to validate their procedure where Pxn was used as a marker of focal adhesions and Transferrin (CD71) as a negative control after high shear flow washing. In our experiments it was difficult to stain after the washing stages so instead figure 3-3 shows staining on un-washed cells using PLL as a negative control for focal adhesion formation. Both methods, in our interpretation, show the concept of focal adhesion enrichment and the PLL negative control functioned as expected.

Figure 3-1 Adhesome Proteins Can be Crosslinked in Endothelial cells and Poly-L-lysine Functions as a Negative Control



A Adhesome enrichment was carried out on $\beta 3^{+/+}$ IMMLECs adhered to fibronectin for 90 minutes before being treated with DMSO or crosslinkers (DSP/DPDPB), lysed with RIPA buffer then shear flow washed. Crosslinked material was eluted using DTT then acetone precipitated and western blotted along with the collected RIPA buffer as Whole Cell Lysate for Nrp1, $\beta 3$, Fak1 and Hspa1a. **B** Adhesome enrichment carried out as above but adhering $\beta 3^{+/+}$ or $\beta 3^{+/-}$ IMMLECs to fibronectin or PLL. Samples were then western blotted for Nrp1, $\beta 3$, Hspa1a and Gapdh.

Figure 3-2 Higher Pressure Washing Reduced Sample Complexity



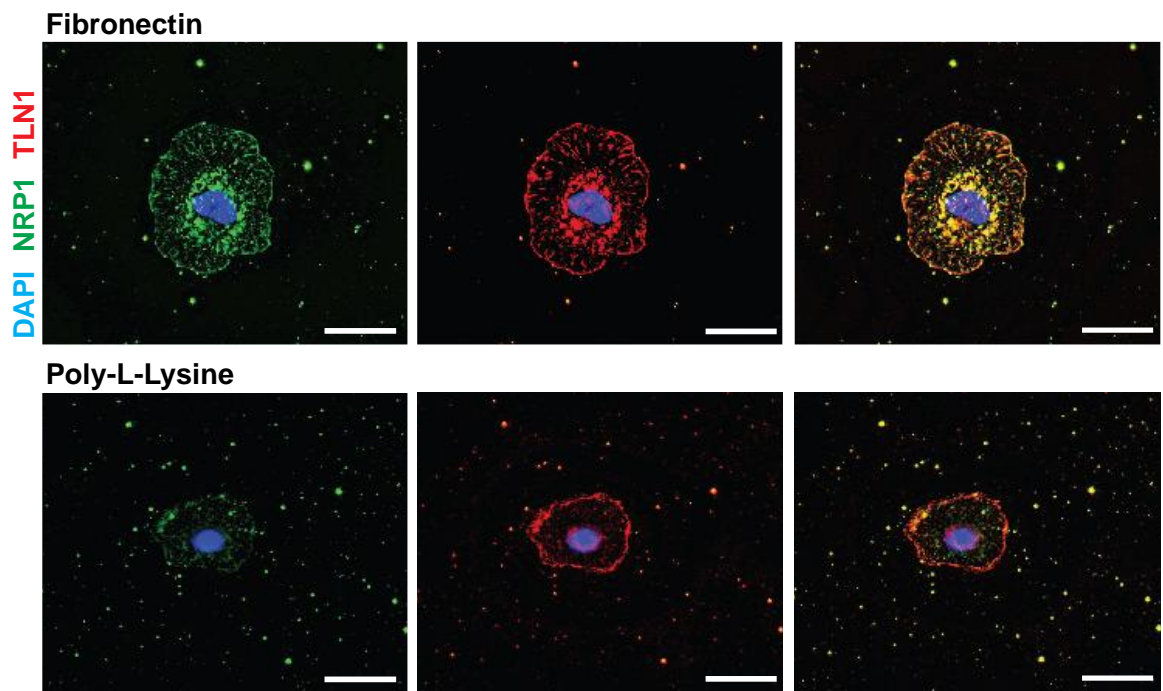
A Adhesome enrichment was carried out on $\beta 3^{+/+}$ and $\beta 3^{+/-}$ IMMLECs adhered to fibronectin or PLL for 75 minutes then stimulated with VEGF(+) or DMSO(-) for 15 minutes before being treated with crosslinkers (DSP/DPDPB), lysed with RIPA buffer then shear flow washed. Crosslinked material was eluted using DTT then acetone precipitated and western blotted along with the collected RIPA buffer as Whole Cell Lysate for Tln1, Nrp1, $\beta 3$,

Hspa1a, Erk1, Erk2 and Gapdh. All adhesome enrichments were carried out with high pressure RO water shear washing except * sample which used a Mill-Q® benchtop system.

B A ponceau stain of the membrane used in panel A before antibody incubation. **C**

Adhesome samples were generated as above except only $\beta 3^{+/+}$ IMMLECs used and all adhered to fibronectin. Samples were western blotted for Filamin-a, $\beta 3$, Vim and Pxn.

Figure 3-3 Endothelial Cells Adhere to Fibronectin and Poly-L-Lysine



$\beta 3^{+/+}$ ECs were adhered to fibronectin (top row) or poly-l-lysine (bottom row) coated/BSA blocked coverslips for 90 minutes before fixing and immunostaining for neuropilin-1 (Nrp1-green) and talin-1 (Tln1-red) along with a nuclear stain (DAPI-blue). Scale bar = 10 μ m.

Quality Control and Experimental Design Development of Adhesome Enrichment

Ponceau-S staining, as seen previously in figure 3-2B, hinted at a possible way of screening for successful adhesome enrichments to use in downstream analysis. The * sample had clearly received insufficient shear washing. However to generate a Ponceau-S stain visible to the naked eye required use of the whole sample meaning it could not be used for anything other than screening ahead of a single western blot. Far more sensitive protein staining methods exist such as Coomassie or silver staining directly on the gel after SDS/PAGE. We wanted to investigate whether using 1/6 of the crosslinked material would be sufficient to screen for successful enrichments, which would leave 5/6 for western blotting or mass spectrometry. Although some Coomassie stains are compatible with mass spectrometry (and only a few silver stains), silver staining was chosen as the preferred method due to its greater sensitivity³¹⁸. Compatibility with mass spectrometry was not considered an issue as we were taking a fraction of the sample for testing and leaving the rest unstained for future analysis.

Figure 3-4A showed the comparison between high and low pressure shear washing using silver staining. Like earlier, the * sample had received insufficient washing compared to the other crosslinked material samples. Interestingly, the * sample closely resembled the RIPA lysate control samples indicating that a large amount of non-adhesome proteins must have remained after blasting and would not have represented a clean adhesome enrichment sample. Silver staining 1/6 of the crosslinked material directly on SDS/PAGE gels was therefore selected as the best screening method: if no bands were detected, then the sample was excluded (most likely due to crosslinking failure or sample loss during acetone precipitation); or if the crosslinked material resembled the RIPA lysate control, then the sample was also excluded.

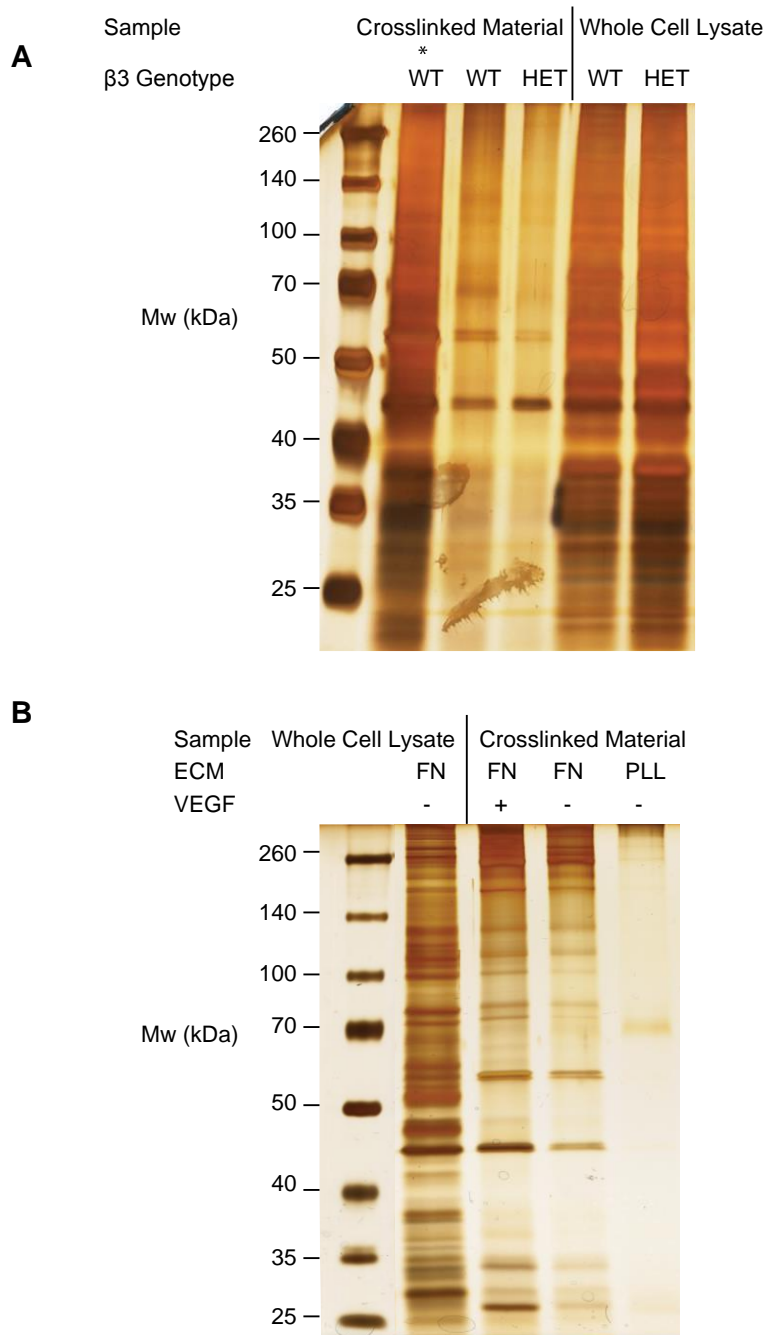
In order to generate a complete picture of the adhesome we needed to generate three datasets for every cell genotype/drug/condition to be tested – fibronectin, fibronectin with VEGF and PLL adhesomes. Fibronectin as a positive control and PLL as a negative control would be essential for defining the endothelial adhesome whereas fibronectin with VEGF would help identify proteins enriched in the adhesome during angiogenic responses. Not including a PLL with VEGF sample saved time and costs, a strategy employed by Schiller et al²³³ where fibronectin, fibronectin with blebbistatin and PLL adhesome enrichments were carried out to define the fibroblast adhesome and the role of myosin II which is inhibited

by blebbistatin³¹⁹. Like blebbistatin, VEGF was not expected to make a big impact on the PLL adhesome and fibronectin vs fibronectin with VEGF two sample comparisons would be able to identify proteins regulated by VEGF.

Silver staining, as well being used as a quality control, was also able to show protein differences between adhesome enrichments. For example, the differences between the FN crosslinked material samples were obvious compared to PLL which had fewer proteins can be seen in figure 3-4B. It was reassuring to observe proteins in the PLL sample as none were seen in the Ponceau-S staining (figure 3-2B); this meant that IMMLECs can both adhere to PLL and still generate a crosslinkable, enrichable adhesome – essential for identifying non-integrin dependent adhesion proteins. Figure 3-4B also revealed subtle differences with VEGF treatment in the crosslinked material therefore it was considered worth the investment to use VEGF treated samples in further analysis. Additionally there were fewer proteins stained in all three crosslinked material samples than the RIPA lysate control indicating successful enrichment. We used the silver stains shown in figure 3-4B as the standard to compare later adhesome enrichments to when carrying out quality control of samples.

Given the successful optimisation of all three kinds of adhesome enrichments we used the schematic outlined in figure 3-5 to generate data for further analysis. Many biological replicates of each type of adhesome enrichment were generated for $\beta 3^{+ / +}$, $\beta 3^{+ / -}$, $\beta 3^{- / -}$ and c(RGDfv) (a specific integrin $\alpha v \beta 3$ inhibitor) treated IMMLECs. The crosslinked material from these enrichments were subjected to silver staining as quality control, with three replicated matching the banding patterns seen in figure 3-4B pooled together. Pooled samples were then sent for Nano LC-MS/MS analysis using an LTQ Orbitrap mass spectrometer as per Schiller at el²³³. Each pooled sample was analysed three times via technical repeats through the mass spectrometer yielding three raw files each. The advantages for analysing pooled samples three times rather than analysing three individual samples once will be discussed below.

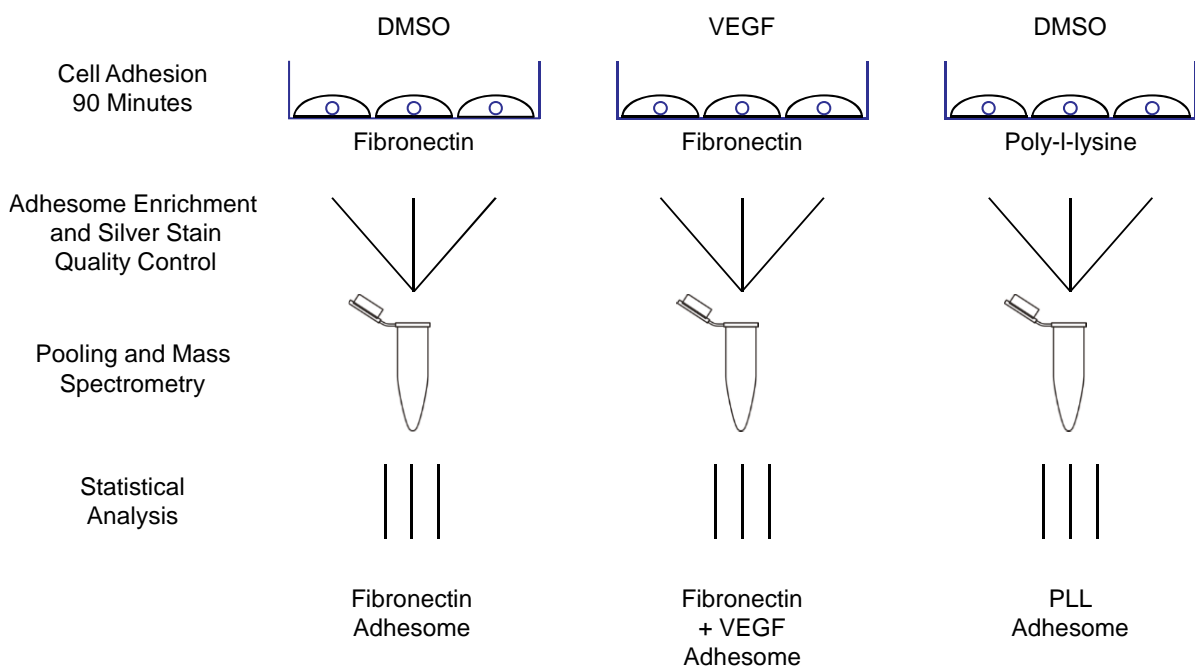
Figure 3-4 Silver Staining as an Indication for Successful Adhesome Enrichment



A Adhesome enrichment was carried out on $\beta 3^{+/+}$ and $\beta 3^{+/-}$ IMMLECs adhered to fibronectin or PLL for 90 minutes before being treated with crosslinkers (DSP/DPDPB), lysed with RIPA buffer then shear flow washed. Crosslinked material was eluted using DTT then acetone precipitated then run of a SDS-PAGE gel before being silver stained. All adhesome enrichments were carried out with high pressure RO water shear washing except * sample which used a Mill-Q[®] benchtop system. **B** Adhesome enrichment was carried out as above

with only $\beta 3^{+}/+$ IMMLECs adhere for 75 minutes before being stimulated with VEGF(+) or DMSO(-) for 15 minutes. Samples were then ran on an SDS-PAGE gel and silver stained.

Figure 3-5 Experimental Design for Defining the Endothelial Adhesome Incorporating Silver Staining Quality Control



A schematic of the experimental design for defining the endothelial adhesome. Triplicate adhesome samples that pass silver stain quality control from IMMLECs adhered to fibronectin or poly-l-lysine and treated with VEGF or DMSO are pooled into a single sample before being analysed by mass spectrometry. Statistical analysis of three LC-MS/MS repeats reveals the fibronectin and VEGF dependent adhesomes of endothelial cells.

Optimisation of MaxQuant Label Free Quantification

Thermo raw files, containing LC-MS/MS spectra, were obtained after sample analysis by LTQ Orbitrap. Briefly, three stages of computation analysis were carried out on the data: MS/MS spectra were identified as peptides using the Andromeda database³²⁰, peptides were matched to proteins predicted from the mouse genome and LFQ (Label free quantification) was carried out to work out the relative abundance of each protein in the samples. All of this was carried out using the quantitative proteomics software package MaxQuant³²¹.

Optimisation of MaxQuant parameters was carried out in order to generate the maximum useful amount of data from the limited three raw files per condition. MaxQuant, like any mass spectrometry software, has a greater chance of identifying and quantifying proteins with a greater number of technical repeats as shown in table 3-1 where increasing the number of samples included gave more protein identifications. Three repeats was the largest viable number of repeats attainable due to cost and time considerations. During optimisation, MaxQuant generated full data files outlining LFQ of proteins in samples however many of these were not useful for further consideration in the context of cell biology due to only a small number of files being analysed at any one time with sometimes incorrect methods. Hence only the metadata of these MaxQuant runs will be included in this thesis, not the full “test” files.

Quality of the MaxQuant runs was assessed using the number of unique proteins identified and the specific identification of the following proteins: β 3, α v, α 5, β 1, Nrp1, Rac1, Tln1 and VE-cadherin. Detection of the fibronectin binding integrins listed was considered critical in order to perform downstream analysis as well as the key focal adhesion marker Tln1. We had previously shown Nrp1 was detectable in the endothelial adhesome²¹⁸ therefore it was important to make sure the “depth” of the dataset was still good enough to do so again. Rac1 detection was considered important as it is a known transient member of the focal adhesions³²² and could have been present at low levels and therefore difficult to detect – much like Erk2/3 was studied previously (figure 3-2A). Finally VE-cadherin was included as an endothelial cell marker³²³ as its detection was evidence of endothelial identify in IMMLECs.

Table 3-1 shows the metadata results of the first four test runs of MaxQuant using adhesome enrichment samples that had been screened by silver staining previously as per figure 3-4. Test 1, as a benchmark, used default settings for MaxQuant which automatically

detected conditions used in the LC-MS/MS runs using the metadata associated with the supplied raw files. It showed that from six runs, 802 proteins could be detected however only 4/8 of the “quality” proteins were detected. Given the successful detection previously by western blot of most of these quality proteins then the failure to detect all eight indicated MaxQuant was not calibrated properly to analyse our LC-MS/MS runs. It was tempting to speculate that some of the undetected quality proteins are ones that are difficult to detect by mass spectrometry. This could be because these proteins do not produce many uniquely identifiable peptides after trypsin cleavage and ion fragmentation, or that the unique peptides they produce are inherently unstable and break down into non unique peptides (shared by other proteins in the sample) before being detected in the spectrometer³²⁴. However all of the chosen quality proteins have been detected by previous groups using mass spectrometry so it should have been possible to detect them in our samples as long as their abundance was not too low^{233,237,245,325}.

Comparing test 1 and test 2 showed us that the match between runs feature of MaxQuant was able to increase the quality of proteins detected in the sample. The match between runs algorithm allowed MaxQuant to use information from one sample to assist in peptide identification in another sample because they were both generated at the same time with identical experimental conditions. Briefly, if within sample X a peptide could be identified from an MS/MS spectra but not in the technical or biological repeats samples Y and Z, then the retention times of unidentified MS/MS spectra in samples Y and Z could be matched (within a certain tolerance depending on the specifications of the mass spectrometer) to the retention time of the successfully identified MS/MS spectra in sample X. If a match is found, then the previously unidentified but retention time matched MS/MS spectra of samples Y and Z are assumed to be the sample peptide identified in sample X – providing of course that the low quality MS/MS spectra in samples X and Y do not show enough information to disprove that assumption. Crucially, the quantification for the identified peptide (and later whole protein) is calculated only from the information in the single samples to give three separate and independently calculated quantifications³²⁶. In test 2, this feature allowed information from multiple runs to detect enough extra peptides to identify two extra quality proteins compared to test 1. The re-quantify feature, used in test 3 for the first time, did not significantly increase the number of proteins detected but also was not detrimental to the quality of the analysis so was used for all subsequent runs. Test 4 showed that more samples supplied to MaxQuant for analysis increased the number of proteins detected and quality, therefore in the next chapter, we aimed to analyse as many

samples simultaneously as was possible for defining the endothelial adhesome. This also meant it was preferable to analyse a single pooled sample three times rather than three individual samples once, as it allowed MaxQuant to achieve a better depth of analysis.

Although match between runs and re-quantify features had increased the quality of the runs, it was still not satisfactory and could have led to our subsequent analysis lacking a strong conclusion due to incomplete mass spectrometry readouts. We suspected that the crosslinkers used in the adhesome enrichment process, DSP and DPDPB, had permanently modified peptides despite the DTT reduction reversing the crosslinking process. These modified peptides would have different mass/charge ratios to unmodified peptides and therefore not match anything present in the Andromeda database so they would remain unidentified.

The DPDPB and DSP crosslinking reactions for adjacent proteins can be seen in figure 3-6A and 3-6B respectively. DPDPB, as a thiol reactive compound, crosslinks cysteine residues with the reducible/reversible sulphur-sulphur bond in close proximity whereas DSP, as an amine reactive compound, crosslinks lysine residues (or the N-terminus of proteins) with its reducible/reversible bond distant from the crosslinked protein. This meant that, as seen in figure 3-6C, DPDPB crosslinker reversal with DTT left the original proteins unchanged but DSP (in figure 3-6D) left behind part of its spacer arm. Adhesome enriched samples were generated by using these crosslinkers to stabilise the adhesome against high pressure shear washing, therefore most of the proteins in our samples were crosslinked with either DSP and/or DPDPB at least once. DPDPB treatment and reversal was “invisible” to MaxQuant but DSP permanently altered peptide mass/charge ratios. If any of these alterations occurred on unique peptides for important proteins then MaxQuant failed to identify these proteins, explaining why the quality of our runs was lower than expected.

Custom modifications can be added into Andromeda and one such modification was automatically included by MaxQuant to account for the acetamidation of thiols by IAA (Iodoacetamide). Disulphide bonds between adjacent cysteines in proteins are strong enough to resist fragmentation in mass spectrometry³²⁷. Therefore, it is common practise to permanently modify cysteines after reduction using IAA to prevent disulphide bonds reforming in downstream sample preparation, as carbamidomethylated cysteine residues cannot form these bonds. The reaction can be seen in figure 3-6E where IAA’s reaction with a thiol side chain is shown. IAA can potentially react with any thiol group so at this point it was unclear whether it would also react with the thiol group generated through the

reduction of DSP crosslinked proteins. If IAA was able to carbamidomethylate the products shown in figure 3-6D it was unknown if it would do so at the same rate as with normal cysteine residues as it could have been slower due to steric hindrance by the DSP spacer arm. Therefore we did not know if the IAA reaction would proceed to completion with reduced DSP crosslinked proteins (i.e. if every DSP modified protein would be carbamidomethylated).

New custom modifications were added to Andromeda searches to account for the possible peptide modifications outlined above: DSP-N-terminus, DSP-lysine, carbamidomethylated DSP-N-terminus and carbamidomethylated DSP-lysine. All of these modifications were included in the MaxQuant test 5 in table 3-2. Whilst this resulted in more proteins being identified than in test 3 (table 3-1) the quality was lower. This suggested that the IAA reaction with DSP treated proteins did proceed to completion and the unnecessary DSP-N-terminus/DSP-lysine modifications were causing MS/MS spectra to be misidentified. We speculated that, because there were no real DSP-N-terminus/DSP-lysine modifications in our samples, this was leading MaxQuant to identify incorrect proteins from the mislabelled MS/MS spectra where it thought it could see modified peptides. This also reduced the pool of correctly identified MS/MS spectra that could be used to search for the quality proteins we were looking for explaining the lower quality of test 5. In test 6 we removed DSP-N-terminus/DSP-lysine modifications but kept the carbamidomethylated versions. This gave a better quality result with less proteins identified so we believed we had removed the incorrect proteins seen in test 5.

In mass spectrometry sample preparation, trypsin was used to digest proteins before LC-MS/MS. Trypsin cleaves C terminally after arginine and lysine residues³²⁸ and the assumption that all proteins would be cleaved in this way before fragmentation into ions was used by MaxQuant to help in the identification of proteins. However trypsin cannot always access its cleavage site if the protein has been post-translationally modified, hence MaxQuant by default tries to account for up to two missed cleavages per protein during its identification algorithms^{239,321,329}. Carbamidomethylated DSP-lysine in our samples also had the potential to block trypsin cleavage therefore we increased the maximum number of permitted missed cleavages to from two to three or four in tests 7 and 8 respectively. Comparing test 6 and 7 revealed that allowing for an extra missed cleavage allowed MaxQuant to identify more proteins but test 8, despite identifying more proteins, gave a much lower quality readout. Test 8's failure was likely due to the same reason as test 5's failure – i.e. “four missed cleavage” proteins did not actually exist in our sample hence the

misidentified MS/MS spectra generated incorrect identifications and subtracted from correct identification of the quality proteins. In summary, the conditions of test 7 in table 3-2 were chosen for use in defining the endothelial adhesome.

Table 3-1 MaxQuant Test Runs – Parameter Optimisation

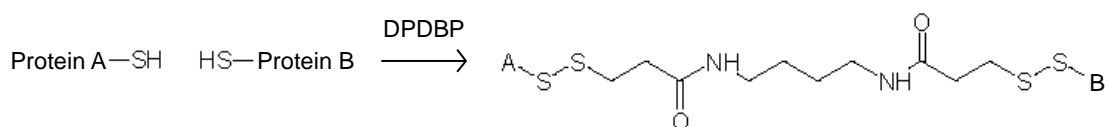
Test ID	Samples Included	MaxQuant Settings	Proteins Identified	Quality
1	FN-β3+/+(x3) and FN-β3+/+ with VEGF(x3)	Default	802	4/8
2	FN-β3+/+(x3) and FN-β3+/+ with VEGF(x3)	Match between runs	797	6/8
3	FN-β3+/+(x3) and FN-β3+/+ with VEGF(x3)	Match between runs; Re-quantify	799	6/8
4	FN-β3+/+(x3), FN-β3+/+ with VEGF(x3), FN-β3+/- (x3) and FN-β3+/- with VEGF(x3)	Match between runs; Re-quantify	977	7/8

Metadata from MaxQuant trial runs of adhesome enrichments from β3+/+ and β3+/- IMMLECs adhered to fibronectin with or without VEGF stimulation.

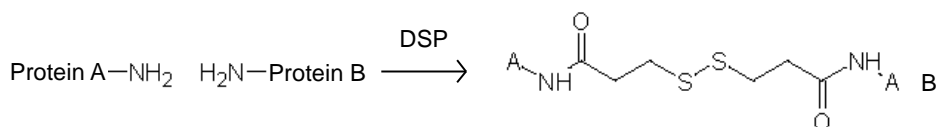
The effects of using MaxQuant setting “match between runs” and “re-quantify” as well as increasing amount of available data (samples included) are shown on the number of proteins identified and the quality of the datasets. Quality was assessed by successful identification of the following 8 proteins: β3, αv, α5, β1, Nrp1, Rac1, Tln1 and VE-cadherin.

Figure 3-6 Reactions of DSP, DPBBP, DTT and IAA in Protein Mass Spectrometry

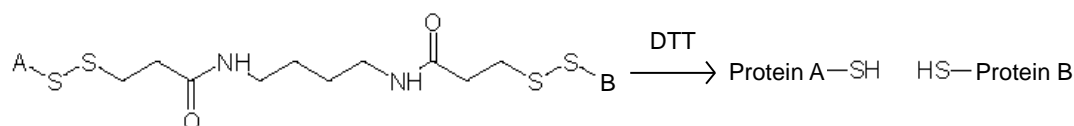
A



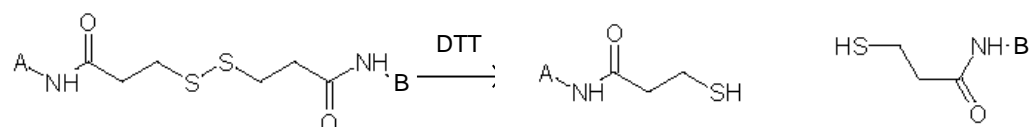
B



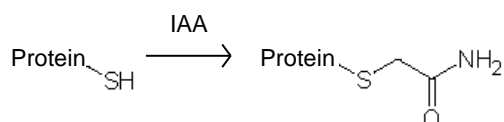
C



D



E



A Reaction of DPDBP crosslinker with adjacent cysteine residues. **B** Reaction of DSP crosslinker with adjacent lysine residues and/or protein n termini. **C** Reaction of the reducing agent DTT with DPDBP crosslinked proteins. **D** Reaction of the reducing agent DTT with DSP crosslinked proteins. **E** Reaction of IAA with thiol groups in proteins. Figure generated using freeware ACD/ChemSketch © Advanced Chemistry Development, Inc.

Table 3-2 MaxQuant Test Runs – Protein Modification

Test ID	Samples Included	MaxQuant Settings	Proteins Identified	Quality
5	FN-β3+/(x3) and FN-β3+/+ with VEGF(x3)	Match between runs; Re-quantify; DSP-lysine; DSP-N-terminus; Carbamidomethylated DSP-lysine; Carbamidomethylated DSP- N-terminus	937	5/8
6	FN-β3+/(x3) and FN-β3+/+ with VEGF(x3)	Match between runs; Re-quantify; Carbamidomethylated DSP-lysine; Carbamidomethylated DSP- N-terminus	856	8/8
7	FN-β3+/(x3) and FN-β3+/+ with VEGF(x3)	Match between runs; Re-quantify; Carbamidomethylated DSP-lysine; Carbamidomethylated DSP- N-terminus; 3 missed cleavages	872	8/8
8	FN-β3+/(x3) and FN-β3+/+ with VEGF(x3)	Match between runs; Re-quantify; Carbamidomethylated DSP-lysine; Carbamidomethylated DSP- N-terminus; 4 missed cleavages	942	6/8

Metadata from MaxQuant trial runs of adhesome enrichments from β3+/+ IMMLECs adhered to fibronectin with or without VEGF stimulation. Additional MaxQuant settings were tested compared to those in 3-1 to assess their effects on the number of proteins identified and the quality of the dataset. Different variable modifications were included in MaxQuant searches resulting from the residue left by the DSP crosslinker after DTT treatment and carbamidomethylation. Quality was assessed by successful identification of the following 8 proteins: β3, αv, α5, β1, Nrp1, Rac1, Tln1 and VE-cadherin.

Chapter four – Analysis of the Endothelial Cell and Integrin $\beta 3$ Dependent Adhesomes

The aim of this chapter is to identify a method of robust statistical analysis to identify the endothelial cell and $\beta 3$ adhesomes from the mass spectrometry data generated using adhesome enrichments. This would begin to identify pathways of interest for further in vitro and in vivo experimentation in later chapters.

Statistical Analysis of the Endothelial Cell Adhesome

In order to define the endothelial adhesome we needed to generate the following $\beta 3/+$ IMMLEC samples: three fibronectin adhered, three fibronectin adhered with VEGF stimulation and three poly-l-lysine adhered. Additionally we needed to define the $\beta 3$ dependent endothelial adhesome using $\beta 3+/-$ and $\beta 3-/-$ IMMLECs later. Given that all sets of samples would have been generated using the same techniques and subjected to the same kinds of statistical analysis it was tempting to generate all samples simultaneously in order to minimise variations between experiments. Long term stability of crosslinking reagents could have, for example, been an issue for generating consistent adhesome samples as they are susceptible to hydrolysis³⁰⁶ and hence degrade over time in normal laboratory conditions. Other experimental variations such as day to day changes in water pressure for high shear washing could have also created large discrepancies between samples not collected at the same time. Our own experience showed that generating adhesome samples on different days gave unacceptable variations between what should have been identical samples. Figure 4-1A showed that samples generated from the same IMMLECs with the same conditions ($\beta 3/+$ on fibronectin) but on different days had a lower correlation than samples generated on the same day with different conditions such as $\beta 3/+$ on fibronectin vs $\beta 3/+$ on fibronectin with VEGF stimulation, seen in figure 4-1B. In a sense, our no VEGF to plus VEGF variations were smaller than our day to day variations i.e. the signal to noise ratio was too low for any meaningful conclusions. This mirrored experiences by Schiller et al²³³ who advised us personally about the need for carrying out all sample generation at once.

However, generating so many samples at once turned out to be impractical given the number of IMMLECs required (five repeats of 6 million IMMLECs per condition) and the processing time required for different stages of enrichment meant having too many samples to process severely impacted our ability to generate useful enrichments. As a

solution, we decided to generate our samples in stages depending on which comparisons we wanted to make. Therefore $\beta 3^{+}/+$ vs $\beta 3^{+}/-$ samples were generated separately from $\beta 3^{+}/+$ vs $\beta 3^{-}/-$ samples (etc. . .). This did create duplicate $\beta 3^{+}/+$ samples but we discovered these could be averaged using MaxQuant to give acceptable correlations between samples, as shown in figure 4-1C.

Our endothelial adhesome data was therefore much more robust than originally planned: three $\beta 3^{+}/+$ day one samples were pooled together and analysed three times by LC-MS/MS; three $\beta 3^{+}/+$ day two samples were pooled together and also analysed by LC-MS/MS three times; this was carried out for all three matrices/conditions. The six LC-MS/MS runs were analysed in three pairs using MaxQuant – $\beta 3^{+}/+$ day one repeat one with $\beta 3^{+}/+$ day two repeat one and so on. The initial MaxQuant dataset, shown in supplementary table 1, contained 1497 identified proteins with LFQ values. MaxQuant, by default, contains FASTA information for common contaminant proteins such as human keratins from skin/hair found in most laboratories, bovine serum proteins found in the BSA fractions used in blocking fibronectin or poly-l-lysine plates and pig trypsin which was used to digest proteins prior to LC-MS/MS analysis. Most of these were identified in our initial dataset along with other human contaminants, but as we were working with mouse derived cells these were easily identified amongst our genuine hits, and subsequently removed. Additionally, MaxQuant controlled for false discoveries by reversing all protein sequences predicted from the mouse genome and searched for their possible existence in our LC-MS/MS runs. Several were identified in our initial dataset which were used to estimate our false discovery rate (used later in statistical calculations). After removal of contaminant and reverse-identified proteins we also filtered our datasets by removing proteins that were not detected in all three LC-MS/MS repeats generated from one pooled sample. We hoped this would give us a reliable and stringent dataset to be used to define the endothelial adhesome. Finally the LFQ values were normalised by a log base 2 transformation and missing values were imputed from the total dataset to fill 0 (undetected) values with low LFQ values. This served to generate normal distributions and fill invalid numbers generated by the log transformation of 0, both of which were necessary for statistical tests carried out later. These data transformations were carried out using Perseus, a statistics programme developed specifically to carry out typically used analyses in mass spectrometry investigations³⁰², as well as all further statistical analysis mentioned in this thesis.

As a first stage of analysis, unsupervised hierarchical clustering based on average Euclidian distance was carried out using the normalised LFQ values to identify clusters of co-regulated proteins in the context of matrix type or VEGF stimulation. This allowed us to distinguish genuine fibronectin adhesome proteins from poly-l-lysine bound nonspecific adhesion proteins as well as any proteins over-represented upon VEGF stimulation i.e. those whose inclusion in the adhesome is VEGF dependent. In figure 4-2, we show that our LC-MS/MS repeats cluster together horizontally, confirming that they all give very similar results. We defined 12 vertical clusters using a distance threshold of 3.34. Based on similar expression patterns between some adjacent clusters we defined clusters A to C as VEGF-enriched proteins, D to F as fibronectin enriched proteins or the non-VEGF adhesome and G-L as poly-l-lysine enriched proteins. As our clusters were based on Euclidian distance and not human intuition and could not therefore be defined manually without the risk of biasing our results, we decided on 12 clusters as this gave the clear separation of A-C, D-F and G-L without introducing too many unnecessary clusters. For example, by eye it appears cluster F should be easy to separate into smaller clusters but the unsupervised clustering algorithm would have only done this after defining many other clusters first.

At this point we also added several annotations to our dataset from publically available GO (Gene ontology)²⁴¹ and KEGG (Kyoto encyclopaedia of genes and genomes)³³⁰ databases, which link proteins together that are known to have similar roles (GOBP), functions (GOMF), sub-cellular localisation (GOCC) or biological pathway (KEGG pathway). Annotation and hierarchical clustering information were combined to generate supplementary table 2 where all 1064 proteins that were clustered after data filtering (see above) are shown along with their corresponding cluster. Additionally, proteins with angiogenesis associated annotations are shown highlighted at the top. Many of the highlighted proteins are specific to endothelial cells confirming the endothelial identity of the IMMLECs used in our investigations as well as other markers in the rest of the table such as VE-cadherin. Supplementary table 2 and figure 4-2 as shown represent our complete endothelial cell adhesome.

Following up changes in 1064 proteins in our endothelial cell adhesome would have been inappropriate and time consuming, especially as we had not yet considered statistical significance, therefore we decided to identify what types of proteins were over-represented in the VEGF, fibronectin or poly-l-lysine groups of clusters. Performing Fisher's exact t tests³³¹ allowed us to investigate "enrichment" using our clustering and annotation datasets. All annotations that passed the FDR (False discovery rate) threshold and were

hence significantly enriched or depleted in the VEGF, fibronectin or poly-l-lysine clusters are listed in table 4-1. Leukocyte trans-endothelial migration (KEGG, $p=9.71 \times 10^{-5}$) proteins were enriched in the fibronectin adhesome but not the VEGF adhesome suggesting our cells represent quiescent vasculature without VEGF-stimulation, as intended. This category also includes many endothelial specific CAMs (Cell adhesion molecules) that have not been detected in other cell adhesomes³³². Critically the focal adhesion category (KEGG, $p = 9.31 \times 10^{-7}$) was enriched in the fibronectin adhesome but also significantly depleted in the poly-l-lysine adhesome ($p= 9.49 \times 10^{-5}$). This finding confirmed to us that the entire process of adhesome enrichment was working successfully, from sample generation to mass spectrometry to statistical analysis, in order for focal adhesion proteins to successfully cluster and be enriched only on fibronectin and not poly-l-lysine. Also reassuring was that many other cell adhesion/migration associate categories were significantly depleted in the poly-l-lysine adhesome: focal adhesion (GOCC, $p=5.99 \times 10^{-5}$), cell projection (GOCC, $p=3.03 \times 10^{-5}$), cell adhesion (GOBP, $p=1.61 \times 10^{-6}$) and lamellipodium (GOCC, $p=1.38 \times 10^{-4}$). These categories were not detected as significant enrichments in the fibronectin (D to F) clusters due to them being separated from the VEGF (A to C) clusters, which were also adhered to fibronectin, when running the Fisher's exact t test. This was done to prevent unnecessary repetition of results.

Separating fibronectin with VEGF and fibronectin without VEGF groups of clusters for enrichment analysis allowed us to detect enrichment of the cell projection category (GOCC, $p=8.62 \times 10^{-5}$) in the adhesome with VEGF stimulation. Given that VEGF induces migration in endothelial cells³³³, normally towards a hypoxic area in response to injury or a tumour, we speculated that the short VEGF stimulation time of 15 mins was sufficient to start this process – beginning with cell projection. Therefore we knew that our VEGF was having the correct effect on our cells under the adhesome enrichment conditions. VEGF stimulation also caused an enrichment of microtubule proteins (GOCC, $p=1.6 \times 10^{-4}$). Microtubules are important to many processes within cell migration, see review by Etienne-Manneville for more information²⁷⁹, and are also known to be involved in VEGFR2 downstream signalling and sorting in response to VEGF²⁸⁶. Given microtubules' known roles in regulating migration, their enrichment in the adhesome suggested that their role in endothelial cell migration was related to focal adhesions.

Another way to visualise the endothelial adhesome was to create an interaction map. Publically available protein-protein interaction databases are commonly used in mass spectrometry investigations to illustrate how networks can be formed between proteins

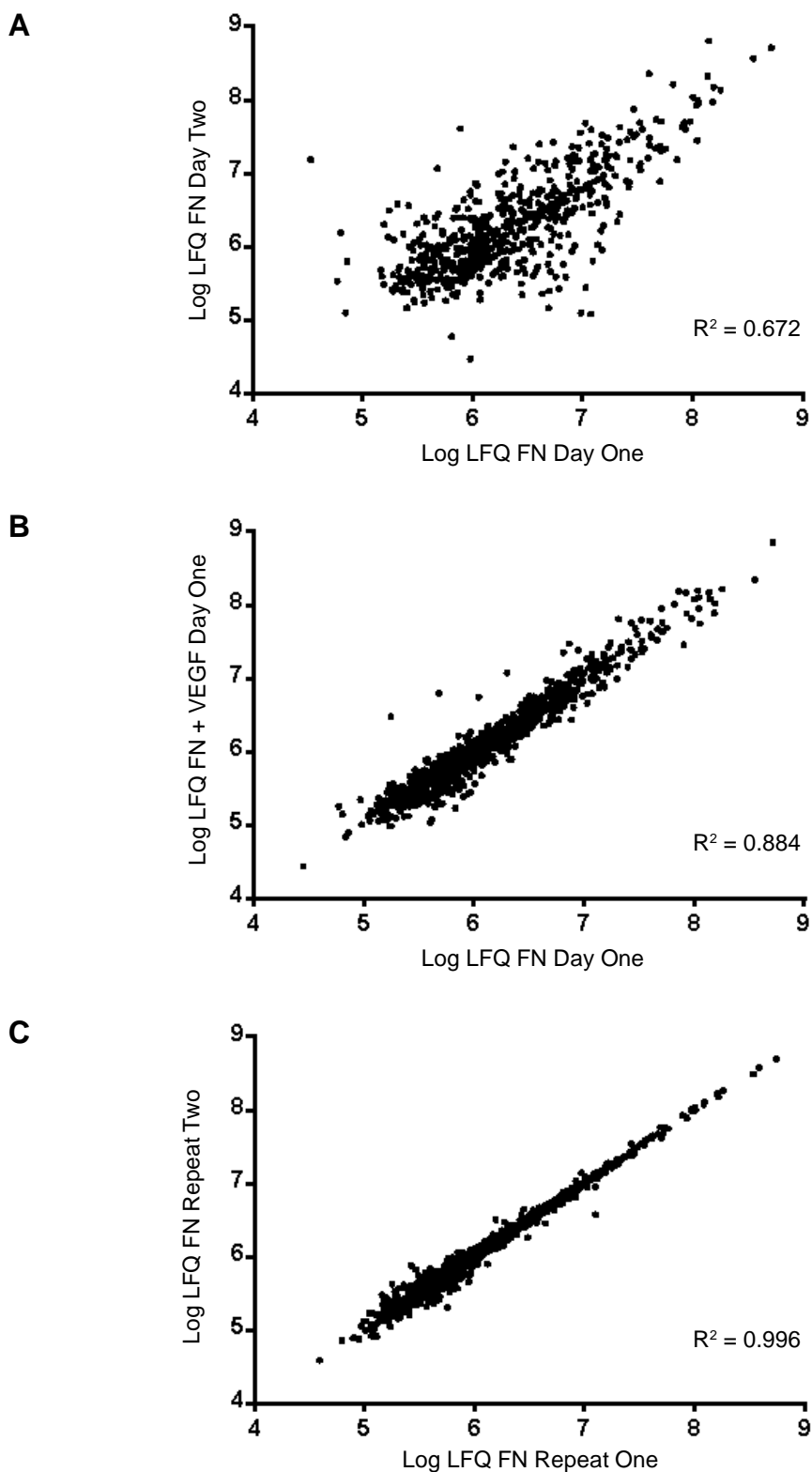
detected. This would help us detect interesting “nodes” or convergent points in our networks that could be manipulated to affect endothelial cell behaviour. Many different protein-protein interaction databases exist, each created from different types of experiments or computationally predicted instead. We chose to use the PINA (Protein interaction network analysis platform) database because it contains a compilation of six manually curated databases - MIPs MPact, HPRD, DIP, BioGRID, MINT and IntAct³³⁴. Another advantage of PINA was that the creators have already filtered out duplicate entries that would have been created from the merging of the six parent databases to create a non-redundant dataset³³⁵. We were able to probe the PINA database to obtain the interactions of our 1064 proteins in the endothelial adhesome. For example β 3 interactors included: α v, Pxn and Filamin-a. Showing the protein-protein interactions of 1064 would be impractical to display, instead we chose to initially create a network for the fibronectin clusters (D-F) defined in figure 4-2 and only show proteins up to two connections from the fibronectin binding integrins detected. Cytoscape, a network interaction visualisation tool designed especially for biomolecular applications³³⁶, was used to visualise the fibronectin (clusters D-F) adhesome in figure 4-3.

Many ribosomal protein were detected in the fibronectin adhesome and labelled black in figure 4-3 where they formed a strong interacting network, indicated by their close proximity derived from the preferred layout algorithm of Cytoscape. It was tempting to speculate that ribosomes/ribosomal proteins are present exclusively in the fibronectin adhesome and not in non-integrin or other adhesomes. However no significant enrichment of such proteins was detected in fisher exact t tests seen in table 4-1. Some ribosomal categories, such as translation pre-initiation and RNA transport, were actually enriched in the poly-l-lysine adhesome which led us to believe instead that these ribosomal proteins are not specific to the fibronectin adhesome. There is some evidence to suggest that proteins can be synthesised at the edges of distance cells and that ribosomes can be targeted to β 3 adhesions³³⁷ therefore it would be interesting to follow these proteins when we studied the β 3 adhesome later. It is worth noting that many of these ribosomal proteins are notoriously nonspecific interactors in mass spectrometry experiments and are well represented in the contaminant repository for affinity purification-mass spectrometry data³³⁸.

Figure 4-3 also demonstrated that Ilk, Pxn, Fak1 and Vcp (Vasolin containing protein), with their unique coloured edges, are key nodes in the endothelial adhesome due to their high number of interactors. If we wanted to influence adhesion of endothelial cells to

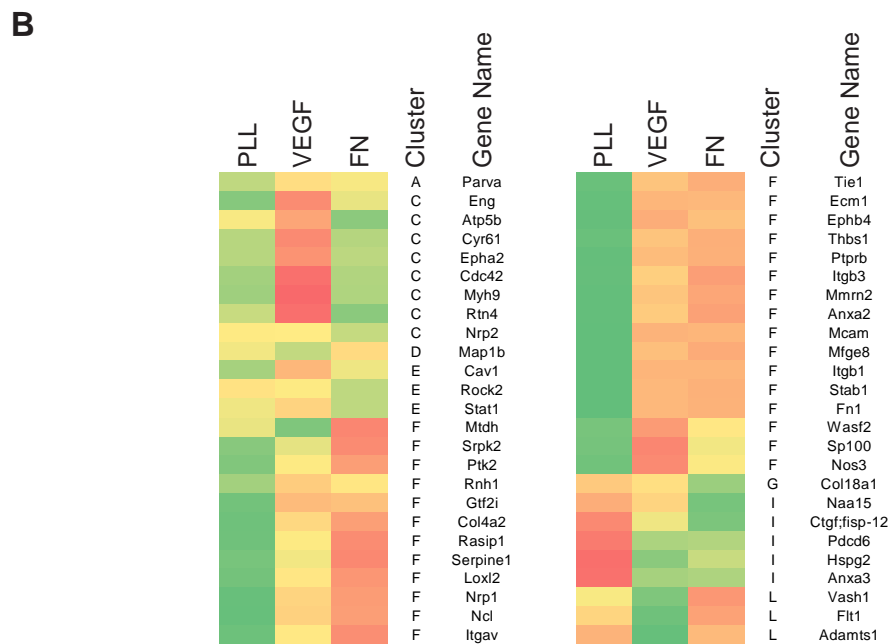
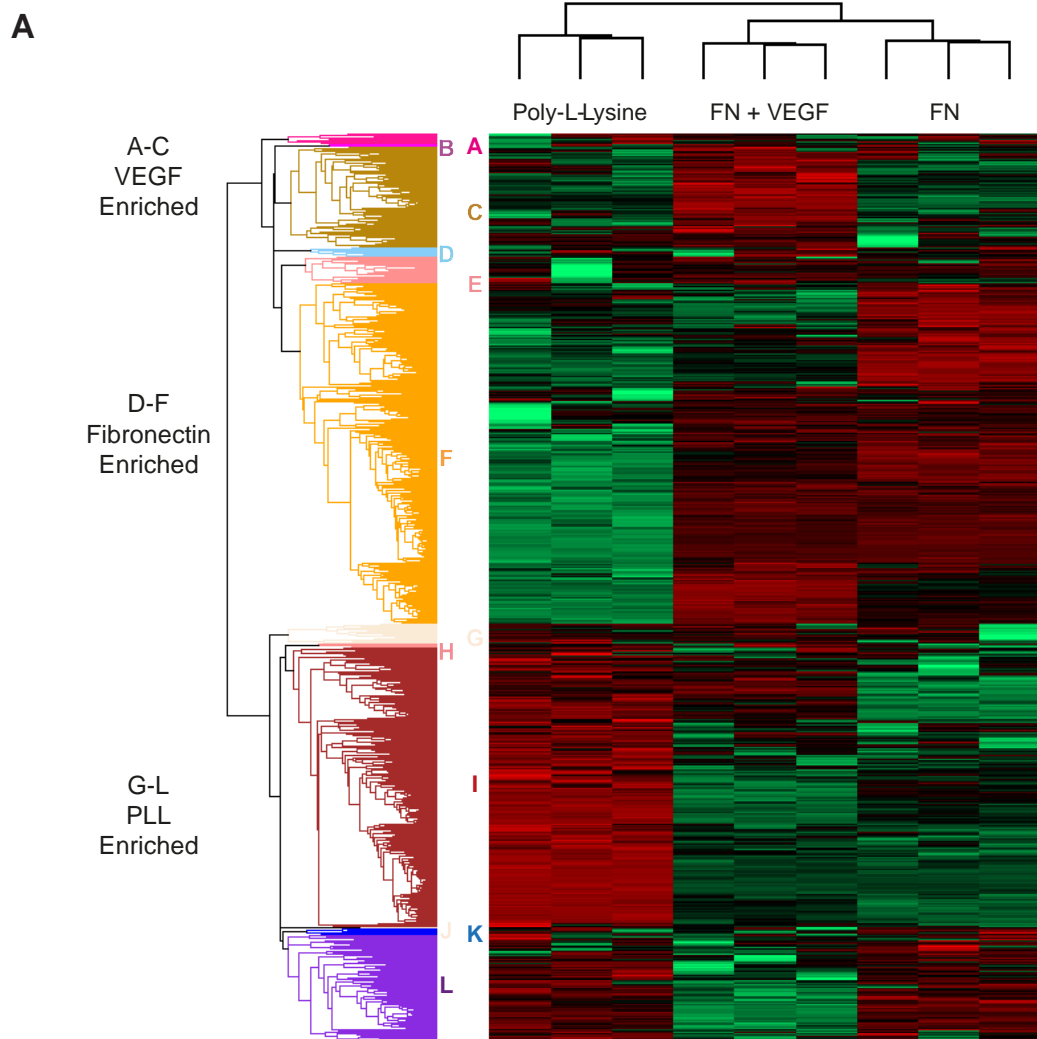
fibronectin then manipulating these four proteins could be a good place to start. Pxn and Fak1 are critical members of focal adhesions, hence their use in optimisation of the adhesome enrichment technique in chapter 3. Ilk, as a kinase, is ubiquitously expressed and essential to the functioning of focal adhesions as it allows integrins who have no intrinsic enzymatic activity to signal downstream as part of outside-in signalling for example³³⁹. It was therefore not surprising that Pxn, Fak1 and Ilk were found as important components in the endothelial adhesome but due to their ubiquitous nature, they would probably not be useful in specifically targeting endothelial cells in anti-angiogenic therapies. Vcp is thought to function as a chaperone and endocytosis regulator^{340,341} but is not known to have any role in angiogenesis or cell migration. Therefore it was possible its position in the endothelial adhesome was due to its localisation near the cell membrane for endocytosis and showed a high number of edges in interaction analysis due to its chaperone abilities.

Figure 4-1 Correlations between Adhesome Samples



Log LFQ values from MaxQuant analysis of $\beta 3^{+/+}$ IMMLECs adhesome samples: **A** fibronectin day one and fibronectin day two, **B** fibronectin day one and fibronectin with VEGF day C and **C** Fibronectin repeat one (average day one and two) and fibronectin repeat two (average day one and two). R^2 correlation is shown for each graph.

Figure 4-2 Hierarchical Clustering of the Endothelial Adhesome



A Unsupervised hierarchical clustering based on Euclidian distance threshold of 3.34 of three fibronectin, three fibronectin with VEGF and three poly-l-lysine $\beta 3^{+}/+$ IMMLEC adesome samples. Clusters were labelled A-L. Generated using Perseus analysis of MaxQuant output. Red indicated high expression and green indicated low expression. **B** Angiogenesis associated proteins were defined using the GOBP annotations: GO:0001525, GO:0002040, GO:0002042, GO:0016525, GO:0045765 and GO:0045766 and displayed in a heatmap (red high expression and green low expression) with their clusters as defined by panel A. The heatmap represents the average Z-score from 3 poly-l-lysine adhesomes (PLL), 3 fibronectin + VEGF adhesomes (VEGF) and 3 fibronectin adhesomes (FN).

Table 4-1 Enrichment Analysis of the Endothelial Adhesome

Clusters	Category column	Category value	Category size	Intersection size	Enrichment factor	P value	Benj. Hoch. FDR
VEGF	GOCC name	mitochondrial inner membrane	19	11	4.6316	2.25E-06	3.93E-04
VEGF	GOCC name	organelle inner membrane	24	12	4	5.75E-06	8.60E-04
VEGF	GOCC name	mitochondrial membrane	25	12	3.84	9.77E-06	1.36E-03
VEGF	GOCC name	microtubule	41	14	2.7317	1.60E-04	9.85E-03
VEGF	GOCC name	myelin sheath	66	20	2.4242	4.26E-05	3.72E-03
FN	KEGG name	Arrhythmogenic right ventricular cardiomyopathy (ARVC)	17	16	2.2708	6.52E-06	1.27E-03
PLL	GOCC name	eukaryotic 43S preinitiation complex	12	12	2.1714	8.46E-05	6.11E-03
PLL	GOCC name	eukaryotic 48S preinitiation complex	13	13	2.1714	3.84E-05	3.66E-03
PLL	GOCC name	eukaryotic translation initiation factor 3 complex	12	12	2.1714	8.46E-05	5.90E-03
PLL	GOCC name	proteasome accessory complex	12	12	2.1714	8.46E-05	5.71E-03
PLL	GOCC name	small nuclear ribonucleoprotein complex	21	21	2.1714	6.70E-08	2.00E-05
PLL	GOCC name	translation preinitiation complex	13	13	2.1714	3.84E-05	3.50E-03
PLL	KEGG name	Proteasome	21	20	2.068	1.72E-06	5.02E-04
FN	KEGG name	Leukocyte transendothelial migration	22	18	1.974	9.71E-05	8.12E-03
PLL	GOCC name	proteasome complex	22	20	1.974	1.04E-05	1.36E-03
FN	KEGG name	Focal adhesion	46	35	1.8357	9.31E-07	5.44E-04

VEGF	GOCC name	cell projection	145	33	1.8207	8.62E-05	5.64E-03
PLL	KEGG name	RNA transport	43	32	1.6159	8.28E-05	9.69E-03
PLL	KEGG name	Spliceosome	62	44	1.541	2.70E-05	3.95E-03
PLL	GOCC name	catalytic step 2 spliceosome	53	37	1.5159	1.99E-04	9.91E-03
PLL	GOCC name	nuclear speck	53	37	1.5159	1.99E-04	9.68E-03
PLL	GOCC name	nucleoplasm part	119	80	1.4598	4.25E-07	9.88E-05
FN	GOCC name	nucleolus	221	127	1.3865	2.97E-08	2.07E-05
FN	GOCC name	intracellular non-membrane-bounded organelle	402	208	1.2484	4.09E-08	2.14E-05
FN	GOCC name	non-membrane-bounded organelle	402	208	1.2484	4.09E-08	1.71E-05
PLL	GOCC name	protein complex	380	210	1.2	2.15E-06	4.10E-04
PLL	GOCC name	macromolecular complex	575	304	1.148	3.93E-07	1.03E-04
FN	GOCC name	macromolecular complex	575	204	0.85598	5.15E-06	8.29E-04
FN	GOCC name	protein complex	380	123	0.78095	2.03E-06	4.25E-04
PLL	GOCC name	intracellular non-membrane-bounded organelle	402	140	0.75622	3.33E-09	6.97E-06
PLL	GOCC name	non-membrane-bounded organelle	402	140	0.75622	3.33E-09	3.49E-06
PLL	GOCC name	plasma membrane	189	64	0.7353	6.11E-05	4.57E-03
PLL	GOCC name	cell junction	197	66	0.72748	2.68E-05	2.80E-03
PLL	GOCC name	cell-substrate adherens junction	155	50	0.70046	5.99E-05	4.82E-03
PLL	GOCC name	focal adhesion	155	50	0.70046	5.99E-05	4.64E-03

PLL	GOCC name	cell-substrate junction	156	50	0.69597	4.55E-05	3.81E-03
PLL	GOCC name	anchoring junction	167	53	0.68914	1.65E-05	1.92E-03
PLL	GOCC name	adherens junction	164	52	0.6885	1.92E-05	2.12E-03
PLL	GOCC name	cell projection	145	45	0.67389	3.03E-05	3.02E-03
PLL	GOCC name	nucleolus	221	67	0.65831	4.09E-08	1.43E-05
PLL	GOBP name	cell adhesion	80	17	0.46143	1.16E-06	8.02E-03
PLL	KEGG name	Focal adhesion	46	9	0.42484	9.46E-05	9.22E-03
PLL	GOCC name	lamellipodium	36	6	0.3619	1.38E-04	8.76E-03
FN	KEGG name	Cell cycle	17	0	0	1.02E-04	7.46E-03
FN	GOCC name	small nuclear ribonucleoprotein complex	21	0	0	1.14E-05	1.40E-03

All significantly enriched or depleted GOMP, GOBP, GOCC or KEGG categories in fibronectin with VEGF (VEGF), fibronectin (FN) or poly-l-lysine (PLL) clusters of the endothelial adhesome defined in figure 4-2 that were detected by Fisher's exact t test's.

Interaction network of only fibronectin adhesome proteins (cluster D-F from figure 4-2) detected in the endothelial adhesome. Mouse and human PINA interaction data was mapped onto the endothelial adhesome in supplementary table 2 using cytoscape. Human gene names are shown in blue except for those of ribosomal proteins which are shown in black. Interactions (edges) are shown in black except for Ilk (red), Pxn (purple), Fak1 (orange) and Vcp (green). Only proteins two interactions from fibronectin binding integrins are shown.

Statistical Analysis of the Integrin $\beta 3$ Dependent Adhesome

Given that $\beta 3^{+/-}$ and $\beta 3^{-/-}$ adhesome samples had been generated separately, due to the day to day consistency problem (outlined above and illustrated in figure 4-1), their statistical analyses were also carried out separately. Normal statistical techniques such as t-tests could not be used here. This was because our datasets contained over 1000 proteins meaning that a standard t-test would indicate 50 proteins to be significantly different with a p value cut off of less than 0.05 by random chance. This could have generated too many unconnected pathways for us to investigate further that would have detracted from unravelling the role of $\beta 3$ in the endothelial adhesome. An appropriate test would have been an ANOVA (Analysis of Variance) test, however this has several assumptions such as a normal distribution and an equal variance in protein changes³⁴². Whilst a normal distribution was corrected for in our data using imputation, equal variances could not be assumed. For example, it could have been possible that in $\beta 3^{-/-}$ cells there were significant changes in proteins that exclusively bind to $\beta 3$ but other proteins that can also bind $\beta 1$ might not have been affected as much.

Similar problems exist in other areas of biological research such as in the analysis of microarray data that produces long lists of genes for which the expression varies between two conditions. A new method of analysis was developed called the Significance Analysis of Microarrays (SAM) method. This carried out independent t tests for each gene/protein in the dataset, but to avoid returning every protein with a p value of less than 0.05 SAM also carries out many randomised permutations (250 in our analysis) to determine if the response in any one protein is different to the response of the whole sample (i.e. to account for proteins that tend to correlate³⁰¹). This permutation based FDR was used to eliminate false positives in our data. Application of SAM to $\beta 3^{+/+}$ vs $\beta 3^{+/-}$ and $\beta 3^{+/+}$ vs $\beta 3^{-/-}$ fibronectin datasets was carried out separately and is shown in supplementary tables 3 and 4 where 269 and 137 proteins respectively were found to be significantly increased (right side of SAM) with Itg3 depletion or significantly decreased in the $\beta 3^{+/+}$ (left side of SAM). Fewer proteins changing significantly was originally considered somewhat counter-intuitive. It was tempting to speculate that a more dramatic change in $\beta 3$ levels in the $\beta 3^{-/-}$ cells would result in a greater number of changes to the adhesome. However we believed that total deletions of $\beta 3$ would result in compensation for the loss of the integrin, such as those seen in $\beta 3^{-/-}$ cells when levels of Flk1 are elevated and drive increased angiogenesis²¹⁵⁻²¹⁷. The compensation by Flk1, possibly through Nrp1 regulation by $\beta 3$ ⁵² and other mechanisms, could have been preventing the need for more dramatic changes in

the adhesome. Moreover, studies in $\beta 3^{-/-}$ cells/animals have been criticised previously as they were not considered physiologically relevant hence there have been efforts to repeat studies in $\beta 3^{+/-}$ or transiently depleted situations^{218,223}. These studies better mimicked $\beta 3$ status when it has been targeted physiologically by current or future generations of integrin inhibitors as it is considered unlikely that any compound, with limitations due to pharmacokinetics, would be able to inhibit all $\beta 3$ in an animal. This could explain why we saw a greater number of statistically significant changes in the $\beta 3^{+/-}$ adhesome than the $\beta 3^{-/-}$ adhesome; that the $\beta 3^{+/-}$ cells do not undergo compensation for the complete loss of $\beta 3$ but instead reveal more about the role of $\beta 3$ in the endothelial adhesome. We still continued to study the $\beta 3^{-/-}$ adhesome though, as the full extent of the compensation mechanisms is of continued interest. Also interesting was that in the $\beta 3^{+/-}$ adhesome, 175 proteins were significantly increased whereas only 94 were decreased in response to $\beta 3$ depletion. In the $\beta 3^{-/-}$ adhesome there were 88 proteins significantly increased and only 49 decreased. Interestingly, in both cases, $\beta 3$ depletion resulted in a greater number of proteins being incorporated into the adhesome than lost despite the apparent loss of an integrin and its cytoplasmic tail as a scaffold for assembly of the outside-in and inside-out signalling machinery³⁴³. This suggested to us that $\beta 3$ may actually be playing a dominant negative role in the adhesome by actively preventing certain proteins from being recruited.

To begin to fully understand the roles of $\beta 3$ in the adhesome, we started by analysing which pathways, cell components, or processes were represented in the $\beta 3^{+/-}$ and $\beta 3^{-/-}$ adhesomes by enrichment analysis as was carried out for defining the $\beta 3^{+/+}$ endothelial adhesome earlier. Tables 4-2 and 4-3 show any categories significantly enriched in the $\beta 3^{+/-}$ and $\beta 3^{-/-}$ adhesomes respectively calculated by Fisher's exact t test. Hierarchically defined clusters from figure 4-2 and supplementary table 2 were also added as annotations, in addition to the normal KEGG, GOCC, GOBP and GOMF annotations, to the $\beta 3^{+/-}$ and $\beta 3^{-/-}$ adhesomes, which allowed us to determine if any of our endothelial adhesome clusters were also significantly enriched upon $\beta 3$ depletion. Initially there were no obvious categories enriched that could easily reveal the role of $\beta 3$ in the endothelial adhesome or the compensation mechanism in $\beta 3^{-/-}$ cells. Taken together with the SAM statistical tests applied earlier, we speculated that the majority of individual focal adhesome components in the endothelial adhesome do not change significantly upon $\beta 3$ depletion. This could have been due to the ability of $\alpha 5\beta 1$ to compensate for the majority of $\alpha \beta 3$'s roles or that the changes in $\beta 3$ are more subtle and only involve certain proteins and not whole pathways, after-all the depletion of $\beta 3$ is not detrimental to the ability of

IMMLEC to adhere or migrate (see figure 5-5). This was demonstrated by the depletion of cytoskeletal parts (GOCC, $p = 4.73 \times 10^{-5}$) from the $\beta 3^{+/+}$ adhesome and a corresponding enrichment in the $\beta 3^{+/-}$ adhesome ($p = 7.01 \times 10^{-5}$) in table 4-2 which suggested that downstream connections to cytoskeletal components change upon $\beta 3$ depletion. Alterations in connections from the cytoskeleton to the adhesome suggested that $\beta 3$, whilst not making a large contribution to the composition of the adhesome, could have an important influence in cellular behaviour through the cytoskeleton. Additionally, there was no indication that ribosomes or ribosomal proteins were of interest to $\beta 3$ depleted adhesion despite their representation in the endothelial adhesome in figure 4-3.

Some interesting enrichments, though, were apparent in the $\beta 3^{+/-}$ adhesome. Table 4-2 showed the enrichment of several endoplasmic reticulum categories in the $\beta 3^{+/-}$ adhesome: protein processing in endoplasmic reticulum (KEGG, $p = 4.01 \times 10^{-7}$), endoplasmic reticulum part (GOCC, $p = 1.21 \times 10^{-7}$) and endoplasmic reticulum (GOCC, $p = 1.39 \times 10^{-6}$). These enrichments suggested the endoplasmic reticulum has become targeted to focal adhesions in $\beta 3^{+/-}$ cells. The endoplasmic reticulum is known to extend along microtubules to focal adhesions where it increases their growth and promotes cell spreading and migration³⁴⁴⁻³⁴⁷. Interestingly microtubule targeting to focal adhesions is thought to destabilise the focal adhesions¹⁹¹ but this destabilisation does not occur when the endoplasmic reticulum also targets focal adhesions³⁴⁸. It was therefore decided important to assess specifically how microtubules were behaving in the endothelial adhesome given that cytoskeletal parts are depleted in $\beta 3^{+/-}$ cells (table 4-2) and microtubules can be recruited to the adhesome with VEGF stimulation (table 4-1) – see figure 5-2 later. Table 4-3, the enrichment analysis of the $\beta 3^{-/-}$ adhesome, showed that several categories of proteins with the ability to bind nucleotides were enriched, specifically those that could bind purines such as ATP (Adenosine Tri Phosphate). The enriched GOMF annotations did not provide much information about what pathways have been potentially enriched in the $\beta 3^{-/-}$ adhesomes as many proteins have the ability to bind ATP. We speculated that this means that $\beta 3^{-/-}$ cells, with their increased complement of ATP binding proteins in the adhesome and therefore near the cell surface, could be “triggered” by ATP signals at lower concentrations than $\beta 3^{+/+}$ cells which potentially explains why $\beta 3^{-/-}$ cells show enhanced angiogenic responses²¹⁵. Increased competition for ATP may also affect $\beta 3^{-/-}$ cells in more specific ways as many signalling proteins important in angiogenesis and focal adhesion regulation use ATP such as Fak1 which can be influenced by both intracellular³⁴⁹ and extracellular³⁵⁰ ATP concentrations. Finally, we

observed that cluster F (fibronectin adhesome) was significantly depleted in both $\beta 3+/-$ and $\beta 3-/-$ adhesomes suggesting there was a conserved core of proteins that can only be recruited to the adhesome by $\beta 3$ and cannot be compensated for by other integrins/mechanisms. The proteins must have been present in cluster F of our $\beta 3+/+$ cell adhesome and hence any depletion of $\beta 3$ resulted in somehow different adhesions. Regardless of whether $\beta 3$ is considered pro or anti-angiogenic in any particular context, see review by Atkinson et al²²⁴, we now realised that targeting $\beta 3$ can have a unique and definitive effect on focal adhesions, meaning properly directed therapies could be developed for potential pro or anti-angiogenic outcomes.

We next decided to utilise our interaction database generated for the endothelial adhesome in figure 4-3 to investigate if $\beta 3$ depletion can affect important nodes in the network. We took the layout defined by Cytoscape previously (from its perforce directed layout algorithm) and incorporated significant changes in the $\beta 3+/-$ or $\beta 3-/-$ adhesome by changing the colour of the nodes in figure 4-4. Most of the critical nodes in the endothelial adhesome such as Ilk, Pxn and Fak1 were not affected by $\beta 3$ depletion, again suggesting that $\beta 3$ depletion can be compensated for in most cases by $\beta 1$. However Vcp, a protein we earlier suggested might be a non-specific interactor, was significantly increased. Although it is unclear if Vcp has a defined role in angiogenesis, its relationship with $\beta 3$ in our adhesome studies suggested it may have a currently unknown but important role. Interestingly, of all adjacent nodes to $\beta 3$ with a significant number of edges, only Filamin-a was significantly increased. We believe the analysis in figure 4-4 demonstrated Filamin-a had the potential to be part of the $\beta 3$ compensation mechanism. The network also reveals that Filamin-a interacts directly with $\beta 1$, the most obvious candidate for $\beta 3$ compensation as another fibronectin binding integrin¹¹⁹. Filamin-a's role in focal adhesions is to link proteins to the actin cytoskeleton, mainly integrins³⁵¹ directly via their cytoplasmic tail³⁵² but also to link other proteins important in cell migration and angiogenesis such as Vim³¹⁵. Filamin-a in the context of the $\beta 3$ dependent adhesome is difficult to unravel due to its many overlapping functions, for example it has been shown to promote focal adhesion stabilisation and migration in breast cancer cells via Mapk/Capn2 signalling³⁵³ but has been shown to be critical for Vim mediated adhesion and spreading of HEK 293 and 3T3 cells³⁵⁴. We thought that the exact contribution of Filamin-a is dependent on the cell type and situation, but given that Filamin-a null mice display severe angiogenesis defects³⁵⁵ and anti-Filamin-a antibody treatments are anti-angiogenic³⁵⁶ we speculated Filamin-a is likely to be pro-angiogenic in endothelial cells and could explain the enhanced pathological

angiogenesis in $\beta 3$ depleted situations. This also meant the Fln1-Vim- $\beta 1$ axis was a more likely candidate for investigation given that Filamin-a knockdown was also shown to decrease $\beta 1$ surface expression and activation^{357,358} and that Vim was also increased in the $\beta 3$ depleted adhesome. No increase in $\beta 1$ levels has been detected in the $\beta 3+/-$ or $\beta 3-/-$ adhesome but it is possible that $\beta 3$ depletion increased Filamin-a levels which in turn activated more of the $\beta 1$ present. Increased $\beta 1$ activity would have allowed $\beta 3$ inhibited cells to continue to adhere to and migrate on fibronectin, although at this point it was not clear if Filamin-a was enough to explain fully the increased angiogenesis phenotypes in $\beta 3+/-$ and $\beta 3-/-$ cells.

Thbs1 (Thrombospondin-1) was an especially interesting as a protein that can interact with both $\alpha v\beta 3$ and $\alpha 5\beta 1$ ³⁵⁹ but was the only protein in figure 4-4 that exhibited a conflict between the $\beta 3+/-$ and $\beta 3-/-$ adhesomes; in $\beta 3+/-$ cells it was increased but in $\beta 3-/-$ cells it was decreased in the adhesome. We thought it was possible that Thbs1 may be upregulated in partial $\beta 3$ depletion but cannot be compensated for in a total deletion although this was unlikely given that Thbs1 can interact with $\beta 1$ which was still present in the $\beta 3-/-$ adhesome. Thbs1 itself has long been known to be a potent inhibitor of angiogenesis³⁶⁰ therefore it was even stranger that it was increased in the $\beta 3+/-$ adhesome; it was also strange that Thbs1 was decreased in the $\beta 3-/-$ adhesome given it could itself bind fibronectin³⁶¹ but considering Thbs1's anti-angiogenic functions would have contradicted the observed $\beta 3-/-$ phenotypes this was not as surprising. One of the main mechanisms thought to be behind the $\beta 3-/-$ enhanced angiogenesis phenotype was the increased Flk1 activation in response to VEGF²¹⁷. We found our adhesome data could be used to expand this mechanism, specific to $\beta 3-/-$ angiogenesis, by rationalising Thbs1 behaviour in the $\beta 3-/-$ adhesome. Thbs1 is known to inhibit angiogenesis by binding to Flk1 and preventing association with integrin complexes³⁶²; VEGF is still able to bind Flk1 but it cannot phosphorylate downstream targets such as Akt1 whilst engaged with Thbs1³⁶³. Therefore in $\beta 3-/-$ cells, lower levels of Thbs1 release Flk1 to participate in angiogenic signalling, enhancing angiogenesis. It is worth noting that the kind of analysis carried out in figure 4-4 is not definitive due to a lack of coverage by publically available interaction databases. For example Nrp1 is not included in figures 4-3 or 4-4 despite it having known interactions with $\beta 3$, Filamin-a and other proteins in the endothelial adhesome^{52,246}. Additionally, to avoid overcomplicating figures we only included proteins who were two interactions away from $\alpha 5$, αv , $\beta 1$ or $\beta 3$ so there may have been additional unseen regulators.

We therefore decided to focus more on the SAM analysis to decide which features of the $\beta 3$ dependent adhesome we should follow up with *in vitro* experimentation. Microtubule related proteins had appeared in our analysis several times above, where they were recruited to the adhesome upon VEGF stimulation (table 4-1) and potentially were involved in endoplasmic reticulum directed regulation of the $\beta 3+/-$ adhesome (table 4-2). Many tubulins, the main components of microtubules, were found to be significantly increased in the $\beta 3+/-$ adhesome as well (supplementary table 3) but strangely no microtubule categories were found to be enriched in the $\beta 3+/-$ adhesome (table 4-2). This was because the defined KEGG, GOCC, GOMF and GOBP microtubule categories contained many microtubule regulators that were not upregulated therefore the entire category was not enriched, just the tubulins themselves and potentially a few select regulators. Additionally, interaction analysis in figure 4-4 did show that a cluster D-F (fibronectin adhesome clusters) tubulin as upregulated upon $\beta 3$ depletion, whereas most of the tubulins detected were in cluster A-C so not shown in figure 4-4. Microtubules, with their varied roles in cell division, focal adhesion regulation and cell migration^{279,291} make them valuable targets in anti-cancer therapies. As well as focal adhesions and cell migration being critical for angiogenesis, microtubules can play roles in angiogenesis through Flk1 signalling regulation²⁸⁶ and growth of cell protrusions along ECM in endothelial cells²⁸⁵ for example. Many microtubule targeting drugs are used clinically as anti-cancer agents such as paclitaxel²⁶⁶ or as direct anti-angiogenic agents (e.g. Foscetabulin³⁶⁴). Indeed, most microtubule targeting drugs are known to have some anti-angiogenic effect in addition to their anti-cancer effects²⁸⁷. Given the prevalence of microtubules in angiogenesis literature and the potential links to $\beta 3$ we had uncovered, we decided to visualise the SAM carried out to generate supplementary table 3 as a volcano plot to help better understand the changes occurring to tubulins. The result, in figure 4-5A, showed that all detected tubulins were significantly upregulated in the $\beta 3+/-$ adhesome. The fact that all tubulins in the endothelial adhesome were on the enriched (right side of SAM analysis) with $\beta 3$ depletion demonstrated to us that part of the microtubule structure itself must be present in the adhesome of $\beta 3+/-$ cells but not $\beta 3+/-$ cells. Initially we were worried that this could be indicative of an artefact in our mass spectrometry data resulting from the chemical modifications carried out³⁶⁵ such as crosslinking or carbamidomethylation. Alternatively, we could have been analysing our LC-MS/MS runs incorrectly in MaxQuant or Perseus and inadvertently skewed our adhesome towards proteins such as tubulins in some samples. To validate our mass spectrometry based findings, we carried out western blots on adhesome samples as per figure 3-2 using a

pan-alpha tubulin antibody as this detected several tubulin proteins we had identified using mass spectrometry. These westerns, quantified in figure 4-5B along with an example blot, showed that increased tubulin presence in the $\beta 3+/-$ adhesome was real and not an artefact of mass spectrometry. Strangely though this upregulation was not apparent in SAM of the $\beta 3-/-$ adhesome data and was not reliably detect by western blot (data not shown). Like Thbs1, it appeared that $\beta 3+/-$ and $\beta 3-/-$ adhesomes might still be behaving differently in response to $\beta 3$ depletion. However, given our earlier conclusions that $\beta 3+/-$ cells better represented a therapeutic targeting of $\beta 3$ than $\beta 3-/-$ cells, we decided that microtubules were worth further investigation.

Additional evidence, not relying on mass spectrometry, for the specific increase in of tubulin the $\beta 3+/-$ adhesome is shown by figure 4-5C. This figure shows that the total cell levels of tubulins are not increased upon $\beta 3$ deletion but figure 4-5B does show an increase in the adhesome in $\beta 3+/-$. Figures 4-5B and 4-5C together show that the increase of tubulin in the $\beta 3+/-$ adhesome is not due to whole cell upregulation of tubulins.

Microtubules, with their complex dynamics in terms of growth, shrinkage, cargo transport and targeting, have many regulators. A lot of these regulators, such as RhoA³⁶⁶ or Cdc42³⁶⁷ are also involved in actin cytoskeleton control³⁶⁸ as well as having their own roles in angiogenesis³⁶⁹. Cytoskeleton regulation and interaction with focal adhesions is an incredibly complex field with dense interaction networks to understand. This kind of analysis is something we specifically set out to accomplish using non-candidate analysis of the endothelial adhesome. We probed our SAM analysed $\beta 3+/-$ and $\beta 3-/-$ adhesomes for all proteins with microtubule associated KEGG, GOCC, GOMF and GOBP annotations. These microtubule regulators, detected in our adhesomes, were used in Cytoscape analysis to attempt to give us a deeper understanding of how $\beta 3$ can regulate microtubules. Despite narrowing down the potential field of candidates, there were still too many possibilities to consider so we organised the network horizontally according to the clusters defined in figure 4-2 for the endothelial adhesome. Additionally we calculated significance for proteins using the adhesomes from which those proteins are clustered in, utilising fresh samples. This meant that, in figure 4-6, the significances of VEGF cluster proteins (A to C) were calculated using SAM of fibronectin with VEGF samples and the significance of poly-l-lysine cluster (G to L) proteins were calculated using SAM of poly-l-lysine samples from $\beta 3+/-$ cells. We hoped this would give us a better chance of uncovering useful information about $\beta 3$ regulation of microtubules by using mass analysis of samples where the regulators were already known to be upregulated (identified by hierarchical clustering). We

took this action because many well-known microtubule regulators with defined roles in angiogenesis²⁸⁵ were not present in any of our adhesome samples, likely because they are present at very low amounts and therefore difficult to detect. Analysis of these microtubule regulators will be carried out in subsequent chapters but it is worth noting that in this figure we have chosen to display both $\beta 3^{+/-}$ and $\beta 3^{-/-}$ data and if they disagree, to choose the one with the greatest difference from the SAM analysis. Despite the $\beta 3^{-/-}$ fibronectin adhesome, without VEGF, not showing an increase in tubulin proteins like the $\beta 3^{+/-}$ adhesome; when treated with VEGF, the $\beta 3^{-/-}$ adhesome did show an increase of tubulin proteins. This suggested to us that both VEGF and $\beta 3$ were important in regulation of microtubules in endothelial cells.

Table 4-2 Enrichment Analysis of the $\beta 3+/-$ Endothelial Adhesome

Adhesome	Category column	Category value	Category size	Intersection size	Enrichment factor	P value	Benj. Hoch. FDR
$\beta 3+ / +$	GOCC name	nucleolus	147	38	1.8221	1.04E-05	7.46E-04
$\beta 3+ / +$	Cluster	F	295	73	1.7442	1.58E-11	1.74E-10
$\beta 3+ / +$	GOCC name	cytoplasm	385	35	0.64078	1.33E-05	8.60E-04
$\beta 3+ / +$	GOCC name	extracellular region part	388	35	0.63582	9.06E-06	7.31E-04
$\beta 3+ / +$	GOCC name	vesicle	384	32	0.58738	8.14E-07	1.31E-04
$\beta 3+ / +$	GOCC name	extracellular vesicular exosome	365	30	0.57933	1.53E-06	1.41E-04
$\beta 3+ / +$	GOCC name	extracellular organelle	365	30	0.57933	1.53E-06	1.65E-04
$\beta 3+ / +$	GOCC name	extracellular membrane-bounded organelle	365	30	0.57933	1.53E-06	1.97E-04
$\beta 3+ / +$	GOCC name	membrane-bounded vesicle	380	31	0.57501	5.06E-07	1.09E-04
$\beta 3+ / +$	GOCC name	protein complex	283	18	0.44832	2.85E-07	9.21E-05
$\beta 3+ / +$	GOCC name	cytosol	136	7	0.36279	1.72E-04	9.28E-03
$\beta 3+ / +$	Cluster	I	220	11	0.35243	3.40E-07	1.87E-06
$\beta 3+ / +$	GOCC name	cytoskeletal part	136	6	0.31097	4.73E-05	2.78E-03
$\beta 3+ / -$	KEGG name	Protein processing in endoplasmic reticulum	26	18	2.9918	4.01E-07	7.05E-05

$\beta 3+/-$	GOCC name	endoplasmic reticulum part	39	24	2.6593	1.12E-07	7.25E-05
$\beta 3+/-$	GOCC name	endoplasmic reticulum	43	24	2.412	1.39E-06	4.50E-04
$\beta 3+/-$	Cluster	I	220	78	1.5321	2.01E-07	1.11E-06
$\beta 3+/-$	GOCC name	protein complex	283	90	1.3743	4.89E-06	7.90E-04
$\beta 3+/-$	GOCC name	cytoplasmic part	407	115	1.221	7.01E-05	9.05E-03
$\beta 3+/-$	Cluster	F	295	30	0.43947	7.51E-13	8.26E-12
$\beta 3+/-$	GOCC name	nucleolus	147	14	0.41156	1.72E-06	3.70E-04

All significantly enriched or depleted GOMP, GOBP, GOCC or KEGG categories in fibronectin adhered $\beta 3+/-$ and fibronectin adhered $\beta 3+/-$ of the $\beta 3+/-$ endothelial adhesion defined in supplementary table 3 that were detected by Fisher's exact t test's.

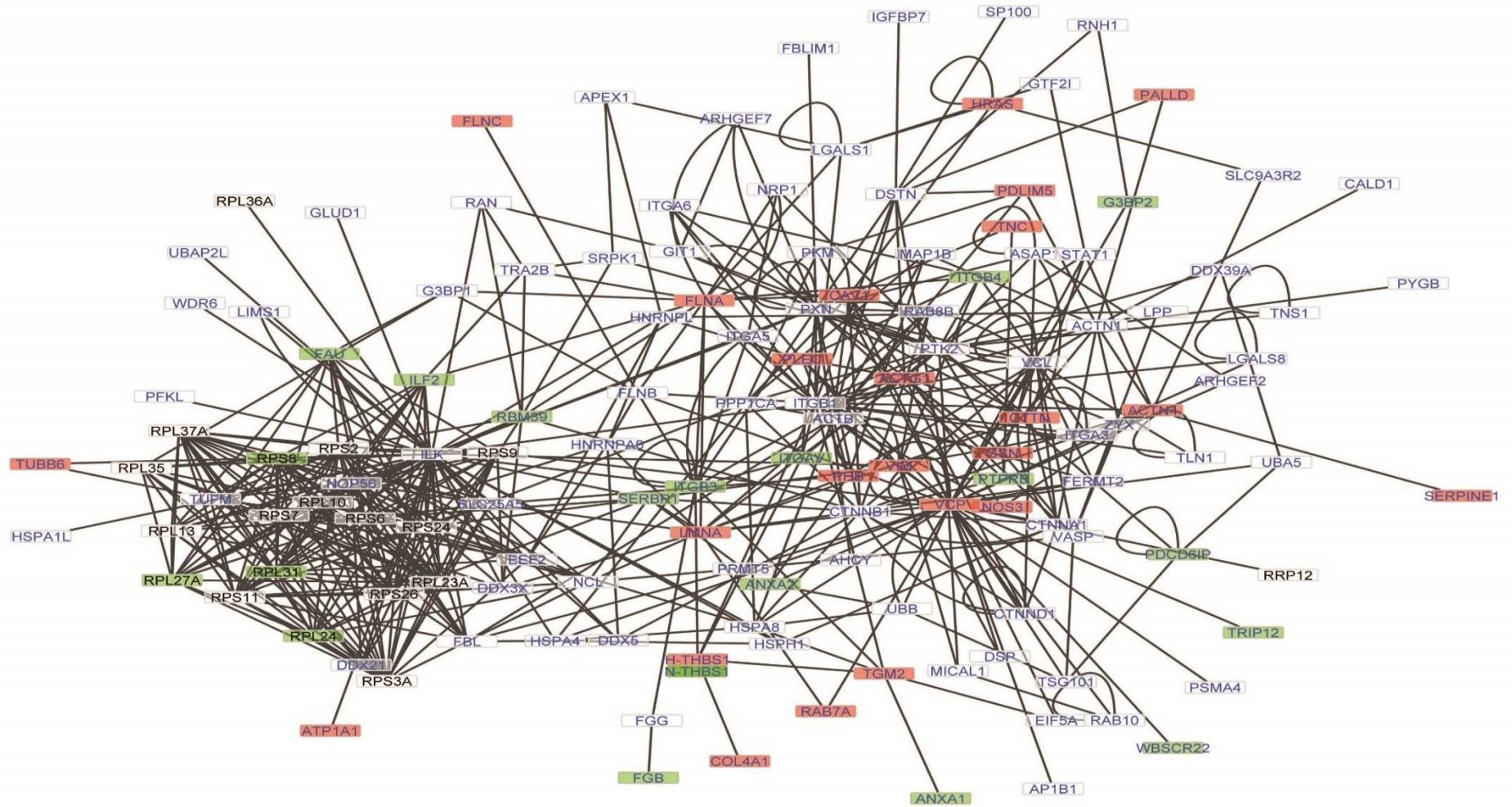
Table 4-3 Enrichment Analysis of the $\beta 3^{-/-}$ Endothelial Adhesome

Adhesome	Category column	Category value	Category size	Intersection size	Enrichment factor	P value	Benj. Hoch. FDR
$\beta 3^{+/-}$	GOCC name	mRNA cleavage and polyadenylation specificity factor complex	6	5	19.533	6.40E-07	4.35E-04
$\beta 3^{+/-}$	GOCC name	mRNA cleavage factor complex	8	5	14.649	5.53E-06	1.88E-03
$\beta 3^{+/-}$	GOCC name	extracellular space	77	12	3.6528	2.97E-05	6.72E-03
$\beta 3^{-/-}$	GOCC name	chaperonin-containing T-complex	8	8	9.3301	1.36E-08	9.21E-06
$\beta 3^{-/-}$	GOBP name	sperm-egg recognition	10	8	7.4641	4.95E-07	5.58E-04
$\beta 3^{-/-}$	GOBP name	cell-cell recognition	10	8	7.4641	4.95E-07	7.45E-04
$\beta 3^{-/-}$	GOBP name	binding of sperm to zona pellucida	10	8	7.4641	4.95E-07	1.12E-03
$\beta 3^{-/-}$	GOCC name	cytosolic part	20	10	4.665	8.77E-06	1.99E-03
$\beta 3^{-/-}$	GOBP name	protein folding	34	16	4.3906	3.84E-08	1.73E-04
$\beta 3^{-/-}$	GOMF name	adenyl nucleotide binding	168	37	2.0548	9.59E-07	9.75E-04
$\beta 3^{-/-}$	GOMF name	ATP binding	167	36	2.0113	2.50E-06	8.49E-04
$\beta 3^{-/-}$	GOMF name	adenyl ribonucleotide binding	167	36	2.0113	2.50E-06	1.27E-03
$\beta 3^{-/-}$	GOMF name	purine nucleotide binding	204	41	1.8752	2.66E-06	6.77E-04
$\beta 3^{-/-}$	GOMF name	ribonucleotide binding	203	40	1.8384	6.44E-06	9.35E-04
$\beta 3^{-/-}$	GOMF name	purine ribonucleotide binding	203	40	1.8384	6.44E-06	1.09E-03

$\beta 3^{-/-}$	GOMF name	purine ribonucleoside triphosphate binding	203	40	1.8384	6.44E-06	1.31E-03
$\beta 3^{-/-}$	Cluster	F	359	21	0.54577	4.63E-05	5.56E-04
$\beta 3^{-/-}$	GOCC name	ribonucleoprotein complex	240	6	0.23325	8.57E-08	2.91E-05
$\beta 3^{-/-}$	GOBP name	RNA processing	177	4	0.21085	3.94E-06	3.55E-03

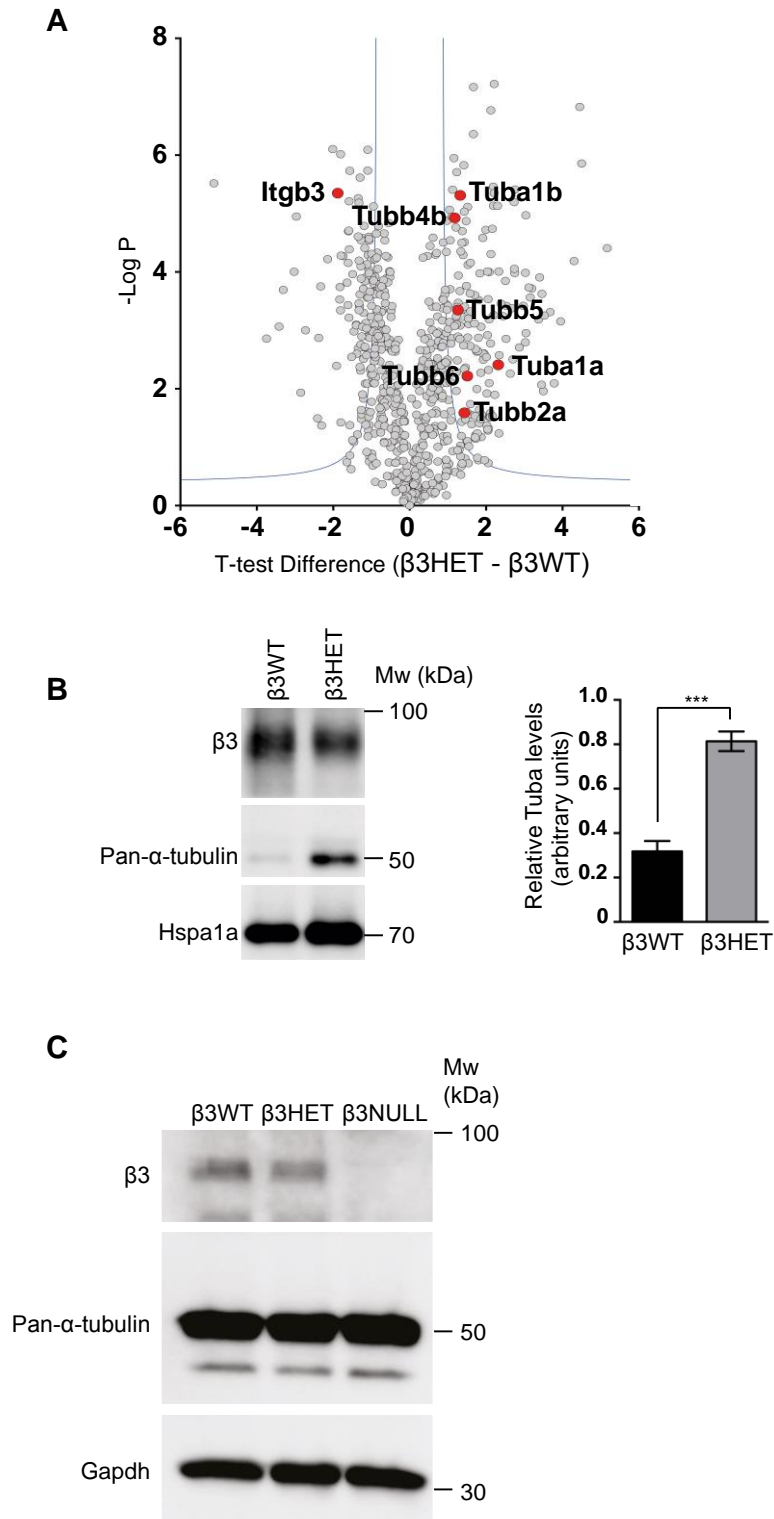
All significantly enriched or depleted GOMP, GOBP, GOCC or KEGG categories in fibronectin adhered $\beta 3^{+/+}$ cells and fibronectin adhered $\beta 3^{-/-}$ cells of the $\beta 3^{-/-}$ -endothelial adhesome defined in supplementary table 4 that were detected by Fisher's exact t test's.

Figure 4-4 Interaction Map of the $\beta 3$ Dependent Adhesome



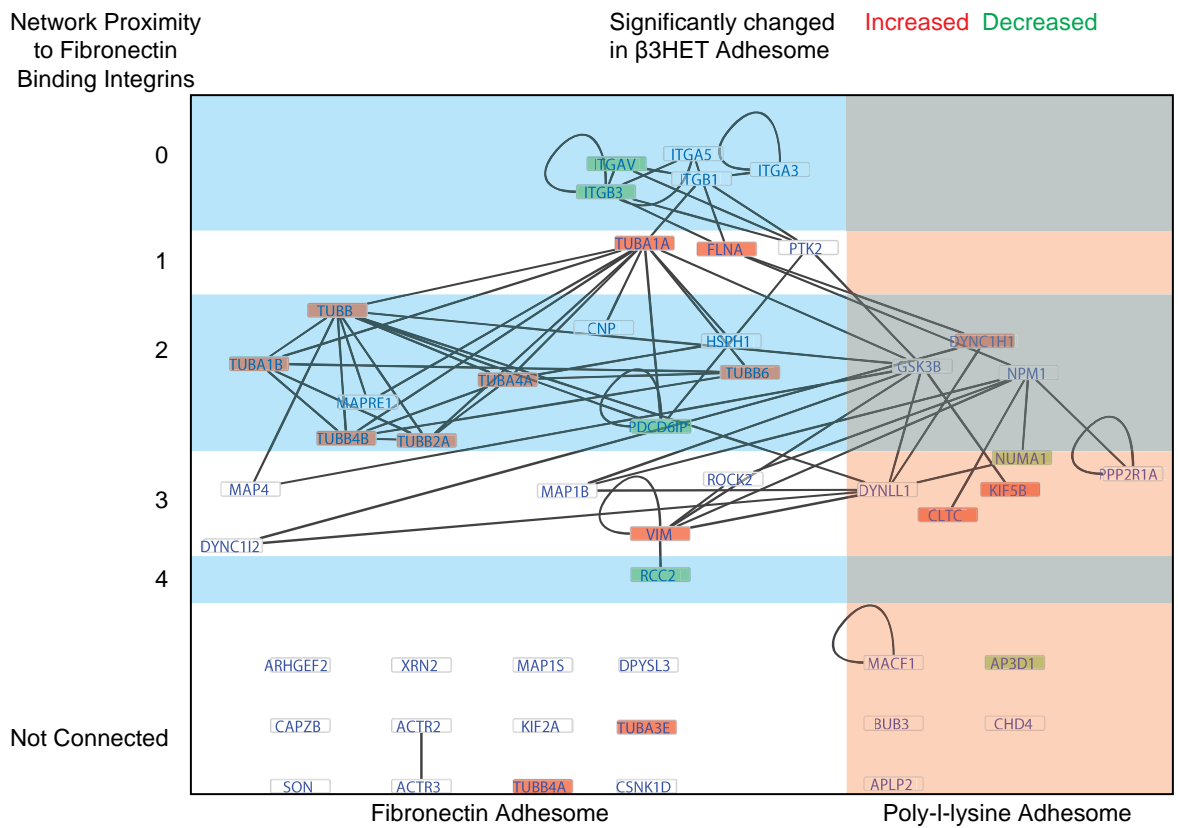
Interaction network of fibronectin adhesome proteins (cluster D-F) detected in the endothelial adhesome taken from figure 4-3. Significant changes in either the $\beta 3^{+/-}$ or $\beta 3^{-/-}$ adhesomes was calculated using SAM analysis and coloured red (increased) and green (decreased). Note Thbs1 is represented as separate nodes for SAM analysis of $\beta 3^{+/-}$ (H-THBS1) or $\beta 3^{-/-}$ (N-THBS1) adhesomes, which was the only node that disagreed between $\beta 3^{+/-}$ and $\beta 3^{-/-}$ adhesome data.

Figure 4-5 Tubulins in the $\beta 3^{+/-}$ Adhesome



A Visual representation of the significant analysis of microarrays (SAM) method as a volcano plot for $\beta3\beta3^{+/+}$ and $\beta3\beta3^{+/-}$ samples (n=3). T-test difference is plotted against $-\log$ of the P value. T-test difference is calculated from the $\beta3\beta3^{+/-}$ t-test value minus the $\beta3\beta3^{+/+}$ t-test value. As \log_2 normalised data was used for SAM analysis, this could also be considered a fold change difference. The blue lines show the cut-off for significance as defined by the SAM. Integrin- $\beta3$ ($\beta3$) as well as all detected tubulins (Tub) have been highlighted as red points. **B** Adhesome samples from $\beta3\beta3^{+/+}$ and $\beta3\beta3^{+/-}$ endothelial cells adhered to fibronectin. Samples were Western blotted for integrin- $\beta3$ ($\beta3$), α -tubulin and heat shock protein 70 (Hspa1a). Blot shown is representative of the 5 individual experiments that are quantified in the bar graph below. Bars = mean (\pm SEM) relative α -tubulin levels normalised to Hspa1a levels. ***= $P < 0.001$ in an unpaired, two-tailed t-test. **C** $\beta3^{+/+}$, $\beta3^{+/-}$ and $\beta3^{-/-}$ endothelial cells were adhered to fibronectin for 90 minutes before being lysed and Western blotted for $\beta3$, α -tubulin and Gapdh (as a loading control).

Figure 4-6 Microtubule Regulators in the $\beta 3$ Dependent Adhesome



Interaction network of microtubule associate proteins, defined by GOCC, GOMF, GOBP and KEGG annotations detected in the endothelial adhesome. Proteins were arranged vertically according to the number of connections from fibronectin binding integrins and horizontally according to whether they are members of the fibronectin or PLL adhesome. Significant changes in the $\beta 3$ +/- fibronectin adhesome (left) was calculated using SAM analysis of fibronectin adhered $\beta 3$ +/+ and $\beta 3$ +/- IMMLECs whereas significant changed for the $\beta 3$ +/- PLL adhesome (right) was calculated using data from PLL adhered cells .

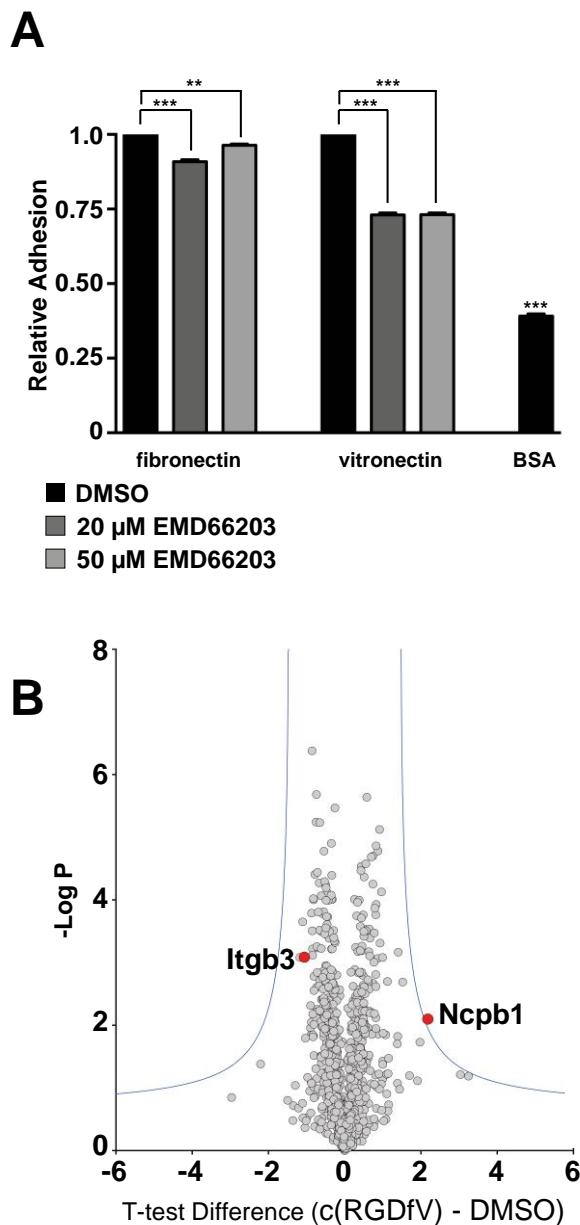
Statistical Analysis of Endothelial Adhesome with c(RGDfV) Treatment

We had observed many interesting changes in the endothelial adhesome upon depletion of $\beta 3$ in both $\beta 3+/-$ and $\beta 3-/-$ cells that had the potential to be exploited for desirable clinical outcomes if we were able to find an effective inhibitor. $\beta 3$ has been of interest as an angiogenesis inhibitor in anti-cancer treatments previously, due to its selective upregulation on only angiogenic vasculature in a heterodimer with αv and the assumption it was a pro-angiogenic molecule²⁰⁵. Efforts were made to target $\beta 3$ in vivo with an RGD-mimetic that could cross the blood brain barrier called Cilengitide[®], but unfortunately this failed clinical trials³⁷⁰. Several reasons have been put forward including: the dual pro and anti-angiogenic roles of $\beta 3$ ^{371,372}, highlighted particularly by pathological analysis observed in mice with complete deletions of $\beta 3$; poor pharmacokinetics and the ability of Cilengitide[®] to actually be pro-angiogenic at low doses²¹⁴; and the off-target effects on other integrins³⁷³. Biphasic effects, i.e. stimulation at low doses but inhibition at high doses, is also seen in other anti-angiogenic compounds such as sulforaphane³⁷⁴

We speculated that the various mechanisms behind RGD-mimetics in general being disappointing in vivo could have been due to compensation in the adhesome and may have already been uncovered in the analysis of the $\beta 3+/-$ and $\beta 3-/-$ adhesomes. We had an opportunity to confirm this by generating an RGD treated adhesome using c(RGDfV), a Cilengitide[®] like compound with greater selectivity towards $\alpha v\beta 3$ ³⁷⁵. We first tested the effectiveness of c(RGDfV) in our cells using adhesion assays carried out with the same amount of fibronectin, cell density and adhesion time as used in generating adhesome samples, shown in figure 4-7A. Vitronectin was used to test the effectiveness of the inhibitor on $\alpha v\beta 3$ based adhesion as it is ligand specific to that integrin and so cannot be compensated for by $\alpha 5\beta 1$ ³⁷⁶. A similar dose to that used in Cilengitide[®] adhesion assays³⁷⁷, 20 μM , was found to be in excess because it inhibited adhesion to vitronectin as well as 50 μM of c(RGDfV). We also showed that 20 μM c(RGDfV) was not detrimental to adhesion on fibronectin in case reports of the integrin specificity were incorrect because we still needed IMMLECs to adhere to fibronectin to generate adhesome samples. We then incubated $\beta 3+/-$ IMMLECs with 20 μM c(RGDfV) during the 90 minute adhesion in generating adhesome samples as per the endothelial adhesome in supplementary table 1. Although small changes in adhesion to fibronectin were observed during c(RGDfV) treatment in figure 4-7A, this could be due to a reduction in cell spreading which was detected using methylene blue staining and so the adhesome (although from less spread cells) would be from the same number of endothelial cells.

Figure 4-7B, a visual representation of SAM analysis of the c(RGDfV) adhesome carried out as per figure 4-5, surprisingly showed only one protein was significantly affected – Ncpb1, a protein involved in mRNA end-capping and export³⁷⁸. We did not think this single protein provided any revelations about pharmacological inhibition of c(RGDfV) and in fact the lack of any other significant changes was itself more interesting. This suggested to us that c(RGDfV) and possibly other RGD mimetics have no effect on β 3 or the adhesome when bound to fibronectin, potentially explaining the disappointing clinical trials. We speculated that binding of c(RGDfV), still triggers the outside-in signalling of β 3 to recruit its intracellular interactors, otherwise we should have seen compensation for loss of integrin function just like in the β 3+/- and β 3-/- adhesomes. Additionally we believed the physical anchorage to the ECM was instead carried out by β 1 when the binding sites of β 3 were occupied as happened in figure 4-7A during adhesion to fibronectin. The c(RGDfV) adhesome and its DMSO control, shown in supplementary table 5, still showed a complete endothelial adhesome like those previously generated with 912 proteins remaining after stringent filtering so we believed our adhesome enrichment and mass spectrometry were still functioning correctly. Other studies have suggested that fibronectin and its receptors are not required for tumour angiogenesis at all and simply our attempts to inhibit these pathways simply result in a dominant negative block, meaning other tumour ECM substrates must be more important³⁷⁹. If this is the case we believe the mode of action behind c(RGDfV) is not able to have this dominant negative effect due to lack of changes in the adhesome.

Figure 4-7 Analysis of the c(RGDfV) Treated Adhesome



A Adhesion analysis of endothelial cells adhered to saturating concentrations of fibronectin or vitronectin in the presence of c(RGDfV), an $\alpha\beta3$ -integrin specific RGD mimetic. Bars = mean (\pm SEM) adhesion relative to vehicle control (DMSO). **B** Visual representation of the significant analysis of microarrays (SAM) method as a volcano plot for DMSO versus 20 μ M c(RGDfV) treated endothelial cell samples (n=3). Endothelial cells were adhered to fibronectin for 90 minutes before being crosslinked, washed and proteins precipitated for mass spectrometry analysis. T-test difference is plotted against $-\log$ of the P value. The blue lines show the cut-off for significance as defined by the SAM. Integrin $\beta3$ ($\beta3$) as well as Ncpb1 (the only significant change) have been highlighted as red points.

Chapter five – Microtubule Behaviour in Integrin $\beta 3$ Depleted Angiogenesis

The aim of this chapter is to investigate the role and behaviour of microtubules in cells depleted for $\beta 3$. Chapter 4 had identified several microtubule components as significantly increased proteins in $\beta 3$ depleted adhesomes and therefore this needed validation with more traditional biochemistry approaches. Once validated, the effectiveness of targeting microtubules in $\beta 3$ depleted angiogenesis can be evaluated.

Microtubules in Endothelial Cells

In the previous chapter, we have highlighted the interesting alterations in intracellular cytoskeletons, particularly microtubules, in the endothelial $\beta 3$ -dependent adhesome. Given the crossover between microtubule and actin cytoskeleton regulation³⁶⁸ we felt it important to assess the state of both of these networks in our IMMLECs. As mentioned previously, microtubules can have diverse roles in focal adhesion regulation, migration and angiogenesis but we had not yet considered the actin cytoskeleton. Table 4-2 showed that the cytoskeletal part category changed significantly upon $\beta 3$ depletion, and the actin cytoskeleton was the most obvious candidate for change. Integrins are linked to the actin cytoskeleton by many critical focal adhesion/actin binding proteins such as Vinculin, Tln1, Fak1, Filamin-a and many others^{351,380,381}. This very strong and well characterised connection is formed during the maturation of a focal adhesion and is responsible for anchoring the cell via the actin cytoskeleton/focal adhesion connection to the ECM as well as playing a role in matrix engagement and matrix rigidity sensing¹⁸⁶. In cell staining experiments across many cell types, focal adhesions are found at the end of actin filaments and this was also true for our IMMLECs as seen in supplementary figure 1 using anti-Pxn and phalloidin staining (using two different methods of image visualisation). We therefore decided to simultaneously image the microtubule and actin cytoskeletons using PHEMO fixation which overcame the issues of fixing actin with methanol (it prefers PFA) or microtubules with PFA (they prefer methanol)³⁸². We used phalloidin and anti-alpha-tubulin (which binds to several actin isoforms identified in our mass spectrometry) to stain actin and microtubules in $\beta 3^{+/+}$ and $\beta 3$ depleted IMMLECs in figure 5-1A. There appeared to be no obvious changes in the actin cytoskeleton structure, despite the complete loss of $\beta 3$ in the $\beta 3^{-/-}$ cells. We speculated that, during the development of a focal adhesion, $\beta 1$ in nascent focal adhesions was able to regulate the actin cytoskeleton sufficiently and that

the additional inclusion of $\beta 3$ in $\beta 3+/+$ or $\beta 3+/-$ mature focal adhesions, did not have a dramatic effect due to the continued presence of $\beta 1$ ³⁸³. We therefore decided to focus our efforts on microtubules, which appeared to show subtle changes upon $\beta 3$ depletion. At first glance, it appeared the organisation of microtubules in $\beta 3+/-$ and $\beta 3-/-$ cells was more chaotic than that of $\beta 3+/+$ cells. From fixed cells it was difficult to draw any substantial conclusions on changes to microtubule organisation but we nevertheless decided it was worth studying microtubules further in $\beta 3$ depleted cells. It also appeared that there could have been more microtubules in the $\beta 3+/-$ and $\beta 3-/-$ than the $\beta 3+/+$ cells. Western blotting for alpha tubulin using whole cell protein extracts from all three genotypes, shown in figure 4-5C, did not show any differences. Therefore we believed there was no global upregulation of tubulin monomers or polymerised microtubules that could have explained the increased tubulin proteins found in the $\beta 3$ depleted adhesome. Additionally we used an alternative imaging technique in figure 5-1C, confocal microscopy, to only image a small z-slice at the very bottom of a $\beta 3+/+$ IMMLEC. As microtubule and actin cytoskeletons extend throughout the entire three-dimensional structure of the cell we felt it important to compare the widefield fluorescent images of figure 5-1A to the gold standard of confocal microscopy to ensure that the cytoskeletons above our plane of interest (focal adhesions being on the bottom of the cell) were not obscuring any phenotypes. The structures observed in figure 5-1C appeared similar to the $\beta 3+/+$ IMMLEC cell in figure 5-1A therefore we continued to use widefield fluorescent imaging in future investigations.

Given that figure 4-5B had shown that increased tubulin in the adhesome was not an artefact of mass spectrometry, and figure 4-5C had shown that there was no whole cell increase in tubulin, we were led to the conclusion that $\beta 3$ must have been specifically affecting the inclusion of tubulin in the adhesome – i.e. the targeting of microtubules to focal adhesions. Whilst other studies have identified roles for $\alpha 5\beta 1$ or focal adhesions generally in microtubule targeting to the cell cortex^{178,237,272} no work considering the role of $\beta 3$ had yet been carried out. Also no investigation into the possible effects of VEGF on microtubule targeting had, to our knowledge, been carried out (n.b. mass spectrometry, see table 4-2, had identified a potential link between VEGF-stimulation and tubulin localisation within the adhesome). To investigate both the role of $\beta 3$ and VEGF in microtubule targeting to focal adhesions we co-stained for alpha-tubulin and Tln1. By counting the number of microtubules that ended at a focal adhesion we were able to assess microtubule targeting. Figure 5-2A shows the result for both $\beta 3$ depleted cells with and without VEGF stimulation, with representative images in figure 5-2C. Without VEGF

stimulation it appears that both $\beta 3^{+/-}$ and $\beta 3^{-/-}$ cells show increased microtubule targeting to focal adhesions compared to $\beta 3^{+/+}$ cells. It is important to note that for $\beta 3^{+/+}$ and $\beta 3^{+/-}$ cells, we observed no difference in the amount or size distributions of focal adhesions when staining for Pxn in figure 5-2B. This fits with earlier results that showed increased tubulin in the adhesome upon $\beta 3$ depletion. Fibronectin binding integrins such as $\alpha 5\beta 1$ are known to target microtubules to focal adhesions possibly via Filamin-a-Iqgap1 (IQ motif containing GTPase activating protein 1)²³⁷ or Tln1-Kank1¹⁷⁸ mechanisms. These focal adhesion proteins are known to bind +TIPs such as Clip1²⁷⁸ and so would be able to anchor the growing ends of microtubules. However which is another fibronectin binding integrin, could be potentially unable to capture microtubules using similar mechanisms as $\alpha 5\beta 1$. At this point it was unclear whether $\beta 3$ was unable to participate in microtubule capture or played a dominant negative role in microtubule stability at focal adhesions, potentially by affecting key microtubule regulators that can induce catastrophe such as Kif2c (Kinesin family member 2C)³⁸⁴. Unfortunately not many of these catastrophe factors were well represented in the microtubule regulatory proteins detected in the endothelial adhesome (figure 4-6), possibly due to difficulties in detection or that they are not relevant to IMMLECs. Those that were detected were not $\beta 3$ dependent, limiting our ability to draw substantive conclusions.

The results of how VEGF affected microtubule targeting were less clear. Figure 5-2A suggested that more microtubules were targeted to focal adhesions in $\beta 3^{+/+}$ cells with VEGF stimulation than without but this was not statistically significant. This was surprising considering earlier enrichment analysis of the VEGF dependent adhesome of $\beta 3^{+/+}$ cells in table 4-1 showed an increase in microtubule proteins and so we would have expected a significant increase in targeting. There was, however, a significant decrease in targeting to focal adhesions in $\beta 3^{-/-}$ cells with VEGF stimulation. Finally $\beta 3^{+/-}$ cells showed no difference with VEGF. Whilst it was possible that $\beta 3$ depletion could change the VEGF response, due to the upregulation of VEGFR2 observed in $\beta 3$ knockouts²¹⁶, the number of contradictions between the VEGF targeting results and the adhesome data suggested to us that the 10 minute VEGF stimulation may not be long enough to trigger dramatic visual changes in the microtubule structure. Live imaging of microtubules (see below) or microtubule regrowth assays (see discussion) may be more appropriate to assess the impact the VEGF, whereas $\beta 3$ gene depletion as a permanent feature of the IMMLECs used was sufficient to show changes consistent with adhesome data.

Microtubules are dynamic structures undergoing constant growth and shrinkage, including dramatic separation of the protofilaments accompanied by rapid disassembly known as catastrophe, which can be reversed in a process known as “rescue”³⁸⁴. As such we decided we should attempt to study microtubule dynamics using live cell imaging where these processes could be observed. Normally microtubule dynamics are assessed using fluorescent protein coupled tubulin constructs to label microtubules or fluorescent protein coupled +TIP constructs to label the ends of microtubules. However, our primary interest was to study microtubule targeting to focal adhesions therefore we needed to label focal adhesions using another construct – GFP-Pxn. The GFP-Pxn construct used was a previously characterised plasmid that was known to traffic to focal adhesions and function correctly as native Pxn^{385,386}, and previously used successfully in our IMMLECs²¹⁸. Despite our best efforts, co-transfection with GFP-Pxn and a labelled tubulin or +TIP construct proved impossible due to very low transfection efficiencies. Instead, we decided to use a docetaxel based fluorescent tubulin binding compound called SiR-Tubulin. To avoid affecting microtubule dynamics with the binding of docetaxel, we used a low concentration of SiR-Tubulin to label microtubules overnight with verapamil to prevent efflux using established protocols³⁸⁷.

With the equipment available, we were unable to image both microtubules and focal adhesions live every three seconds, as required to measure microtubule dynamics accurately³⁸⁸. When focusing on imaging just microtubules using a single channel (SiR-Tubulin) we were able to capture images every 3 seconds but they were not of sufficient quality to make meaningful measurements (data not shown). We decided to measure microtubule targeting instead of dynamics as this required only taking an image every minute. When carried out in $\beta 3^{+/-}$, $\beta 3^{+/-}$ and $\beta 3^{-/-}$ cells, we were still unable to generate enough quality images to make an assessment of microtubule targeting to individual focal adhesions. Instead we measured the growth/targeting of microtubules into the lamellipodia, a focal adhesion rich membrane extension seen in migrating cells^{389,390}, as a proxy for microtubules being associated with adhesive areas of the cell. We were able to distinguish lamellipodia from other types of membrane extensions using the GFP-Pxn signal as an indicator of adhesions forming in lamellipodia. Figure 5-3B shows an example where we measured the area of the lamellipodia that formed over half an hour; then were able to count the number of microtubules that moved into the lamellipodia and normalised to the area measured. The results, as seen in figure 5-3A, showed that with $\beta 3$ depletion there were significantly more microtubules targeting the lamellipodia. This was consistent with

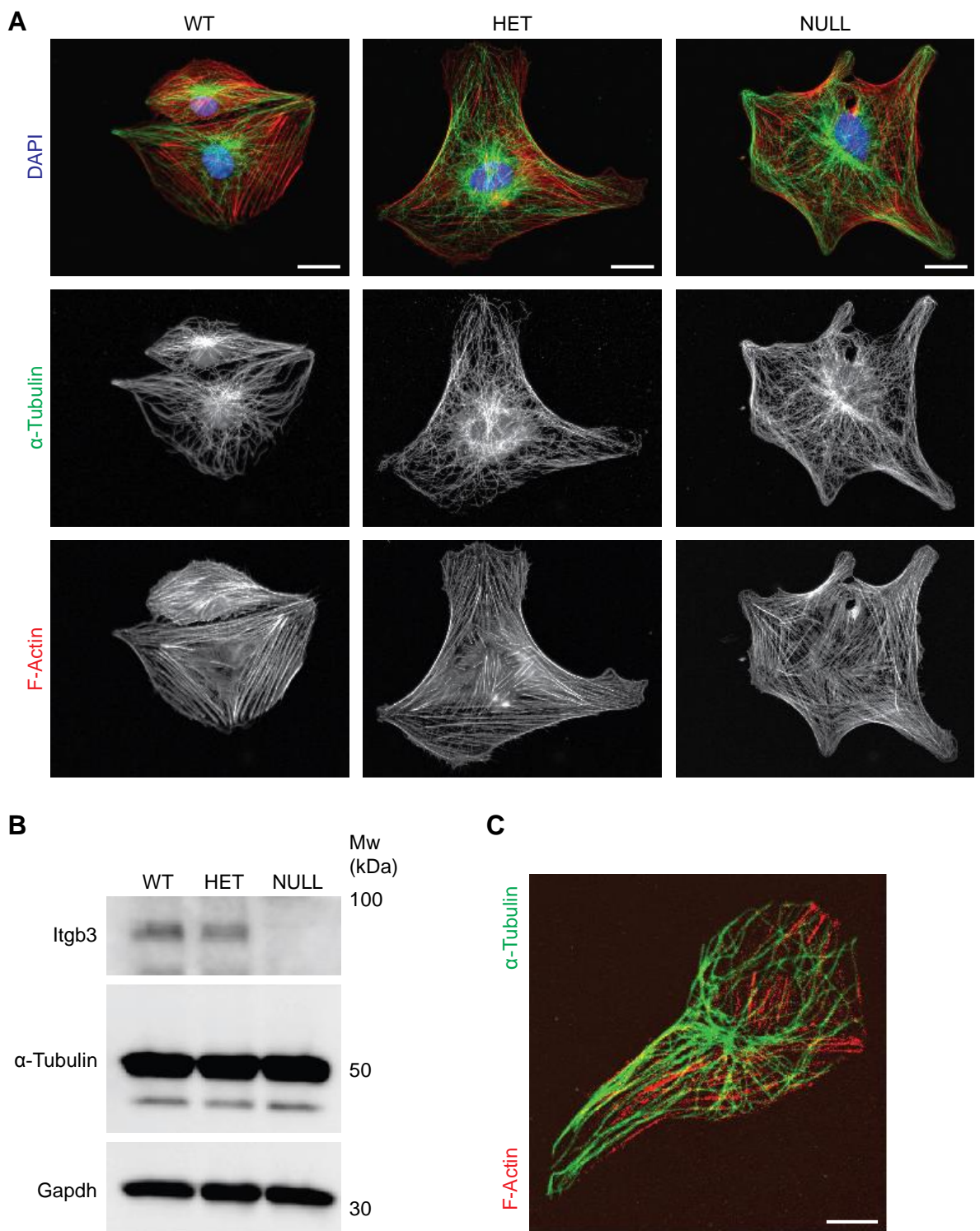
adhesome data and microtubule targeting in figure 5-2A. Interestingly, unlike in figure 5-2A which did not show increased targeting in $\beta 3^{-/-}$ cells compared to $\beta 3^{+/-}$, $\beta 3^{-/-}$ cells showed a much higher number of microtubules targeting lamellipodia than $\beta 3^{+/-}$ cells. We speculated this was because of the different criteria being used for measuring microtubule targeting to focal adhesions in the two experiments. In figure 5-2 we counted only microtubules whose ends overlapped with the Tln1 staining signal, whereas in figure 5-3 we counted microtubules that terminated anywhere inside a lamellipodia and not necessarily in direct contact with a focal adhesion. As a result, figure 5-2 quantified microtubule targeting to adhesions in $\beta 3^{+/-}$ above $\beta 3^{-/-}$ but in figure 5-3 the opposite was true. $\beta 3^{-/-}$ cells are exclusively reliant on $\alpha 5\beta 1$ for adhesion to fibronectin and current thinking suggests that this integrin dimer is able to stabilise microtubules whereas our data so far suggests $\alpha v/\beta 1$ cannot. If this was true then we would have expected $\beta 3^{-/-}$ to show greater microtubule targeting to focal adhesions than $\beta 3^{+/-}$. One mechanism for $\alpha 5\beta 1$ stabilisation of microtubules suggests that the stabilisation effect of the engaged integrin can be observed across a wider area of the cell²³⁷ possibly by using lipid rafts³⁹¹ and another suggests that Tln1 found at engaged integrins recruits Kank1 as a scaffold for microtubule stabilising factors where the size of this macromolecular complex means that microtubules targeted end up stabilised at a significant distance from the focal adhesion, but still anchored to the membrane using PIP₃. This remote Tln1-Kank1 scaffold means that fluorescent signals for Tln1 and microtubules do not overlap at all¹⁷⁸. Both of these mechanisms might explain why we observed an apparent under-representation of microtubule targeting to focal adhesions in $\beta 3^{-/-}$ cells in figure 5-2.

Although previous adhesome results have shown no difference in integrin levels in the adhesome, it is important to remember that the enrichment technique and mass spectrometry, carried out after 90 minutes adhesion, represents a brief snapshot in time. Changes in $\beta 3$ could have profound consequences for the behaviour of other integrins. For example, it has been shown that $\beta 3$ can sequester Nrp1 in the plasma membrane⁵². However, with the loss of $\beta 3$, Nrp1 is free to promote further angiogenesis through several mechanisms^{215,218} such as through interaction with Gipc1 (GPIC PDZ domain containing family member 1) which facilitates endocytosis of $\alpha 5\beta 1$ ¹⁹⁵. Increased trafficking of $\alpha 5\beta 1$ could therefore facilitate increased cell migration, enhancing angiogenic responses³⁹². Many other mechanisms of integrin recycling could be affected by the loss of $\beta 3$, but our study has not studied these further. Rab4, a key component in the recycling of $\alpha v\beta 3$ ³⁹³ can also recycle $\alpha 5\beta 1$ ³⁹⁴ and we speculate this could be another reason why $\beta 3$ loss does not

detrimentally affect endothelial cells on fibronectin because the increased recycling of $\alpha 5\beta 1$ can compensate. For a full review of integrin trafficking see Bridgewater et al¹⁹⁴. It is necessary to repeat this staining in future experiments for specific integrins such as $\alpha 5$ and/or $\beta 1$ to see if they are indeed present at the focal adhesions being increasingly targeted in $\beta 3+/-$ and $\beta 3-/-$ cells. In our hands, $\beta 3$ antibodies were not specific enough for use and we were concerned that following the more promiscuous αv would complicate analysis, but better antibodies are always in development and this should be revisited or alternatives such as labelled RGD mimetics could be explored²²⁴. The development of specific antibodies for both the inactive and active confirmation of $\alpha 5\beta 1$ and their use has shown how this integrin, when active, can target microtubules to focal adhesions²³⁷

Figure 5-2A showed how depletion of $\beta 3$ in $\beta 3+/+$ and $\beta 3+/-$ cells resulted in increased microtubule targeting to focal adhesions. Microtubule targeting of focal adhesions is known to be important throughout their lifecycle but particularly for maturation and disassembly²⁹¹. The ability of microtubules to increase focal adhesion disassembly rates is dependent on Kif5b, suggesting this function is dependent on the cargo delivered by kinesins¹⁹². Delivery of clathrin internalisation pathway components such as clathrin and Dab2 (DAB2, Clathrin adaptor protein) by microtubules increases focal adhesion disassembly³⁹⁵. Prolonged targeting of microtubules to areas of important cell-ECM contacts has also been shown to promote integrin internalisation/recycling by the exocytosis of MT1-MMP which severs connections between integrins and their ligands³⁹⁶.

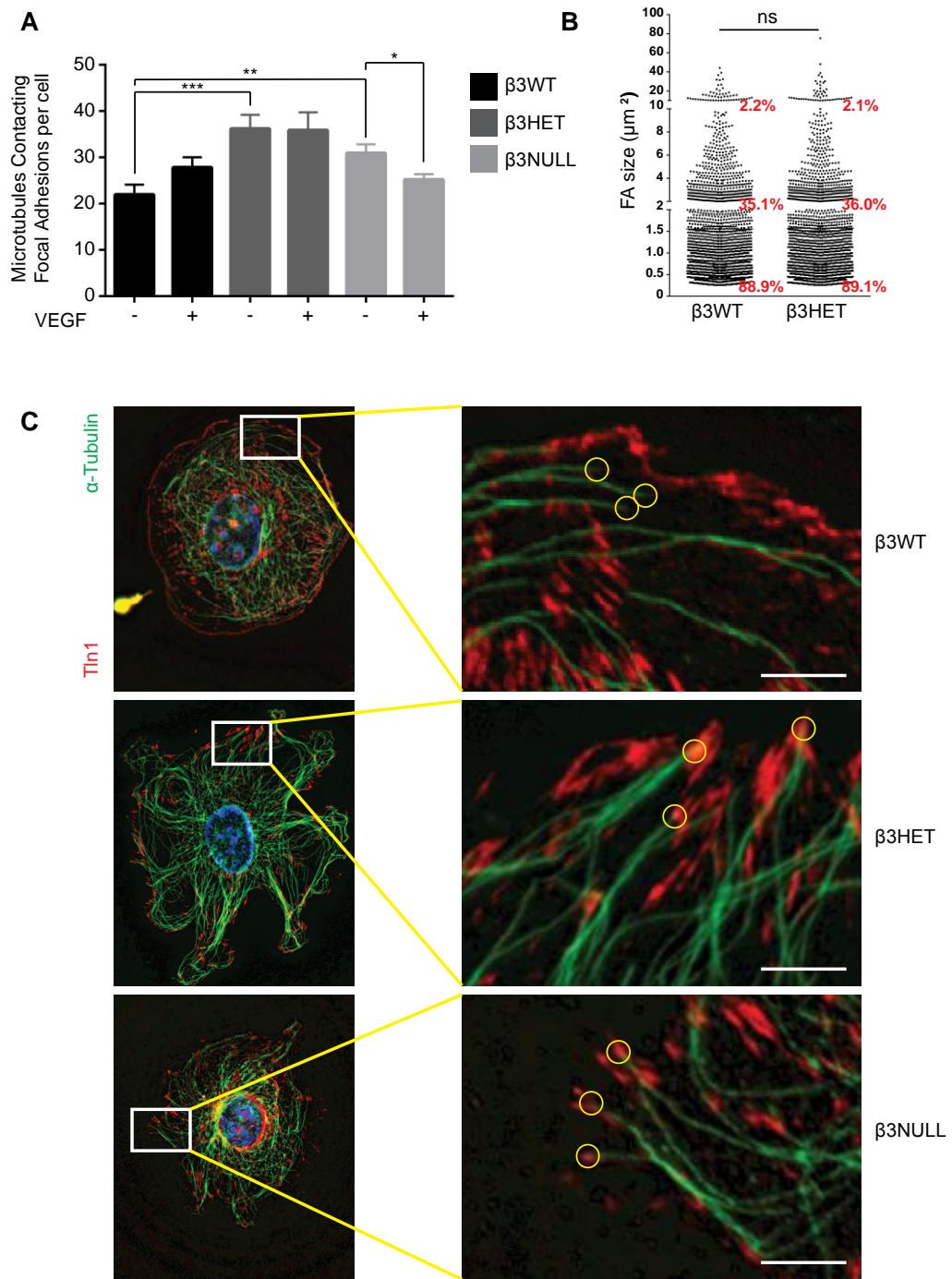
Figure 5-1 Microtubule and Actin Cytoskeletons in Endothelial Cells



A $\beta 3^{+/+}$, $\beta 3^{+/-}$ and $\beta 3^{-/-}$ endothelial cells were adhered to fibronectin coated coverslips for 90 minutes before being PHEMO fixed and immunostained for α -tubulin (green). Nuclear (DAPI-blue) and Phalloidin (F-actin - red) stains were also used. Greyscale images of α -tubulin and F-actin are shown below the three-colour overlays. Scale bar = 20 μ m **B** $\beta 3^{+/+}$, $\beta 3^{+/-}$ and $\beta 3^{-/-}$ endothelial cells were adhered to fibronectin for 90 minutes before being

lysed and Western blotted for $\beta 3$, α -tubulin and Gapdh (as a loading control). **C** Single $\beta 3^{+/+}$ cell adhered and stained as per panel A but imaged using a confocal microscope. Scale bar = 10 μm .

Figure 5-2 Microtubule Targeting to Focal Adhesions in Endothelial Cells

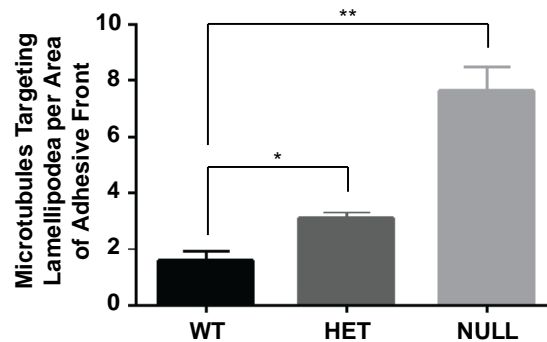


A $\beta 3^{+/+}$, $\beta 3^{+/-}$ and $\beta 3^{-/-}$ IMMLECs were adhered to fibronectin coated coverslips for 80 minutes then treated with VEGF for 10 minutes before being methanol fixed and immunostained for α -tubulin (green) and Tln1 (red). The number of microtubules that terminated at a focal adhesion per cell were counted for each genotype (n=15 from three independent experiments). Statistical significances between means were calculated using Student's t-test where *, ** and *** represent $p \leq 0.05$, $p \leq 0.01$ and $p \leq 0.001$ respectively.

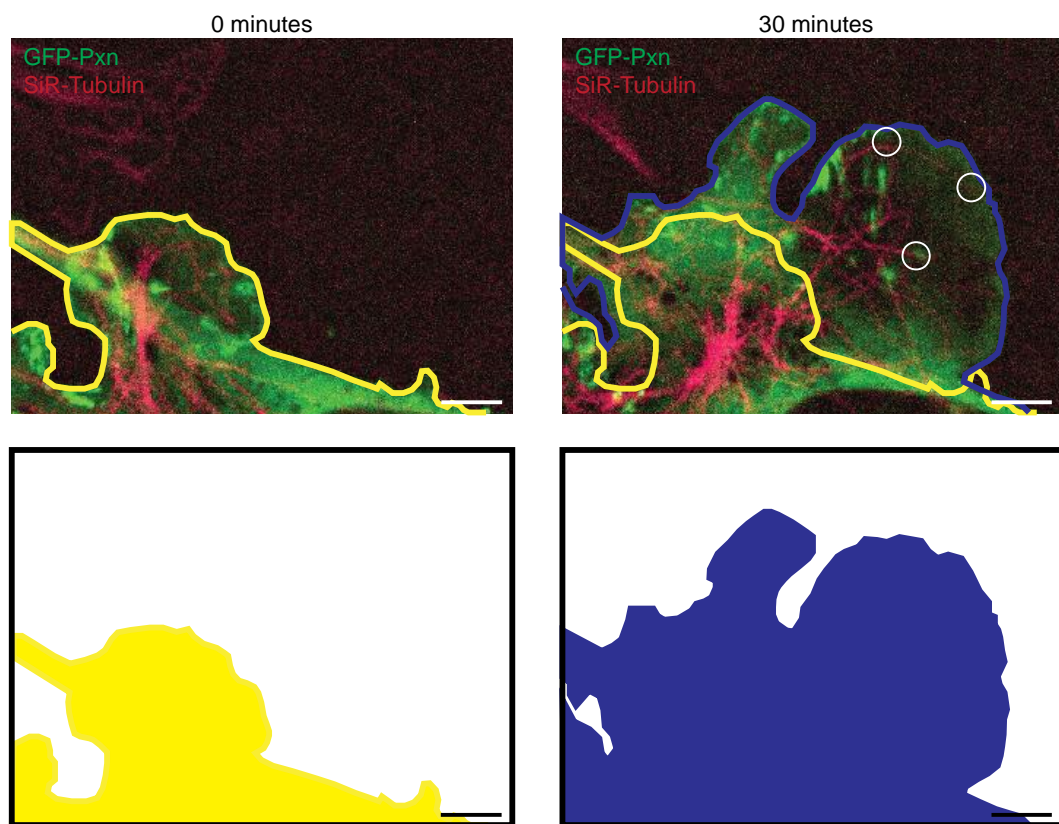
B $\beta 3^{+/+}$ and $\beta 3^{+/-}$ IMMLECs were adhered to fibronectin coated coverslips for 90 minutes before being methanol fixed and stained for Tln1. Images were taken of multiple cells across two independent experiments totalling >1,400 focal adhesions. ImageJ was used to measure sizes of focal adhesions and they were binned into groups of less than 2 μm , 2-10 μm and greater than 10 μm . N.s. indicated no significant difference found using student's t-test. **C** Examples of the staining images used above with yellow circles indicating example microtubules that were counted. Scale bar = 5 μm .

Figure 5-3 Microtubule Live Imaging in Endothelial Cells

A



B



A $\beta 3^{+/+}$, $\beta 3^{+/-}$ and $\beta 3^{-/-}$ cells were transfected with Pxn-GFP and left to recover overnight. The cells were then adhered to fibronectin coated coverslips and allowed to recover for 3 hours before being treated with 100 nM SiR Tubulin and 1 μ M verapamil overnight. The next day, fresh media containing SiR Tubulin and verapamil (same dose) was added cells were imaged every minute for 30 minutes ($n=3$). Areas of adhesive fronts were assessed by measuring the growth of Pxn-GFP positive areas between the 1st and 30th image. The number of microtubules that entered the adhesive front (GFP positive area) was quantified to give the number of microtubules entering lamellipodia relative to the area of adhesive fronts for each cell. **B** A Schematic demonstrating how panel A was calculated. Yellow

indicates the edge of Pxn-GFP (green) positive areas at 0 minutes and blue indicated the edge at the end of 30 minutes. Microtubules were labelled red with SiR Tubulin, with example counts circled in white. The bottom panels show the area measured in yellow for the 0 minute image and the area measured in blue for the 30 minute image. The area of adhesive front is calculated by subtracting the yellow area from blue. Scale bar = 5 μm .

Microtubule Inhibitors in Endothelial Cells

We have shown that microtubules are upregulated in the endothelial adhesome upon $\beta 3$ depletion by mass spectrometry, biochemically by western blotting and visually by fixed/live cell imaging. We decided the next stage was to see if this increased targeting of microtubules to focal adhesions was relevant to the behaviour of $\beta 3$ depleted cells. Microtubules have the ability to control focal adhesion dynamics²⁷⁹ and in particular disassembly through Dnm2, a microtubule binding protein³⁹⁷ and its interaction with Fak1 in focal adhesions¹⁹¹. Both focal adhesion assembly and disassembly must be tightly controlled and synchronised during cellular migration to maintain the optimal focal adhesion size and tread-milling ability³⁹⁸. Therefore we felt it highly likely that targeting microtubule behaviour would have a downstream effect on cell migration in our cells, as has been seen in other cell types^{263,284,399}, and this could have been greater in $\beta 3$ depleted IMMLECs. Luckily there are a vast array of microtubule inhibitor compounds available for use *in vitro* and *in vivo* with good pharmacokinetics, many of which are used as anti-cancer therapies²⁶⁴. To test our hypothesis, we selected a wide variety of microtubule inhibitors with different modes of action and effectiveness: microtubule stabilisers paclitaxel²⁸⁸ and epothilone B⁴⁰⁰ which prevent depolymerisation; microtubule destabilisers colchicine⁴⁰¹, fosbretabulin³⁶⁴ and mebendazole⁴⁰² which induce depolymerisation; and a mechanistically unique destabiliser known as eribulin⁴⁰³. Different cells can have vastly different responses to these inhibitors, for example endothelial cells are very sensitive to fosbretabulin which is being used specifically as an anti-angiogenic compound²⁸⁹, so we initially needed to test the response of our IMMLECs to each of these compounds. We used an overnight survival assay to determine the dose that allowed 90% of the cells to survive. As shown for paclitaxel and colchicine in figure 5-4A, we first used a logarithmic dose range before narrowing down to a more specific dose of 5 nM. We settled on the following doses for the remaining inhibitors: epothilone B – 1 nM, colchicine – 10 μ M, fosbretabulin – 0.5 μ M, mebendazole – 0.4 μ M and eribulin – 1 μ M. We then visualised whether these doses affected microtubule organisation in IMMLECs by treating cells overnight with one compound from each of the three classes mentioned above followed by fixation and staining for α -tubulin and Pxn. Colchicine and paclitaxel were used and the results shown in figure 5-4B; eribulin was also tested in IMMLECs but the staining was identical to colchicine treated cells so is not shown. Interestingly, at the dose of colchicine used, there were no microtubules present in $\beta 3+/+$, $\beta 3+/-$ or $\beta 3-/-$ cells after treatment. Given the specific targeting of microtubules to focal adhesions in $\beta 3$ depleted cells we might have expected

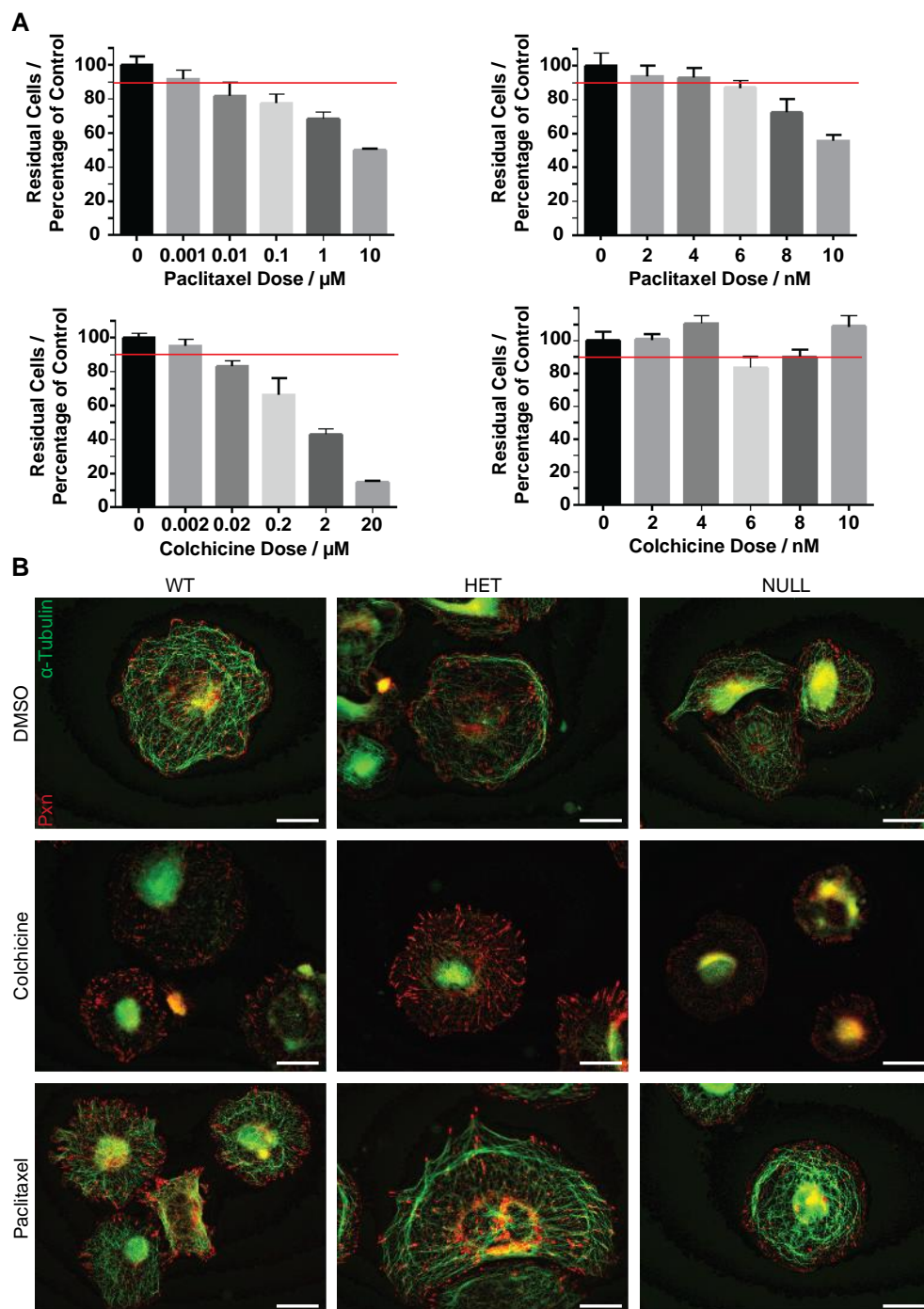
to see microtubules resisting the colchicine in these cells but this was not the case. As for paclitaxel, strong and numerous stained microtubules were detected in all three genotypes reflecting the stabilising ability of the drug. We also checked that $\beta 3$ cells were not more sensitive to microtubule destabilising drugs than $\beta 3+/+$ cells, an example is shown in supplementary figure 2.

Once we had decided on doses for our microtubule inhibitors we tested their effects on random cell migration in $\beta 3+/+$, $\beta 3+/-$ and $\beta 3-/-$ cells. The results, as seen in figure 5-5A, showed that all microtubule targeting drugs, regardless of mechanism of action, seemed to significantly affect the migration of $\beta 3$ depleted cells compared to $\beta 3+/+$ cells. Additionally it was interesting that the microtubule stabilisers, paclitaxel and epothilone b, significantly affected all three genotypes but decreased the migration of $\beta 3+/-$ and $\beta 3-/-$ the most. The other drugs, microtubule destabilisers, however did not have any effect on $\beta 3+/+$ cell migration, but still significantly slowed down $\beta 3+/-$ and $\beta 3-/-$ cells. Even with its unique mechanism of action, eribulin showed the same affects as the other destabilisers. Of all the drugs tested, only mebendazole failed to inhibit $\beta 3+/-$ cell migration significantly but it was still able to affect $\beta 3-/-$ migration. We speculated this was due to the weaker action of mebendazole against mammalian microtubules; the drug itself is currently used as an anthelmintic⁴⁰⁴. Figure 5-5B shows a limited example of random migration tracking used in the generation of figure 5-5A for $\beta 3-/-$ cells treated with colchicine – the most dramatic example. From this it was clear to see how colchicine has affected the normally highly migratory $\beta 3-/-$ cells, although it is possible at the dose used (10 μ M) we have begun to induce apoptosis in cells and hence are seeing a reduction in cell migration due to cell death. However at the same dose, $\beta 3+/+$ cells did not see a significant reduction in migration speed in figure 5-5A. Regardless of the exact mechanisms i.e. migration inhibition or cell death promotion we were confident that the colchicine affect was more selective for $\beta 3-/-$ cells. Interestingly, enrichment analysis of the $\beta 3$ depleted adhesomes in chapter four, suggested that microtubule categories were upregulated in $\beta 3+/-$ cells but not so much in $\beta 3-/-$. Despite this, we had observed in figure 5-5A that $\beta 3-/-$ cells were equally or sometimes more susceptible to microtubule inhibitors than $\beta 3+/-$. Looking back at supplementary tables 3 and 4 we observed that Dnm2 was significantly increased in the $\beta 3-/-$ but not the $\beta 3+/-$ adhesome upon $\beta 3$ depletion. If Dnm2 was, through increased targeting to focal adhesions by microtubules, promoting focal adhesion disassembly^{191,279} then this could be assisting $\beta 3-/-$ migration. $\beta 3+/-$ do not appear to have increased Dnm2 in our data, but instead have more robust microtubule associations. We speculated there

could be subtle differences in the mechanisms of compensation for total and partial depletions of $\beta 3$ but given the trend of increasing susceptibility to microtubule targeting drugs from $\beta 3^{+/-}$ to $\beta 3^{-/-}$ ECs we believed there would also be a common mechanism for compensation to any level of $\beta 3$ depletion. Non-normalised random migration data for figure 5-5A can be seen in supplementary figure 6.

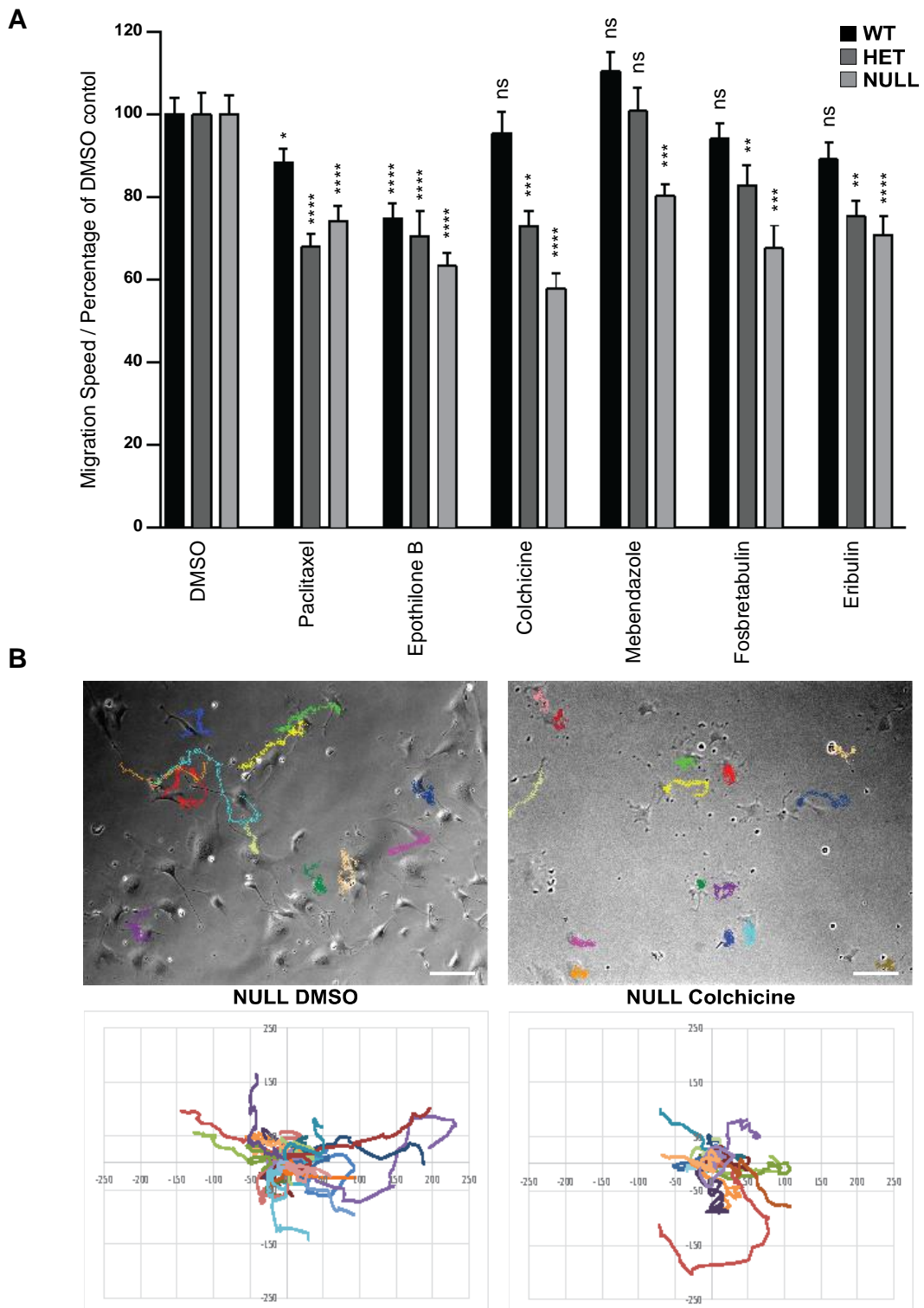
We next attempted to co-target $\beta 3$ and microtubules with microtubule inhibitors and c(RGDfV). Figure 4-7B had demonstrated it was unlikely that c(RGDfV) had any effect on the adhesome. We still felt it was worthwhile to check if changes outside the adhesome, caused by c(RGDfV), would make IMMLEC migration susceptible to microtubule inhibition; especially given that most microtubule regulatory proteins, as mentioned earlier, were not detected in the adhesome and so could be further downstream. Additionally, c(RGDfV) does have some influence on adhesion to vitronectin (figure 4-7A) so we thought it could also affect migration. However, when testing random migration in figure 5-6A with c(RGDfV), there was no significant effect on cell movement in combination with any microtubule inhibitor on fibronectin. To confirm this finding we took colchicine, as the inhibitor closest to significance with c(RGDfV) co-treatment, and obtained fresh supplies of both drugs in case there were unforeseen stability issues in storing these compounds. In figure 5-6B, new experiments were carried out using the fresh colchicine and c(RGDfV) where the lack of affect was shown to be consistent with figure 5-6A. Finally, we suspected that part of the apparent lack of c(RGDfV) effects could have been due to the length of inhibition. Earlier work in our lab had shown that tumour growth and angiogenesis was reduced using short term deletion of $\beta 3$ using an inducible cre with acute tamoxifen doses. However, long term inhibition using constitutive cre or inducible cre with chronic tamoxifen administration had no effect on angiogenesis²²³. We therefore tested whether an alternative method of inhibition, using a siRNA against $\beta 3$, would sensitise IMMLEC migrations to microtubule inhibition where c(RGDfV) could not. Figure 5-6C shows that, despite $\beta 3$ siRNA knockdown, there was no synergistic effect with additional colchicine treatment. This led us to the interesting conclusion that no mode of short term depletion/inhibition of $\beta 3$ was able to induce microtubule based changes and therefore the increased microtubule targeting of the adhesome could be the mechanism behind long term adaptation to long term $\beta 3$ loss observed by Steri et al²²³.

Figure 5-4 Use of Microtubule Inhibitors in Endothelial Cells



A $\beta 3^{+/+}$ endothelial cells were adhered to fibronectin before being treated with a range of paclitaxel or colchicine doses overnight. Residual cells after treatment was assessed using methylene blue staining followed by de-staining and absorption measurements. Red line indicates 90% cell survival $n = 8$. **B** $\beta 3^{+/+}$, $\beta 3^{+/-}$ and $\beta 3^{-/-}$ endothelial cells were adhered to fibronectin coated coverslips for 60 minutes before treated with colchicine (10 μM), paclitaxel (5 nM) or DMSO then fixed and immunostained for α -tubulin (green) and Pxn (red). Scale bar = 20 μm .

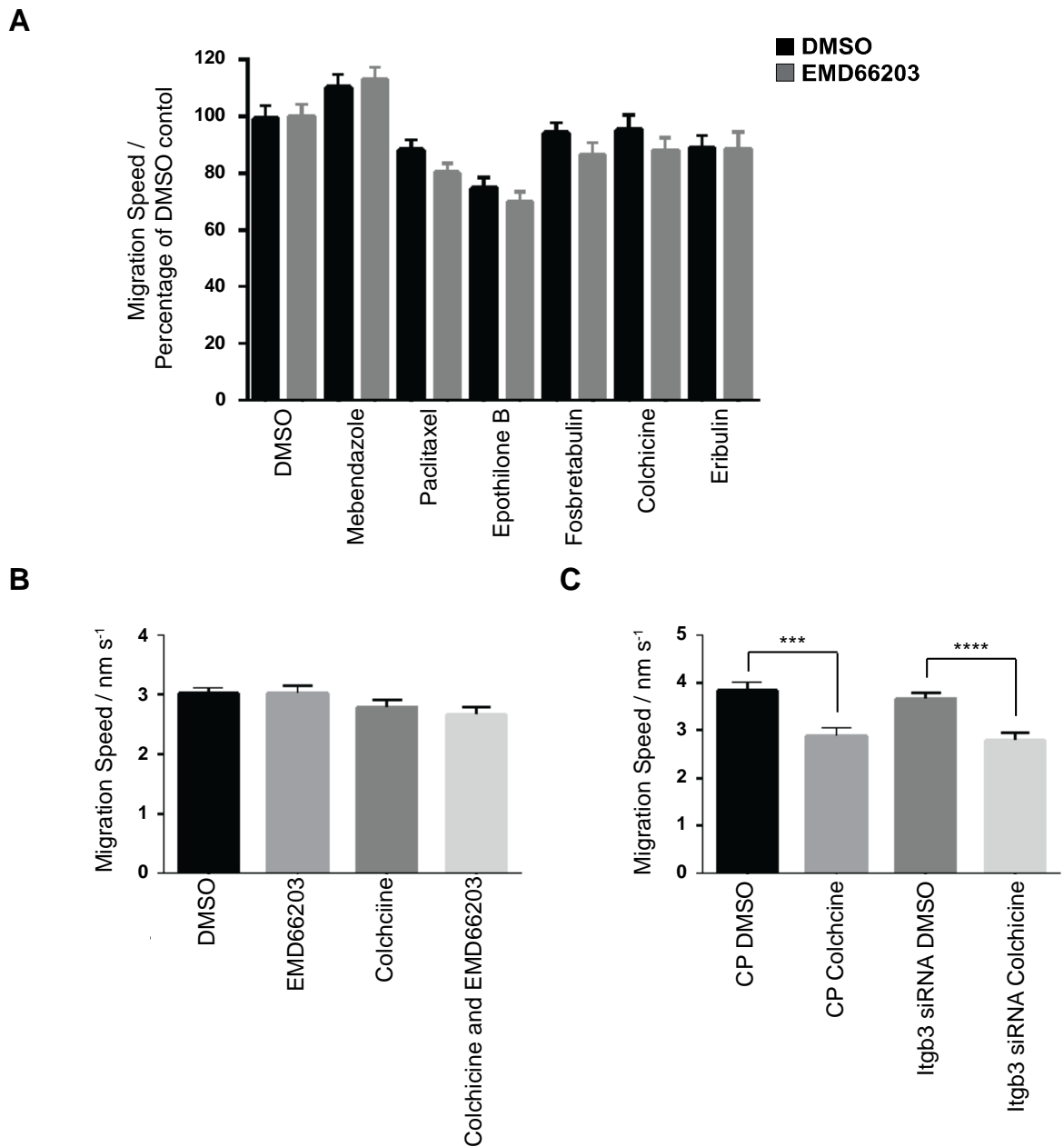
Figure 5-5 Random Migration in $\beta 3$ Depleted Endothelial Cells with Microtubule Inhibitors



A $\beta 3^{+/+}$, $\beta 3^{+/-}$ and $\beta 3^{-/-}$ endothelial cells were adhered to fibronectin overnight. Migration speed of individual cells was measured over 15 hours using the MTrackJ plugin for ImageJ whilst under the influence of the indicated microtubule agent. Migration speeds are shown

as a percentage of the speed of the corresponding genotype under DMSO (vehicle) treatment (n=46). **B** Example of tracking data generated for $\beta 3^{-/-}$ cells treated with DMSO or colchicine (10 μM) with graphs showing paths taken from a unified starting point. Scale bar = 100 μm .

Figure 5-6 Random Migration in Microtubule Inhibitor Treated Endothelial Cells with Alternative Modes of $\beta 3$ Inhibition



A $\beta 3^{+/+}$ endothelial cells were adhered to fibronectin overnight. Migration speed of individual cells was measured over 15 hours using the MTrackJ plugin for ImageJ whilst under the influence of the indicated microtubule agent and either DMSO or c(RGDfV) (20 μ M). Migration speeds are shown as a percentage of the speed under DMSO (vehicle) treatment alone (n=49). **B** $\beta 3^{+/+}$ endothelial cells adhered and quantified as in panel A. Treated with DMSO, c(RGDfV) (20 μ M), Colchicine (10 μ M) or a combination (n=59) **C** $\beta 3^{+/+}$ endothelial cells were treated with control pool (CP) or $\beta 3$ siRNA and allowed to recover

overnight. The next day they were adhered to fibronectin overnight and migration speed was measured as per panel A. Treated with colchicine (10 μ M) or DMSO (n=45).

Microtubule Inhibitors in vivo

We were confident in our studies that showed microtubule inhibition lead to a reduction of migration in long term $\beta 3$ depleted cells. Our wide choice of drugs with their distinct mechanisms, targets, off-targets and pharmacokinetics made it very unlikely that off-target effects on another protein were causing the phenotype. Additionally, the experiments of figures 5-5 and 5-6 had confirmed to us that changes in the adhesome translate to changes in migration behaviour, which was strengthened by the negative case of c(RGDfV) where no changes in the adhesome translated to no changes in migration behaviour. We decided the next step was to test if microtubule inhibition affected $\beta 3$ depleted angiogenesis in a more complete system using *in vivo* tumour growth assays. This also gave us the opportunity to confirm that the phenotypes observed so far were not an artefact of *in vitro* experimentation or a quirk unique to IMMLECs.

Tie1 cre²⁹⁴ driven deletion of $\beta 3$ specifically in endothelial cells had been observed successfully in our mice^{218,223}. This cre is also constitutively active so would closely mimic the genetically deleted IMMLECs used so far without having to use $\beta 3$ +/- or $\beta 3$ -/- mice that would have global $\beta 3$ depletion, complicating analysis due to the potential involvement of other cell types expressing $\beta 3$ in tumour growth. We crossed $\beta 3$ floxed mice²⁹⁵ with Tie1 cre mice to produce Tie1 cre negative $\beta 3$ floxed/floxed and Tie1 cre positive $\beta 3$ floxed/floxed mice which were littermates to reduce genetic differences across or experimental animals. CMT19T, a lung carcinoma cell line, was chosen because it develops well vascularised tumours^{218,223}, grow predictably in our experience, and can be used to produce allograft tumours without immune suppression in our animals⁴⁰⁵. We also chose to use eribulin as the microtubule targeting drug. Figure 5-4 had shown that eribulin, like all destabilisers, had no effect on $\beta 3$ +/+ cells. Part of the issue with anti-angiogenic treatments to date is the toxicity or bleeding side effects observed⁴⁰⁶. As a result, significant efforts are being made in treatment of cancer to target therapies more accurately to just tumours^{224,407} and not systemically exposing the whole body to these toxic agents. Even though $\beta 3$ is only expressed on angiogenic vasculature, this still includes events such as wound healing; therefore we wanted to choose a microtubule targeting drug that would be compatible with targeted $\beta 3$ depletion in the future. Using a destabiliser allowed us to do this as it would not affect $\beta 3$ +/+ vasculature unlike stabilisers which could stop any angiogenesis from occurring (see above), regardless of $\beta 3$ co-depletion, and cause side effects. Eribulin is also well tolerated in mice and actively being developed for use in human breast cancer⁴⁰⁸.

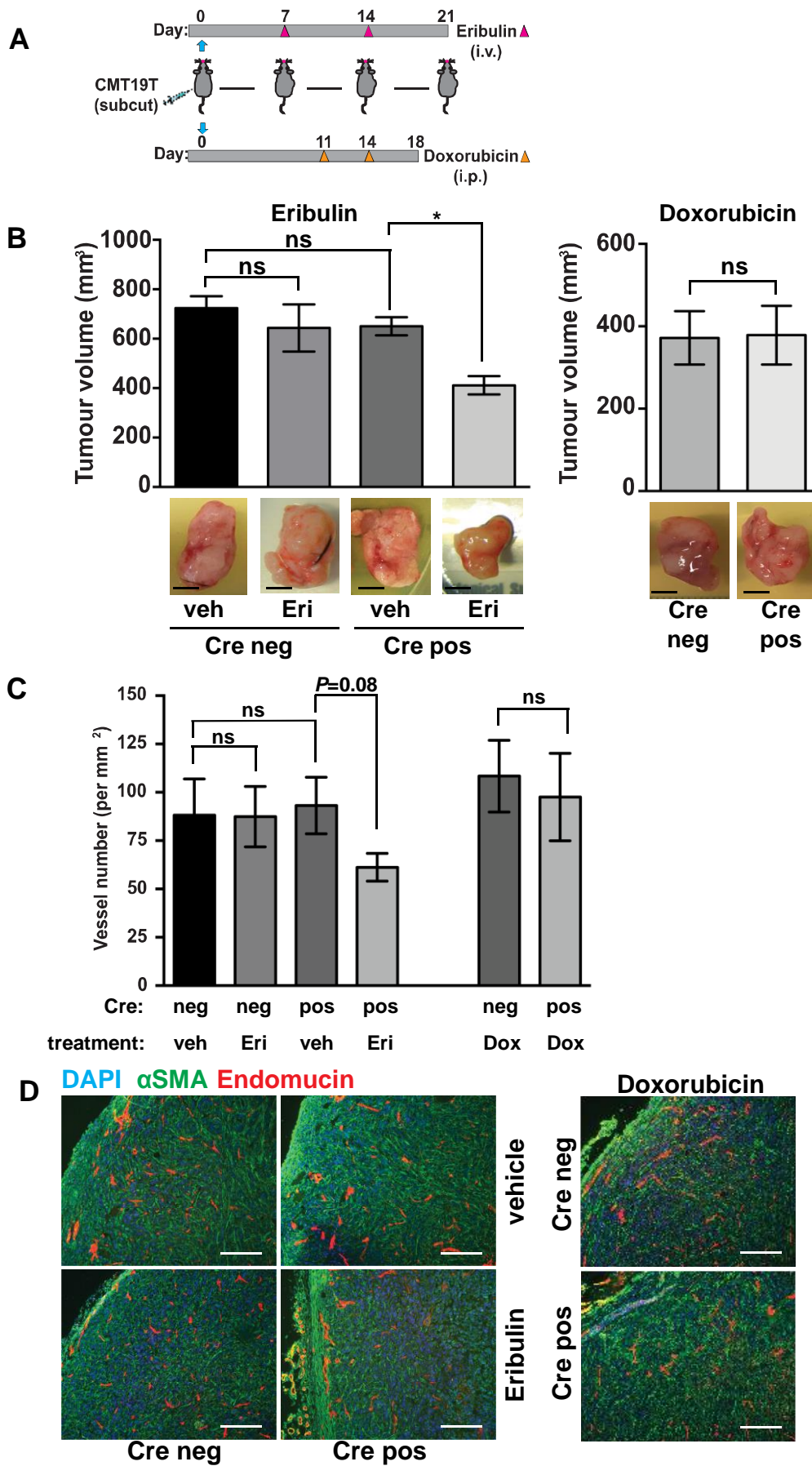
We grew subcutaneous CMT19T tumours for a week before intravenous administration of eribulin once a week for two weeks then harvesting the tumours a week later, see schematic in figure 5-7A. There have been reports that $\beta 3$ depletion can make vasculature leaky⁴⁰⁹, potentially allowing more chemotherapeutic agents to reach the tumour; tumours themselves also have leaky vasculature⁴¹⁰ that could become even more so under $\beta 3$ depletion. Therefore we also used a non-microtubule targeting drug, doxorubicin⁴⁰⁵, as a control for this possibility. Doxorubicin, a DNA damaging agent, is known to have significant issues with toxicity, particularly cardiomyopathy⁴¹¹. We decided to use a sub-optimal dose of eribulin to strengthen our results if we did see significant reductions in tumour growth but for doxorubicin we needed to use an optimal dose i.e. a dose that would definitely affect tumour growth in order for us to be able to make a conclusion on possible vessel leakiness. As a result the doxorubicin treated mice experienced significant toxicity hence the decision was taken to use doxorubicin over a shorter time frame as shown in figure 5-7A.

Firstly, the results in figure 5-7B showed there was no difference in tumour growth between control Tie1 cre positive and negative mice meaning that, in agreement with literature assessing why $\beta 3$ treatments failed clinically, there was no effect from $\beta 3$ depletion. Additionally there was no difference observed in tumour growth between Tie1 cre negative mice treated with vehicle control or eribulin, demonstrating that our dose chosen was indeed sub-optimal. There was however a significant reduction in tumour growth when Tie1 cre positive mice were treated with eribulin. This synergy is in agreement with *in vitro* random migration data in figure 5-5A for eribulin's effects on $\beta 3^{+/-}$ and $\beta 3^{-/-}$ cell migration. Doxorubicin did not show similar synergy, demonstrating the reduction observed with eribulin was most likely due to action on vasculature rather than a consequence of exceptional leakage of drugs into the tumour stroma in Tie1 cre positive animals killing tumour cells directly. Vessel density, shown in figure 5-7C with example staining in figure 5-7D, directly correlated with the tumour volumes measured in figure 5-7B. We therefore came to the conclusions that targeting microtubules in endothelial cells with destabilising drugs in long term $\beta 3$ depleted animals was potentially a viable anti-angiogenic/anti-cancer strategy *in vivo* and not an artefact of *in vitro* experimentation. Additionally the synergy observed using a sub-optimal dose of eribulin had the potential to lower side effects observed with any chemotherapeutic agent.

Next, we wanted to test whether acute deletions of $\beta 3$ would reduce tumour growth and angiogenesis *in vivo*. We speculated it could have also been an artefact/quirk of *in vitro*

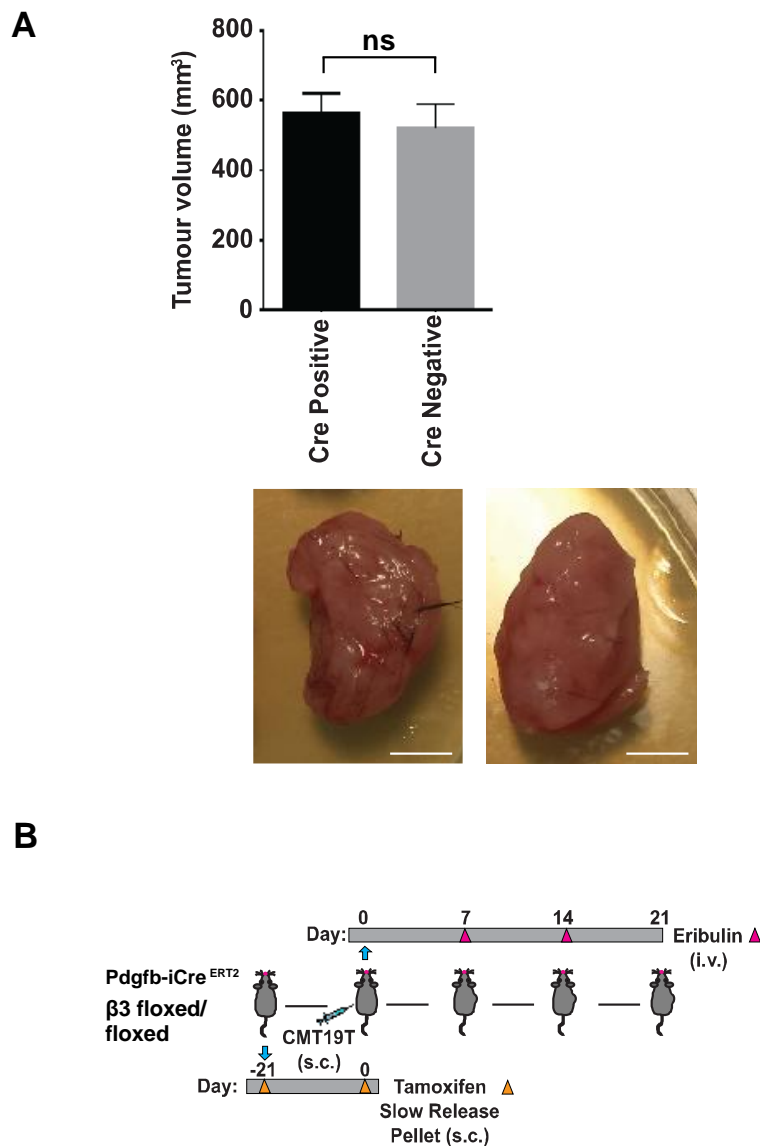
experimentation on IMMLECs that c(RGDfV) or $\beta 3$ siRNA treatment in figure 5-6 did not have any additional reduction in migration speed when microtubule inhibitors were used. Tamoxifen induced deletions of $\beta 3$ using $\beta 3$ flox/flox Pdgfb-iCre^{ERT2} mice (Pdgfb cre) have also been used to great effect in proving acute deletions of $\beta 3$ can reduce tumour growth²²³. We therefore used the same model and induction schedule as described for the Tie1 cre model. In figure 5-8 we compared tumour growth in Pdgfb cre positive $\beta 3$ floxed/floxed and Pdgfb cre negative $\beta 3$ floxed/floxed littermates, both treated with eribulin as above. This time we observed no difference in tumour growth, consistent with figure 5-6 where short term depletions of $\beta 3$ had no synergy with microtubule inhibitors. Again this suggested that increased microtubule targeting to focal adhesions is not a symptom of $\beta 3$ loss but is a long term compensation for its complete removal from the cells. Both Tie1 and Pdgfb cre driven deletions of $\beta 3$ have been shown to be specific and effective in our mice²²³.

Figure 5-7 Constitutive Integrin $\beta 3$ Depletion in Tumour Vasculature



B $\beta 3$ flox/flox Tie1 cre positive (pos) and negative (neg) animals were injected subcutaneously with 1×10^6 CMT19T lung carcinoma cells and then treated with eribulin, doxorubicin or vehicle control according to the indicated schematic (**A**). Bar graph shows mean tumour volumes at the end of the experiment. Micrographs (below) show representative tumours from 2 independent experiments ($n \geq 5$). Scale bars = 5 mm. **C** After excision, tumours from $\beta 3$ flox/flox Tie1 cre positive (pos) and negative (neg) animals were processed and endomucin staining was assessed over entire tumour sections to measure vascular density. Bars = mean vessel number per mm^2 ($n \geq 5$). Micrographs (**D**) show representative images of sections stained for alpha smooth muscle actin (αSMA =green), Endomucin (red) DAPI (blue). Scale bars = $100\mu\text{m}$.

Figure 5-8 Inducible Integrin $\beta 3$ Depletion in Tumour Vasculature



A $\beta 3$ flox/flox Pdgfb-iCre^{ERT2} positive (pos) and negative (neg) animals were treated with tamoxifen as per Steri et al²²³ for acute $\beta 3$ depletion, injected subcutaneously with 1×10^6 CMT19T lung carcinoma cells and then treated with eribulin as seen in the schematic (**B**). Bar graph shows mean tumour volumes at the end of the experiment. Micrographs (below) show representative tumours ($n \geq 5$). Scale bars = 5 mm.

Chapter six – Mechanisms of Integrin $\beta 3$ Regulation of Microtubule Stability

After confirming the potential of inhibiting microtubules to halt endothelial cell migration and tumour growth in $\beta 3$ depleted angiogenesis, this chapter aims to explain the mechanisms behind these observations. This was achieved by using microtubule stability assays and further mining the endothelial adhesome plus other datasets for the additional proteins in the pathways involved before validating their participation.

Microtubule Stability in Integrin $\beta 3$ Depleted Cells

We had so far demonstrated in chapter five that migration in $\beta 3$ depleted endothelial cells is more susceptible to microtubule inhibitors than in $\beta 3+ / +$. This was also replicated *in vivo*, where microtubule inhibitors reduced the growth of tumours in $\beta 3$ depleted mice. We needed to establish how $\beta 3$, using the tools established earlier such as the endothelial and $\beta 3$ dependent adhesomes, influenced microtubule behaviour. Microtubules have many roles themselves in regulating focal adhesion behaviour especially during directional migration such as by trafficking focal adhesion components to the cell cortex or by participating in signalling²⁷⁹, and because of this they can often be stabilised near or at focal adhesions via +TIPs^{272,412}. Given that focal adhesions are known to capture and promote stability of microtubules^{280,413} it was interesting that the presence of an integrin, $\beta 3$, was apparently preventing the targeting of microtubules to focal adhesions in figures 5-2 and 5-3. It seemed that $\beta 3$ was playing an opposing role in microtubule regulation to $\beta 1$ which can capture and stabilise microtubules²³⁷. This could have explained why $\beta 3+ / -$ and $\beta 3- / -$ endothelial cells have more microtubules in the adhesome/at focal adhesions and that this could act as a compensation for the loss of $\beta 3$, making them more reliant on microtubules and therefore vulnerable to microtubule targeting agents.

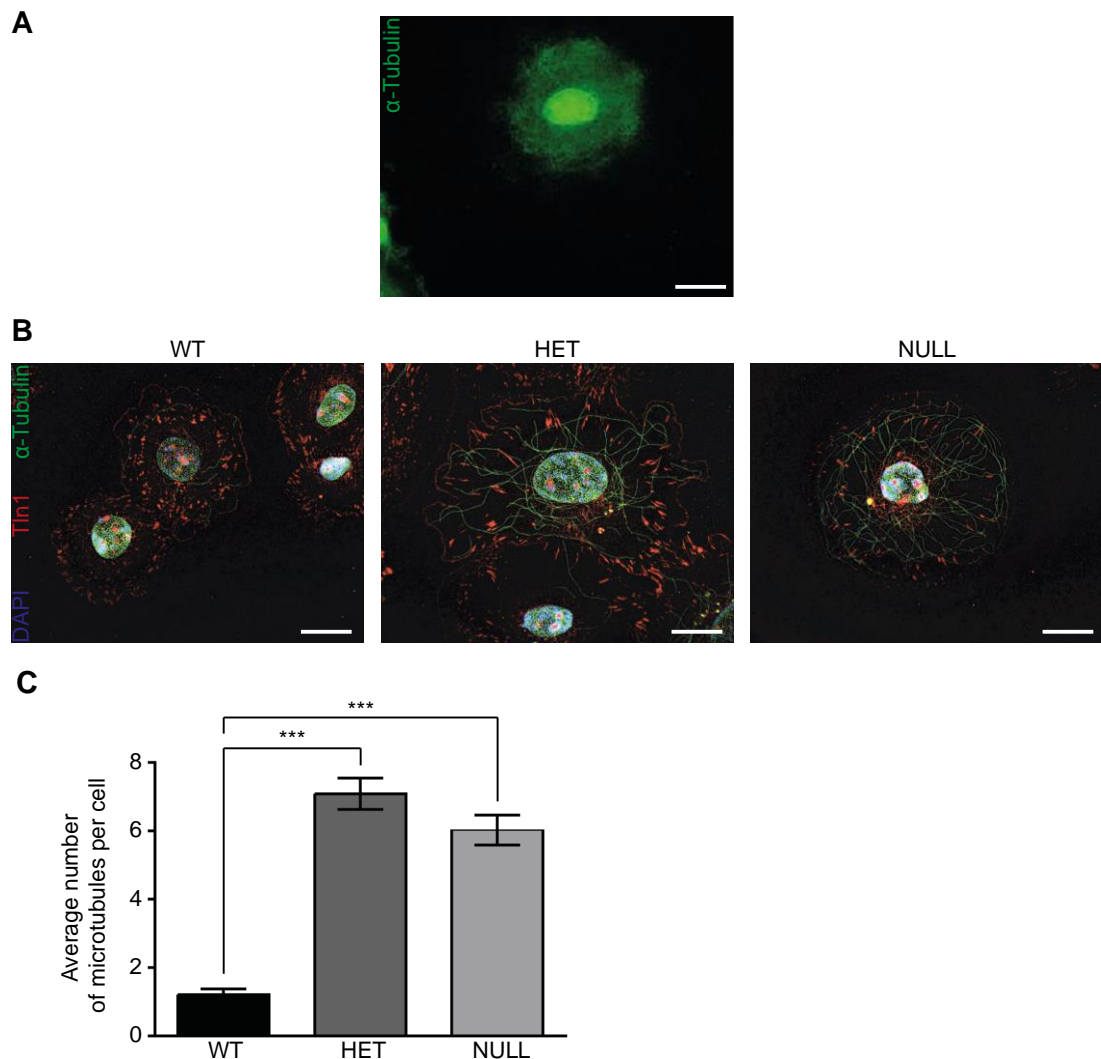
We already knew that $\beta 3$ was not promoting targeting of microtubules to focal adhesions but to completely test if $\beta 3$ was opposing $\beta 1$ in other modes of microtubule regulation, we needed to assess the stability of microtubules in our endothelial cells as well. Microtubule stability can be assessed by their post-translational modifications such as acetylation⁴¹⁴, however in our hands the antibodies for acetylated mouse tubulin were unreliable preventing us from obtaining reliable staining or western blots. As an alternative we investigated microtubule stability in response to cold treatment. Low temperatures are known to induce disassembly of microtubules in a short time^{258,260}. Some cell types, including endothelial cells, also have microtubules that are permanently resistant to cold

treatment known as cold stable microtubules due to the action of protective capping proteins such as Map6²⁵⁹. We designed experiments where cells were adhered to fibronectin for 90 minutes, to be consistent with adhesion samples and figure 5-2, but exposed to cold treatment in the last 15 minutes before fixation. In preliminary experiments we discovered the vast majority of microtubules were indeed depolymerised during the cold exposure but, as shown in figure 6-1A, the resulting cloud of liberated tubulin monomers preventing us from being able to quantify cold stable microtubules when staining for α -tubulin. To overcome this we used a gentle lysis buffer (PEM) to wash out soluble tubulin, leaving behind insoluble tubulin, before fixation as per Ochoa et al²⁵⁹. The washout step allowed us to only stain cold stable microtubules, making quantification much easier as can be seen for $\beta 3^{+/+}$, $\beta 3^{+/-}$ and $\beta 3^{-/-}$ cells in figure 6-1B.

Figure 6-1C compares the average number of cold stable microtubules between $\beta 3^{+/+}$, $\beta 3^{+/-}$ and $\beta 3^{-/-}$ IMMLECs. The difference observed between $\beta 3^{+/+}$ cells and *Itb3* depleted ones was astounding, and in most cases $\beta 3^{+/+}$ cells had no stable microtubules remaining. This result suggested that in endothelial cells expressing $\beta 3$ there are very low levels of microtubule stabilisation or conversely cells without $\beta 3$ undergo more stabilisation. The very simple but time-consuming technique of counting microtubules was, we believe, sufficient to accurately reflect the phenotype of increased microtubule stability upon $\beta 3$ depletion but was not flawless. For example this technique did not discriminate between long microtubules travelling from the centrosome to the cell cortex or short ones just beginning to be nucleated. Additionally microtubules were occasionally broken in the middle making counting difficult, likely due to mechanical destruction during washing/washouts/fixation rather than spontaneous breakdown because microtubules tend to disassemble from the plus end⁴¹⁵. To confirm that the dramatic difference in microtubule stability was not an artefact of staining during this experiment, we also tested microtubule stability biochemically using western blotting. In figure 6-2 we used the same procedure as before except capturing and western blotting the washout material for α -tubulin to quantify soluble tubulin. After washout we were then able to lyse the cells separately to assess the amount of insoluble tubulin. The amount of cold soluble tubulin washed out of the endothelial cells, in figure 6-2A, was greatest in the $\beta 3^{+/+}$ and the least in the $\beta 3^{-/-}$. Conversely in figure 6-2B, the amount of cold insoluble tubulin remaining behind after the washout was greatest in the $\beta 3^{-/-}$ and the least in the $\beta 3^{+/+}$. Not only did this experiment confirm the findings in figure 6-1 that decreasing levels of $\beta 3$ led to increased microtubule it was also able to validate our cold stability and washout technique

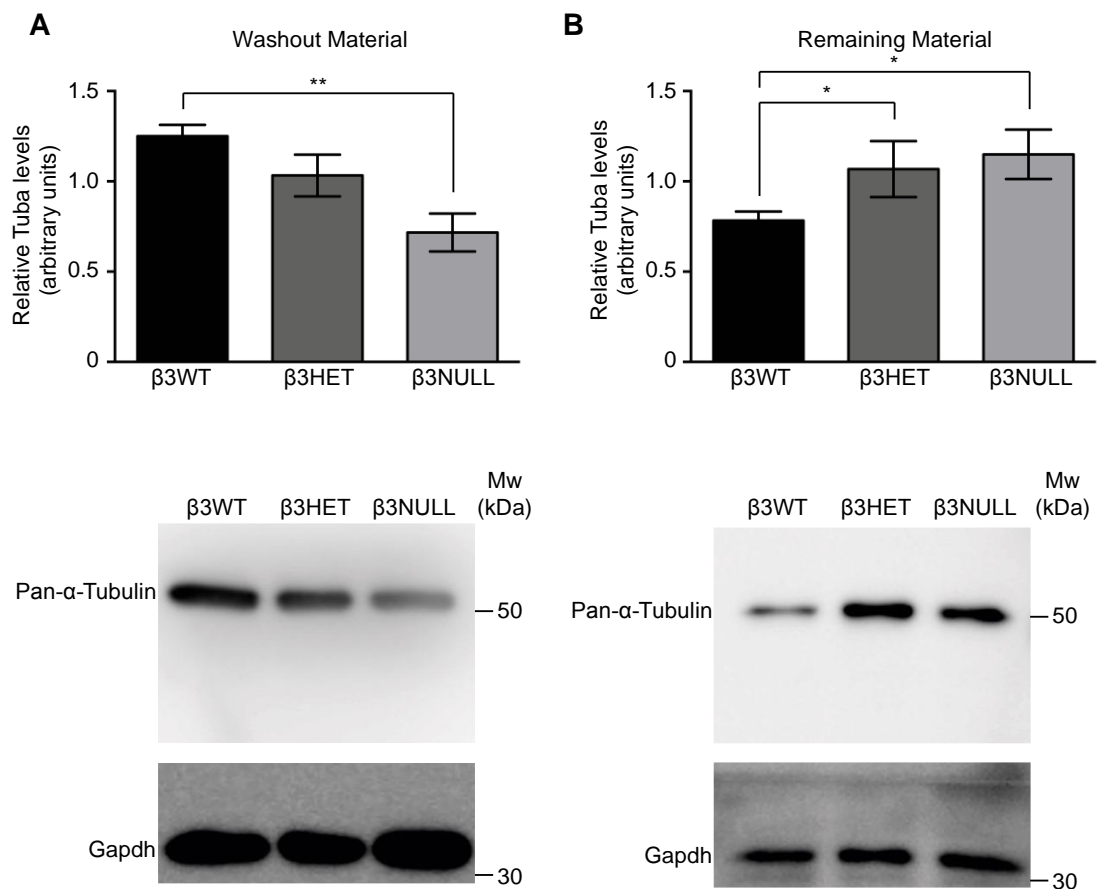
for cell staining. The graphs presented in figure 6-2 are near mirror images of each other meaning that the entire cellular pool of tubulin was represented in our cold soluble or cold insoluble samples; no tubulin was lost during washing stages and hence the staining approach was also a good indicator of the number of cold stable microtubules. We speculated that the difference between figures 6-1 and 6-2 concerning stability in $\beta 3^{+/-}$ vs $\beta 3^{-/-}$ was part of a trend discussed in earlier chapters and possibly down to the length/breakages of microtubules that could be accounted for in figure 6-2 but not 6-1.

Figure 6-1 Cold Stable Microtubule Staining in $\beta 3$ Depleted Endothelial Cells



A $\beta 3^{+/+}$ IMMLECs adhered to fibronectin coated coverslips for 75 minutes at 37°C before being moved to ice for 15 minutes and then fixed with methanol. Immunostaining was carried out for α -tubulin (green) scale bar = 20 μ m. **B** $\beta 3^{+/+}$, $\beta 3^{+/-}$ and $\beta 3^{-/-}$ IMMLECs treated as in A except soluble tubulin washed out using PEM buffer before fixation. Immunostaining was carried out for α -tubulin (green) and Tln1 (red). DAPI (blue) was used as a nuclear stain scale bar = 20 μ m. **C** Quantification of microtubules per cell treated as in B. Bars represent mean \pm SEM n = 519.

Figure 6-2 Cold Soluble Microtubules in $\beta 3$ Depleted Endothelial Cells



A $\beta 3^{+/+}$, $\beta 3^{+/-}$ and $\beta 3^{-/-}$ IMMLECs were adhered to fibronectin for 75 minutes before being moved to ice for 15 minutes. Soluble tubulin was washed out using PEM buffer, collected and western blotted for α -tubulin and Gapdh as a loading control. Bars represent mean soluble tubulin \pm SEM $n = 5$ with a representative blot shown below. **B** Cells used in generating panel A were then lysed after PEM washout and western blotted for α -tubulin and Gapdh as a loading control. Bars represent mean insoluble tubulin \pm SEM $n = 5$ with a representative blot shown below.

β 3 Dependent Microtubule Stability Regulators in Endothelial Cells

We next turned our attention to elucidating the mechanism behind changes in microtubule stability in β 3 depleted endothelial cells. We had the possibility of searching for a protein that was recruited to the adhesome upon β 3 depletion to promote stability or one that was displaced from the adhesome to destabilise microtubules. We knew that β 1 is known to stabilise microtubules at focal adhesions²³⁷, however none of the proteins involved in that mechanism such as β 1, α 5, Tln1, and Kank1¹⁷⁸ or similar proposed mechanisms involving Iqgap1²⁷⁸ were detected or upregulated upon β 3 depletion in the endothelial adhesome (see supplementary tables 3 and 4). Therefore we attributed the changes in microtubule stability to a dominant negative role played by β 3, supported by the fact that β 1 was still present in β 3+/+ cell adhesomes at equal levels to that of β 3+/- and β 3-/- cells; narrowing down candidate regulators to those that were lost from the adhesome upon β 3 depletion. We also knew that from figures 5-2 and 5-3 that β 3 containing cells show less targeting of microtubules, which was also not VEGF dependent, leading us to the conclusion to search for microtubule regulating proteins in the fibronectin adhesome. Figure 4-6, which was built from our adhesome data, identified a number of candidate proteins that could have been behind the increased microtubule stability of β 3 depleted cells using our adhesome data. Only two proteins were labelled green (decreased abundance in the adhesome upon β 3 depletion) and in the central column (the fibronectin adhesome): Rcc2 and Pcd6ip (Programmed cell death 6 interacting protein). Of the two, Rcc2 appeared a much more promising candidate as a microtubule regulator that could explain our phenotypes according to literature.

Rcc2 is known to interact with microtubules and be important in spindle assembly during early mitosis^{243,416}. Recently, Rcc2 has been found to possess GEF ability and can use this to control Rac1 activity²⁴⁴ through its interaction with Coro1c (Coronin, actin binding protein 1c) which can assist with directional migration^{417,418}. Figure 4-6 suggested that Rcc2 is only recruited to the adhesome with β 3 presence making Rcc2 a likely candidate in our cells for β 3 driven microtubule regulation. We initially tested this candidate using siRNA to produce a knockdown of Rcc2 protein levels. We were reliably able to knockdown Rcc2 in β 3+/+ IMMLEC cells, with an example blot shown in figure 6-3A. After Rcc2 knockdown we subjected our cells, along with control pool siRNA treated control cells, to the same cold stability assay used in figure 6-1. Staining and counting of microtubules revealed a significant increase in the number of cold stable microtubules upon Rcc2 knockdown, shown in figure 6-3B with example images in figure 6-3C. Even with incomplete

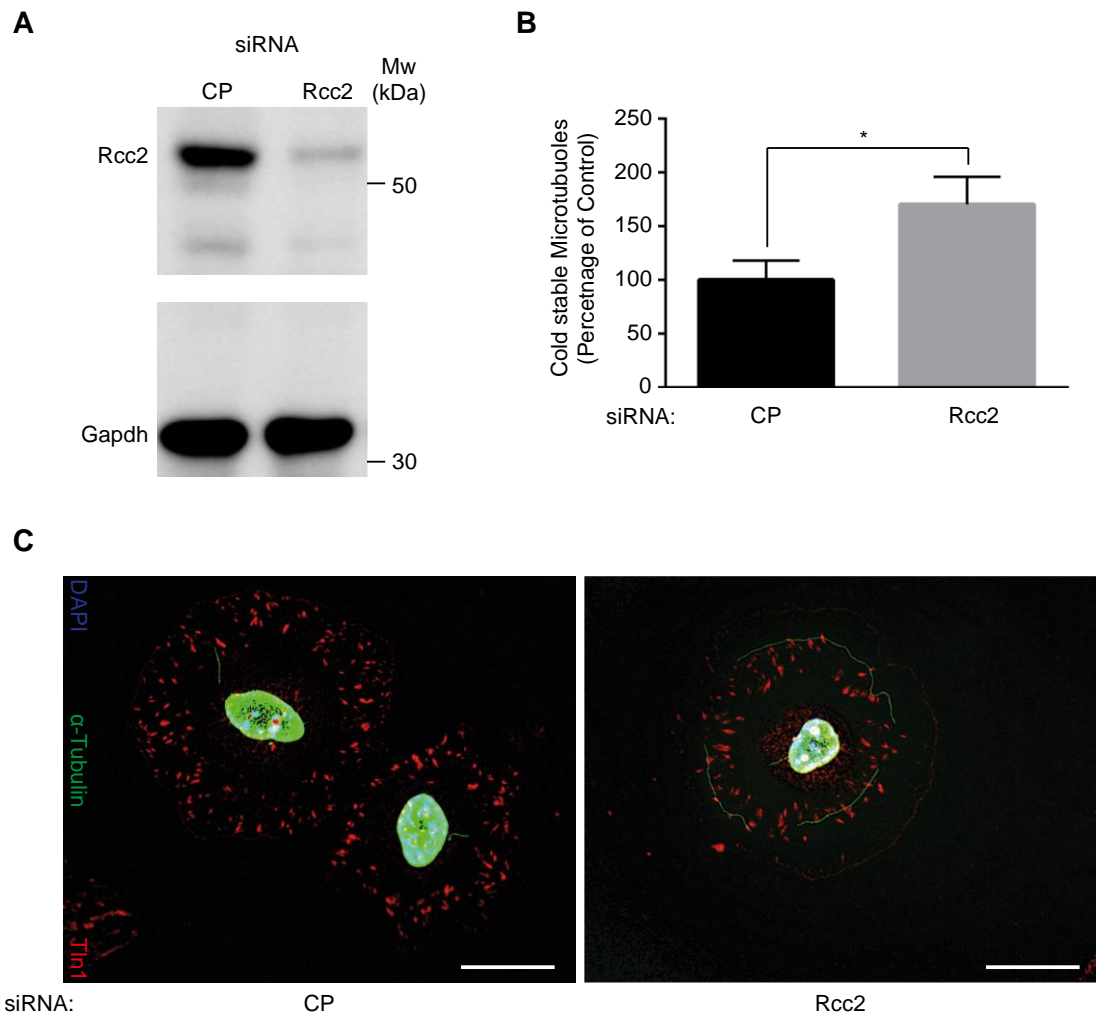
knockdown, the increase in microtubule stability with lower levels of Rcc2 lead us to the conclusion that Rcc2 is at least partially responsible for the effects of $\beta 3$ on microtubules. Also, we had shown that our adhesome data could be used to successfully identify targets relevant to endothelial cell behaviour and perhaps with future uses in anti-angiogenic therapies.

Although the interactions of Rcc2 with microtubules are quite well known, and we had shown this was somehow inhibitory to stability in endothelial cells, we did not yet know how Rcc2 interacts with $\beta 3$. Figure 4-6, as the culmination of different sources of adhesome data, showed Rcc2 and $\beta 3$ to be in the same adhesome cluster; which gave a higher probability these proteins were involved in the same complex than if Rcc2 was found in a different cluster. Williamson et al⁴¹⁸ had previously carried out GFP-Rcc2 fusion protein pulldowns and compared this with GFP-only control pulldowns using mass spectrometry in HEK-293T cells but had only published part of the dataset. We believed the full dataset could provide us with more information about Rcc2 interactions and potentially reveal the link to $\beta 3$. Through a collaborative agreement, we obtained the full list of proteins which we found in higher abundance in GFP-Rcc2 pulldowns compared to GFP control pulldowns which is shown in supplementary table 6. We correlated this data with our adhesome data, specifically to identify proteins in the same cluster as $\beta 3$ and Rcc2 but also decreased in the adhesome with $\beta 3$ depletion like Rcc2. We found Anxa2 correlated in this manner between the Rcc2 pulldown and in both the $\beta 3+/-$ (supplementary table 3 row 185) and $\beta 3-/-$ (supplementary table 4 row 111) adhesomes. Anxa2 is a calcium dependent phospholipid binding protein found in many cellular compartments including on the cell surface and involved in many different roles, cell types and diseases including a strong association with cancer when misregulated⁴¹⁹; Anxa2 also has specific roles in angiogenesis during tumour growth⁴²⁰. Additionally Anxa2 has been shown to interact with $\beta 1$ ⁴²¹ and αm ⁴²² and can therefore influence focal adhesion behaviour such as recycling⁴²³.

We set out to prove the relevance of Anxa2 in $\beta 3$ dependent microtubule stability using knockdown experiments as before with Rcc2. Knockdowns of Anxa2 using siRNA proved to be more difficult and were not overly successful as shown in figure 6-4A however across multiple experiments the reduction of Anxa2 protein level, shown in figure 6-4B was significant. Despite the modest knockdown, figure 6-4C shows that there was still a significant increase in cold stable microtubules compared to control pool siRNA treated cells. Example images shown in figure 6-4D illustrate how dramatic the increase was and

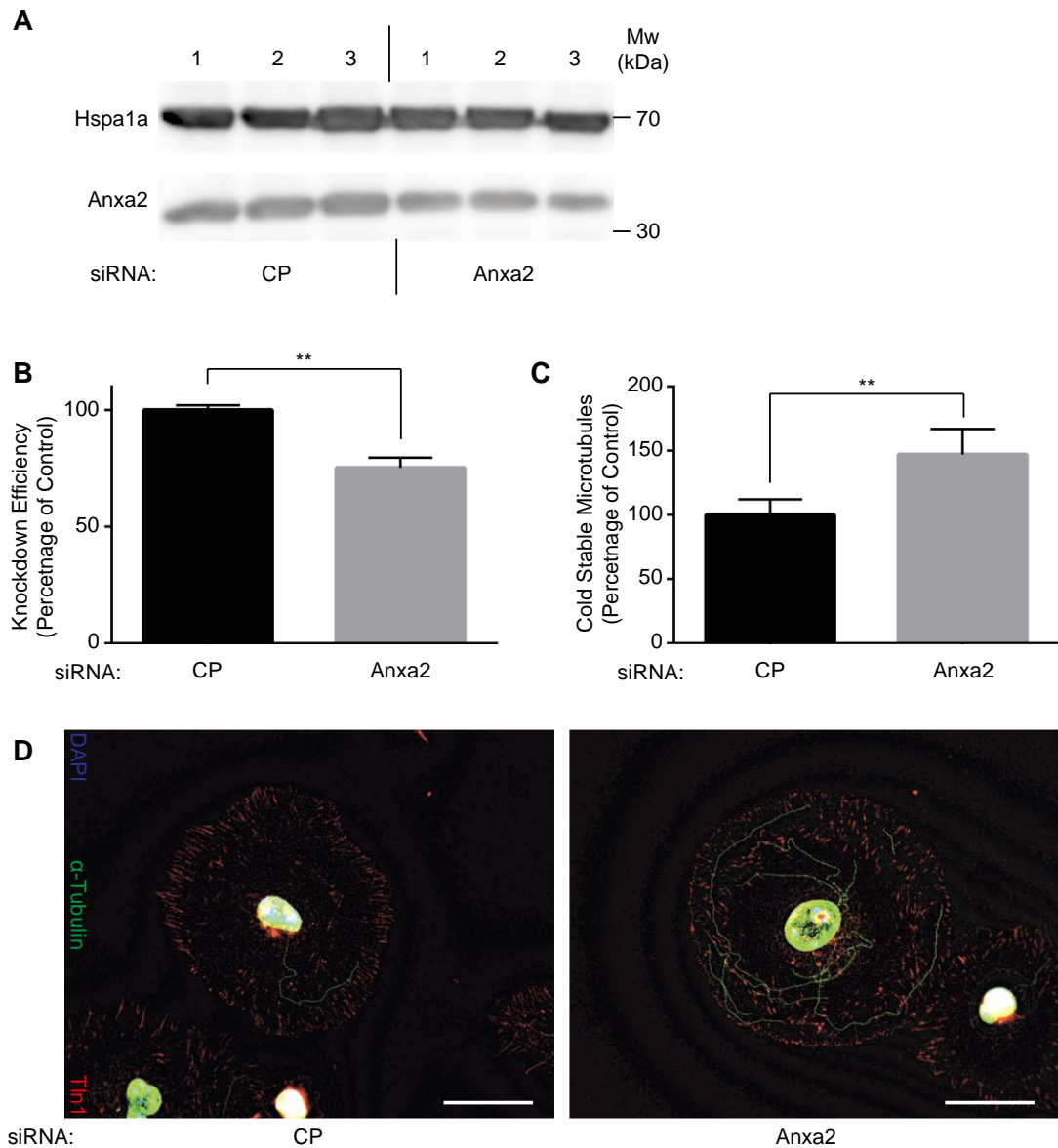
hence we believed Anxa2 to be very important in the mechanism of β 3 dependent microtubule stability considering the strong phenotype on top of a modest knockdown.

Figure 6-3 Rcc2 Regulates Microtubule Stability in Endothelial Cells



A $\beta 3^{+}/+$ IMMLECs were transfected with control pool (CP) or Rcc2 smart pool siRNA and allowed to recover for 48 hours. Cells were lysed and western blotted for Rcc2 or Gapdh as a loading control. Blot is representative of all Rcc2 knockdowns used in this figure. **B** Cells transfected as per panel A were adhered to fibronectin coated coverslips for 75 minutes at 37°C before being moved to ice for 15 minutes. Soluble tubulin was washed out using PEM buffer before fixing with -20°C methanol. Immunostaining for α -tubulin was carried out to allow counting of cold stable microtubules per cell. Bars = mean number of cold stable microtubules shown as a percentage relative to CP treated cells \pm SEM n = 224. **C** Representative immunostaining of cells used from panel B. α -tubulin (green), Tln1 (red) and DAPI (blue) as a nuclear stain. Scale bar = 20 μ m.

Figure 6-4 Anxa2 Regulates Microtubule Stability in Endothelial Cells



A $\beta 3^{+/+}$ IMMLECs were transfected with control pool (CP) or Anxa2 smart pool siRNA and allowed to recover for 48 hours before being lysed and western blotted for Anxa2 or Hspa1a as a loading control. Three different knockdowns are shown to illustrate the small but consistent knockdown. **B** Quantification of knockdown efficiency of Anxa2 shown in panel A as a percentage of control pool signal. Bars = mean \pm SEM. **C** Cells transfected as per panel A were adhered to fibronectin coated coverslips for 75 minutes at 37°C before being moved to ice for 15 minutes. Soluble tubulin was then washed out using PEM buffer before fixing with -20°C methanol. Immunostaining was carried out for α -tubulin to allow counting of cold stable microtubules. Bars = mean number of cold stable microtubules per

cell as a percentage of control pool \pm SEM n = 100. **D** Representative images of cells used in panel C. Immunostained for α -tubulin (green), Tln1 (red) and nuclear stained using DAPI (blue). Scale bar = 20 μ m.

Rac1 Drives Microtubule Stability in $\beta 3$ Depleted Endothelial Cells

The next stage in our investigation was to explain how $\beta 3$ directed changes in Rcc2 and Anxa2 affected microtubule stability. We had shown earlier that Rcc2 and Anxa2 knockdowns had increased microtubule stability in $\beta 3^{+/+}$ cells and that Rcc2 and Anxa2 are lost from the adhesome upon $\beta 3$ depletion. Therefore it was reasonable to believe that Rcc2 and Anxa2 function were related to or responsible for the increased microtubule stability in $\beta 3$ depleted cells seen in figures 6-1 and 6-2. Previous work from our collaborators and others had shown that Rcc2 is able to bind Rac1 directly and in doing so can control its access to GEFs which would alter its activity⁴¹⁶⁻⁴¹⁸. Rac1 is of considerable interest in anti-angiogenesis and anti-cancer treatments due to its many roles in cell migration²⁷⁵, either through direct effects on actin dynamics or on downstream signals also affecting cell survival, growth or pro-angiogenic signalling utilising important pathways such as Erk1/Erk2⁴²⁴. Interestingly Rac1 has also been associated with $\beta 3$ in endothelial cells. D'Amico et al⁴²⁵ showed that, in tumour angiogenesis, Rac1 depletion has no effect on angiogenic responses in $\beta 3^{+/+}$ mice or cells. However, upon $\beta 3$ depletion, Rac1 co-depletion did affect angiogenesis. It appeared to us that Rac1 driven processes were not sensitive to depletion unless $\beta 3$ was also depleted or that Rac1 somehow became more important for endothelial cells in $\beta 3$ depleted situations. The mechanisms behind this $\beta 3$ dependence were never fully derived but we believed we may have found them in the form of microtubule stability. Rac1 is currently known to have several mechanisms through which it can influence microtubule stability⁴²⁶⁻⁴²⁸ including capture through Iqgap1 and Clip1²⁷⁴.

Given we had successfully shown tumour growth and endothelial migration was sensitive to microtubule inhibitors during $\beta 3$ depletion in figure 5-5 and that this correlated with microtubule stability in figures 6-1 and 6-2, we decided to test if Rac1 activity was behind these effects using further microtubule cold stability assays as before. We chose to use a Rac1 inhibitor known as NSC23766 which can reduce Rac1 activity by inhibiting specific Rac1 GEFs without inhibiting the binding of Rac1 to downstream effectors or the activity of closely related Rho-GTPases such as Cdc42 or RhoA⁴²⁹. Figure 6-5A shows that NSC23766 only affects microtubule stability in $\beta 3^{+/-}$ or $\beta 3^{-/-}$ cells but not $\beta 3^{+/+}$ cells, which can also be seen in the representative pictures of figure 6-5B. This key finding indicated to us that the increased microtubule stability in $\beta 3$ depleted cells is dependent on Rac1 activity.

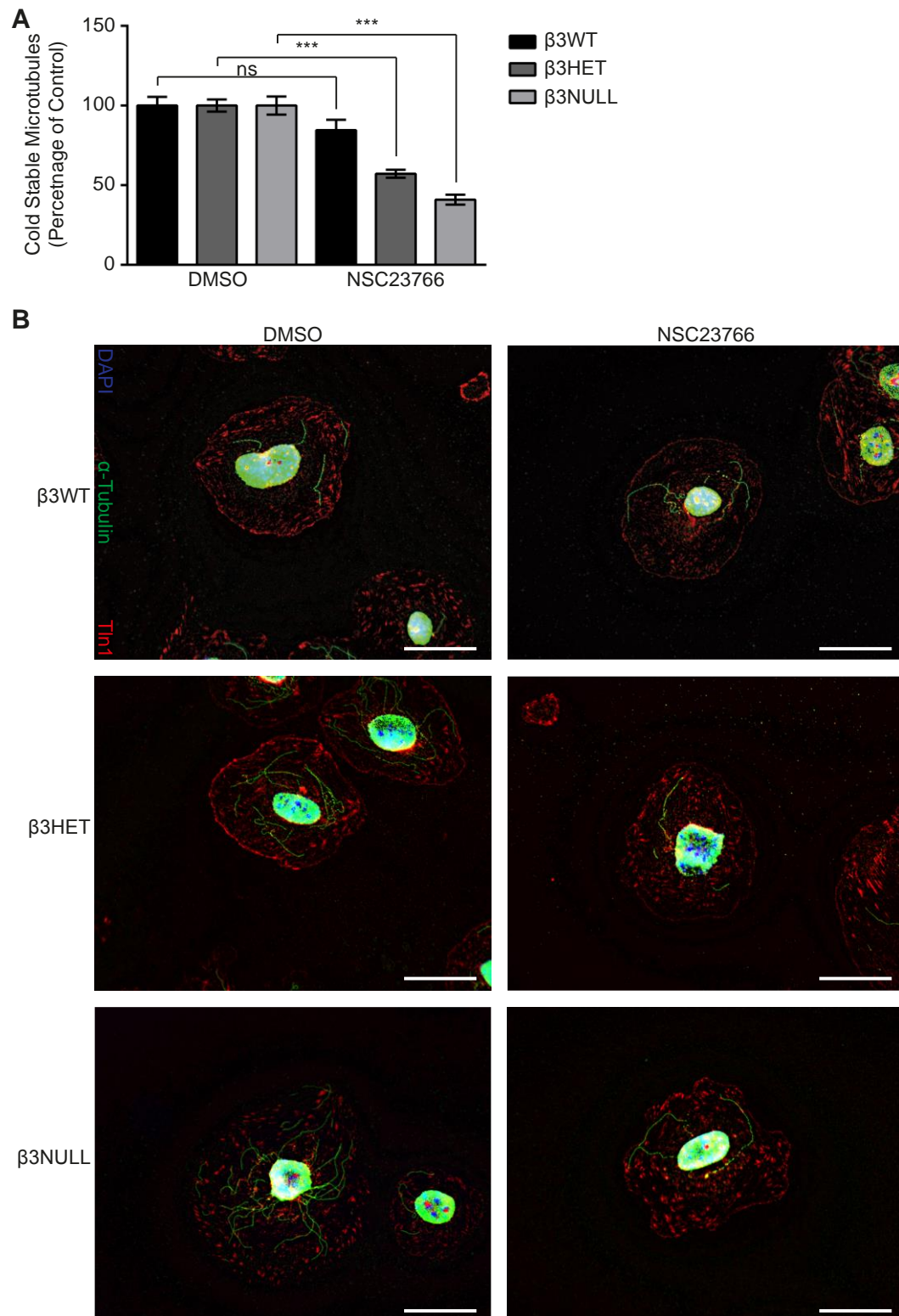
We were tempted to speculate that the simplest explanation of Rac1 involvement would have been true; that Rac1 recruitment to the endothelial adhesome was dependent on $\beta 3$.

However this was not the case in supplementary table 3 or 4-5. Rcc2's role in regulating GEF exposure of Rac1 therefore seemed more a more likely explanation instead of Rac1's localisation being the driving factor of phenotypes observed so far. Additionally we believed Anxa2 was able to bind Rcc2, as shown in supplementary table 6, and assist in Rcc2 localisation to the adhesome by interaction with β 3. If true, then both Rcc2 and Anxa2 would have a role to play in making Rac1 activity important for microtubule stability. Anxa2 has also been shown to interact itself with Rac1 and control its localisation to the membrane⁴³⁰. We tested this theory using Rcc2 and Anxa2 siRNA knockdowns as before in figures 6-3 and 6-4 in microtubule cold stability assays along with the Rac1 inhibitor NSC23766. Figure 6-6A, along with representative pictures in figure 6-6B, show that the increased microtubule stability observed with Rcc2 and Anxa2 depletion earlier is dependent on Rac1 activity. I.e. without Rac1 activity, Rcc2 and Anxa2 depletion had no effect.

We believed, from the combination of experiments carried out in this investigation, that Rcc2 and Anxa2 loss from the adhesome was causing an increase in Rac1 activity which lead to an increase in microtubule stability in β 3 depleted cells. In β 3+/+ cells Rac1 activity was held in check by its association with Rcc2/Anxa2/ β 3 in the adhesome, preventing microtubule capture at or around focal adhesions by not allowing Rac1 directed microtubule stability to occur. To investigate this mechanism further we decided to assess the amount of active Rac1 in β 3+/+, β 3+/- and β 3-/- cells using a Pak1-PBD pulldown assay which worked on the principle that Pak1-PBD coated magnetic beads would only bind to GTP-Rac1. This assay proved to somewhat unreliable, likely due to rapid hydrolysis of GTP to GDP preventing the successful pulldown of GTP-bound (active) Rac1, therefore we did not apply a full statistical analysis to the results however figure 6-7A does show increased active Rac1 in β 3+/- cells compared to β 3+/+ cells. We were not able to reliably detect an increase in active Rac1 in β 3-/- cells however. Given the conclusions of how important Rac1 activity was shown to be important in figures 6-5 and 6-6 to explain β 3 driven changes in microtubule stability, and that Rac1 is actually a cluster I protein in the endothelial adhesome (figure 4-2 and supplementary table 2) meaning it was found more in the non-focal adhesion areas of the adhesome but still present in focal adhesions, we came to the conclusion that both Rac1 activity and localisation of active Rac1 were important. Adhesome enrichment and mass spectrometry experiments were not able to distinguish from inactive or active Rac1 to support this conclusion, however we were able to probe for several proteins that complex with active Rac1 in IMMLEC cells using the Pak1-PBD

pulldowns. In figures 6-7A ad 6-7B, $\beta 3$ was detected in association with active Rac1 only in $\beta 3^{+/+}$ but not $\beta 3^{+/-}$ cells, and obviously none in $\beta 3^{-/-}$ cells. Additionally greater associations were detected between Rcc2 and active Rac1 in $\beta 3$ depleted cells, and a similar result for Anxa2 strengthening our conclusion. Finally, much greater $\alpha 5$ associations were detected in $\beta 3$ depleted cells suggesting that without $\beta 3$ there was more active Rac1 associated with $\alpha 5$. Active Rac1 associations with $\alpha 5$ offer a different interpretation of $\alpha 5\beta 1$ directed microtubule stabilisation than is often found in the literature such as via Tln1 and Kank1¹⁷⁸ which will be discussed in the next chapter.

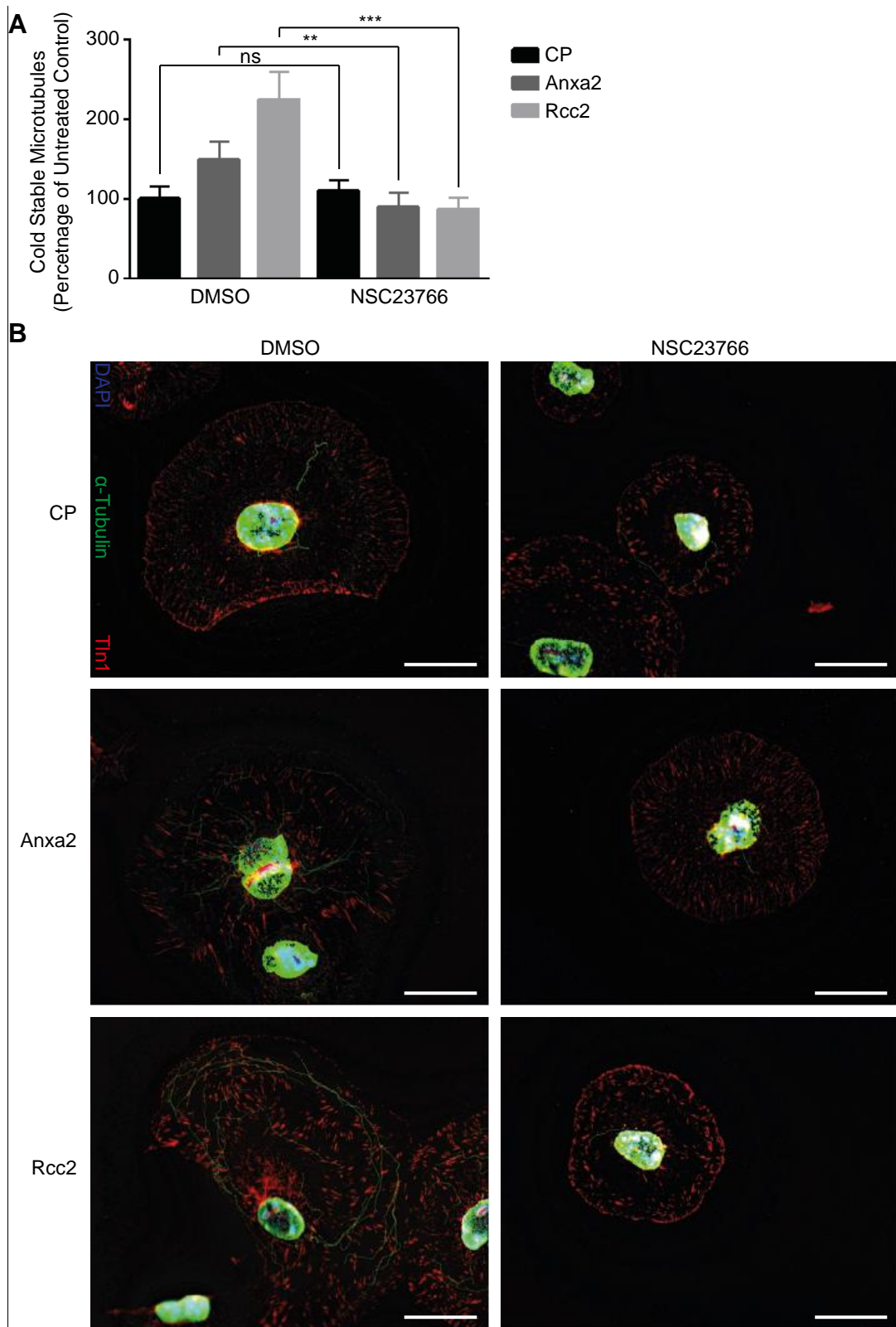
Figure 6-5 Rac1 Inhibition Decreases Microtubule Stability in $\beta 3$ Depleted Endothelial Cells



A $\beta 3^{+/+}$, $\beta 3^{+/-}$ and $\beta 3^{-/-}$ IMMLECs were adhered to fibronectin coated coverslips for 60 minutes at 37°C before being treated with DMSO (control) or 50 μ M NSC23766 and

incubated at 37°C for a further 15 minutes. Coverslips were moved to ice for 15 minutes. Soluble tubulin was then washed out using PEM buffer before fixing with -20°C methanol. Immunostaining was carried out for α -tubulin to allow for counting of cold stable microtubules. Bars = mean number of microtubules per cell shown as a percentage relative to the DMSO control \pm SEM n = 218. **B** Representative images of cells treated as in panel A, immunostained for α -tubulin (green), Tln1 (red) with DAPI (blue) as a nuclear stain. Scale bar = 20 μ m.

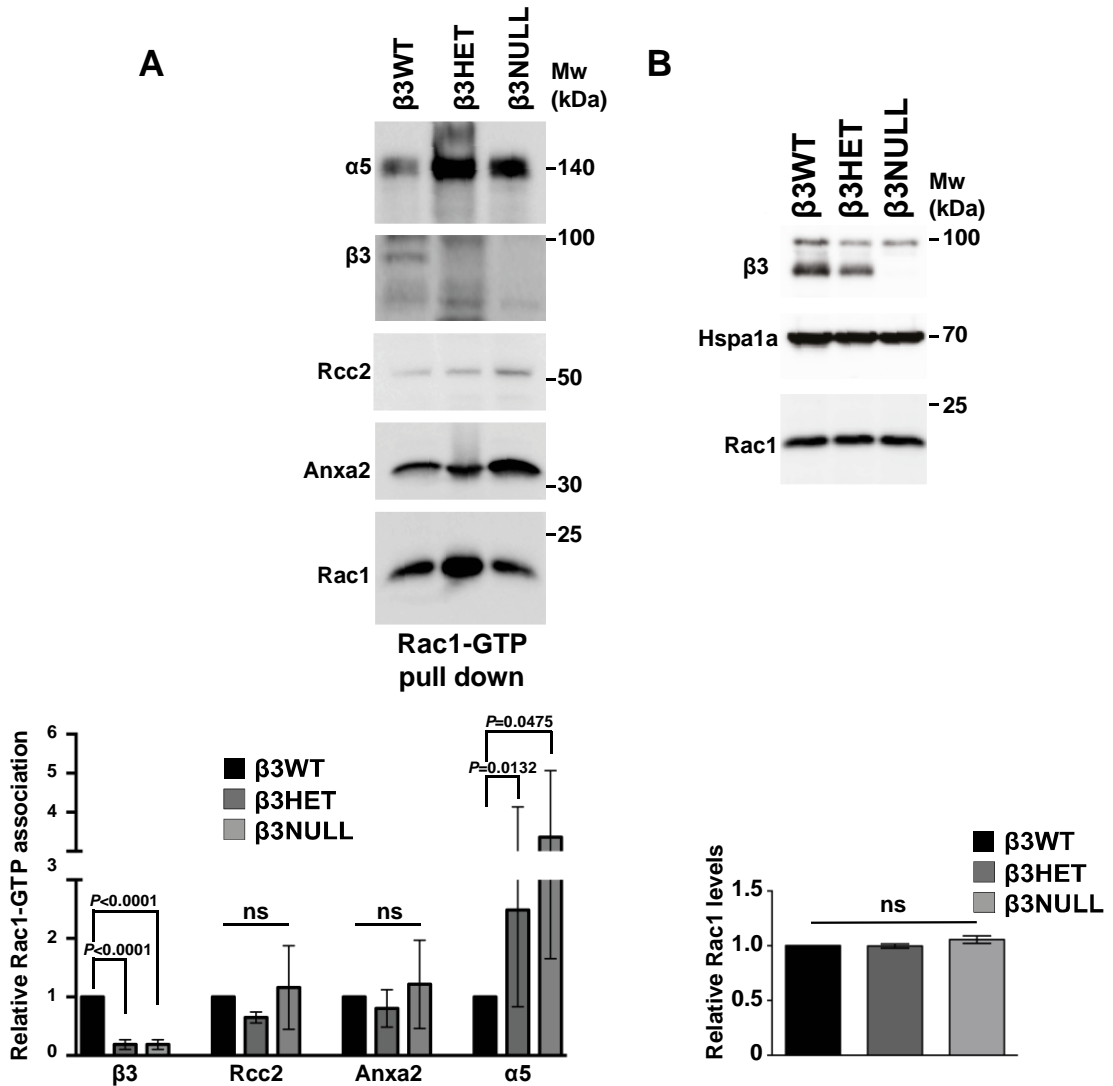
Figure 6-6 Rcc2 and Anxa2 Dependent Microtubule Stability is driven by Rac1 in Endothelial Cells



A $\beta 3^{+/+}$ IMMLECs were transfected with control pool (CP), Anxa2 or Rcc2 smart pool siRNA and allowed to recover for 48 hours then were adhered to fibronectin coated coverslips for

75 minutes at 37°C before being moved to ice for 15 minutes. Soluble tubulin was then washed out using PEM buffer before fixing with -20°C methanol. Immunostaining was carried out for α -tubulin to allow counting of cold stable microtubules. Bars = mean number of cold stable microtubules per cell as a percentage of DMSO treated control pool cells \pm SEM n = 100. **B** Representative images of cells from panel A, immunostained for α -tubulin (green), Tln1 (red) with DAPI (blue) as a nuclear stain. Scale bar = 20 μ m.

Figure 6-7 Active Rac1 Associates with Different Microtubule Regulators in Itb3 Depleted Endothelial Cells



A $\beta 3^{+/+}$, $\beta 3^{+/-}$ and $\beta 3^{-/-}$ IMMLECs were adhered to fibronectin coated plates for 90 minutes before being lysed in MLB. GTP-Rac1 and bound proteins were extracted from cleared MLB using Pak1-PBD magnetic beads at 4°C for an hour as per manufacturer’s instructions before being western blotted for $\alpha 5$, $\beta 3$, Rcc2, Anxa2 and Rac1. Blot (top) is representative of at least 3 independent experiments. Quantification of experiments is shown in bottom panel. Bars = mean level of association of the indicated protein with GTP-Rac1, shown relative to $\beta 3^{+/+}$ associations \pm SEM. **B**. Independently of panel A, $\beta 3^{+/+}$, $\beta 3^{+/-}$ and $\beta 3^{-/-}$ endothelial cells were adhered to fibronectin for 90 minutes before being lysed and Western blotted for $\beta 3$, Hspa1a (Hsc70; as a loading control) and Rac1. Blot is representative of 3 independent experiments with quantification of experiments shown in

bottom panel. Bars = mean relative amount of Rac1 \pm SEM. Panel B experiments were performed with assistance from Abdullah Alghamdi, University of East Anglia.

Chapter seven – Discussion

Modes of Integrin $\beta 3$ Inhibition

In order to define the role $\beta 3$ plays in the endothelial cell adhesome we had to find ways of inhibiting it. We used various methods throughout this investigation in an attempt to strengthen our conclusions by overcoming the possibility that one method could have an inherent flaw. As a by-product we discovered that the method of $\beta 3$ disruption greatly affects the outcome. It had previously been observed that $\beta 3^{-/-}$ mice show increased angiogenic responses²¹⁵ and that this was due to a combination of increased VEGFR2 signalling and an increase in $\beta 1$ focal adhesion formation through decreases in Vasp (Vasodilator stimulated phosphoprotein) and RIAM^{216,386}. These mechanisms are primarily driven by phosphorylation and hence would not necessarily be evident in our quantitative mass spectrometry datasets and indeed no total protein levels of VEGFR2, Vasp or RIAM were upregulated in any of our adhesome datasets in chapter 4. These $\beta 3^{-/-}$ studies had previously been criticised in that a global and complete knockout of $\beta 3$ was not physiologically relevant and would not represent a cancer treatment setting where an inhibitor would not be perfectly efficient. $\beta 3^{+/-}$ mice had also showed enhanced angiogenesis with the study by Ellison et al and others expanding the mechanism of $\beta 3$ angiogenesis suppression to include the VEGF co-receptor Nrp1^{52,218}. Supplementary figure 3 shows that there is a linear relationship between $\beta 3$ gene deletion and migration speed i.e. $\beta 3^{-/-}$ IMMLECs migrate faster than $\beta 3^{+/-}$ which migrate faster than $\beta 3^{+/+}$ on fibronectin, which suggested to us that there may be similarities in the adaption to partial and total losses of $\beta 3$. However adhesome results in chapter 4 casted doubt on this suggestion, where significant changes in supplementary tables 3 and 4 were not similar. Enrichment analysis of the adhesome results in tables 4-2 and 4-3 confirmed this dissimilarity between $\beta 3^{+/-}$ and $\beta 3^{-/-}$ $\beta 3$ gene deletion as no similarities were shown with the exception of cluster F, a focal adhesion cluster defined in figure 4-2, suggesting that a minority of core focal adhesion proteins were affected in the same way, possibly ones that bind directly to $\beta 3$ only, but that this led to no meaningful downstream consequences. We speculated the lack of similarities in the $\beta 3^{+/-}$ and $\beta 3^{-/-}$ adhesomes could have been due to the samples being prepared in difference experiments, however the $\beta 3^{+/+}$ controls used in both the generation of the $\beta 3^{+/-}$ and $\beta 3^{-/-}$ samples did show a reasonable correlation in figure 4-1C. An alternative explanation was that there are different compensation mechanisms for total and partial loss of $\beta 3$ and that it is merely coincidence that this results in a linear relationship between migration speed and extent of gene deletion in

supplementary figure 3. The true answer is likely somewhere in between and would require further investigation.

Significant increases in microtubule recruitment to the adhesome in $\beta 3^{+/-}$ cells was the most striking finding from our adhesome analysis. Yet, every readout of microtubule function tested in this investigation suggested that $\beta 3^{-/-}$ cells were just as susceptible to microtubule inhibition as $\beta 3^{+/-}$ cells and, as mentioned in chapter 4, the $\beta 3^{-/-}$ adhesome with VEGF stimulation does include some significant enrichment of microtubule categories. Figure 5-2, showing the effects of $\beta 3$ deletion and VEGF in targeting microtubules to focal adhesions and in this case there was a significant decrease of microtubule targeting to focal adhesions in $\beta 3^{-/-}$ cells with VEGF compared to without, but $\beta 3^{+/-}$ cells appeared unaffected by VEGF. The differences in the way VEGF affects adaptation to $\beta 3$ is possibly due to the increased VEGFR2 expression reported in $\beta 3^{-/-}$ mice and liberation of Nrp1 to participate in VEGF signalling^{52,215}. We considered the investigation into why both $\beta 3^{-/-}$ and $\beta 3^{+/-}$ cells were more sensitive to microtubule inhibition a more pressing subject, but we have not fully explored the adhesome datasets for $\beta 3^{+/-}$ and $\beta 3^{-/-}$ cells with VEGF stimulation which could be investigated further.

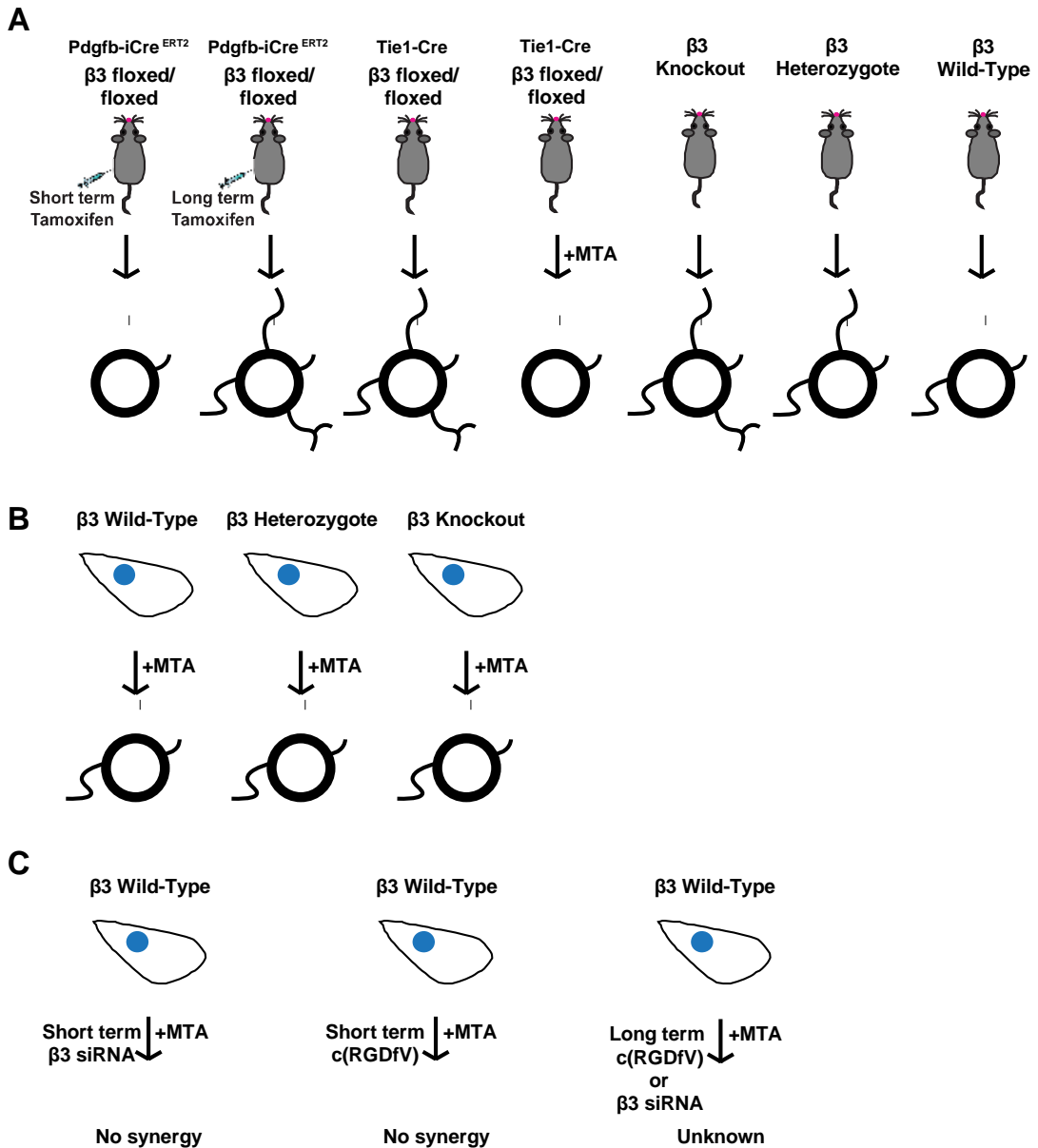
We also wanted to investigate how inhibitors like RGD mimetics affected the endothelial adhesome and if these were similar to that of genetic deletions in the $\beta 3^{+/-}$ and $\beta 3^{-/-}$ IMMLECs; we also hoped this would explain the disappointing clinical data behind drugs such as Cilengitide^{®212}. Figure 4-7B and supplementary table 5 showed that c(RGDfV) had no effect on the composition of the adhesome, despite figure 4-7A showing the dose of c(RGDfV) used was able to inhibit $\alpha v\beta 3$ dependent vitronectin binding. Concerned a problem with the mass spectrometry dataset had obscured any potential findings, we tested the c(RGDfV) inhibitor on random migration in combination with microtubule inhibitors, shown in figure 5-6A, as this had a dramatic effect on IMMLECs with a genetic deletion of $\beta 3$ but no synergy between the inhibitors was observed. This led us to the conclusion that c(RGDfV), and possibly other RGD mimetics, had no effect on the endothelial adhesome and hence would likely have little impact on tumour growth. We believe this tells us that in endothelial cells, $\beta 3$ ligation is enough to trigger recruitment of $\beta 3$ dependent members of the adhesome. RGD mimetics are designed to fit into the fibronectin binding site of $\alpha v\beta 3$, in an attempt to prevent matrix engagement and pro-angiogenic signalling. However it appears that RGD mimetics like Cilengitide[®] are actually able to activate $\beta 3$ in a similar way to matrix engagement³⁷⁷ which could be part of the reason that Cilengitide[®] has been found to be pro-angiogenic in low doses²¹⁴. Ligation to a

small molecule like c(RGDfV) would not provide the same stiffness response as that of a complex matrix, but this may be beyond the range of normal $\beta 3$ function in endothelial cells. Schiller et al¹⁸⁶ had already shown that $\beta 1$ containing integrins are responsible for stiffness sensing in fibroblasts via Myh2. They showed that if a fibroblast was able to sense a matrix stiff enough using $\beta 1$, then mature focal adhesions would develop containing $\beta 3$. If we assume this is also true in endothelial cells, then it would make sense that soluble RGD mimetic ligation is sufficient to activate $\beta 3$ and recruit its mediators to the adhesome because the stiffness sensing is carried out by $\beta 1$ instead. As a result there would be no difference in downstream signalling from c(RGDfV) binding as fibronectin ligation, which is supported by our adhesome data showing no differences between c(RGDfV) and DMSO control treated IMMLECs, as stiffness sensing is not within the “repertoire” of $\beta 3$. This is consistent with our adhesion assays showing c(RGDfV) reduces adhesion to vitronectin in figure 4-7A: whilst c(RGDfV) may induce similar signalling to matrix ligation, it does not form a physical connection to anchor the cell. As a future investigation, it would be interesting to evaluate whether $\alpha 5\beta 1$ blocking peptides or antibodies^{431,432} also have no effect on the endothelial adhesome with and without constitutive activation of Myh2, to induce the matrix stiffness response.

Finally, in an attempt to explain the conflicting pro and anti-angiogenic roles of $\beta 3$, Steri et al²²³ had observed that acute genetic depletion of $\beta 3$ inhibited tumour growth and angiogenesis whereas long term depletion promoted it. We thought this could also offer some insight into the differences between our c(RGDfV) treated IMMLECs and $\beta 3+/-/\beta 3-/-$ as our pharmacological inhibition was always a short term treatment during the 90 minute adhesions of the cell. We had shown that $\beta 3+/-$ and $\beta 3-/-$ IMMLECs were sensitive to microtubule inhibition during random migration in figure 5-5 and that tumour growth and angiogenesis in Tie1 cre $\beta 3$ floxed/floxed mice was decreased when $\beta 3$ was deleted along with eribulin treatment in figure 5-7. Tie1 driven cre is a constitutively active cre in endothelial cells, therefore we used an inducible cre in figure 5-8 to test whether eribulin treatment would synergise with acute $\beta 3$ loss. It turned out that it did not, confirming the findings that the method and length of $\beta 3$ depletion is important in determining the angiogenic responses that arise from compensation for its loss. A useful further investigation would be to disentangle the length and method of inhibition further to allow us to develop better therapeutic strategies. For example, Steri et al used tamoxifen to induce $\beta 3$ depletion over a long time and this phenocopied the constitutive Tie1 cre deletion. A similar investigation using c(RGDfV) or other RGD mimetics should be carried

out to see if long term pharmacological inhibition of $\beta 3$ has a similar effect, which could also explain why the c(RGDfV) adhesome showed no differences compared to control in the short experiments we carried out. A summary of how different modes of $\beta 3$ inhibition affects angiogenesis can be seen in figure 7-1.

Figure 7-1 Effects of Different Modes of $\beta 3$ Inhibition During Angiogenesis



A schematic overview showing how different modes of $\beta 3$ Inhibition can affect angiogenesis, which is represented by the numbers of sprouts coming from the rings. **A** Different mouse studies show that: $\beta 3$ knockouts can result in increased angiogenesis²¹⁵, acute deletion of $\beta 3$ driven by Pdgfb cre prevents angiogenesis but chronic does not²²³ and this study demonstrates how angiogenesis with constitutive Tie1-cre deletion of $\beta 3$ is vulnerable to microtubule targeting agents (MTAs). **B** Processes important in angiogenesis such as cell migration can be inhibited or brought down to $\beta 3^{+/+}$ levels in $\beta 3^{+/-}$ and $\beta 3^{-/-}$ cells with MTA treatment. **C** Preliminary results in this study suggests that short term $\beta 3$ inhibition with siRNA or c(RGDfV) does not synergize with MTA treatment but based on results shown in panel A and B, we believe it should be important to investigate long term siRNA or c(RGFfV).

Microtubule Regulation by Integrin $\beta 3$

Much of the evidence provided in this thesis points to $\beta 3$ having a dominant negative role on the recruitment of microtubules to the endothelial adhesome. Without $\beta 3$ present there is an increase in microtubule components at the adhesion, which was particularly evident in the $\beta 3+/-$ adhesome. Additionally there was a significant increase in both microtubule targeting to focal adhesions and lamellipodia in $\beta 3+/-$ and $\beta 3-/-$ endothelial cells shown in figures 5-2 and 5-3 respectively. Prevention of microtubule recruitment to focal adhesions by $\beta 3$ appears to be the opposite to the role of $\beta 1$, which is thought to recruit microtubules to focal adhesions²³⁷. Increased microtubule targeting, due to the lack of $\beta 3$, seems to aid the migration of the $\beta 3+/-$ and $\beta 3-/-$ cells shown in supplementary figure 3, probably by increasing focal adhesion turnover^{189,291}. This greater use of microtubules makes $\beta 3+/-$ and $\beta 3-/-$ cells susceptible to microtubule inhibitors as shown in figure 5-5. Interestingly though, we found that microtubules in the $\beta 3+/-$ and $\beta 3-/-$ cells were more stable compared to those in $\beta 3+/+$ cells, despite this increased susceptibility to inhibitors. Cold stability assays showed, by both staining and biochemical methods in figures 6-1 and 6-2, that more $\beta 3+/-$ and $\beta 3-/-$ microtubules resisted cold induced depolymerisation. Ochoa et al²⁵⁹ have suggested that Map6 is responsible for protecting microtubules during low temperatures and was observed that pulmonary endothelial cells have a permanent cold stable microtubule population as a result. We did not observe Map6, or many microtubule +TIPs at all, in any adhesome datasets, likely due to the difficulty of detecting them and their low abundance. We also did not observe a permanent cold stable microtubule population in our IMMLECs, as was seen in the study identifying Map6. The vast majority of $\beta 3+/+$ IMMLECs in the cold stability assays were observed with no microtubules at all indicating that our cells may not have Map6. However, it was not clear that from if the work by Ochoa et al on cold stability in endothelial cells whether cells were adhered to any matrix prior to cold stability testing. In our assays cells were adhered to fibronectin so it is possible that over 90 minutes, matrix engagement prevented microtubule stabilisation in an $\alpha v\beta 3$ dependent manner not possible if cells were simply adhered to uncoated glass coverslips.

It was tempting to speculate that the increased stability and targeting of microtubules to focal adhesions was due to an increase in $\beta 1$ in order to compensate for the loss of $\beta 3$ as has been observed previously³⁸⁶. However, no adhesome datasets showed a significant increase in $\alpha 5$ or $\beta 1$. Additionally, proteins involved in the two known mechanisms behind microtubule capture by $\beta 1$ via Tln1-Kank1 or via Iqgap1^{178,278} were not significantly

increased in any adhesome datasets. Therefore, the other possible explanation is that $\beta 3$ presence inhibits microtubule recruitment to focal adhesions via a novel mechanism. We mined our adhesome dataset for proteins that appeared to be recruited to the adhesome by $\beta 3$ according to SAM analysis and were known to have a role in microtubule regulation. The result of this analysis, as seen in figure 4-6, was that we identified Rcc2 as a possible mediator of the $\beta 3$ effects on microtubules. Rcc2 has been shown to interact with microtubules during mitosis but has recently been found to have other roles in cell migration^{244,433}. Knockdown of Rcc2 in $\beta 3+/+$ endothelial cells increased the number of cold stable microtubules which suggested Rcc2 was negatively regulating microtubule stability. Although Rcc2 had been detected in adhesome enrichments previously²⁴⁴, the mechanism behind its apparent $\beta 3$ dependent recruitment was unknown. Mass spectrometry analysis of Rcc2 pulldowns had previously been carried out but only partially published⁴¹⁸. Through collaborative arrangements we obtained the full dataset and carried out a comparison with our mass spectrometry datasets to identify Rcc2 interactors that were also dependent on $\beta 3$ for adhesome inclusion. Our conclusion was that Anxa2 was the most likely candidate, given it had been previously shown to interact with some integrins^{421,422} and has known roles in angiogenesis⁴²⁰. Like Rcc2, Anxa2 knockdown increased the number of cold stable microtubules in figure 6-4. It was suggested to us by reviewers that we should also knockdown Rcc2 and Anxa2 in combination to double confirm that they were part of the same system as both knockdowns were incomplete, the results in supplementary figure 4 showed that the double knockdown significantly increased microtubule stability more than single knockdowns.

We believed we had begun to develop an understanding of a protein complex which gave $\beta 3$ the ability to negatively regulate microtubule stability: $\beta 3$ recruits Anxa2 to the adhesome which is bound to Rcc2. We reasoned that the other unknown members of the $\beta 3$ /Anxa2/Rcc2 complex must be the driving force behind the microtubule recruitment and stability phenotypes observed so far. Rcc2 was originally thought to act as a Rac1 GEF but now is thought to bind it and control its access to GEFs through changing Rac1 localisation and inclusion into certain complexes^{417,418}. We knew Rac1 itself had multiple roles in cell migration and itself has been shown to recruit microtubules through Iqgap1 and Clip170 when activated²⁷⁴, hence the localisation and GTP status of Rac1 was of great interest to us in potentially explaining how $\beta 3$ regulated microtubules. Studying Rac1 is always hard due to the difficulty of distinguishing the active GTP bound and inactive GDP forms, with the GTP being unstable and easily hydrolysable, compared to proteins that are regulated by

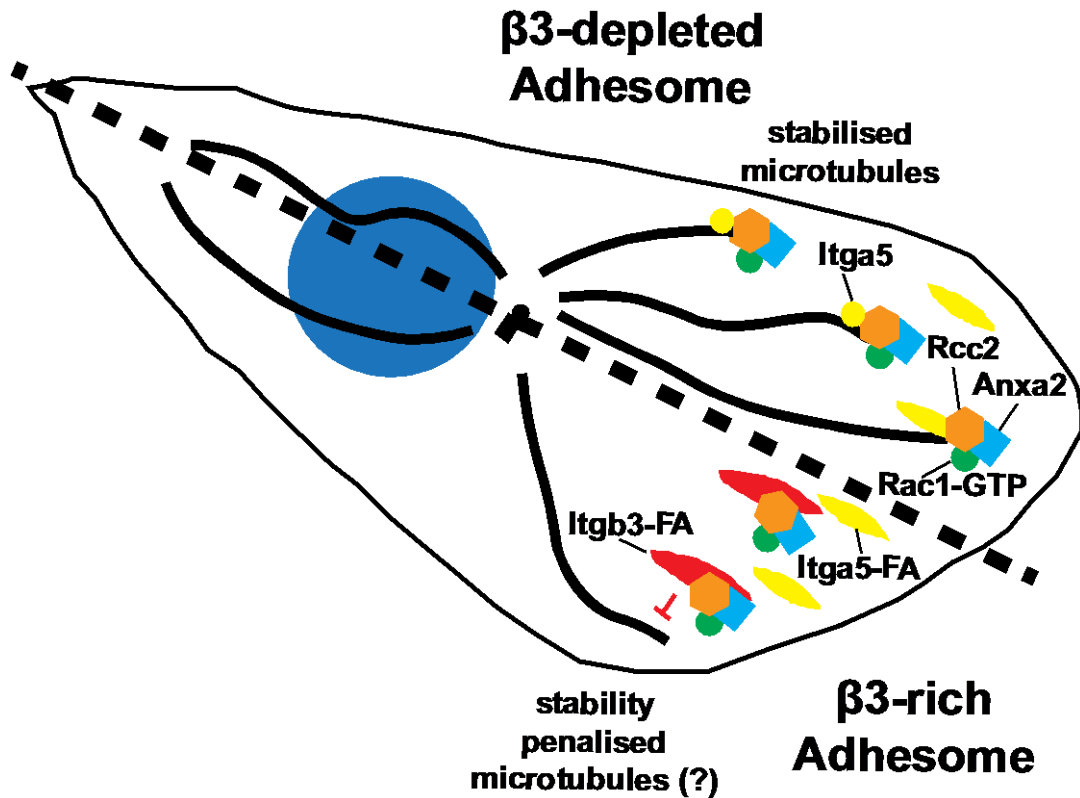
phosphorylation which often have phospho-specific antibody tools. Instead we initially turned to studying Rac1 indirectly through use of the inhibitor NSC23766 where, in figure 6-5. We found NSC23766 suppressed the increase microtubule stability observed in $\beta 3^{+/-}$ and $\beta 3^{-/-}$ cells. Additionally, in case the roles of Rac1 in regulating microtubules were unrelated to the $\beta 3$ /Anxa2/Rcc2 system we had identified, we also observed that NSC23766 prevented the increased stability of microtubules when Rcc2 or Anxa2 were reduced.

Normally active Rac1 is able to recruit microtubules through Iqgap1²⁷⁴, therefore we considered it unlikely that the recruitment of Rac1 by Rcc2 and Anxa2 to $\beta 3$ containing focal adhesions was activating. However, Humphries et al²⁴⁴ noted that when Rcc2 was found in focal adhesions, its role was primarily to inhibit cell migration, which would fit with our finding that the $\beta 3$ /Anxa2/Rcc2 complex is inhibiting Rac1 and therefore microtubule stability and cell migration on fibronectin; we believed we could have found the mechanism behind Rcc2's influence. For this to occur the localisation of Rac1 to focal adhesions by $\beta 3$ /Anxa2/Rcc2 must be to prevent Rac1 from interacting with GEFs. In figure 6-7 we measured protein associations with active Rac1 using Pak1-PBD coated bead pulldowns, which preferentially interacts with GTP-bound Rac1⁴³⁴. We found that GTP-Rac1 only interacts with $\beta 3$ in $\beta 3^{+/+}$ cells and not in $\beta 3^{+/-}$ or $\beta 3^{-/-}$ cells. We suspect there was likely some low level interaction in the $\beta 3^{+/-}$ cells as well, but at a level too low to detect by western blotting. We also found an increased association with Anxa2 and Rcc2 in $\beta 3$ depleted cells suggesting that Anxa2/Rcc2/Rac1 still form a complex even in the absence of $\beta 3$. Additionally the observation of increased $\alpha 5$ association with active Rac1 in $\beta 3^{+/-}$ and $\beta 3^{-/-}$ cells suggested that the documented interaction of $\alpha 5$ with Rac1 is still the primary method of microtubule recruitment to focal adhesions that do not contain $\beta 3$. We concluded that the most likely explanation for our observations is that the Anxa2/Rcc2 complex localises Rac1 to focal adhesions. If the adhesion contains $\beta 3$ then Rac1 is not activated but if the adhesion contains $\alpha 5$ then Rac1 is activated by GEFs. Williamson et al⁴¹⁸ have identified several Rcc2 interacting proteins that are Rac1 GEFs which could be responsible for this activity and we believe one or more of these are missing from $\beta 3$ containing focal adhesions, or alternatively a new Rac1 GAP (GTPase activating protein) is present in the $\beta 3$ adhesome. Unfortunately the coverage of Rac1 GEFs/GAPs is low in our adhesome studies but a key future experiment would be to repeat active Rac1 pulldowns in $\beta 3^{+/+}$, $\beta 3^{+/-}$ and $\beta 3^{-/-}$ endothelial cells using quantitative mass spectrometry instead of

candidate western blotting to further elucidate our mechanism. A schematic outlining the basics of this mechanism can be seen in figure 7-1.

Although we have highlighted, in this work, some novel ways that $\beta 3$ can affect microtubule behaviour, it is important to consider that $\beta 3$ could also affect microtubule behaviour indirectly through known pathways such as with $\alpha 5$. $\alpha 5$ and its common heterodimer $\beta 1$ are known to capture microtubules through a number of adapters such as *Iqgap1*^{237,291}. Therefore, any changes in $\alpha 5$ behaviour or trafficking from $\beta 3$ inhibition could have profound consequences. For example it has been shown that inhibiting $\alpha v\beta 3$ short-loop recycling can dramatically increase the rate of $\alpha 5\beta 1$ recycling through *Rab11*⁴³⁵. A recent study by Mana et al⁴³⁶ highlighted how *Rab11* along with *Ppfia1* (Protein Tyrosine Phosphatase, Receptor Type, F Polypeptide (PTPRF), Interacting Protein (Liprin), Alpha 1) directs and localises $\alpha 5\beta 1$ recycling as well as promoting microtubule targeting to *Ppfia1* positive areas. To further our study into the role of $\beta 3$ in regulating microtubule behaviour, it would be important to measure $\alpha 5$ recycling, potentially by surface biotinylation¹⁹⁵. We should also determine if inhibition of $\alpha 5$ recycling is responsible for any of the phenotypes observed in IMMLECs from $\beta 3$ depletion by inhibiting known recycling pathways through *Rab* knockdowns, pharmacological inhibitors such as primaquine or depletion of $\alpha 5$ ^{437,438}.

Figure 7-2 Possible Mechanisms Behind $\beta 3$ Regulation of Microtubules



A model representing how $\beta 3$ could control microtubule behaviour in fibronectin adhered endothelial cells. A line drawn through the cell allows the comparison of two scenarios: one where there are normal levels of $\beta 3$ (bottom) and another where there is $\beta 3$ depletion (top). $\beta 3$ recruits a complex of Rac1-GTP, Rcc2 and Anxa2 which can reduce the stability of microtubules at focal adhesions. When $\beta 3$ is absent, $\alpha 5$ instead can recruit the same complex which leads to stabilisation of microtubules.

Microtubules as Targets for Integrin $\beta 3$ Treatment Escape

Regardless of the exact mechanism behind $\beta 3$ control of microtubule targeting and stability, we have shown that using microtubule targeting agents is a potentially powerful anti-cancer tool in combination with $\beta 3$ inhibition. Steri et al²²³ observed that short term depletion of $\beta 3$ decreased tumour growth and angiogenesis whereas long term depletion increased it. Although done with genetic tools, this kind of investigation could be considered a surrogate for $\beta 3$ treatment escape. Tumours grown in mice tend to develop a lot quicker than in humans and partly this is by design as a mouse's lifespan is much shorter than a human's. Therefore it is impossible to model a slow development of a tumour over several years as sometimes happens in humans⁴³⁹. This is a problem in many studies into tumour angiogenesis where drugs like Cilengitide® could be successful in a fast growing mouse tumour but fail in a slow growing human tumour due to a long term treatment escape. We found that microtubule inhibition did not synergise with c(RGDfV) treatment, siRNA or Pdgfb cre inducible $\beta 3$ depletion as it did with global knockouts or Tie1 cre constitutive depletions, offering further explanations for the failure of RGD mimetics but hope that $\beta 3$ is still a valid target. Therefore we concluded that a possible mechanism behind long term anti- $\beta 3$ treatment escape is the increased targeting and stability of microtubules to focal adhesions, aiding in cell migration.

It was interesting to us that despite increased microtubule stability in response to cold treatment, $\beta 3+/-$ and $\beta 3-/-$ endothelial cells were more sensitive to microtubule inhibitors. We thought that because the microtubule phenotypes were likely a compensation mechanism for loss of $\beta 3$, then it made sense that $\beta 3+/-$ and $\beta 3-/-$ cells were dependent on microtubule function. We have not in this investigation considered what the effects of extra microtubule interaction with focal adhesions are in $\beta 3$ depleted cells but it appears to be pro-angiogenic due to the increased migration speed observed in supplementary figure 3 and the increased tumour growth observed in $\beta 3$ depleted mice^{223,440}. Additionally, it is worth considering that the doses of microtubule destabilising drugs were high enough to depolymerise all microtubules in figure 5-4B, and we assumed stabilising drugs doses were enough to polymerise all microtubules, with no differences between $\beta 3+/+$, $\beta 3+/-$ and $\beta 3-/-$ cells observed, which we believed was due to our doses being much higher than the increased cold stability effect could cope with. Interestingly, with the same doses of inhibitors and presumably completely rigid or no microtubules, $\beta 3+/+$ endothelial cell migration was unaffected in figure 5-5 unlike $\beta 3+/-$ and $\beta 3-/-$ cells for microtubule destabilisers. This indicated that microtubules were not essential for $\beta 3+/+$ cell migration

but are for $\beta 3$ depleted cells, backing up the theory that the microtubule phenotype is a compensation for loss of $\beta 3$. We presumed that overly stabilised microtubules, such as from the action of paclitaxel and epothilone B, in figure 5-5 were still able to affect $\beta 3+ / +$ migration because the rigid microtubules physically resisted the rear edge of cells contracting²⁶³. However it was still promising that $\beta 3+ / -$ and $\beta 3- / -$ cells migrated slower than $\beta 3+ / +$ possibly due to the fact $\beta 3$ containing focal adhesions do not attract as many focal adhesions to the lamellipodia of the cell in the first place as shown in figure 5-3, reducing hindrance in the event of microtubule stabilisation treatment.

Microtubule inhibitors are already being used as anti-angiogenic treatments and, even at sub toxic doses, stabilisers such as docetaxel have been observed to inhibit endothelial cell migration and tube formation in a mechanism also thought to involve Rac1^{441,442}. These results have been exciting clinically because it means that lower doses can be used to achieve the desired therapeutic outcome with fewer side effects²⁸⁹. Our results have shown that efficacy of microtubule stabilisers can be increased even further in combination with $\beta 3$ inhibition, which could be used to widen the therapeutic window further with even lower doses or more aggressively inhibit tumour vascularisation. We have also shown that microtubule destabilising drugs could become even more useful clinically if sufficient $\beta 3$ depletion can be achieved. Drugs such as eribulin had a powerful effect on $\beta 3+ / -$ and $\beta 3- / -$ endothelial cell migration but left $\beta 3+ / +$ cells completely unaffected suggesting that side effects could be lower in patients. Indeed, when we tested a low dose of eribulin in mice in figure 5-7 it reduced tumour growth at sub toxic doses in combination with $\beta 3$ deletion with no side effects but doses of a non-microtubule targeting drug, doxorubicin, were met with significant side effects.

For these strategies to work in human tumours, there is an urgent need for effective integrin inhibitors. We have shown that RGD mimetics like c(RGDfV) induce no changes to the adhesome in figure 4-7 despite still being able to physically block cell adhesion likely because they still trigger outside-in integrin signalling. RGD mimetics may still be useful in targeting other fibronectin binding integrins such as $\alpha 5$ as this could interfere with their stress sensing abilities as hypothesised earlier¹⁸⁶. Function blocking antibodies for certain integrins do exist such as Volociximab for $\alpha 5\beta 1$ which have been shown to suppress angiogenesis and tumour growth⁴⁴³. So far only an effective function blocking antibody is available for use against human $\alpha v\beta 3$ known as LM609⁴⁴⁴, which would not function in our mice. However it would function in human endothelial cells such as HUVECs (Human umbilical vein endothelial cells) and so it would be fairly straight forward to test if it

synergised with microtubule inhibition during random migration or cold stability assays in future studies. Additionally, allosteric inhibitors of $\beta 3$ are being developed such as ProAgi⁴⁴⁵ which could have the potential to inhibit $\beta 3$ without triggering outside-in signalling i.e. prevent the recruitment of the $\beta 3$ adhesome. Alternatively, there are a large number of proteins in the $\beta 3$ dependent adhesome for which we have not characterised their contribution to angiogenesis. Some of them will be unique mediators of $\beta 3$ functions and could include Rac1 effectors. Targeting these proteins instead with inhibitors could be easier using pre-existing compounds that do not have the same issues as RGD mimetics. Any of these strategies would allow us to continue to use $\beta 3$ as a therapeutic target due to its excellent restriction to only angiogenic vasculature³⁷¹ to reduce side effects in vivo.

Further Work – Other Adhesome Targets

Aside from further developing our $\beta 3$ /Anxa2/Rcc2/Rac1 mechanism of microtubule stability in endothelial cells, there is still a vast array of data within our adhesome datasets that likely does not affect microtubule stability but could still contribute to the long term escape from $\beta 3$ inhibition. For example there are enrichments of several endoplasmic reticulum categories in table 4-2 and enrichment of protein folding categories in table 4-3 suggesting that endoplasmic reticulum stress is increasing without $\beta 3$ which has been linked to angiogenesis⁴⁴⁶. Many endoplasmic proteins have been found at focal adhesions and the association of the organelle with adhesions can promote focal adhesion turnover and growth³⁴⁸. At first glance this appears to be a similar phenotype to microtubules in $\beta 3$ depleted cells, where the integrin is preventing the association of the otherwise pro-migratory organelle and so would be worth investigating in the future.

Alternatively, there are many individual proteins that may have unique roles in the adhesome that are recruited to the adhesome upon $\beta 3$ loss and could be equally useful combination therapy targets like microtubules. We have begun to characterise a few of these with the most notable targeting so far being Hsp90, where different isoforms are significantly increased in the $\beta 3$ +/- adhesome as shown in supplementary table 3 lines 37, 66 and 107. Additionally, some but not all of the isoforms detected were significantly increased in the $\beta 3$ -/- adhesome as shown in supplementary table 4 line 86. Heat shock proteins like Hsp90 often act as chaperones to ensure correct folding of proteins under normal and stress conditions but Hsp90 is unusual as its activity is ATP dependent⁴⁴⁷. The ATP binding site of Hsp90 therefore is unique and drugs such as tanespimycin show incredible specificity and, when used clinically, few side effects^{448,449}. Hsp90 is of considerable interest in cancer therapies due to its increased expression in some cancer cells⁴⁴⁸. Interestingly Hsp90, and its ATP metabolising functionality, are thought to be involved in the cross talk between VEGFR2 and Fak1 in an $\beta 3$ dependent mechanism⁴⁴⁷ although why Hsp90 is increased in $\beta 3$ depleted adhesomes is unclear. However, it is worth noting that VEGFR2 is also not present in the adhesome, suggesting there may be alterations to the VEGFR2/Hsp90 interactions by moving Hsp90 to the adhesome without $\beta 3$.

To begin to understand Hsp90's role in the $\beta 3$ depleted adhesome, we tested the effects of its inhibitor in $\beta 3$ +/, $\beta 3$ +/- and $\beta 3$ -/- IMMLECs in random migration assays similar to figure 5-5. The results, as shown in supplementary figure 5, indicated that tanespimycin significantly inhibited the migration of $\beta 3$ +/- and $\beta 3$ -/- endothelial cells much like

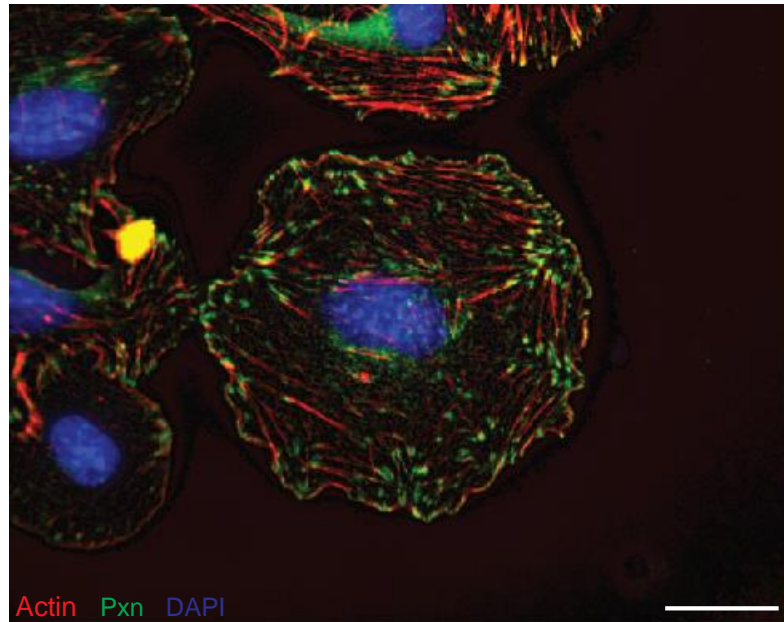
microtubule inhibitors did. $\beta 3^{+/+}$ cells were not affected which suggests that, Hsp90 is not required for endothelial cell migration when $\beta 3$ is present. Hsp90 therefore may represent another aspect of compensation for $\beta 3$ loss in endothelial cells and is therefore a good target for further investigation, especially given the availability of effective pharmacological inhibitors. The full extent and diversity of hidden targets in the $\beta 3$ adhesome like Hsp90 has yet to be realised, so this investigation into $\beta 3$ is only just beginning.

Appendix

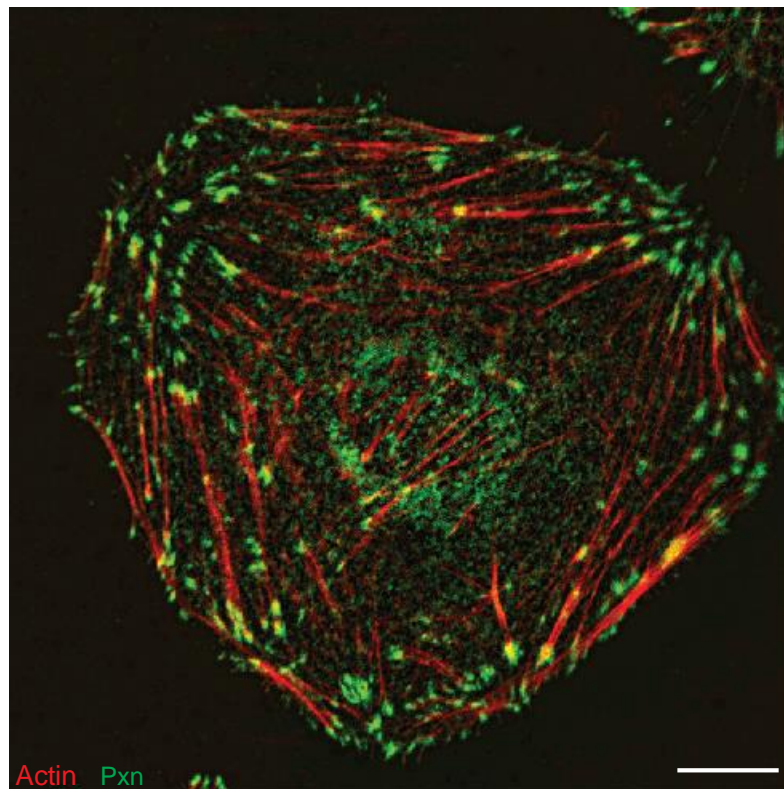
Supplementary Figures

Supplementary Figure 1 Comparison of Microscopy Techniques

A



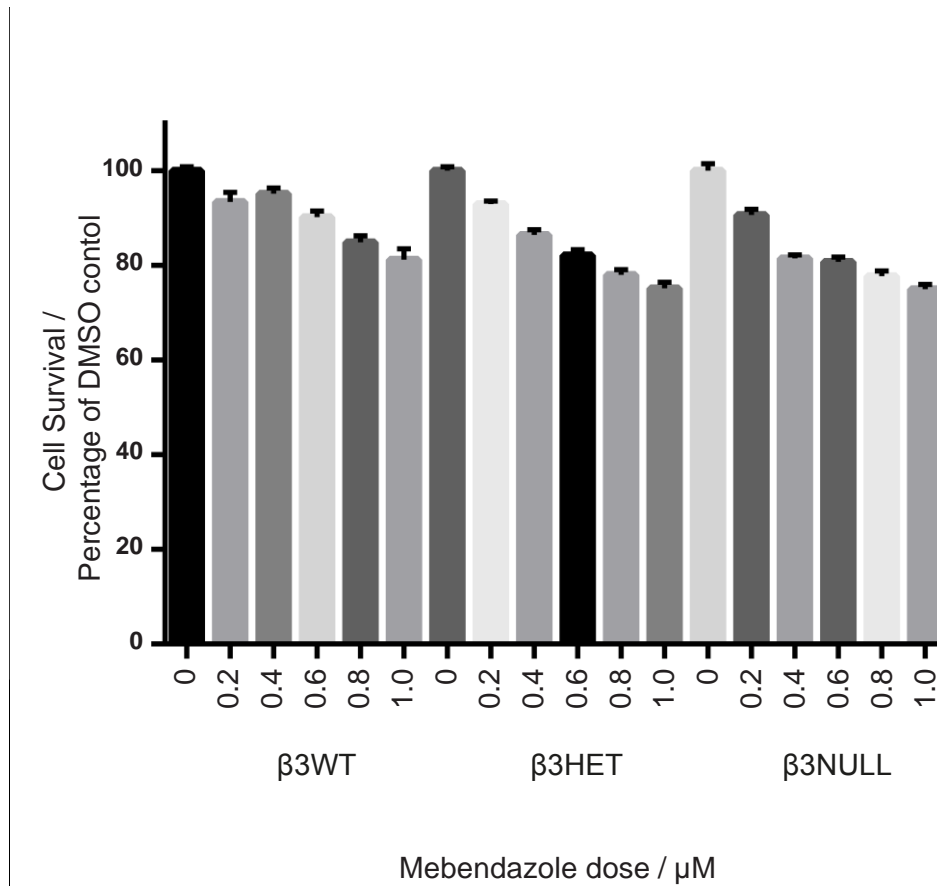
B



$\beta 3^{+/+}$ endothelial cells were adhered to fibronectin coated coverslips for 90 minutes then treated with VEGF for 10 minutes before being PHEMO fixed and immunostained for Pxn

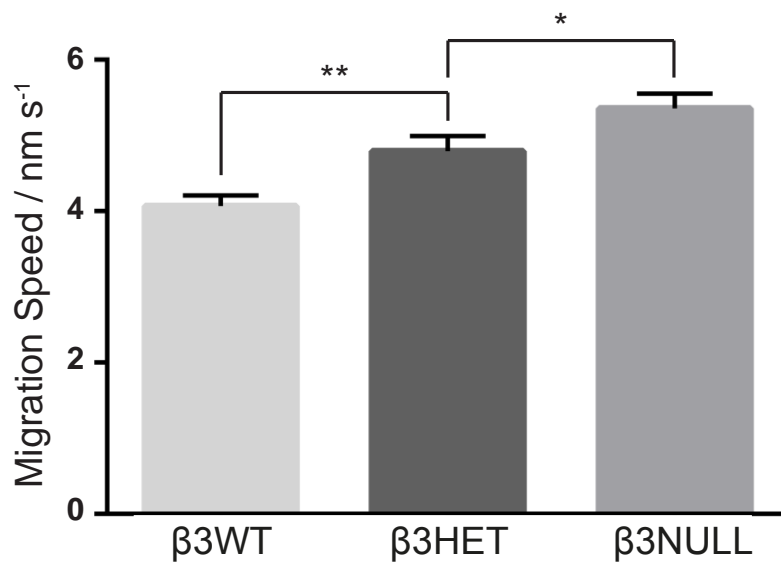
(green). DAPI (blue) and Phalloidin-actin (Red) staining were also used. Images taken using a **A** widefield microscope (scale bar = 20 μm) or a **B** confocal microscope (scale bar = 10 μm)

Supplementary Figure 2 Resistance to Mebendazole treatment by $\beta 3$ Depleted Endothelial Cells



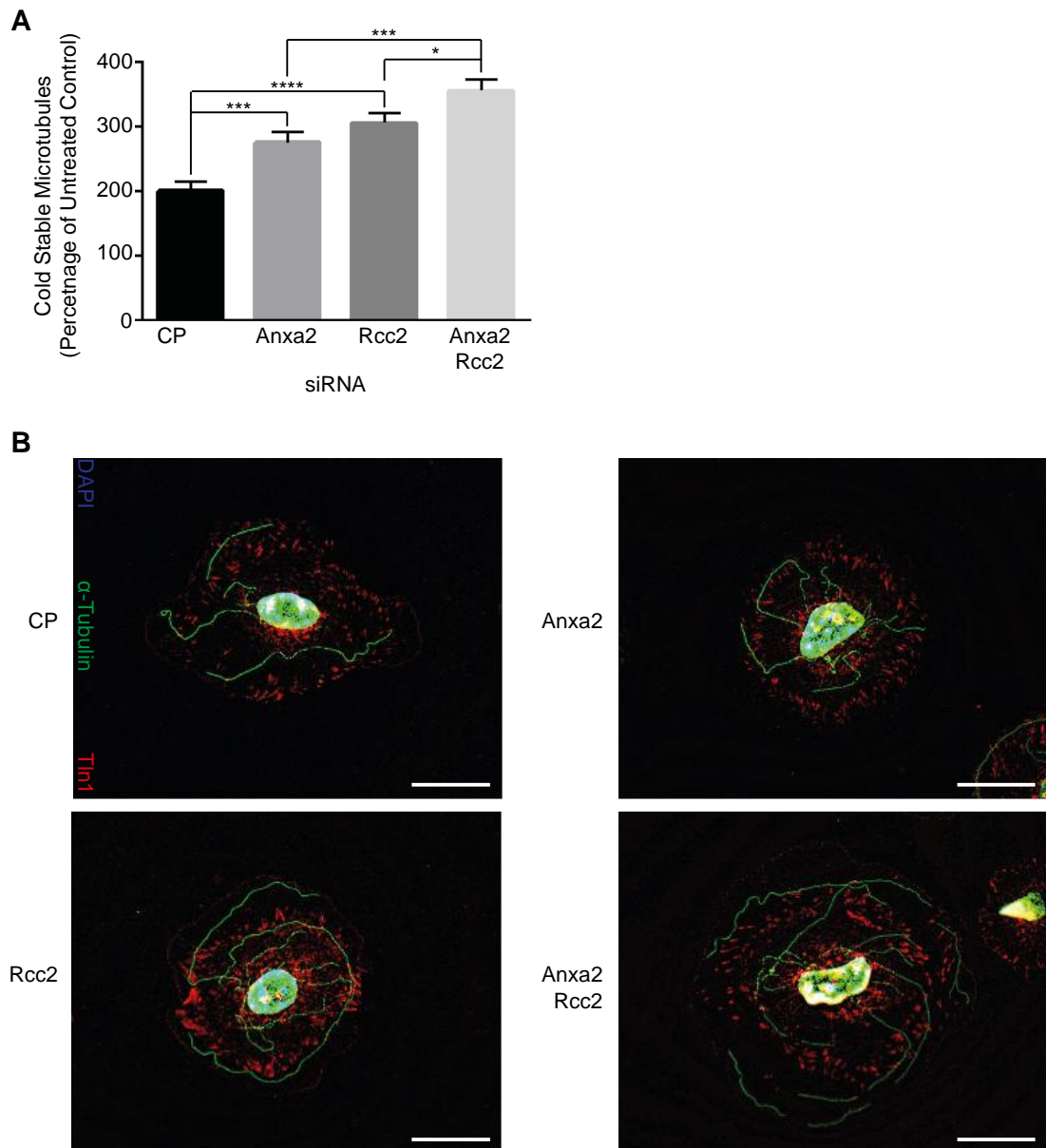
$\beta 3^{+/+}$ endothelial cells were adhered to fibronectin before being treated with a range of Mebendazole doses overnight. Cell survival was assessed using methylene blue staining of cells followed by de-staining and absorption measurements $n = 16$.

Supplementary Figure 3 Random Migration of $\beta 3$ Depleted Endothelial Cells



$\beta 3^{+/+}$, $\beta 3^{+/-}$ and $\beta 3^{-/-}$ endothelial cells were adhered to fibronectin overnight. Migration speed of individual cells was measured over 15 hours using the MTrackJ plugin for ImageJ (n=69).

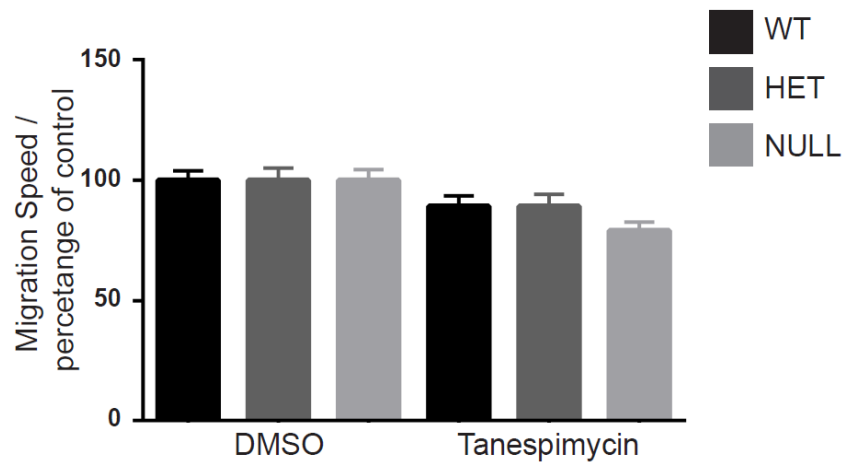
Supplementary Figure 4 Dual Knockdown of Rcc2 and Anxa2 Cumulatively Increases Microtubule Stability



A $\beta 3^{+/+}$ IMMLECs were transfected with control pool (CP) or Rcc2 smart pool siRNA and allowed to recover for 48 hours then were adhered to fibronectin coated coverslips for 75 minutes at 37°C before being moved to ice for 15 minutes. Soluble tubulin was washed out using PEM buffer before fixing with -20°C methanol. Immunostaining for α -tubulin was carried out to allow counting of cold stable microtubules per cell. Bars = mean number of cold stable microtubules shown as a percentage relative to CP treated cells \pm SEM n = 224.

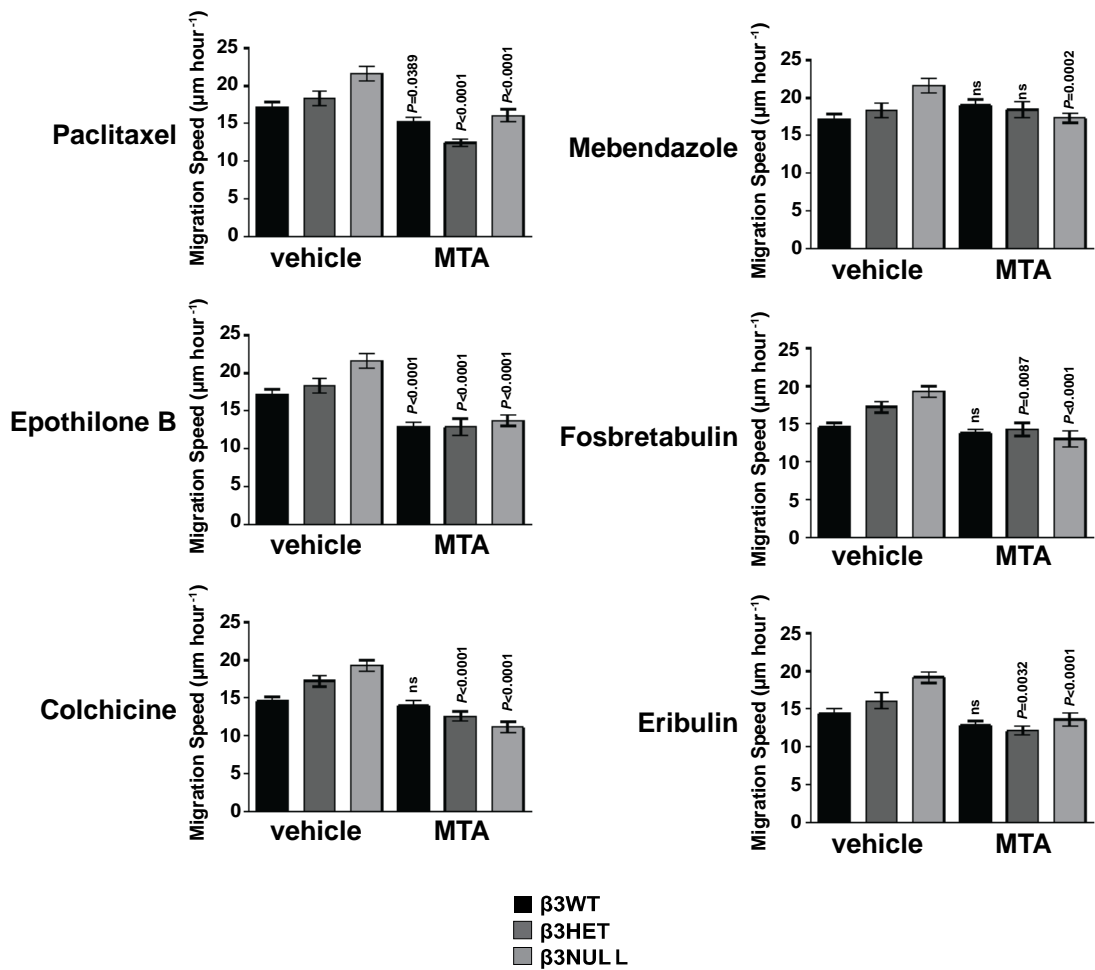
B Representative immunostaining of cells used from panel A. α -tubulin (green), Tln1 (red) and DAPI (blue) as a nuclear stain. Scale bar = 20 μ m.

Supplementary Figure 5 Hsp90 Inhibition in $\beta 3$ Depleted Endothelial Cell Migration



$\beta 3^{+/+}$, $\beta 3^{+/-}$ and $\beta 3^{-/-}$ endothelial cells were adhered to fibronectin overnight. Migration speed of individual cells was measured over 15 hours using the MTrackJ plugin for ImageJ whilst under the influence of the tanespimycin ($0.08 \mu\text{M}$). Migration speeds are shown as a percentage of the speed of the corresponding genotype under DMSO (vehicle) treatment ($n=58$).

Supplementary Figure 6 Non-normalised Random Migration of Endothelial Cells with Microtubule Inhibitors



$\beta3^{+/+}$, $\beta3^{+/-}$ and $\beta3^{-/-}$ endothelial cells were adhered to fibronectin overnight. Migration speed of individual cells was measured over 15 hours using the MTrackJ plugin for ImageJ whilst under the influence of the indicated microtubule agent (MTA) or DMSO (vehicle) treatment (n=46).

Supplementary Tables

Table 1 Raw MaxQuant Output of the Endothelial Adhesome

Unaltered MaxQuant output from analysis of the endothelial adhesome. Fibronectin adhered (FN), fibronectin adhered with VEGF (VEGF) and poly-L-lysine adhered (PLL) triplicate adhesome samples were used in MaxQuant analysis. Ordered alphabetically by gene name.

Table 2 LFQ of the Endothelial Adhesome

Normalised and filtered MaxQuant output from analysis of the endothelial adhesome generated in table 1. Listed in the same order defined by unsupervised hierarchical clustering in figure 4-2. Angiogenesis associated proteins, highlighted at the start of the table, were defined using the GOBP annotations: GO:0001525, GO:0002040, GO:0002042, GO:0016525, GO:0045765 and GO:0045766

Table 3 $\beta 3+/-$ Endothelial Cell Adhesome

Normalised and filtered MaxQuant output from analysis of the $\beta 3+/-$ endothelial adhesome. Fibronectin adhered $\beta 3+/+$ cell and fibronectin adhered $\beta 3+/-$ cell triplicate adhesome samples were used in MaxQuant analysis. Ordered by significance defined by SAM analysis.

Table 4 $\beta 3^{-/-}$ Endothelial Cell Adhesome

Normalised and filtered MaxQuant output from analysis of the $\beta 3^{-/-}$ endothelial adhesome. Fibronectin adhered $\beta 3^{+/+}$ cell and fibronectin adhered $\beta 3^{-/-}$ cell triplicate adhesome samples were used in MaxQuant analysis. Ordered by significance defined by SAM analysis.

Table 5 c(RGDfV) Treated Endothelial Cell Adhesome

Normalised and filtered MaxQuant output from analysis of the c(RGDfV) treated endothelial adhesome. Fibronectin adhered $\beta 3^{+/+}$ cells treated with c(RGDfV) (RGD) and fibronectin adhered $\beta 3^{+/+}$ cells treated with DMSO (DMSO) triplicate adhesome samples were used in MaxQuant analysis. Ordered by t test difference defined by SAM analysis with Ncbp1 (Nuclear cap binding protein subunit 1) as the only significant change on top.

Table 6 Mass Spectrometry of Rcc2 Pulldown

SILAC mass spectrometry of GFP-Rcc2 vs GFP control pulldown represented as heavy/light ratio. Full details of experiment can be found in Williamson et al⁴¹⁸

Abbreviations

$\alpha 5$ – Integrin $\alpha 5$ (mouse)

$\alpha 6$ – Integrin $\alpha 6$ (mouse)

αv – Integrin αv (mouse)

αm – Integrin αm (mouse)

Acta2 – Actin alpha 2 smooth muscle (mouse)

ADAM10 - A disintegrin and metalloproteinase domain 10

ADAM17 - A disintegrin and metalloproteinase domain 17

Akt1 – AKT serine/threonine kinase 1 (mouse)

ANOVA – Analysis of Variance

Anxa2 – Annexin A2 (mouse)

Arf6 – ADAP-ribosylation factor 6 (mouse)

ATP – Adenosine tri-phosphate

$\beta 1$ – Integrin $\beta 1$ (mouse)

$\beta 3$ – Integrin $\beta 3$ (mouse)

$\beta 3^{+/+}$ – Integrin $\beta 3$ Wild-type (for the $\beta 3$ gene)

$\beta 3^{+/-}$ – Integrin $\beta 3$ Heterozygous (for the $\beta 3$ gene)

$\beta 3^{-/-}$ – Integrin $\beta 3$ Null Homozygous (for the $\beta 3$ gene)

$\beta 5$ – Integrin $\beta 5$ (mouse)

$\beta 6$ – Integrin $\beta 6$ (mouse)

Bcar1 – Breast Cancer Anti-Estrogen Resistance Protein 1 (mouse)

BSA – Bovine serum albumin

CAF – Cancer associated fibroblasts

CAM – Cell adhesion molecule

Capn2 – Calpain 2(mouse)

Cdc42 – Cell division cycle 42 (mouse)

Clip1 – CAP-Gly domain containing linker protein 1 (mouse) (aka CLIP-170)

Coro1c – Coronin, actin binding protein 1c (mouse)

Crebbp – Creb binding protein (mouse)

c(RGDfV) - Cyclo(-Arg-Gly-Asp-D-Phe-Val) trifluoroacetate (aka Bachem H-2574)

Crk – CRK proto-oncogene, adaptor protein (mouse)

Dab2 – DAB2, Clathrin adaptor protein (mouse)

DAG – Diacylglycerol

Dll4 - Delta like canonical notch ligand 4 (mouse)

DMSO – Dimethyl sulfoxide

Dnm2 – Dynamin-2 (mouse)

Dock1 – Deducator of cytokinesis 1 (mouse)

DPDPB - 1,4-Bis[3-(2-pyridyldithio)propionamido]butane

DSP - Dithiobis(succinimidyl propionate)

DTT – Dithiothreitol

Dyn2 – Dynamin 2

EB2 - Microtubule Associated Protein RP/EB Family Member 2 (mouse)

ECM – Extracellular matrix

Egfr – Epidermal growth factor receptor (mouse)

Emcn – Endomucin (mouse)

Ep300 – E1a binding protein p300 (mouse)

Epo – Erythropoietin (mouse)

ErbB2 – Erb-B2 receptor tyrosine kinase 2 (mouse)

Erk1 – Extracellular regulated kinase 1 aka Mitogen-activated protein kinase 3 (mouse)

Erk2 – Extracellular regulated kinase 2 aka Mitogen-activated protein kinase 1 (mouse)

Fak1 – Focal adhesion kinase 1 aka Ptk2 (mouse)

FDR – False discovery rate

FN – Fibronectin

GAP – GTPase activating protein

Gapdh - Glyceraldehyde-3-phosphate dehydrogenase (mouse)

GDP – Guanine di-phosphate

GEF – Guanine exchange factor

Gipc1 – GPIC PDZ domain containing family member 1 (mouse)

GOBP – Gene ontology: biological process

GOCC – Gene ontology: cellular compartment

GOMF – Gene ontology: molecular function

Gpcr – G protein coupled receptor

Grb7 – Growth factor receptor bound protein 7 (mouse)

GTP – Guanine tri-phosphate

Hif1a – Hypoxia inducible factor 1 alpha subunit (mouse)

Hif1b – Hypoxia inducible factor 1 beta subunit (mouse)

Hsp90 – Heat shock protein 90 (mouse)

Hspa1a – Heat shock protein family A (Hsc70) member 1A (mouse)

HUVECs – Human umbilical vein endothelial cells

IAA – Iodoacetamide

ICAM1 – Intracellular adhesion molecule 1

ICAM2 – Intracellular adhesion molecule 2

Il6 – Interleukin 6 (mouse)

Ilk – Integrin linked kinase (mouse)

IMMLEC – Immortalised mouse lung endothelial cell

IP₃ - Inositol trisphosphate

lqgap1 – IQ motif containing GTPase activating protein 1 (mouse)

ltp3 - Inositol 1,4,5-trisphosphate receptor type 3 (mouse)

Kank1 – KN Motif and Ankyrin Repeat Domains 1 (mouse)

KEGG – Kyoto encyclopaedia of genes and genomes

Kif2c – Kinesin family member 2C (mouse)

Kif5b – Kinesin family member 5B (mouse)

LC-MS/MS – Liquid chromatography tandem mass spectrometry

LFQ – Label free quantification

LTQ – Linear trap quadrupole (mass spectrometer)

Macf1 – Microtubule actin crosslinking factor 1 (mouse)

Map6 – Microtubule associated protein 6 (mouse)

Map4k4 - Mitogen-Activated Protein Kinase Kinase Kinase Kinase 4 (mouse)

MAP – Microtubule associated protein

Met – MET proto-oncogene, receptor tyrosine kinase (mouse)

MLB – Magnesium lysis buffer

MMP9 – Matrix metalloproteinase 9

MMP14 – Matrix metalloproteinase 14

Mtor - Mechanistic Target Of Rapamycin (mouse)

Myc - MYC proto-oncogene, BHLH transcription factor (mouse)

Myh2 – Myosin heavy chain 2 (mouse)

Ncbp1 – Nuclear cap binding protein subunit 1 (mouse)

Nfatc1 - Nuclear factor of activated T-cells 1 (mouse)

Nos2 – Nitric oxide synthase 2 (mouse)

Nrp1 – Neuropilin-1 (mouse)

PAGE – Polyacrylamide gel electrophoresis

Pak1 – P21 (Rac1) activated kinase 1 (mouse)

PBD – P21 (Rac1) binding domain

PBS – Phosphate buffered saline

Pdcd6ip – Programmed cell death 6 interacting protein (mouse)

Pdgfb – Platelet derived growth factor subunit b (mouse)

PEM – PIPES, EGTA, MgCl₂ buffer

PFA – Paraformaldehyde

Pgf – Placental growth factor (mouse)

PHD2 – Prolyl hydroxylase domain containing protein 2

PHEMO – PIPES, HEPES, EGTA, MgCl₂ and DMSO containing buffer

PI3K-alpha - Phosphatidylinositol 4,5-bisphosphate 3-kinase catalytic subunit alpha isoform (mouse)

PINA – Protein interaction network analysis platform

PIP₂ - Phosphatidylinositol 4,5-bisphosphate

PIP₃ - Phosphatidylinositol 3,4,5-trisphosphate

Pkcb – Protein kinase c beta (mouse)

PLL – Poly-l-lysine

Ppfia1 - Protein Tyrosine Phosphatase, Receptor Type, F Polypeptide (PTPRF), Interacting Protein (Liprin), Alpha 1 (mouse)

Pxn – Paxillin (mouse)

Rab4 – Ras-related protein Rab-4 (mouse)

Rab6 – Ras-related protein Rab-6 (mouse)

Rab11 - Ras-related protein Rab-11 (mouse)

Rac1 - Ras-related C3 botulinum toxin substrate 1 (mouse)

Raf1 - Raf-1 proto-oncogene, serine/threonine kinase (mouse)

Rcc2 – Regulator of Chromatin Condensation 2 (mouse) (aka TD-60)

RGD – Arginine, glycine, asparagine tri-peptide

RhoA – Ras homologue family member A (mouse)

RIAM – Rap1-GTP Adapter Interacting Molecule (APBB1IP)

RIPA – Radioimmunoprecipitation assay buffer

RO – Reverse osmosis

Rock1 - Rho associated coiled-coil containing protein kinase 1 (mouse)

SAM – Significance analysis of microarrays

Sdc1 – Syndecan-1

SDS - Sodium dodecyl sulphate

Sem3a – Semaphorin 3a (mouse)

SH2 – Src homology domain 2

Slc2a1 – Solute carrier family 2, facilitated glucose transporter member 1 (mouse)

Src - SRC proto-oncogene, non-receptor tyrosine kinase (mouse)

Tie1 – Tyrosine-protein kinase receptor 1 (mouse)

Thbs1 – Thrombospondin-1 (mouse)

TIPS – Microtubule plus end tracking proteins

Tln1 – Talin 1 (mouse)

Tsc2 – Tuberous sclerosis 2 (mouse)

Vasp – Vasodilator stimulated phosphoprotein (mouse)

VCAM1 – Vascular cell adhesion protein 1

Vcp – Vasolin containing protein (mouse)

VEGF – Vascular endothelial growth factor

VEGFR2 – Vascular endothelial growth factor receptor 2

VE-cadherin – Vascular endothelial cadherin (mouse) (aka Cdh5)

Vhl – Von Hippel-Lindau tumour suppressor (mouse)

Vim – Vimentin (mouse)

Zyx – Zyxin (mouse)

References

1. Baish, J. W. *et al.* Scaling rules for diffusive drug delivery in tumor and normal tissues. *Proc. Natl. Acad. Sci.* **108**, 1799–1803 (2011).
2. Wallez, Y. & Huber, P. Endothelial adherens and tight junctions in vascular homeostasis, inflammation and angiogenesis. *Biochim. Biophys. Acta - Biomembr.* **1778**, 794–809 (2008).
3. Yurchenco, P. D. *et al.* Basement Membranes : Cell Scaffoldings and Signaling Platforms. 1–28 (2012). doi:10.1101/cshperspect.a004911
4. Townsley, M. I. Structure and composition of pulmonary arteries, capillaries and veins. *Compr. Physiol.* **2**, 675–709 (2012).
5. Michiels, C. Endothelial cell functions. *J. Cell. Physiol.* **196**, 430–443 (2003).
6. Kubis, N. & Levy, B. I. Vasculogenesis and angiogenesis: molecular and cellular controls. Part 1: growth factors. *Interv. Neuroradiol.* **9**, 227–37 (2003).
7. Fehling, H. J. Tracking mesoderm induction and its specification to the hemangioblast during embryonic stem cell differentiation. *Development* **130**, 4217–4227 (2003).
8. Basak, G. W. *et al.* Human embryonic stem cells hemangioblast express HLA-antigens. *J. Transl. Med.* **7**, 27 (2009).
9. LaRue, A. C., Lansford, R. & Drake, C. J. Circulating blood island-derived cells contribute to vasculogenesis in the embryo proper. *Dev. Biol.* **262**, 162–172 (2003).
10. Drake, C. J. Embryonic and adult vasculogenesis. *Birth Defects Res. Part C - Embryo Today Rev.* **69**, 73–82 (2003).
11. Patan, S. Vasculogenesis and angiogenesis as mechanisms of vascular network formation, growth and remodeling. *J. Neurooncol.* **50**, 1–15 (2000).
12. Djonov, V., Baum, O. & Burri, P. H. Vascular remodeling by intussusceptive angiogenesis. *Cell Tissue Res.* **314**, 107–117 (2003).
13. Krock, B. L., Skuli, N. & Simon, M. C. Hypoxia-Induced Angiogenesis: Good and Evil. *Genes Cancer* **2**, 1117–1133 (2011).
14. Aragonés, J., Fraisl, P., Baes, M. & Carmeliet, P. Oxygen Sensors at the Crossroad of

- Metabolism. *Cell Metab.* **9**, 11–22 (2009).
15. Kaelin, W. G. & Ratcliffe, P. J. Oxygen Sensing by Metazoans: The Central Role of the HIF Hydroxylase Pathway. *Mol. Cell* **30**, 393–402 (2008).
 16. Chan, D. a, Sutphin, P. D., Yen, S. & Giaccia, A. J. Coordinate Regulation of the Oxygen-Dependent Degradation Domains of Hypoxia-Inducible Factor 1 α
Coordinate Regulation of the Oxygen-Dependent Degradation Domains of Hypoxia-Inducible Factor 1 α . *Mol. Cell. Biol.* **25**, 6415–6426 (2005).
 17. Buckley, D. L. *et al.* Targeting the von Hippel-Lindau E3 ubiquitin ligase using small molecules to disrupt the VHL/HIF-1 α interaction. *J Am Chem Soc* **134**, 4465–4468 (2012).
 18. Zheng, X. *et al.* Cell-Type-Specific Regulation of Degradation of Hypoxia-Inducible Factor 1 α : Role of Subcellular Compartmentalization Cell-Type-Specific Regulation of Degradation of Hypoxia-Inducible Factor 1 α : Role of Subcellular Compartmentalization. *Society* **26**, 4628–4641 (2006).
 19. Jiang, B. H., Zheng, J. Z., Leung, S. W., Roe, R. & Semenza, G. L. Transactivation and inhibitory domains of hypoxia-inducible factor 1 α . Modulation of transcriptional activity by oxygen tension. *J. Biol. Chem.* **272**, 19253–19260 (1997).
 20. Arany, Z. *et al.* An essential role for p300/CBP in the cellular response to hypoxia. *Cell Biol.* **93**, 12969–12973 (1996).
 21. Wenger, R. H., Stiehl, D. P. & Camenisch, G. Integration of Oxygen Signaling at the Consensus HRE. *Sci. Signal.* **2005**, re12–re12 (2005).
 22. Jung, F., Palmer, L. A., Zhou, N. & Johns, R. A. Hypoxic regulation of inducible nitric oxide synthase via hypoxia inducible factor-1 in cardiac myocytes. *Circ Res* **86**, 319–325 (2000).
 23. Iyer, N. V *et al.* Cellular and developmental control of O₂ homeostasis by hypoxia-inducible factor 1 α . 149–162 (1998). doi:10.1101/gad.12.2.149
 24. Feilim Mac Gabhann and Aleksander S. Popel. Systems Biology of Vascular Endothelial Growth Factors. *Microcirculation* **15**, 715–738 (2009).
 25. Koch, S., Tugues, S., Li, X., Gualandi, L. & Claesson-Welsh, L. Signal transduction by

- vascular endothelial growth factor receptors. *Biochem. J.* **437**, 169–83 (2011).
26. Harper, S. J. & Bates, D. O. VEGF-A splicing: the key to anti-angiogenic therapeutics? *Nat. Rev. Cancer* **8**, 880–7 (2008).
 27. Perrin, R. M. *et al.* Diabetic retinopathy is associated with a switch in splicing from anti- to pro-angiogenic isoforms of vascular endothelial growth factor. *Diabetologia* **48**, 2422–2427 (2005).
 28. Mac Gabhann, F., Ji, J. W. & Popel, A. S. VEGF gradients, receptor activation, and sprout guidance in resting and exercising skeletal muscle. *J. Appl. Physiol.* **102**, 722–34 (2007).
 29. Lee, S., Jilan, S. M., Nikolova, G. V., Carpizo, D. & Luisa Iruela-Arispe, M. Processing of VEGF-A by matrix metalloproteinases regulates bioavailability and vascular patterning in tumors. *J. Cell Biol.* **169**, 681–691 (2005).
 30. Vempati, P., Popel, A. S. & Mac Gabhann, F. Extracellular regulation of VEGF: Isoforms, proteolysis, and vascular patterning. *Cytokine Growth Factor Rev.* **25**, 1–19 (2014).
 31. Hawinkels, L. J. A. C. *et al.* VEGF release by MMP-9 mediated heparan sulphate cleavage induces colorectal cancer angiogenesis. *Eur. J. Cancer* **44**, 1904–1913 (2008).
 32. Lemmon, M. a & Schlessinger, J. Cell signaling by receptor-tyrosine kinases Mark. *Biochemistry* **141**, 1117–1134 (2011).
 33. Shibuya, M. Vascular endothelial growth factor receptor-1 (VEGFR-1/Flt-1): a dual regulator for angiogenesis. *Angiogenesis* **9**, 225–230; discussion 231 (2006).
 34. Kendall, R. L. & Thomas, K. A. Inhibition of vascular endothelial cell growth factor activity by an endogenously encoded soluble receptor (endothelial cells/mitogenic inhibitor/alternative transcription/angiogenesis). *Biochemistry* **90**, 10705–10709 (1993).
 35. Deng, Y., Zhang, X. & Simons, M. Molecular controls of lymphatic VEGFR3 signaling. *Arterioscler. Thromb. Vasc. Biol.* **35**, 421–429 (2015).
 36. Dixelius, J. *et al.* Ligand-induced Vascular Endothelial Growth Factor Receptor-3 (VEGFR-3) Heterodimerization with VEGFR-2 in Primary Lymphatic Endothelial Cells

- Regulates Tyrosine Phosphorylation Sites. *J. Biol. Chem.* **278**, 40973–40979 (2003).
37. Shibuya, M. Vascular Endothelial Growth Factor (VEGF) and Its Receptor (VEGFR) Signaling in Angiogenesis: A Crucial Target for Anti- and Pro-Angiogenic Therapies. *Genes Cancer* **2**, 1097–1105 (2011).
 38. Tzima, E. *et al.* A mechanosensory complex that mediates the endothelial cell response to fluid shear stress. *Nature* **437**, (2005).
 39. Cudmore, M. J. *et al.* The role of heterodimerization between VEGFR-1 and VEGFR-2 in the regulation of endothelial cell homeostasis. *Nat. Commun.* **3**, 972 (2012).
 40. Cai, M., Wang, K., Murdoch, C. E., Gu, Y. & Ahmed, A. Heterodimerisation between VEGFR-1 and VEGFR-2 and not the homodimers of VEGFR-1 inhibit VEGFR-2 activity. *Vascul. Pharmacol.* **88**, 11–20 (2017).
 41. Carmeliet, P. & Jain, R. K. Molecular mechanisms and clinical applications of angiogenesis. *Nature* **473**, 298–307 (2011).
 42. Ochsenbein, A. M. *et al.* Endothelial cell-derived semaphorin 3A inhibits filopodia formation by blood vascular tip cells. *Development* **143**, 589–594 (2016).
 43. Kawasaki, T. *et al.* A requirement for neuropilin-1 in embryonic vessel formation. *Development* **126**, 4895–4902 (1999).
 44. Jones, E. A. V, Yuan, L., Breant, C., Watts, R. J. & Eichmann, A. Separating genetic and hemodynamic defects in neuropilin 1 knockout embryos. *Development* **135**, 2479–88 (2008).
 45. Sawamiphak, S. *et al.* Ephrin-B2 regulates VEGFR2 function in developmental and tumour angiogenesis. *Nature* **465**, 487–491 (2010).
 46. Wang, Y. *et al.* Ephrin-B2 controls VEGF-induced angiogenesis and lymphangiogenesis. *Nature* **465**, 483–486 (2010).
 47. Chen, T. T. *et al.* Anchorage of VEGF to the extracellular matrix conveys differential signaling responses to endothelial cells. *J. Cell Biol.* **188**, 595–609 (2010).
 48. Soldi, R. *et al.* Role of α v β 3 integrin in the activation of vascular endothelial growth factor receptor-2. *EMBO J.* **18**, 882–92 (1999).
 49. Rapraeger, A. C. *et al.* Vascular endothelial-cadherin stimulates syndecan-1-coupled

- insulin-like growth factor-1 receptor and cross-talk between α v β 3 integrin and vascular endothelial growth factor receptor 2 at the onset of endothelial cell dissemination during angiogenesis. *FEBS J.* **280**, 2194–2206 (2013).
50. West, X. Z. *et al.* Integrin β 3 crosstalk with VEGFR accommodating tyrosine phosphorylation as a regulatory switch. *PLoS One* **7**, (2012).
 51. Coon, B. G. *et al.* Intramembrane binding of VE-cadherin to VEGFR2 and VEGFR3 assembles the endothelial mechanosensory complex. *J. Cell Biol.* **208**, 975–986 (2015).
 52. Robinson, S. D. *et al.* α v β 3 integrin limits the contribution of neuropilin-1 to vascular endothelial growth factor-induced angiogenesis. *J. Biol. Chem.* **284**, 33966–81 (2009).
 53. Simons, M., Gordon, E. & Claesson-Welsh, L. Mechanisms and regulation of endothelial VEGF receptor signalling. *Nat. Rev. Mol. Cell Biol.* **10**, 611–25 (2016).
 54. Mikoshiba, K. IP3 receptor/ Ca^{2+} channel: From discovery to new signaling concepts. *J. Neurochem.* **102**, 1426–1446 (2007).
 55. Corbit, K. C. *et al.* Activation of Raf-1 signaling by protein kinase C through a mechanism involving Raf kinase inhibitory protein. *J. Biol. Chem.* **278**, 13061–13068 (2003).
 56. Srinivasan, R. *et al.* Erk1 and erk2 regulate endothelial cell proliferation and migration during mouse embryonic angiogenesis. *PLoS One* **4**, (2009).
 57. Ye, Q. *et al.* Structural basis of calcineurin activation by calmodulin. *Cell. Signal.* **25**, 2661–2667 (2013).
 58. Zaichuk, T. a *et al.* Nuclear factor of activated T cells balances angiogenesis activation and inhibition. *J. Exp. Med.* **199**, 1513–1522 (2004).
 59. Jinnin, M. *et al.* Suppressed NFAT-dependent VEGFR1 expression and constitutive VEGFR2 signaling in infantile hemangioma. *Nat Med.* **14**, 1236–1246 (2008).
 60. Carmeliet, P. *et al.* Targeted deficiency or cytosolic truncation of the VE-cadherin gene in mice impairs VEGF-mediated endothelial survival and angiogenesis. *Cell* **98**, 147–157 (1999).
 61. Shiojima, I. & Walsh, K. Role of Akt signaling in vascular homeostasis and

- angiogenesis. *Circ. Res.* **90**, 1243–1250 (2002).
62. Chen, J. *et al.* Akt1 regulates pathological angiogenesis, vascular maturation and permeability in vivo. *Nat. Med.* **11**, 1188–96 (2005).
 63. Hahn-Windgassen, A. *et al.* Akt activates the mammalian target of rapamycin by regulating cellular ATP level and AMPK activity. *J. Biol. Chem.* **280**, 32081–32089 (2005).
 64. Farhan, M. A., Carmine-Simmen, K., Lewis, J. D., Moore, R. B. & Murray, A. G. Endothelial cell mTOR complex-2 regulates sprouting angiogenesis. *PLoS One* **10**, 1–20 (2015).
 65. Sun, Z. *et al.* VEGFR2 induces c-Src signaling and vascular permeability in vivo via the adaptor protein TSA. *J. Exp. Med.* **209**, 1363–1377 (2012).
 66. Westhoff, M. A., Serrels, B., Fincham, V. J., Frame, M. C. & Carragher, N. O. Src-Mediated Phosphorylation of Focal Adhesion Kinase Couples Actin and Adhesion Dynamics to Survival Signaling. *Mol Cell Biol* **24**, 8113–8133 (2004).
 67. Ferrando, I. M. *et al.* Identification of Targets of c-Src Tyrosine Kinase by Chemical Complementmentation and Phosphoproteomics. *Mol. Cell. Proteomics* **11**, 355–369 (2012).
 68. Ucuzian, A. A., Gassman, A. A., East, A. T. & Greisler, P. Molecular Mediators of Angiogenesis. *J Burn Care Res.* **31**, 1–28 (2011).
 69. McKeown, S. R. Defining normoxia, physoxia and hypoxia in tumours - Implications for treatment response. *Br. J. Radiol.* **87**, 1–12 (2014).
 70. Carreau, A., Hafny-Rahbi, B. El, Matejuk, A., Grillon, C. & Kieda, C. Why is the partial oxygen pressure of human tissues a crucial parameter? Small molecules and hypoxia. *J. Cell. Mol. Med.* **15**, 1239–1253 (2011).
 71. Adams, R. H. & Alitalo, K. Molecular regulation of angiogenesis and lymphangiogenesis. *Nat Rev Mol Cell Biol* **8**, 464–478 (2007).
 72. Herbert, S. P. & Stainier, D. Y. R. Molecular control of endothelial cell behavior during blood vessel morphogenesis. *Nat. Rev. Mol. Cell. Biol.* **12**, 551–564 (2012).

73. Bhattacharya, R. *et al.* Distinct role of PLCbeta3 in VEGF-mediated directional migration and vascular sprouting. *J. Cell Sci.* **122**, 1025–1034 (2009).
74. Herbert, S. P., Cheung, J. Y. M. & Stainier, D. Y. R. Determination of endothelial stalk versus tip cell potential during angiogenesis by H2.0-like homeobox-1. *Curr. Biol.* **22**, 1789–1794 (2012).
75. Roca, C. & Adams, R. H. Regulation of vascular morphogenesis by Notch signaling Regulation of vascular morphogenesis by Notch signaling. **21**, 2511–2524 (2007).
76. Gerhardt, H. *et al.* VEGF guides angiogenic sprouting utilizing endothelial tip cell filopodia. *J. Cell Biol.* **161**, 1163–1177 (2003).
77. Suchting, S. *et al.* The Notch ligand Delta-like 4 negatively regulates endothelial tip cell formation and vessel branching. *Proc. Natl. Acad. Sci. U. S. A.* **104**, 3225–3230 (2007).
78. Phng, L.-K. & Gerhardt, H. Angiogenesis: a team effort coordinated by notch. *Dev. Cell* **16**, 196–208 (2009).
79. Sainson, R. C. *et al.* Cell-autonomous notch signaling regulates endothelial cell branching and proliferation during vascular tubulogenesis. *Faseb J* **19**, 1027–1029 (2005).
80. Blanco, R. & Gerhardt, H. VEGF and Notch in tip and stalk cell selection. *Cold Spring Harb. Perspect. Med.* **3**, 1–19 (2013).
81. Gerhardt, H. VEGF and endothelial guidance in angiogenic sprouting. *Organogenesis* **4**, 241–246 (2008).
82. Stupack, D. G. & Cheresh, D. a. ECM remodeling regulates angiogenesis: endothelial integrins look for new ligands. *Sci. STKE* **2002**, pe7 (2002).
83. Brooks, P. C., Clark, R. a & Cheresh, D. a. Requirement of vascular integrin alpha v beta 3 for angiogenesis. *Science* **264**, 569–571 (1994).
84. Creamer, D., Allen, M., Sousa, a, Poston, R. & Barker, J. Altered vascular endothelium integrin expression in psoriasis. *Am. J. Pathol.* **147**, 1661–7 (1995).
85. Yana, I. *et al.* Crosstalk between neovessels and mural cells directs the site-specific expression of MT1-MMP to endothelial tip cells. *J. Cell Sci.* **120**, 1607–1614 (2007).

86. Arroyo, A. G. & Iruela-Arispe, M. L. Extracellular matrix, inflammation, and the angiogenic response. *Cardiovasc. Res.* **86**, 226–235 (2010).
87. Anderson, D. E. J. & Hinds, M. T. Extracellular matrix production and regulation in micropatterned endothelial cells. *Biochem. Biophys. Res. Commun.* **427**, 159–164 (2012).
88. Kusuma, S., Zhao, S. & Gerecht, S. The extracellular matrix is a novel attribute of endothelial progenitors and of hypoxic mature endothelial cells. *FASEB J.* **26**, 4925–4936 (2012).
89. Tung, J. J., Tattersall, I. W. & Kitajewski, J. Tips, stalks, tubes: Notch-mediated cell fate determination and mechanisms of tubulogenesis during angiogenesis. *Cold Spring Harb. Perspect. Med.* **2**, 1–14 (2012).
90. Davis, G. E., Stratman, A. N., Sacharidou, A. & Koh, W. *Molecular Basis for Endothelial Lumen Formation and Tubulogenesis During Vasculogenesis and Angiogenic Sprouting.* *Int. Rev. Cell Mol. Biol.* **288**, (2011).
91. Stratman, A. N. *et al.* Endothelial cell lumen and vascular guidance tunnel formation requires MT1-MMP-dependent proteolysis in 3-dimensional collagen matrices. *Blood* **114**, 237–247 (2009).
92. Davis, G. E. & Camarillo, C. W. An alpha 2 beta 1 integrin-dependent pinocytic mechanism involving intracellular vacuole formation and coalescence regulates capillary lumen and tube formation in three-dimensional collagen matrix. *Exp. Cell Res.* **224**, 39–51 (1996).
93. Bayless, K. J., Salazar, R. & Davis, G. E. RGD-dependent vacuolation and lumen formation observed during endothelial cell morphogenesis in three-dimensional fibrin matrices involves the alpha(v)beta(3) and alpha(5)beta(1) integrins. *Am. J. Pathol.* **156**, 1673–83 (2000).
94. Lizama, C. O. & Zovein, A. C. Polarizing pathways: Balancing endothelial polarity, permeability, and lumen formation. *Exp. Cell Res.* **319**, 1247–1254 (2013).
95. Zeeb, M., Strilic, B. & Lammert, E. Resolving cell-cell junctions: Lumen formation in blood vessels. *Curr. Opin. Cell Biol.* **22**, 626–632 (2010).
96. Potente, M., Gerhardt, H. & Carmeliet, P. Basic and therapeutic aspects of angiogenesis. *Cell* **146**, 873–887 (2011).

97. Fantin, A. *et al.* Tissue macrophages act as cellular chaperones for vascular anastomosis downstream of VEGF-mediated endothelial tip cell induction. *Blood* **116**, 829–840 (2010).
98. Song, J. W., Bazou, D. & Munn, L. L. Anastomosis of endothelial sprouts forms new vessels in a tissue analogue of angiogenesis. *Integr. Biol.* **4**, 857–862 (2012).
99. Ricard, N. & Simons, M. When It Is Better to Regress: Dynamics of Vascular Pruning. *PLoS Biol.* **13**, 1–6 (2015).
100. Murakami, M. Signaling required for blood vessel maintenance: Molecular basis and pathological manifestations. *Int. J. Vasc. Med.* **2012**, (2012).
101. Bazmara, H. *et al.* The vital role of blood flow-induced proliferation and migration in capillary network formation in a multiscale model of angiogenesis. *PLoS One* **10**, (2015).
102. Folkman, J. Role of angiogenesis in tumor growth and metastasis. *Semin. Oncol.* **29**, 15–18 (2002).
103. Inoue, M., Hager, J. H., Ferrara, N., Gerber, H. P. & Hanahan, D. VEGF-A has a critical, nonredundant role in angiogenic switching and pancreatic ?? cell carcinogenesis. *Cancer Cell* **1**, 193–202 (2002).
104. Du, Y. C. N., Lewis, B. C., Hanahan, D. & Varmus, H. Assessing tumor progression factors by somatic gene transfer into a mouse model: Bcl-xL promotes islet tumor cell invasion. *PLoS Biol.* **5**, 2255–2269 (2007).
105. Oberstein, P. E. & Olive, K. P. Pancreatic cancer: Why is it so hard to treat? *Therap. Adv. Gastroenterol.* **6**, 321–337 (2013).
106. Delbaldo, C., Faivre, S., Dreyer, C. & Raymond, E. Sunitinib in advanced pancreatic neuroendocrine tumors: Latest evidence and clinical potential. *Ther. Adv. Med. Oncol.* **4**, 9–18 (2012).
107. Rampetsreiter, P., Casanova, E. & Eferl, R. Genetically modified mouse models of cancer invasion and metastasis. *Drug Discov. Today Dis. Model.* **8**, 67–74 (2011).
108. Semenza, G. L. Regulation of metabolism by hypoxia-inducible factor 1. *Cold Spring Harb Symp Quant Biol* **76**, 347–353 (2011).
109. Eales, K. L., Hollinshead, K. E. R. & Tennant, D. A. Hypoxia and metabolic adaptation

- of cancer cells. *Oncogenesis* **5**, e190 (2016).
110. Bielenberg, D. R., Zetter, B. R. & Program, V. B. The Contribution of Angiogenesis to the Process of Metastasis. *Cancer J.* **21**, 267–273 (2015).
 111. Liberti, M. V. & Locasale, J. W. The Warburg Effect: How Does it Benefit Cancer Cells? *Trends Biochem. Sci.* **41**, 211–218 (2016).
 112. Lee, S. H., Jeong, D., Han, Y.-S. & Baek, M. J. Pivotal role of vascular endothelial growth factor pathway in tumor angiogenesis. *Ann. Surg. Treat. Res.* **89**, 1–8 (2015).
 113. Guppy, M. The hypoxic core: A possible answer to the cancer paradox. *Biochem. Biophys. Res. Commun.* **299**, 676–680 (2002).
 114. Nagy, J. A., Chang, S. H., Shih, S. C., Dvorak, A. M. & Dvorak, H. F. Heterogeneity of the tumor vasculature. *Semin. Thromb. Hemost.* **36**, 321–331 (2010).
 115. Ziyad, S. & Iruela-Arispe, M. L. Molecular mechanisms of tumor angiogenesis. *Genes Cancer* **2**, 1085–96 (2011).
 116. Shiga, K. *et al.* Cancer-associated fibroblasts: Their characteristics and their roles in tumor growth. *Cancers (Basel)*. **7**, 2443–2458 (2015).
 117. Gopinathan, G. *et al.* Europe PMC Funders Group Interleukin-6 stimulates defective angiogenesis. **75**, 3098–3107 (2016).
 118. Xing, F., Saidou, J. & Watabe, K. Cancer associated fibroblasts (CAFs) in tumor microenvironment. *Front. Biosci. (Landmark Ed.)* **15**, 166–79 (2010).
 119. Serini, G., Valdembri, D. & Bussolino, F. Integrins and angiogenesis: a sticky business. *Exp. Cell Res.* **312**, 651–8 (2006).
 120. Lee, P. F., Bai, Y., Smith, R. L., Bayless, K. J. & Yeh, A. T. Angiogenic responses are enhanced in mechanically and microscopically characterized, microbial transglutaminase crosslinked collagen matrices with increased stiffness. *Acta Biomater.* **9**, 7178–7190 (2013).
 121. Levental, K. R. *et al.* Matrix Crosslinking Forces Tumor Progression by Enhancing Integrin signaling. *Cell* **139**, 891–906 (2009).
 122. Kessenbrock, K., Plaks, V. & Werb, Z. Matrix Metalloproteinases: Regulators of the Tumor Microenvironment. *Cell* **141**, 52–67 (2010).

123. Stockmann, C., Schadendorf, D., Klose, R. & Helfrich, I. The impact of the immune system on tumor: angiogenesis and vascular remodeling. *Front. Oncol.* **4**, 69 (2014).
124. Riabov, V. *et al.* Role of tumor associated macrophages in tumor angiogenesis and lymphangiogenesis. *Front. Physiol.* **5 MAR**, 1–13 (2014).
125. Dvorak, H. F. Tumors: Wounds That Do Not Heal. *N. Engl. J. Med.* **315**, 1650–1659 (1986).
126. Holohan, C., Van Schaeybroeck, S., Longley, D. B. & Johnston, P. G. Cancer drug resistance: an evolving paradigm. *Nat. Rev. Cancer* **13**, 714–726 (2013).
127. Shojaei, F. & Ferrara, N. Antiangiogenic therapy for cancer: an update. *Cancer J.* **13**, 345–348 (2013).
128. Jain, R. K. Normalizing tumor vasculature with anti-angiogenic therapy: a new paradigm for combination therapy. *Nat. Med.* **7**, 987–989 (2001).
129. Keating, G. M. Bevacizumab: A review of its use in advanced cancer. *Drugs* **74**, 1891–1925 (2014).
130. Goel, S., Wong, A. H. K. & Jain, R. K. Vascular normalization as a therapeutic strategy for malignant and nonmalignant disease. *Cold Spring Harb. Perspect. Med.* **2**, 1–24 (2012).
131. Pozarowska, D. & Pozarowski, P. The era of anti-vascular endothelial growth factor (VEGF) drugs in ophthalmology, VEGF and anti-VEGF therapy. *Cent. Eur. J. Immunol.* **41**, 311–316 (2016).
132. Amadio, M., Govoni, S. & Pascale, A. Targeting VEGF in eye neovascularization: What's new?: A comprehensive review on current therapies and oligonucleotide-based interventions under development. *Pharmacol. Res.* **103**, 253–269 (2016).
133. Bottsford-Miller, J. N., Coleman, R. L. & Sood, A. K. Resistance and escape from antiangiogenesis therapy: Clinical implications and future strategies. *J. Clin. Oncol.* **30**, 4026–4034 (2012).
134. Loges, S., Schmidt, T. & Carmeliet, P. Mechanisms of resistance to anti-angiogenic therapy and development of third-generation anti-angiogenic drug candidates. *Genes Cancer* **1**, 12–25 (2010).
135. Thirlwell, C., Schulz, L., Dibra, H. & Beck, S. Suffocating cancer: hypoxia-associated

- epimutations as targets for cancer therapy. *Clin. Epigenetics* **3**, 9 (2011).
136. Holmes, K., Roberts, O. L., Thomas, A. M. & Cross, M. J. Vascular endothelial growth factor receptor-2: Structure, function, intracellular signalling and therapeutic inhibition. *Cell. Signal.* **19**, 2003–2012 (2007).
 137. Reinhart-King, C. A. Chapter 3 Endothelial Cell Adhesion and Migration. *Methods Enzymol.* **443**, 45–64 (2008).
 138. Barczyk, M., Carracedo, S. & Gullberg, D. Integrins. *Cell Tissue Res.* **339**, 269–280 (2010).
 139. Avraamides, C. J., Garmy-susini, B. & Varnier, J. A. Integrins in angiogenesis and lymphangiogenesis. *Nat Rev Cancer* **8**, 604–617 (2008).
 140. Shen, B., Delaney, M. K. & Du, X. Inside-out, outside-in, and inside-outside-in: G protein signaling in integrin-mediated cell adhesion, spreading, and retraction. *Curr. Opin. Cell Biol.* **24**, 600–606 (2012).
 141. Hyun, Y. M., Lefort, C. T. & Kim, M. Leukocyte integrins and their ligand interactions. *Immunol. Res.* **45**, 195–208 (2009).
 142. Lau, T.-L. T.-L., Kim, C., Ginsberg, M. H. & Ulmer, T. S. The structure of the integrin α 5 β 3 transmembrane complex explains integrin transmembrane signalling. *EMBO J.* **28**, 1351–61 (2009).
 143. Li, R. Activation of Integrin α 5 β 3 by Modulation of Transmembrane Helix Associations. *Science (80-.).* **300**, 795–798 (2003).
 144. Kim, C., Ye, F. & Ginsberg, M. H. Regulation of Integrin Activation. *Annu. Rev. Cell Dev. Biol.* **27**, 321–345 (2011).
 145. Hemmings, L. *et al.* Talin contains three actin-binding sites each of which is adjacent to a vinculin-binding site. *J. Cell Sci.* **109 (Pt 1)**, 2715–2726 (1996).
 146. Calderwood, D. A. *et al.* The talin head domain binds to integrin β subunit cytoplasmic tails and regulates integrin activation. *J. Biol. Chem.* **274**, 28071–28074 (1999).
 147. Moes, M. *et al.* The integrin binding site 2 (IBS2) in the talin rod domain is essential for linking integrin α subunits to the cytoskeleton. *J. Biol. Chem.* **282**, 17280–17288 (2007).

148. Tadokoro, S. Talin Binding to Integrin Tails: A Final Common Step in Integrin Activation. *Science (80-.)*. **302**, 103–106 (2003).
149. Calderwood, D., Campbell, I. D. & Critchley, D. R. Talins and kindlins: partners in integrin-mediated adhesion. *Nat. Rev. Mol. Cell Biol.* **14**, 503–17 (2013).
150. Bialkowska, K. *et al.* The integrin co-activator kindlin-3 is expressed and functional in a non-hematopoietic cell, the endothelial cell. *J. Biol. Chem.* **285**, 18640–18649 (2010).
151. Hodivala-Dilke, K. M. *et al.* Beta3-integrin-deficient mice are a model for Glanzmann thrombasthenia showing placental defects and reduced survival. *J. Clin. Invest.* **103**, 229–38 (1999).
152. Moser, M., Nieswandt, B., Ussar, S., Pozgajova, M. & Fässler, R. Kindlin-3 is essential for integrin activation and platelet aggregation. *Nat. Med.* **14**, 325–30 (2008).
153. Moser, M., Legate, K. R., Zent, R. & Fässler, R. The tail of integrins, talin, and kindlins. *Science* **324**, 895–9 (2009).
154. Montanez, E. *et al.* Kindlin-2 controls bidirectional signaling of integrins. *Genes Dev.* **22**, 1325–1330 (2008).
155. Tu, Y., Wu, S., Shi, X., Chen, K. & Wu, C. Migfilin and Mig-2 link focal adhesions to filamin and the actin cytoskeleton and function in cell shape modulation. *Cell* **113**, 37–47 (2003).
156. Ithychanda, S. S. *et al.* Migfilin, a molecular switch in regulation of integrin activation. *J. Biol. Chem.* **284**, 4713–4722 (2009).
157. Su, W., Mruk, D. D. & Cheng, C. Y. Filamin A A regulator of blood-testis barrier assembly during post-natal development Wenhui. *Spermatogenesis* **2**, 73–78 (2012).
158. Tigges, U., Koch, B., Wissing, J., Jockusch, B. M. & Ziegler, W. H. The F-actin cross-linking and focal adhesion protein filamin A is a ligand and in vivo substrate for protein kinase C α . *J. Biol. Chem.* **278**, 23561–23569 (2003).
159. Das, M., Ithychanda, S. S., Qin, J. & Plow, E. F. Migfilin and filamin as regulators of integrin activation in endothelial cells and neutrophils. *PLoS One* **6**, (2011).
160. Paoli, P., Giannoni, E. & Chiarugi, P. Anoikis molecular pathways and its role in cancer progression. *Biochim. Biophys. Acta - Mol. Cell Res.* **1833**, 3481–3498 (2013).

161. Vachon, P. H. Integrin Signaling, Cell Survival, and Anoikis: Distinctions, Differences, and Differentiation. *J. Signal Transduct.* **2011**, 1–18 (2011).
162. Lefort, C. T. *et al.* Outside-In Signal Transmission by Conformational Changes in Integrin Mac-1. *J. Immunol.* **183**, 6460–6468 (2009).
163. Zhao, X. & Guan, J.-L. Focal adhesion kinase and its signaling pathways in cell migration and angiogenesis. *Adv. Drug Deliv. Rev.* **63**, 610–5 (2011).
164. Lietha, D. *et al.* Structural Basis for the Autoinhibition of Focal Adhesion Kinase. *Cell* **129**, 1177–1187 (2007).
165. Klemke, R. L. *et al.* CAS/Crk coupling serves as a ‘molecular switch’ for induction of cell migration. *J. Cell Biol.* **140**, 961–972 (1998).
166. Cho, S. Y. & Klemke, R. L. Extracellular-regulated kinase activation and CAS/Crk coupling regulate cell migration and suppress apoptosis during invasion of the extracellular matrix. *J. Cell Biol.* **149**, 223–236 (2000).
167. Reiske, H. R. *et al.* Requirement of phosphatidylinositol 3-kinase in focal adhesion kinase-promoted cell migration. *J. Biol. Chem.* **274**, 12361–12366 (1999).
168. Han, D. C., Shen, T. L. & Guan, J. L. Role of Grb7 targeting to focal contacts and its phosphorylation by focal adhesion kinase in regulation of cell migration. *J. Biol. Chem.* **275**, 28911–28917 (2000).
169. Pradip, D., Bouzyk, M., Dey, N. & Leyland-Jones, B. Dissecting GRB7-mediated signals for proliferation and migration in HER2 overexpressing breast tumor cells: GTP-ase rules. *Am. J. Cancer Res.* **3**, 173–95 (2013).
170. Kallergi, G., Agelaki, S., Markomanolaki, H. & Stournaras, C. Cellular Physiology and Biochemistry Activation of FAK / PI3K / Rac1 Signaling Controls Actin Reorganization and Inhibits Cell Motility in Human Cancer Cells. 977–986 (2007).
171. Costa, P., Scales, T. M. E., Ivaska, J. & Parsons, M. Integrin-Specific Control of Focal Adhesion Kinase and RhoA Regulates Membrane Protrusion and Invasion. *PLoS One* **8**, (2013).
172. Schaller, M. D. Paxillin: a focal adhesion-associated adaptor protein. *Oncogene* **20**, 6459–6472 (2001).
173. Turner, C. E. Paxillin interactions. *J Cell Sci* **113 Pt 23**, 4139–4140 (2000).

174. Turner, C. E., Glenney, J. R. & Burridge, K. Paxillin: A new vinculin-binding protein present in focal adhesions. *J. Cell Biol.* **111**, 1059–1068 (1990).
175. Kumar, A. *et al.* Talin tension sensor reveals novel features of focal adhesion force transmission and mechanosensitivity. *J. Cell Biol.* **213**, 371–383 (2016).
176. Yan, J., Yao, M., Goult, B. T. & Sheetz, M. P. Talin Dependent Mechanosensitivity of Cell Focal Adhesions. *Cell. Mol. Bioeng.* **8**, 151–159 (2015).
177. Lee, H. S., Lim, C. J., Puzon-McLaughlin, W., Shattil, S. J. & Ginsberg, M. H. RIAM activates integrins by linking talin to Ras GTPase membrane-targeting sequences. *J. Biol. Chem.* **284**, 5119–5122 (2009).
178. Bouchet, B. P. *et al.* Talin-KANK1 interaction controls the recruitment of cortical microtubule stabilizing complexes to focal adhesions. *Elife* **5**, 1–23 (2016).
179. Plow, E. F., Haas, T. A., Zhang, L., Loftus, J. & Smith, J. W. Ligand binding to integrins. *J. Biol. Chem.* **275**, 21785–21788 (2000).
180. Knight, C. G. *et al.* The collagen-binding A-domains of integrins alpha(1)beta(1) and alpha(2)beta(1) recognize the same specific amino acid sequence, GFOGER, in native (triple-helical) collagens. *J. Biol. Chem.* **275**, 35–40 (2000).
181. Dzamba, B. J., Wu, H., Jaenisch, R. & Peters, D. M. Fibronectin binding site in type I collagen regulates fibronectin fibril formation. *J. Cell Biol.* **121(5)**, 1165–1172 (1993).
182. Chen, C. S., Alonso, J. L., Ostuni, E., Whitesides, G. M. & Ingber, D. E. Cell shape provides global control of focal adhesion assembly. *Biochem. Biophys. Res. Commun.* **307**, 355–361 (2003).
183. Zamir, E. & Geiger, B. Molecular complexity and dynamics of cell-matrix adhesions. *J. Cell Sci.* **114**, 3583–3590 (2001).
184. Beningo, K. A., Dembo, M., Kaverina, I., Small, J. V. & Wang, Y. L. Nascent focal adhesions are responsible for the generation of strong propulsive forces in migrating fibroblasts. *J. Cell Biol.* **153**, 881–887 (2001).
185. Wu, C. Focal Adhesion. *Cell Adh. Migr.* **1**, 13–18 (2007).
186. Schiller, H. B. *et al.* β 1- and α v-class integrins cooperate to regulate myosin II during rigidity sensing of fibronectin-based microenvironments. *Nat. Cell Biol.* **15**, 625–36 (2013).

187. Zamir, E. *et al.* Molecular diversity of cell-matrix adhesions. *J. Cell Sci.* **112**, 1655–1669 (1999).
188. Nagano, M., Hoshino, D., Koshikawa, N., Akizawa, T. & Seiki, M. Turnover of focal adhesions and cancer cell migration. *Int. J. Cell Biol.* **2012**, (2012).
189. Zamir, E. *et al.* Dynamics and segregation of cell-matrix adhesions in cultured fibroblasts. *Nat. Cell Biol.* **2**, 191–6 (2000).
190. Small, J. V., Stradal, T., Vignat, E. & Rottner, K. The lamellipodium: Where motility begins. *Trends Cell Biol.* **12**, 112–120 (2002).
191. Ezratty, E. J., Partridge, M. A. & Gundersen, G. G. Microtubule-induced focal adhesion disassembly is mediated by dynamin and focal adhesion kinase. *Nat. Cell Biol.* **7**, 581–590 (2005).
192. Krylyshkina, O. *et al.* Modulation of substrate adhesion dynamics via microtubule targeting requires kinesin-1. *J. Cell Biol.* **156**, 349–359 (2002).
193. Franco, S. J. *et al.* Calpain-mediated proteolysis of talin regulates adhesion dynamics. *Nat. Cell Biol.* **6**, 977–983 (2004).
194. Bridgewater, R. E., Norman, J. C. & Caswell, P. T. Integrin trafficking at a glance. *J. Cell Sci.* **125**, 3695–3701 (2012).
195. Valdembri, D. *et al.* Neuropilin-1/GIPC1 signaling regulates alpha5beta1 integrin traffic and function in endothelial cells. *PLoS Biol.* **7**, e25 (2009).
196. Hongu, T. *et al.* Arf6 regulates tumour angiogenesis and growth through HGF-induced endothelial β 1 integrin recycling. *Nat. Commun.* **6**, 1–12 (2015).
197. Ikeda, S. *et al.* Novel role of ARF6 in vascular endothelial growth factor-induced signaling and angiogenesis. *Circ. Res.* **96**, 467–75 (2005).
198. Yue, J. *et al.* Microtubules Regulate Focal Adhesion Dynamics through MAP4K4. *Dev. Cell* **31**, 572–585 (2014).
199. Eliceiri, B. P. Integrin and growth factor receptor crosstalk. *Circ. Res.* **89**, 1104–1110 (2001).
200. Klemke, R. L., Yebra, M., Bayna, E. M. & Cheresch, D. A. Receptor tyrosine kinase signaling required for integrin alpha v beta 5- directed cell motility but not adhesion

- on vitronectin. *J Cell Biol* **127**, 859–866 (1994).
201. Falcioni, R. *et al.* Alpha 6 beta 4 and alpha 6 beta 1 integrins associate with ErbB-2 in human carcinoma cell lines. *Exp. Cell Res.* **236**, 76–85 (1997).
 202. Sen, B. & Johnson, F. M. Regulation of Src Family Kinases in Human Cancers. *J. Signal Transduct.* **2011**, 1–14 (2011).
 203. Playford, M. P. & Schaller, M. D. The interplay between Src and integrins in normal and tumor biology. *Oncogene* **23**, 7928–7946 (2004).
 204. Lu, Y. *et al.* Src family protein-tyrosine kinases alter the function of PTEN to regulate phosphatidylinositol 3-kinase/AKT cascades. *J. Biol. Chem.* **278**, 40057–40066 (2003).
 205. Brooks, P. C., Clark, R. A. F. & Cheresh, D. A. Requirement of Vascular Integrin alpha v beta 3 for Angiogenesis. **353**, 21–23 (1994).
 206. Hynes, R. O. Integrins: Bidirectional, allosteric signaling machines. *Cell* **110**, 673–687 (2002).
 207. Brooks, P. C. *et al.* Integrin alpha v beta 3 antagonists promote tumor regression by inducing apoptosis of angiogenic blood vessels. *Cell* **79**, 1157–1164 (1994).
 208. Oliveira-Ferrer, L. *et al.* Cilengitide induces cellular detachment and apoptosis in endothelial and glioma cells mediated by inhibition of FAK/src/AKT pathway. *J Exp Clin Cancer Res* **27**, 86 (2008).
 209. Mahabeleshwar, G. H., Feng, W., Reddy, K., Plow, E. F. & Byzova, T. V. Mechanisms of integrin-vascular endothelial growth factor receptor cross-activation in angiogenesis. *Circ. Res.* **101**, 570–80 (2007).
 210. Byzova, T. V *et al.* A mechanism for modulation of cellular responses to VEGF: activation of the integrins. *Mol. Cell* **6**, 851–60 (2000).
 211. Buerkle, M. a *et al.* Inhibition of the alpha-nu integrins with a cyclic RGD peptide impairs angiogenesis, growth and metastasis of solid tumours in vivo. *Br. J. Cancer* **86**, 788–95 (2002).
 212. Stupp, R., Picard, M. & Weller, M. Does cilengitide deserve another chance?- Authors' reply. *Lancet Oncol.* **15**, e585–e586 (2014).

213. Mas-Moruno, C., Rechenmacher, F. & Kessler, H. Cilengitide: the first anti-angiogenic small molecule drug candidate design, synthesis and clinical evaluation. *Anticancer. Agents Med. Chem.* **10**, 753–768 (2010).
214. Reynolds, A. R. *et al.* Stimulation of tumor growth and angiogenesis by low concentrations of RGD-mimetic integrin inhibitors. *Nat. Med.* **15**, 392–400 (2009).
215. Reynolds, L. E. *et al.* Enhanced pathological angiogenesis in mice lacking beta3 integrin or beta3 and beta5 integrins. *Nat. Med.* **8**, 27–34 (2002).
216. Robinson, S. D., Reynolds, L. E., Wyder, L., Hicklin, D. J. & Hoidalva-Dilke, K. M. Beta3-integrin regulates vascular endothelial growth factor-A-dependent permeability. *Arterioscler. Thromb. Vasc. Biol.* **24**, 2108–14 (2004).
217. Reynolds, A. R. *et al.* Elevated Flk1 (Vascular Endothelial Growth Factor Receptor 2) Signaling Mediates Enhanced Angiogenesis in β 3 -Integrin – Deficient Mice Elevated Flk1 (Vascular Endothelial Growth Factor Receptor 2) Signaling Mediates Enhanced Angiogenesis in β 3 -Int. **1**, 8643–8650 (2004).
218. Ellison, T. S. *et al.* Suppressing β -integrin triggers a neuropilin-1 dependent change in focal adhesion remodelling that can be targeted to block pathological angiogenesis. *Dis. Model. Mech.* 1105–1119 (2015). doi:10.1242/dmm.019927
219. Fantin, A. *et al.* The cytoplasmic domain of neuropilin 1 is dispensable for angiogenesis, but promotes the spatial separation of retinal arteries and veins. *Development* **138**, 4185–4191 (2011).
220. Hamano, Y. *et al.* Physiological levels of tumstatin, a fragment of collagen IV alpha3 chain, are generated by MMP-9 proteolysis and suppress angiogenesis via alphaVbeta3 integrin. *Cancer Cell* **3**, 589–601 (2003).
221. Loriger, M., Krueger, J. S., O’Neal, M., Staflin, K. & Felding-Habermann, B. Activation of tumor cell integrin alphaVbeta3 controls angiogenesis and metastatic growth in the brain. *Proc. Natl. Acad. Sci. U. S. A.* **106**, 10666–10671 (2009).
222. Kaur, S. *et al.* {Beta}3-Integrin Expression on Tumor Cells Inhibits Tumor Progression, Reduces Metastasis, and Is Associated With a Favorable Prognosis in Patients With Ovarian Cancer. *Am. J. Pathol.* **175**, 2184–96 (2009).
223. Steri, V. *et al.* Acute depletion of endothelial β 3-integrin transiently inhibits tumor

growth and angiogenesis in mice. *Circ. Res.* (2013). at
<<http://www.ncbi.nlm.nih.gov/pubmed/24103390>>

224. Atkinson, S. J., Ellison, T. S., Steri, V., Gould, E. & Robinson, S. D. Redefining the role(s) of endothelial $\alpha v\beta 3$ -integrin in angiogenesis. *Biochem. Soc. Trans.* **42**, 1590–5 (2014).
225. Schaffner, F., Ray, A. M. & Dontenwill, M. Integrin $\alpha 5\beta 1$, the fibronectin receptor, as a pertinent therapeutic target in solid tumors. *Cancers (Basel)*. **5**, 27–47 (2013).
226. Sudhakar, A. *et al.* Human tumstatin and human endostatin exhibit distinct antiangiogenic activities mediated by alpha v beta 3 and alpha 5 beta 1 integrins. *Proc. Natl. Acad. Sci. U. S. A.* **100**, 4766–71 (2003).
227. Springer, T. A., Zhu, J. & Xiao, T. Structural basis for distinctive recognition of fibrinogen γC peptide by the platelet integrin $\alpha IIb\beta 3$. *J. Cell Biol.* **182**, 791–800 (2008).
228. Zhu, J. *et al.* Structure of a Complete Integrin Ectodomain in a Physiologic Resting State and Activation and Deactivation by Applied Forces. *Mol. Cell* **32**, 849–861 (2008).
229. Wegener, K. L. *et al.* Structural Basis of Integrin Activation by Talin. *Cell* **128**, 171–182 (2007).
230. Zaidel-Bar, R., Itzkovitz, S., Ma'ayan, A., Iyengar, R. & Geiger, B. Functional atlas of the integrin adhesome. *Nat. Cell Biol.* **9**, 858–867 (2007).
231. Zaidel-Bar, R. & Geiger, B. The switchable integrin adhesome. *J. Cell Sci.* **123**, 1385–1388 (2010).
232. Hu, Q. *et al.* The Orbitrap: A new mass spectrometer. *J. Mass Spectrom.* **40**, 430–443 (2005).
233. Schiller, H. B., Friedel, C. C., Boulegue, C. & Fässler, R. Quantitative proteomics of the integrin adhesome show a myosin II-dependent recruitment of LIM domain proteins. *EMBO Rep.* **12**, 259–266 (2011).
234. Bantscheff, M., Schirle, M., Sweetman, G., Rick, J. & Kuster, B. Quantitative mass spectrometry in proteomics: a critical review. *Anal. Bioanal. Chem.* **389**, 1017–31 (2007).

235. Fabre, B. *et al.* Comparison of label-free quantification methods for the determination of protein complexes subunits stoichiometry. *EuPA Open Proteomics* **4**, 82–86 (2014).
236. Zhang, B. *et al.* Detecting Differential and Correlated Protein Expression in Label-Free Shotgun Proteomics Detecting Differential and Correlated Protein Expression in Label-Free Shotgun Proteomics. *J. Proteome Res.* 2909–2918 (2006).
doi:10.1021/pr0600273
237. Byron, A. *et al.* A proteomic approach reveals integrin activation state-dependent control of microtubule cortical targeting. *Nat. Commun.* **6**, 6135 (2015).
238. Mattson, G. *et al.* A practical approach to crosslinking. *Mol. Biol. Rep.* **17**, 167–183 (1993).
239. Rappsilber, J. The beginning of a beautiful friendship: Cross-linking/mass spectrometry and modelling of proteins and multi-protein complexes. *J. Struct. Biol.* **173**, 530–540 (2011).
240. Yoshigi, M., Hoffman, L. M., Jensen, C. C., Yost, H. J. & Beckerle, M. C. Mechanical force mobilizes zyxin from focal adhesions to actin filaments and regulates cytoskeletal reinforcement. *J. Cell Biol.* **171**, 209–215 (2005).
241. Ashburner, M. *et al.* Gene Ontology: Tool for The Unification of Biology. *Nat. Genet.* **25**, 25–29 (2000).
242. Blake, J. A. *et al.* Gene ontology consortium: Going forward. *Nucleic Acids Res.* **43**, D1049–D1056 (2015).
243. Papini, D. *et al.* TD-60 links RalA GTPase function to the CPC in mitosis. *Nat. Commun.* **6**, 7678 (2015).
244. Humphries, J. D. *et al.* Proteomic analysis of integrin-associated complexes identifies RCC2 as a dual regulator of Rac1 and Arf6. *Sci. Signal.* **2**, ra51 (2009).
245. Horton, E. R. *et al.* Definition of a consensus integrin adhesome and its dynamics during adhesion complex assembly and disassembly. *Nat. Cell Biol.* **17**, (2015).
246. Seerapu, H. R. *et al.* The cytoplasmic domain of neuropilin-1 regulates focal adhesion turnover. *FEBS Lett.* **587**, 3392–9 (2013).
247. Fantin, A. *et al.* NRP1 acts cell autonomously in endothelium to promote tip cell

- function during sprouting angiogenesis. *Blood* **121**, 2352–62 (2013).
248. Weber, G. F., Bjerke, M. A. & DeSimone, D. W. Integrins and cadherins join forces to form adhesive networks. *J. Cell Sci.* **124**, 1183–1193 (2011).
249. Nelson, C. M., Pirone, D. M., Tan, J. L. & Chen, C. S. Vascular Endothelial-Cadherin Regulates Cytoskeletal Tension, Cell Spreading, and Focal Adhesions by Stimulating RhoA. *Mol. Biol. Cell* **15**, 2943–2953, (2004).
250. Le Boeuf, F., Houle, F. & Huot, J. Regulation of vascular endothelial growth factor receptor 2-mediated phosphorylation of focal adhesion kinase by heat shock protein 90 and Src kinase activities. *J. Biol. Chem.* **279**, 39175–39185 (2004).
251. Schiller, H. B. & Fässler, R. Mechanosensitivity and compositional dynamics of cell-matrix adhesions. *EMBO Rep.* **14**, 509–519 (2013).
252. Akhmanova, A. & Steinmetz, M. O. Control of microtubule organization and dynamics: two ends in the limelight. *Nat. Rev. Mol. Cell Biol.* **16**, 711–726 (2015).
253. Chretien, D., Metoz, F., Verde, F., Karsenti, E. & Wade, R. H. Lattice defects in microtubules: Protofilament numbers vary within individual microtubules. *J. Cell Biol.* **117**, 1031–1040 (1992).
254. Desai, A. & Mitchison, T. J. Microtubule Polymerization Dynamics. *Annu. Rev. Cell Dev. Biol.* **13**, 83–117 (1997).
255. Slep, K. C. A microtubule dynamics reconstitutive convention. *J. Cell Biol.* **215**, 305–307 (2016).
256. Bowne-Anderson, H., Zanic, M., Kauer, M. & Howard, J. Microtubule dynamic instability: A new model with coupled GTP hydrolysis and multistep catastrophe. *BioEssays* **35**, 452–461 (2013).
257. Akhmanova, A. & Hoogenraad, C. C. Microtubule plus-end-tracking proteins: Mechanisms and functions. *Curr. Opin. Cell Biol.* **17**, 47–54 (2005).
258. Delphin, C. *et al.* MAP6-F is a temperature sensor that directly binds to and protects microtubules from cold-induced depolymerization. *J. Biol. Chem.* **287**, 35127–35138 (2012).
259. Ochoa, C. D., Stevens, T. & Balczon, R. Cold exposure reveals two populations of microtubules in pulmonary endothelia. *Am. J. Physiol. Lung Cell. Mol. Physiol.* **300**,

- L132–8 (2011).
260. Breton, S. & Brown, D. Cold-induced microtubule disruption and relocalization of membrane proteins in kidney epithelial cells. *J Am Soc Nephrol* **9**, 155–166 (1998).
 261. Hancock, W. O. Bidirectional cargo transport: moving beyond tug of war. *Nat. Rev. Mol. Cell Biol.* **15**, 615–628 (2014).
 262. Schmoranzler, J. & Simon, S. M. Role of Microtubules in Fusion of Post-Golgi Vesicles to the Plasma Membrane. *Mol. Biol. Cell* **14**, 1558–1569 (2003).
 263. Yang, H., Ganguly, A. & Cabral, F. Inhibition of cell migration and cell division correlates with distinct effects of microtubule inhibiting drugs. *J. Biol. Chem.* **285**, 32242–32250 (2010).
 264. Dumontet, C. & Jordan, M. A. Microtubule-binding agents: a dynamic field of cancer therapeutics. *Nat. Rev. Drug Discov.* **9**, 790–803 (2010).
 265. Elie-Caille, C. *et al.* Straight GDP-Tubulin Protofilaments Form in the Presence of Taxol. *Curr. Biol.* **17**, 1765–1770 (2007).
 266. Khanna, C., Rosenberg, M. & Vail, D. M. A review of paclitaxel and novel formulations including those suitable for use in dogs. *J. Vet. Intern. Med.* **29**, 1006–1012 (2015).
 267. Kowalski, R. J., Giannakakous, P. & Hamel, E. Activities of the microtubule-stabilizing agents epothilone A and B with purified and in cells resistant to paclitaxel (Taxol). *J. Biol. Chem.* **272**, 2534–2541 (1997).
 268. Rai, S. S. & Wolff, J. Localization of the vinblastine-binding site on β -tubulin. *J. Biol. Chem.* **271**, 14707–14711 (1996).
 269. Stanton, R. A., Gernert, K. M., Nettles, J. H. & Aneja, R. Drugs That Target Dynamic Microtubules: A New Molecular Perspective. *Med Res Rev* **31**, 443–481 (2011).
 270. Dhamodharan, R., Jordan, M. A., Thrower, D., Wilson, L. & Wadsworth, P. Vinblastine Suppresses Dynamics of Individual Microtubules in Living Interphase Cells. *Mol. Biol. Cell* **6**, 1215–1229 (1995).
 271. Downing, K. H. STRUCTURAL BASIS FOR THE INTERACTION OF TUBULIN WITH PROTEINS AND DRUGS THAT AFFECT MICROTUBULE DYNAMICS. *Annu Rev Cell Dev Biol* **16**, 89–111 (2000).

272. Kaverina, I., Rottner, K. & Small, J. V. Targeting, capture, and stabilization of microtubules at early focal adhesions. *J. Cell Biol.* **142**, 181–190 (1998).
273. Rooney, C. *et al.* The Rac activator STEF (Tiam2) regulates cell migration by microtubule-mediated focal adhesion disassembly. *EMBO Rep.* **11**, 292–298 (2010).
274. Fukata, M. *et al.* Rac1 and Cdc42 capture microtubules through IQGAP1 and CLIP-170. *Cell* **109**, 873–885 (2002).
275. Faix, J. & Weber, I. A dual role model for active Rac1 in cell migration. *Small GTPases* **4**, 110–5 (2013).
276. Bretscher, M. S. & Aguado-Velasco, C. Membrane traffic during cell locomotion. *Curr. Opin. Cell Biol.* **10**, 537–541 (1998).
277. Spiczka, K. S. & Yeaman, C. Ral-regulated interaction between Sec5 and paxillin targets Exocyst to focal complexes during cell migration. *J. Cell Sci.* **121**, 2880–2891 (2008).
278. Gundersen, G. G. Microtubule capture: IQGAP and CLIP-170 expand the repertoire. *Curr. Biol.* **12**, 645–647 (2002).
279. Etienne-Manneville, S. Microtubules in cell migration. *Annu. Rev. Cell Dev. Biol.* **29**, 471–99 (2013).
280. Krylyshkina, O. *et al.* Nanometer targeting of microtubules to focal adhesions. *J. Cell Biol.* **161**, 853–859 (2003).
281. Applewhite, D. A. *et al.* The Spectraplakins Short Stop Is an Actin–Microtubule Cross-Linker That Contributes to Organization of the Microtubule Network. *Mol. Biol. Cell* **21**, 1713–1724 (2010).
282. Wu, X., Kodama, A. & Fuchs, E. ACF7 Regulates Cytoskeletal-Focal Adhesion Dynamics and Migration and Has ATPase Activity. *Cell* **135**, 137–148 (2008).
283. Efimov, A. *et al.* Paxillin-dependent stimulation of microtubule catastrophes at focal adhesion sites. *J. Cell Sci.* **121**, 196–204 (2008).
284. Ganguly, A., Yang, H., Zhang, H., Cabral, F. & Patel, K. D. Microtubule Dynamics Control Tail Retraction in Migrating Vascular Endothelial Cells. *Mol. Cancer Ther.* **12**, 2837–2846 (2013).

285. Lyle, K. S., Corleto, J. a & Wittmann, T. Microtubule dynamics regulation contributes to endothelial morphogenesis. *Bioarchitecture* **2**, 220–227 (2012).
286. Czeisler, C. & Mikawa, T. Microtubules Coordinate VEGFR2 Signaling and Sorting. *PLoS One* **8**, 1–11 (2013).
287. Bijman, M. N. a, van Nieuw Amerongen, G. P., Laurens, N., van Hinsbergh, V. W. M. & Boven, E. Microtubule-targeting agents inhibit angiogenesis at subtoxic concentrations, a process associated with inhibition of Rac1 and Cdc42 activity and changes in the endothelial cytoskeleton. *Mol. Cancer Ther.* **5**, 2348–2357 (2006).
288. Pasquier, E. *et al.* Antiangiogenic activity of paclitaxel is associated with its cytostatic effect , mediated by the initiation but not completion of a mitochondrial apoptotic signaling pathway. **3**, 1301–1311 (2004).
289. Mooney, C. J. *et al.* A Phase II Trial of Fosbretabulin in Advanced Anaplastic Thyroid Carcinoma and Correlation of Baseline Serum-Soluble Intracellular Adhesion Molecule-1 with Outcome. *Thyroid* **19**, 233–240 (2009).
290. Shi, Y.-W. *et al.* Combretastatin A-4 efficiently inhibits angiogenesis and induces neuronal apoptosis in zebrafish. *Sci. Rep.* **6**, 30189 (2016).
291. Stehbens, S. & Wittmann, T. Targeting and transport: How microtubules control focal adhesion dynamics. *J. Cell Biol.* **198**, 481–489 (2012).
292. Krilleke, D. *et al.* Molecular mapping and functional characterization of the VEGF164 heparin-binding domain. *J. Biol. Chem.* **282**, 28045–28056 (2007).
293. Claxton, S. *et al.* Efficient, inducible cre-recombinase activation in vascular endothelium. *Genesis* **46**, 74–80 (2008).
294. Gustafsson, E., Brakebusch, C., Hietanen, K. & Fässler, R. Tie-1-directed expression of Cre recombinase in endothelial cells of embryoid bodies and transgenic mice. *J. Cell Sci.* **114**, 671–6 (2001).
295. Morgan, E. A. *et al.* Dissection of platelet and myeloid cell defects by conditional targeting of the α 3-integrin subunit. *FASEB J.* **24**, 1117–1127 (2010).
296. Reynolds, L. E. & Hodivala-dilke, K. M. Primary Mouse Endothelial Cell Culture for Assays of Angiogenesis. *Methods Mol. Biol.* **120**, 503–509 (2006).
297. Bellett, G. *et al.* Microtubule plus-end and minus-end capture at adherens junctions

- is involved in the assembly of apico-basal arrays in polarised epithelial cells. *Cell Motil. Cytoskeleton* **66**, 893–908 (2009).
298. Iversen, N., Birkenes, B., Torsdalen, K. & Djurovic, S. Electroporation by nucleofector is the best nonviral transfection technique in human endothelial and smooth muscle cells. *Genet. Vaccines Ther.* **3**, 1–13 (2005).
 299. Jayo, A., Parsons, M. & Adams, J. C. A novel Rho-dependent pathway that drives interaction of fascin-1 with p-Lin-11/Isl-1/Mec-3 kinase (LIMK) 1/2 to promote fascin-1/actin binding and filopodia stability. *BMC Biol.* **10**, 1–19 (2012).
 300. Meijering, E., Dzyubachyk, O. & Smal, I. Methods for cell and particle tracking. *Methods Enzymol.* **504**, 183–200 (2012).
 301. Tusher, V. G., Tibshirani, R. & Chu, G. Significance analysis of microarrays applied to the ionizing radiation response. *Proc. Natl. Acad. Sci. U. S. A.* **98**, 5116–21 (2001).
 302. Tyanova, S. *et al.* The Perseus computational platform for comprehensive analysis of (prote)omics data. *Nat. Methods* **13**, 731–40 (2016).
 303. Ivaska, J. & Ivaska, J. Unanchoring integrins in focal adhesions. *Nat. Cell Biol.* **14**, 981–983 (2012).
 304. Mould, A. P., Garratt, A. N., Askari, J. A., Akiyama, S. K. & Humphries, M. J. Identification of a novel anti-integrin monoclonal antibody that recognises a ligand-induced binding site epitope on the $\beta 1$ subunit. *FEBS Lett.* **363**, 118–122 (1995).
 305. Mazia, D., Schatten, G. & Sale, W. Adhesion of cells to surfaces coated with polylysine. Applications to electron microscopy. *J. Cell Biol.* **66**, 198–200 (1975).
 306. Lomant, A. J. & Fairbanks, G. Chemical probes of extended biological structures: Synthesis and properties of the cleavable protein cross-linking reagent [35S]dithiobis(succinimidyl propionate). *J. Mol. Biol.* **104**, 243–261 (1976).
 307. Somanath, P. R., Malinin, N. L. & Byzova, T. V. Cooperation between integrin $\alpha v\beta 3$ and VEGFR2 in angiogenesis. *Angiogenesis* **12**, 177–85 (2009).
 308. Barber, R. D., Harmer, D. W., Coleman, R. a & Clark, B. J. GAPDH as a housekeeping gene: analysis of GAPDH mRNA expression in a panel of 72 human tissues. *Physiol. Genomics* **21**, 389–395 (2005).
 309. Chen, L. *et al.* Smooth muscle- α actin inhibits vascular smooth muscle cell

- proliferation and migration by inhibiting rac1 activity. *PLoS One* **11**, 1–10 (2016).
310. Horton, E. R. *et al.* The integrin adhesome network at a glance. *J. Cell Sci.* 1–5 (2016). doi:10.1242/jcs.192054
311. Fincham, V. J., James, M., Frame, M. C. & Winder, S. J. Active ERK/MAP kinase is targeted to newly forming cell-matrix adhesions by integrin engagement and v-Src. *EMBO J.* **19**, 2911–23 (2000).
312. Lawson, C. *et al.* FAK promotes recruitment of talin to nascent adhesions to control cell motility. *J. Cell Biol.* **196**, 223–232 (2012).
313. Hoeben, A. N. N. *et al.* Vascular endothelial growth factor and angiogenesis. *Pharmacol. Rev.* **56**, 549–580 (2004).
314. Herzog, B., Pellet-Many, C., Britton, G., Hartzoulakis, B. & Zachary, I. C. VEGF binding to NRP1 is essential for VEGF stimulation of endothelial cell migration, complex formation between NRP1 and VEGFR2, and signaling via FAK Tyr407 phosphorylation. *Mol. Biol. Cell* **22**, 2766–76 (2011).
315. Yue, J., Huhn, S. & Shen, Z. Complex roles of filamin-A mediated cytoskeleton network in cancer progression. *Cell Biosci.* **3**, 7 (2013).
316. Tsuruta, D. & Jones, J. C. R. The vimentin cytoskeleton regulates focal contact size and adhesion of endothelial cells subjected to shear stress. *J. Cell Sci.* **116**, 4977–4984 (2003).
317. Deakin, N. O. & Turner, C. E. Paxillin comes of age. *J. Cell Sci.* **121**, 2435–44 (2008).
318. Winkler, C., Denker, K., Wortelkamp, S. & Sickmann, A. Silver- and Coomassie-staining protocols: Detection limits and compatibility with ESI MS. *Electrophoresis* **28**, 2095–2099 (2007).
319. Choi, C. K. *et al.* Actin and alpha-actinin orchestrate the assembly and maturation of nascent adhesions in a myosin II motor-independent manner. *Nat. Cell Biol.* **10**, 1039–50 (2008).
320. Cox, J. *et al.* Andromeda: A peptide search engine integrated into the MaxQuant environment. *J. Proteome Res.* **10**, 1794–1805 (2011).
321. Cox, J. & Mann, M. MaxQuant enables high peptide identification rates, individualized p.p.b.-range mass accuracies and proteome-wide protein

- quantification. *Nat. Biotechnol.* **26**, 1367–72 (2008).
322. Jacquemet, G. *et al.* Rac1 is deactivated at integrin activation sites through an IQGAP1-filamin-A-RacGAP1 pathway. *J. Cell Sci.* **126**, 4121–35 (2013).
323. Yamamoto, H. *et al.* Integrin β 1 controls VE-cadherin localization and blood vessel stability. *Nat. Commun.* **6**, 6429 (2015).
324. Cottrell, J. S. Protein identification using MS/MS data. *J. Proteomics* **74**, 1842–1851 (2011).
325. Flemming, S. *et al.* Soluble VE-cadherin is involved in endothelial barrier breakdown in systemic inflammation and sepsis. *Cardiovasc. Res.* **107**, 32–44 (2015).
326. Tyanova, S., Temu, T. & Cox, J. The MaxQuant computational platform for mass spectrometry-based shotgun proteomics. *Nat. Protoc.* **11**, 2301–2319 (2016).
327. Gorman, J. J., Wallis, T. P. & Pitt, J. J. Protein disulfide bond determination by mass spectrometry. *Mass Spectrom. Rev.* **21**, 183–216 (2002).
328. Olsen, J. V., Ong, S.-E. & Mann, M. Trypsin Cleaves Exclusively C-terminal to Arginine and Lysine Residues. *Mol. Cell. Proteomics* **3**, 608–614 (2004).
329. Holding, A. N. XL-MS: Protein cross-linking coupled with mass spectrometry. *Methods* **89**, 54–63 (2015).
330. Kanehisa, M., Furumichi, M., Tanabe, M., Sato, Y. & Morishima, K. KEGG: new perspectives on genomes, pathways, diseases and drugs. *Nucleic Acids Res.* **45**, 1–15 (2016).
331. Rivals, I., Personnaz, L., Taing, L. & Potier, M. C. Enrichment or depletion of a GO category within a class of genes: Which test? *Bioinformatics* **23**, 401–407 (2007).
332. Johnson-Léger, C., Aurrand-Lions, M. & Imhof, B. a. The parting of the endothelium: miracle, or simply a junctional affair? *J. Cell Sci.* **113** (Pt 6, 921–933 (2000).
333. Bernatchez, P. N., Soker, S. & Sirois, M. G. Vascular endothelial growth factor effect on endothelial cell proliferation, migration, and platelet-activating factor synthesis is Flk-1-dependent. *J Biol Chem* **274**, 31047–31054 (1999).
334. Wu, J. *et al.* Integrated network analysis platform for protein-protein interactions. *Nat. Methods* **6**, 75–7 (2009).

335. Cowley, M. J. *et al.* PINA v2.0: Mining interactome modules. *Nucleic Acids Res.* **40**, 862–865 (2012).
336. Shannon, P. *et al.* Cytoscape: a software environment for integrated models of biomolecular interaction networks. *Am. Assoc. Cancer Res. Educ. B.* 12–16 (2005). doi:10.1101/gr.1239303.metabolite
337. Willett, M., Pollard, H. J., Vlasak, M. & Morley, S. J. Localization of ribosomes and translation initiation factors to talin/beta3-integrin-enriched adhesion complexes in spreading and migrating mammalian cells. *Biol. Cell* **102**, 265–276 (2010).
338. Mellacheruvu, D. *et al.* The CRAPome: a contaminant repository for affinity purification-mass spectrometry data. *Nat. Methods* **10**, 730–6 (2013).
339. Widmaier, M., Rognoni, E., Radovanac, K., Azimifar, S. B. & Fassler, R. Integrin-linked kinase at a glance. *J. Cell Sci.* **125**, 1839–1843 (2012).
340. Bug, M. & Meyer, H. Expanding into new markets - VCP/p97 in endocytosis and autophagy. *J. Struct. Biol.* **179**, 78–82 (2012).
341. Meyer, H., Bug, M. & Bremer, S. Emerging functions of the VCP/p97 AAA-ATPase in the ubiquitin system. *Nat. Cell Biol.* **14**, 117–23 (2012).
342. Jeffery, I. B., Higgins, D. G. & Culhane, A. C. Comparison and evaluation of methods for generating differentially expressed gene lists from microarray data. *BMC Bioinformatics* **7**, 359 (2006).
343. Shattil, S. J. The $\beta 3$ integrin cytoplasmic tail: Protein scaffold and control freak. *J. Thromb. Haemost.* **7**, 210–213 (2009).
344. Friedman, J. R., Webster, B. M., Mastronarde, D. N., Verhey, K. J. & Voeltz, G. K. ER sliding dynamics and ER-mitochondrial contacts occur on acetylated microtubules. *J. Cell Biol.* **190**, 363–375 (2010).
345. Ng, I. C. *et al.* Kinectin-dependent ER transport supports the focal complex maturation required for chemotaxis in shallow gradients. *J. Cell Sci.* **129**, 2660–2672 (2016).
346. Arregui, C. O., Balsamo, J. & Lilien, J. Impaired integrin-mediated adhesion and signaling in fibroblasts expressing a dominant, negative mutant PTP1B. *J. Cell Biol.* **143**, 861–873 (1998).

347. Hernández, M. V, Sala, M. G. D., Balsamo, J., Lilien, J. & Arregui, C. O. ER-bound PTP1B is targeted to newly forming cell-matrix adhesions. *J. Cell Sci.* **119**, 1233–1243 (2006).
348. Zhang, X. *et al.* Kinectin-mediated endoplasmic reticulum dynamics supports focal adhesion growth in the cellular lamella. *J. Cell Sci.* **123**, 3901–12 (2010).
349. Zhou, J., Bronowska, A., Le Coq, J., Lietha, D. & Gr??ter, F. Allosteric regulation of focal adhesion kinase by PIP2 and ATP. *Biophys. J.* **108**, 698–705 (2015).
350. Bae, Y. S. & Ryu, S. H. ATP-induced focal adhesion kinase activity is negatively modulated by phospholipase D2 in PC12 cells. *Exp. Mol. Med.* **33**, 150–155 (2001).
351. Kiema, T. *et al.* The molecular basis of filamin binding to integrins and competition with talin. *Mol. Cell* **21**, 337–347 (2006).
352. Morse, E. M., Brahme, N. N. & Calderwood, D. a. Integrin Cytoplasmic Tail Interactions. *Biochemistry* (2014). doi:10.1021/bi401596q
353. Xu, Y. *et al.* Filamin A regulates focal adhesion disassembly and suppresses breast cancer cell migration and invasion. *J. Exp. Med.* **207**, 2421–37 (2010).
354. Kim, H. *et al.* Filamin A is required for vimentin-mediated cell adhesion and spreading. *Am J Physiol Cell Physiol* **298**, 221–236 (2010).
355. Feng, Y. *et al.* Filamin A (FLNA) is required for cell-cell contact in vascular development and cardiac morphogenesis. *Proc. Natl. Acad. Sci. U. S. A.* **103**, 19836–41 (2006).
356. Bu, Z. *et al.* A monoclonal antibody SZ-117 that recognizes filamin A derived from tumor cells. *Hybrid.* **31**, 214–218 (2012).
357. Kim, H., Sengupta, A., Glogauer, M. & McCulloch, C. A. Filamin A regulates cell spreading and survival via β 1 integrins. *Exp. Cell Res.* **314**, 834–846 (2008).
358. Meyer, S. C., Sanan, D. A. & Fox, J. E. B. Role of actin-binding protein in insertion of adhesion receptors into the membrane. *J. Biol. Chem.* **273**, 3013–3020 (1998).
359. Resovi, A., Pinessi, D., Chiorino, G. & Taraboletti, G. Current understanding of the thrombospondin-1 interactome. *Matrix Biol.* **37**, 83–91 (2014).
360. Lawler, J. Thrombospondin-1 as an endogenous inhibitor of angiogenesis and tumor

- growth. *J Cell Mol Med* **6**, 1–12 (2002).
361. LAHAV, J., LAWLER, J. & GIMBRONE, M. A. Thrombospondin interactions with fibronectin and fibrinogen: Mutual inhibition in binding. *Eur. J. Biochem.* **145**, 151–156 (1984).
 362. Kaur, S. *et al.* Thrombospondin-1 inhibits VEGF receptor-2 signaling by disrupting its association with CD47. *J. Biol. Chem.* **285**, 38923–38932 (2010).
 363. Chu, L. Y., Ramakrishnan, D. P. & Silverstein, R. L. Thrombospondin-1 modulates VEGF signaling via CD36 by recruiting SHP-1 to VEGFR2 complex in microvascular endothelial cells. *Blood* **122**, 1822–1832 (2013).
 364. Iyer, S. *et al.* Induction of Apoptosis in Proliferating Human Endothelial Cells by the Tumor-specific Antiangiogenesis Agent Combretastatin. *Cancer Res.* **58**, 4510–4514 (1998).
 365. Lapko, V. N., Smith, D. L. & Smith, J. B. Identification of an artifact in the mass spectrometry of proteins derivatized with iodoacetamide. *J. Mass Spectrom.* **35**, 572–575 (2000).
 366. Zaoui, K., Honor??, S., Isnardon, D., Braguer, D. & Badache, A. Memo - RhoA - mDia1 signaling controls microtubules, the actin network, and adhesion site formation in migrating cells. *J. Cell Biol.* **183**, 401–408 (2008).
 367. Cau, J. & Hall, A. Cdc42 controls the polarity of the actin and microtubule cytoskeletons through two distinct signal transduction pathways. *J. Cell Sci.* **118**, 2579–2587 (2005).
 368. Spiering, D. & Hodgson, L. Dynamics of the rho-family small GTPases in actin regulation and motility. *Cell Adhes. Migr.* **5**, 170–180 (2011).
 369. Fantin, A. *et al.* NRP1 Regulates CDC42 Activation to Promote Filopodia Formation in Endothelial Tip Cells. *Cell Rep.* **11**, 1577–1590 (2015).
 370. Carter, P. Merck: Phase III Trial of Cilengitide Did Not Meet Primary Endpoint in Patients With Newly Diagnosed Glioblastoma. **49**, (2013).
 371. Liu, Z., Wang, F. & Chen, X. Integrin alpha v beta 3 targeted cancer therapy. **69**, 329–339 (2010).
 372. Tarui, T., Miles, L. A. & Takada, Y. Specific Interaction of Angiostatin with Integrin

- alphavbeta3 in Endothelial Cells. *J. Biol. Chem.* **276**, 39562–39568 (2001).
373. Loges, S. *et al.* Cilengitide inhibits proliferation and differentiation of human endothelial progenitor cells in vitro. *Biochem. Biophys. Res. Commun.* **357**, 1016–20 (2007).
374. Liu, P. *et al.* Sulforaphane exerts anti-angiogenesis effects against hepatocellular carcinoma through inhibition of STAT3/HIF-1 α /VEGF signalling. *Sci. Rep.* **7**, 1–11 (2017).
375. Pfaff, M. *et al.* Selective recognition of cyclic RGD peptides of NMR defined conformation by alpha IIb beta 3, alpha V beta 3, and alpha 5 beta 1 integrins. *J. Biol. Chem.* **269**, 20233–20238 (1994).
376. Hermann, P. *et al.* The vitronectin receptor and its associated CD47 molecule mediates proinflammatory cytokine synthesis in human monocytes by interaction with soluble CD23. *J. Cell Biol.* **144**, 767–775 (1999).
377. Alghisi, G. C., Ponsonnet, L. & Rüegg, C. The integrin antagonist cilengitide activates α V β 3, disrupts VE-cadherin localization at cell junctions and enhances permeability in endothelial cells. *PLoS One* **4**, (2009).
378. Gebhardt, A. *et al.* mRNA export through an additional cap-binding complex consisting of NCBP1 and NCBP3. *Nat. Commun.* **6**, 8192 (2015).
379. Murphy, P. A., Begum, S. & Hynes, R. O. Tumor Angiogenesis in the Absence of Fibronectin or Its Cognate Integrin Receptors. 1–16 (2015).
doi:10.1371/journal.pone.0120872
380. Vicente-Manzanares, M., Choi, C. K. & Horwitz, A. R. Integrins in cell migration - the actin connection. *J. Cell Sci.* **122**, 1473–1473 (2009).
381. Calderwood, D. A., Shattil, S. J. & Ginsberg, M. H. Integrins and actin filaments: Reciprocal regulation of cell adhesion and signaling. *J. Biol. Chem.* **275**, 22607–22610 (2000).
382. Whelan, D. R. & Bell, T. D. M. Image artifacts in Single Molecule Localization Microscopy: why optimization of sample preparation protocols matters. *Sci. Rep.* **5**, 7924 (2015).
383. Zamir, E. *et al.* Dynamics and segregation of cell – matrix adhesions in cultured

- fibroblasts. **2**, (2000).
384. Gardner, M. K., Zanic, M. & Howard, J. Microtubule catastrophe and rescue. *Curr. Opin. Cell Biol.* **25**, 1–9 (2013).
385. Goult, B. T. *et al.* RIAM and vinculin binding to talin are mutually exclusive and regulate adhesion assembly and turnover. *J. Biol. Chem.* **288**, 8238–49 (2013).
386. Worth, D. C. *et al.* Alpha v beta3 integrin spatially regulates VASP and RIAM to control adhesion dynamics and migration. *J. Cell Biol.* **189**, 369–83 (2010).
387. Lukinavičius, G. *et al.* Fluorogenic probes for live-cell imaging of the cytoskeleton. *Nat. Methods* **11**, 731–3 (2014).
388. Goldspink, D. a *et al.* The microtubule end-binding protein EB2 is a central regulator of microtubule reorganisation in apico-basal epithelial differentiation. *J. Cell Sci.* **126**, 4000–14 (2013).
389. Parsons, J. T., Horwitz, A. R. & Schwartz, M. A. Cell adhesion: integrating cytoskeletal dynamics and cellular tension. *Nat. Rev. Mol. Cell Biol.* **11**, 633–643 (2010).
390. Zaidel-Bar, R., Milo, R., Kam, Z. & Geiger, B. A paxillin tyrosine phosphorylation switch regulates the assembly and form of cell-matrix adhesions. *J. Cell Sci.* **120**, 137–48 (2007).
391. Balasubramanian, N., Scott, D. W., Castle, J. D., Casanova, J. E. & Schwartz, M. A. Arf6 and microtubules in adhesion-dependent trafficking of lipid rafts. *Nat. Cell Biol.* **9**, 1381–1391 (2007).
392. Paul, N. R., Jacquemet, G. & Caswell, P. T. Endocytic Trafficking of Integrins in Cell Migration. *Curr. Biol.* **25**, R1092–R1105 (2015).
393. Roberts, M., Barry, S., Woods, A., Van der Sluijs, P. & Norman, J. PDGF-regulated rab4-dependent recycling of alpha v beta 3 integrin from early endosomes is necessary for cell adhesion and spreading. *Curr. Biol.* **11**, 1392–1402 (2001).
394. Fang, Z. *et al.* The Membrane-Associated Protein, Supervillin, Accelerates F-Actin-Dependent Rapid Integrin Recycling and Cell Motility. *Traffic* **11**, 782–799 (2010).
395. De Franceschi, N., Hamidi, H., Alanko, J., Sahgal, P. & Ivaska, J. Integrin traffic - the update. *J. Cell Sci.* **128**, 839–852 (2015).

396. Shi, F. & Sottile, J. MT1-MMP regulates the turnover and endocytosis of extracellular matrix fibronectin. *J. Cell Sci.* **124**, 4039–4050 (2011).
397. Tanabe, K. & Takei, K. Dynamic instability of microtubules requires dynamin 2 and is impaired in a Charcot-Marie-Tooth mutant. *J. Cell Biol.* **185**, 939–948 (2009).
398. Kim, D.-H. & Wirtz, D. Focal adhesion size uniquely predicts cell migration. *FASEB J.* **27**, 1351–61 (2013).
399. Ganguly, A., Yang, H., Sharma, R., Patel, K. D. & Cabral, F. The role of microtubules and their dynamics in cell migration. *J. Biol. Chem.* **287**, 43359–43369 (2012).
400. Cheng, K. L., Bradley, T. & Budman, D. R. Novel microtubule-targeting agents - the epothilones. *Biol. Targets Ther.* **2**, 789–811 (2008).
401. Asahina, a, Tada, Y., Nakamura, K. & Tamaki, K. Colchicine and griseofulvin inhibit VCAM-1 expression on human vascular endothelial cells - evidence for the association of VCAM-1 expression with microtubules. *J. Dermatol. Sci.* **25**, 1–9 (2001).
402. Pantziarka, P., Bouche, G., Meheus, L., Sukhatme, V. & Sukhatme, V. P. Repurposing Drugs in Oncology (ReDO)-mebendazole as an anti-cancer agent. *Ecancermedicalscience* **8**, 443 (2014).
403. Dybdal-Hargreaves, N. F., Risinger, A. L. & Mooberry, S. L. Eribulin Mesylate: Mechanism of action of a unique microtubule-Targeting agent. *Clin. Cancer Res.* **21**, 2445–2452 (2015).
404. Pawluk, S. A., Roels, C. A., Wilby, K. J. & Ensom, M. H. H. A Review of Pharmacokinetic Drug–Drug Interactions with the Anthelmintic Medications Albendazole and Mebendazole. *Clin. Pharmacokinet.* **54**, 371–383 (2015).
405. Tavora, B. *et al.* Endothelial-cell FAK targeting sensitizes tumours to DNA-damaging therapy. *Nature* **514**, 112–6 (2014).
406. Leighl, N. B. *et al.* Bleeding events in bevacizumab-treated cancer patients who received full-dose anticoagulation and remained on study. *Br. J. Cancer* **104**, 413–418 (2011).
407. Danhier, F., Le Breton, A. & Pr eat, V. RGD-based strategies to target alpha(v) beta(3) integrin in cancer therapy and diagnosis. *Mol. Pharm.* **9**, 2961–73 (2012).

408. Su, X. *et al.* Antagonizing integrin $\beta 3$ increases immunosuppression in cancer. *Cancer Res.* **76**, 3484–3495 (2016).
409. Su, G. *et al.* Absence of integrin $\alpha 3$ enhances vascular leak in mice by inhibiting endothelial cortical actin formation. *Am. J. Respir. Crit. Care Med.* **185**, 58–66 (2012).
410. Nagy, J. A., Chang, S.-H., Dvorak, A. M. & Dvorak, H. F. Why are tumour blood vessels abnormal and why is it important to know? *Br. J. Cancer* **100**, 865–869 (2009).
411. Chatterjee, K., Zhang, J., Honbo, N. & Karliner, J. S. Doxorubicin cardiomyopathy. *Cardiology* **115**, 155–162 (2010).
412. Straube, A. & Merdes, A. EB3 Regulates Microtubule Dynamics at the Cell Cortex and Is Required for Myoblast Elongation and Fusion. *Curr. Biol.* **17**, 1318–1325 (2007).
413. Stehbens, S. J. *et al.* CLASPs link focal-adhesion-associated microtubule capture to localized exocytosis and adhesion site turnover. *Nat. Cell Biol.* **16**, 561–73 (2014).
414. Howes, S. C., Alushin, G. M., Shida, T., Nachury, M. V. & Nogales, E. Effects of tubulin acetylation and tubulin acetyltransferase binding on microtubule structure. *Mol. Biol. Cell* **25**, 257–266 (2014).
415. Howard, J. & Hyman, A. A. Dynamics and mechanics of the microtubule plus end. *Nature* **422**, 753–758 (2003).
416. Yenjerla, M., Panopoulos, A., Reynaud, C., Fotedar, R. & Margolis, R. L. TD-60 is required for interphase cell cycle progression. *Cell Cycle* **12**, 837–841 (2013).
417. Tilley, F. C., Williamson, R. C., Race, P. R., Rendall, T. C. & Bass, M. D. Integration of the Rac1- and actin-binding properties of Coronin-1C. *Small GTPases* **6**, 41–47 (2015).
418. Williamson, R. C. *et al.* Coronin-1C and RCC2 guide mesenchymal migration by trafficking Rac1 and controlling GEF exposure. *J. Cell Sci.* 4292–4307 (2014). doi:10.1242/jcs.154864
419. Xu, X. H., Pan, W., Kang, L. H., Feng, H. & Song, Y. Q. Association of Annexin A2 with cancer development (review). *Oncol. Rep.* **33**, 2121–2128 (2015).

420. Liu, W. & Hajjar, K. A. The annexin A2 system and angiogenesis. *Biol. Chem.* **397**, 1005–1016 (2016).
421. Rankin, C. R. *et al.* Annexin A2 regulates Beta1 integrin internalization and intestinal epithelial cell migration. *J. Biol. Chem.* **288**, 15229–15239 (2013).
422. Lin, L., Wu, C. & Hu, K. Tissue Plasminogen Activator Activates NF- B through a Pathway Involving Annexin A2/CD11b and Integrin-Linked Kinase. *J. Am. Soc. Nephrol.* **23**, 1329–1338 (2012).
423. Hitchcock, J. K., Katz, A. A. & Schäfer, G. Dynamic reciprocity: The role of annexin A2 in tissue integrity. *J. Cell Commun. Signal.* **8**, 125–133 (2014).
424. Bid, H. K., Roberts, R. D., Manchanda, P. K. & Houghton, P. J. RAC1: An Emerging Therapeutic Option for Targeting Cancer Angiogenesis and Metastasis. *Mol. Cancer Ther.* **12**, 1925–1934 (2013).
425. D’Amico, G. *et al.* Endothelial-Rac1 Is Not Required for Tumor Angiogenesis unless $\alpha\beta 3$ -Integrin Is Absent. *PLoS One* **5**, (2010).
426. Wittmann, T., Bokoch, G. M. & Waterman-Storer, C. M. Regulation of Microtubule Destabilizing Activity of Op18/Stathmin Downstream of Rac1. *J. Biol. Chem.* **279**, 6196–6203 (2004).
427. Daub, H., Gevaert, K., Vandekerckhove, J., Sobel, A. & Hall, A. Rac/Cdc42 and p65PAK regulate the microtubule-destabilizing protein stathmin through phosphorylation at serine 16. *J. Biol. Chem.* **276**, 1677–1680 (2001).
428. Banerjee, M., Worth, D., Prowse, D. M. & Nikolic, M. Pak1 phosphorylation on T212 affects microtubules in cells undergoing mitosis. *Curr. Biol.* **12**, 1233–1239 (2002).
429. Gao, Y., Dickerson, J. B., Guo, F., Zheng, J. & Zheng, Y. Rational design and characterization of a Rac GTPase-specific small molecule inhibitor. *Proc. Natl. Acad. Sci. U. S. A.* **101**, 7618–23 (2004).
430. Hansen, M. D. H., Ehrlich, J. S. & Nelson, W. J. Molecular mechanism for orienting membrane and actin dynamics to nascent cell-cell contacts in epithelial cells. *J. Biol. Chem.* **277**, 45371–45376 (2002).
431. Marshall, J. F. *et al.* Alpha v beta 1 is a receptor for vitronectin and fibrinogen, and acts with alpha 5 beta 1 to mediate spreading on fibronectin. *J. Cell Sci.* **108**, 1227–

- 1238 (1995).
432. Stoeltzing, O. *et al.* Inhibition of integrin alpha5beta1 function with a small peptide (ATN-161) plus continuous 5-fu infusion reduces colorectal liver metastases and improves survival in mice. *Int. J. Cancer* **104**, 496–503 (2003).
433. Mollinari, C. *et al.* The mammalian passenger protein TD-60 is an RCC1 family member with an essential role in prometaphase to metaphase progression. *Dev. Cell* **5**, 295–307 (2003).
434. Shin, Y. J., Kim, E. H., Roy, A. & Kim, J. H. Evidence for a Novel Mechanism of the PAK1 Interaction with the Rho-GTPases Cdc42 and Rac. *PLoS One* **8**, (2013).
435. White, D. P., Caswell, P. T. & Norman, J. C. $\alpha\beta3$ and $\alpha5\beta1$ integrin recycling pathways dictate downstream Rho kinase signaling to regulate persistent cell migration. *J. Cell Biol.* **177**, 515–525 (2007).
436. Mana, G. *et al.* PPFIA1 drives active $\alpha5\beta1$ integrin recycling and controls fibronectin fibrillogenesis and vascular morphogenesis. *Nat. Commun.* **7**, (2016).
437. Van Weert, A. W. M., Geuze, H. J., Groothuis, B. & Stoorvogel, W. Primaquine interferes with membrane recycling from endosomes to the plasma membrane through a direct interaction with endosomes which does not involve neutralisation of endosomal pH nor osmotic swelling of endosomes. *Eur. J. Cell Biol.* **79**, 394–399 (2000).
438. Aizawa, M. & Fukuda, M. Small GTPase Rab2B and Its specific binding protein golgiassociated rab2b interactor-like 4 (GARI-I4) regulate golgi morphology. *J. Biol. Chem.* **290**, 22250–22261 (2015).
439. Loizides, C. *et al.* Model-based tumor growth dynamics and therapy response in a mouse model of de novo carcinogenesis. *PLoS One* **10**, 1–18 (2015).
440. Taverna, D. *et al.* Increased primary tumor growth in mice null for beta3- or beta3/beta5-integrins or selectins. *Proc. Natl. Acad. Sci. U. S. A.* **101**, 763–8 (2004).
441. Su, M. *et al.* The anti-angiogenic effect and novel mechanisms of action of Combretastatin A-4. *Sci. Rep.* **6**, 28139 (2016).
442. Bijman, M. N. A. Microtubule-targeting agents inhibit angiogenesis at subtoxic concentrations, a process associated with inhibition of Rac1 and Cdc42 activity and

- changes in the endothelial cytoskeleton. *Mol. Cancer Ther.* **5**, 2348–2357 (2006).
443. Bhaskar, V. *et al.* A function blocking anti-mouse integrin $\alpha 5\beta 1$ antibody inhibits angiogenesis and impedes tumor growth in vivo. *J. Transl. Med.* **5**, 61 (2007).
444. Mitjans, F. *et al.* An anti- αv -integrin antibody that blocks integrin function inhibits the development of a human melanoma in nude mice. *J. Cell Sci.* **108 (Pt 8)**, 2825–2838 (1995).
445. Turaga, R. C. *et al.* Rational design of a protein that binds integrin $\alpha\beta 3$ outside the ligand binding site. *Nat Commun* **7**, 11675 (2016).
446. Binet, F. & Sapieha, P. ER stress and angiogenesis. *Cell Metab.* **22**, 560–575 (2015).
447. Masson-Gadais, B., Houle, F., Laferrière, J. & Huot, J. Integrin $\alpha v\beta 3$, requirement for VEGFR2-mediated activation of SAPK2/p38 and for Hsp90-dependent phosphorylation of focal adhesion kinase in endothelial cells activated by VEGF. *Cell Stress Chaperones* **8**, 37–52 (2003).
448. Rodrigues, L. M. *et al.* Effects of HSP90 inhibitor 17-allylamino-17-demethoxygeldanamycin (17-AAG) on NEU/HER2 overexpressing mammary tumours in MMTV-NEU-NT mice monitored by Magnetic Resonance Spectroscopy. *BMC Res. Notes* **5**, 250 (2012).
449. Sanderson, S. *et al.* Benzoquinone ansamycin heat shock protein 90 inhibitors modulate multiple functions required for tumor angiogenesis. *Mol. Cancer Ther.* **5**, 522–32 (2006).